MECHANISM OF ACTION OF CYCLIC ANTIMICROBIAL PEPTIDES

Anna DÍAZ i CIRAC

Dipòsit legal: GI-1303-2011
http://hdl.handle.net/10803/38252

PhD Thesis

Mechanism of Action of Cyclic Antimicrobial Peptides

Anna Díaz Cirac

2011

Doctorat Interuniversitari en Química Teòrica Computacional

Dirigida per

Pedro Salvador Sedano

Marta Planas Grabuleda

Lidia Feliu Soley

Memòria presentada per optar al títol de Doctor per la Universitat de Girona

Universitat de Girona

Pedro Salvador Sedano, Marta Planas Grabuleda i Lidia Feliu Soley professors titulars del Departament de Química de la Universitat de Girona,

CERTIFIQUEM:

Que aquest treball titulat **"Mechanism of Action of Cyclic Antimicrobial Peptides"**, que presenta l'Anna Díaz Cirac per a l'obtenció del títol de Doctor, ha estat realitzat sota la nostra direcció i que compleix els requeriments per poder optar a Menció Europea.

Signatura

Pedro Salvador Sedano Marta Planas Grabuleda Lidia Feliu Soley

Girona, 26 d'Abril de 2011

A la meva mare

Summary of the Thesis

Antimicrobial peptides (AMPs) are currently in the spotlight as potential candidates to overcome bacterial resistance to conventional antibiotics. However, how these molecules kill bacteria by interacting with the cell membrane is not fully understood. Studying the biophysical processes of antimicrobial activity of these peptides can provide excellent information for the rational design of new improved candidates for the development of effective antibacterial agents. Amongst the large number of AMPs present in nature, cyclic peptides have emerged as good antimicrobial candidates due to their robust secondary structure and high activity.

The starting point of this thesis is a library of *de novo* cyclic decapeptides which showed high antimicrobial activity against three plant pathogenic bacteria, namely *Pseudomonas syringae*, *Erwinia amylovora* and *Xanthomonas vesicatoria*, and low hemolytic activity. These cyclic peptides consisted of alternating cationic (lysine) and hydrophobic (leucine and phenylalanine) amino acids, with a general formula of c(X_5-Phe-X_3-Gln) where X can be either lysine or leucine. In order to devise a general procedure for designing new cyclic antimicrobial candidates with improved activity, this work is devoted to the understanding of i) the factors governing the activity and ii) the mechanism of action at the atomistic level of these peptides, principally by making use of well-established computational molecular modeling tools such as Molecular Dynamics (MD) simulations.

This thesis is divided into two parts, one of them focused on the synthesis and evaluation of the biological activity of a series of cyclic AMPs, and another one where MD simulations of these peptides were carried out in order to shed light on their conformational preferences, stability in water phase and their mechanism of action upon lipid membrane.

In the first part, the experimental procedure covered the optimization of the synthesis of a particular cyclic decapeptide in different solid supports, namely resin and lanterns. We show how by changing the coupling reagents an improved head-to-tail cyclization over dimerization is reached. Also the influence of replacing the phenylalanine residue by a tryptophan for the cyclic peptides from the library is evaluated in detail. Even though the tryptophan analogue shows

a higher antimicrobial activity, its cytotoxic activity is also affected giving rise to higher hemolytic activity. Moreover, the evaluation of the stability of some of the cyclic peptides in human serum is tested to study their potential therapeutic application for cancer therapy. Those active peptides prove to be more stable compared to their linear analogues.

The second part of the thesis comprises the computational modeling of several specific cyclic AMPs from the library. In a first study, we describe a comprehensive conformational search of the cyclic peptide BPC16, c(KLKLKFKLKQ) by means of several strategies rooted on the use of MD simulations. The analysis of the large set of conformers obtained revealed higher stability of structures with smaller radius of gyration. Dynamical studies showed a high stability of a compact structure both in gas phase and in solution. In the water phase, the effect of water molecules caused more fluctuations in the formation of hydrogen bonds but a stable secondary structure consisting of a β-turn I and α-turn structure was established as the conformation of the peptide in solution.

In a second study, and in collaboration with the Molecular Dynamics group of Groningen, we used the best candidate from the library of cyclic peptides, BPC194 (c(KKLKKFKKLQ)) and its non-active linear analogue (BPC193) to study the molecular basis for their antimicrobial activity. To do so, a number molecular dynamics simulations upon anionic lipid bilayer models were carried out. We show here that the cyclic peptide is able to fold in an amphypathic-like manner, which helps in the stabilization of a disordered toroidal pore. Furthermore, a structure-function relationship is derived from the careful analysis of a stable conformation of the peptides directly involved in the formation and stabilization of the porated state, best characterized by a β-structure with a spatially-symmetric arrangement of the lysine side-chains. In the last part of this section, bigger systems consisting of two sets of lipid bilayers were modeled in order to examine alternative modes of antimicrobial action. These simulations manifest the ability of the cyclic peptide BPC194 to both porate and fuse lipid membranes simultaneously. Such multi-mode process may be functionally relevant and contribute to the high effectiveness of this peptide towards bacteria killing.

In the last part of this thesis we work with the hypothesis that the distinct structural motif found for the BPC194 peptide in the porated state plays a fundamental role in its antimicrobial activity, and therefore can be a key element for a rational design of new cyclic peptides with similar or enhanced activity. Principally based on the bioactive conformation of BPC194, nine cyclic peptides were designed and synthesized. Remarkably, peptide BPC490 exhibits improved activ-

ity against all three bacteria compared to the most active peptide of the original library, yet keeping its hemolytic activity still very low. Such high antimicrobial activity found for some of these new peptides evidences the effectiveness of our rational design approach, by combining both experiment and computational modeling.

Resum de la Tesi

Els pèptids antimicrobians (AMPs) es troben actualment en el centre d'atenció com a possibles candidats per superar la resistència bacteriana als antibiòtics convencionals. El mecanisme pel qual aquestes molècules maten els bacteris per interacció amb la membrana cel.lular no està completament entès. L'estudi dels processos biofísics de l'activitat antimicrobiana d'aquests pèptids poden proporcionar informació rellevant per al disseny racional de nous candidats per al millor desenvolupament d'eficaços agents antibacterians. D'entre el gran nombre de AMPs presents en la natura, els pèptids cíclics s'han convertit en bons candidats a compostos antimicrobians a causa de la seva robusta estructura secundària i la seva elevada activitat.

El punt de partida d'aquesta tesi és una biblioteca de *de novo* decapèptids cíclics sintetitzat al laboratori LIPPSO de la Universitat de Girona, que va mostrar una elevada activitat antimicrobiana contra tres bacteris patògens de plantes (*Pseudomonas syringae*, *Erwinia amylovora* i *Xanthomonas vesicatoria*), així com una activitat hemolítica baixa. L'estructura primària d'aquests pèptids cíclics alternava aminoàcids catiònics (lisina) i hidrofòbiques (leucina i fenilalanina), per donar lloc a la fórmula general c(X_5-Phe-X_3-Gln), on X poden ser lisines o leucines.

Per tal d'elaborar un procediment general per al disseny de nous pèptids cíclics antimicrobians amb activitat millorada, aquest treball està dedicat a la comprensió i) dels factors que regulen llur activitat i ii) del mecanisme d'acció a nivell atòmic d'aquests pèptids, principalment per mitjà de l'ús d'eines computacionals de modelatge molecular com les simulacions de dinàmica molecular clàssica.

Aquesta tesi es divideix en dues parts, una d'elles es centra en la síntesi i la posterior avaluació de l'activitat biològica d'una sèrie de pèptids antimicrobians cíclics, i una altra a on es duen a terme simulacions de dinàmica molecular d'aquests pptids terme per tal d'elucidar les seves preferències conformacionals, l'estabilitat en fase aquosa i el seu mecanisme d'acció en membrana lipídica.

La primera part es centra en els procediments experimentals, que inclouen l'optimització de la síntesi d'un decapèptid cíclic particular en diferents suports

sòlids com resines i llanternes. Es mostra com, en canviar el reactiu d'acoblament, s'aconsegueix un millor rendiment de la reacció de ciclació respecte la de dimerització. També s'avalua en detall la influència de la substitució dels residus de fenilalanina per triptòfan als pèptids cíclics de la biblioteca. Tot i que l'anàleg de triptòfan mostra una major activitat antimicrobiana, la seva activitat citotòxica també es veu afectada, donant lloc a una major hemòlsi. D'altra banda, també s'avalua l'estabilitat d'alguns dels pèptids cíclics en el sèrum humà, per tal de valorar la seva possible aplicació terapèutica envers el càncer. Aquests pèptids actius s'han mostrat més estables en comparació als seus anàlegs lineals.

La segona part de la tesi abasta el modelatge computacional de diversos pèptids cíclics antimicrobians de la biblioteca. En un primer estudi es descriu una cerca conformacional exhaustiva del pèptid cíclic BPC16, c(KLKLKFKLKQ) per mitjà de diversos protocols basats en l'ús de simulacions de dinàmica molecular clàssica. L'anàlisi del gran conjunt de confòrmers obtinguts va revelar una tendència cap a una major estabilitat de les estructures amb radi de gir menor. Els estudis dinàmics posteriors van corroborar l'elevada estabilitat d'una estructura compacta, tant en fase gasosa com en dissolució aquosa. En fase aquosa, l'efecte entròpic de molècules d'aigua provoca més fluctuacions en la formació d'enllaços per pont d'hidrogen, però es va establir que la conformació estable del pèptid en solució presentava els elements *β-turn* tipus I *α-turn*.

En un segon estudi, i en col.laboració amb el grup de dinàmica molecular de Groningen, es va utilitzar el pèptid BPC194 (c(KKLKKFKKLQ)), millor candidat de la biblioteca de pèptids cíclics, i el seu anàleg lineal no actiu (BPC193) per establir la base molecular de la seva activitat antimicrobiana. Per aquest fi, es van dur a terme diverses simulacions de dinàmica molecular amb models aniònics de bicapa lipídica. Aquí es mostra com el pèptid cíclic és capaç de plegar-se d'una manera amfipàtica, el que ajuda a l'estabilització d'un porus toroidal desordenat a la membrana lipídica. D'altra banda, s'ha establert una relació estructura-funció derivada de l'anàlisi permenoritzada de la conformació estable dels pèptids que participen directament en la formació i estabilització de l'estat porat. Aquesta presenta una β-estructura amb un arranjament espacial simètric i alineat de les cadenes laterals dels residus de lisina. En l'última part d'aquesta secció es descriu l'estudi de sistemes més complexos que consten de dues bicapes de lípids, que es van dur a terme amb la finalitat d'examinar possibles modes alternatius d'acció antimicrobiana. Aquestes simulacions posen de manifest la capacitat del pèptid cíclic BPC194 per formar poros estables i induir fusió de membranes lipídiques a la vegada. Aquest procés *multi-mode* pot ser funcionalment rellevant i contribuir a l'elevada activitat antibacteriana d'aquest

pèptid.

A la darrera part d'aquesta tesi s'explota la hipòtesi de que el motiu estructural trobat pel pèptid BPC194 en l'estat porat juga un paper fonamental en la seva activitat antimicrobiana, i per tant pot ser un element clau per a un disseny racional de nous pèptids cíclics amb activitat similar o millorada. Basats principalment en la conformació bioactiva del BPC194, s'ha dissenyat i sintetitzat una nova llibreria de nou pèptids cíclics. Notablement, el pèptid BPC490 sembla presentar una millor activitat contra les tres bacteries estudiades en comparació amb el pèptid més actiu de la llibreria original, i, a més a més, mantenint la seva relativament baixa activitat hemolítica. Aquesta elevada activitat antimicrobiana que s'ha trobat per alguns d'aquests nous pèptids evidecia l'eficàcia del disseny racional proposat, que combina tant els experiments com la modelització computacional.

Acknowledgments/Agraïments

Sembla mentida que estigui escribint els agraïments. Com tot en aquesta vida sempre es fa molt difícil començar qualsevol cosa, però quan una persona s'ho proposa i posa empemta, les coses acaben sortint sigui com sigui. Això si, al llarg dels anys fent el Doctorat he aprés moltíssimes coses perque aquesta empemta sigui constant en el temps, com per exemple que un no s'ha d'estressar, que mes val poc a poc i bona lletra, que les coses en fred tenen un altre color, be ... moltíssimes, però una d'elles i molt important es que la gent que t'envolta, que et dona suport i et fa riure, fa possible que acabi sortint bé. Com que durant aquest temps he conegut i hi han intervingut moltíssimes persones en aquest procés, intentaré ordenar les meves idees per no deixar-me ningú.

Què millor començar per el començament. Primer de tot m'agradaria agrair a en Miquel Duran per donar-me la possibilitat de gaudir de la beca de Doctorat i poder combinar lliurement el món experimental i teòric. Per altra banda també m'agradaria agrair a les meves directores de la part experimental, la Marta Planas i la Lidia Feliu. Gràcies per donar-me la possibilitat de treballar en el món de la síntesi de pèptids. Tot i la meva transformació al camp de la química computacional, sempre recordaré els primers anys de creixament al LIPPSO. No vull oblidar-me d'agrair primer a l'Eduard Bardají per l'oportunitat de treballar al grup i segon i no menys important a la Montse Heras, que tot i que no ha sigut directora meva, sempre ha tingut un somriure que oferir.
Vull agrair en especial a en Pedro (Salvador, poco mordedor? era així?) que a mesura que ha anat passant el temps s'ha acabat convertint en el director de la meva Tesi. Gràcies Pedro per tot plegat, per ajudar-me els meus primers inicis amb l'AMBER, per donar-me la llibertat de marxar a Groningen tantes vegades com he necessitat, i per fer l'esforç de dirigir una Tesi que no formava part dels esquemes inicials. Però també per les llargues bicicletades que hem fet en totes les condicions, aranyes, pluja, pedra, vent, etc ... (no cridem al mal temps que tot pot empitxorar!).

Com que els meus inicis van ser a la part experimental, m'agradaria començar per agrair totes les persones que he anat coneixen en el grup, els

LIPPSIANS i *LIPPSIANES* (això, això ho sap tothom!). Vull donar les gràcies a en Rafael (incloent les bromes per telèfon), la Vane, la Marta D., la Cristina C., la Montse T. en Marc, l'Ana (ànims queda poc per la teva tesi també!), en Tifa (le hip-hoperoo du grup, PALANGANA!), l'Imma (la noia mes energètica del lippso, merci!), la Cristina R., la Iteng (ehh hola?) i la Silvia. Sobretot gràcies per enfiar-vos de mi al tornar al laboratori, després de pasar al *lado oscuro* =)!. No em vull oblidar a les *CATS*! l'Anna (Dachs, especifiquem eh!jeje), la Lidia, la Sandra, l'Anna Pla, la Magda i la Monica R. Gràcies per tots els moments, tant alhora de dinar, cafés, sopars que hem fet, en especial al trio lalala (Anna, Lidia i Sandra).

Això van ser els meus 2 anys de doctorat, que es diuen aviat! Ara ve, quan creues el pont aeri de la facultat, et trobes a la zona freaky, alies *IQC*. I en aquest cas a qui et trobes, als *IQCIANS* (això, això també ho sap tothom!). Aixo si que sembla ahir que entrava al despatx 177 i no sabia el que m'esperava. Vull donar les gràcies a en Ferran (Ferram! son bones aquestes xopes?), en Pata, la Mireia, la Silvia, l'Oscar, en David H, l'Eloy (Carambidurí Carambidurà!), en Lluís, la Cristina, en Sergi (vull sortir a l'APM!), la Laia (never gonna give you up, lalala), en Majid, en Marc (abracadabra ...) , l'Eugeni, en Carles i la Carme!. En especial, voldria donar les gràcies primer a la Laia, per tornar-se tan freaky (vegila que aixo creix exponencialment ehhh! Al loro!), i per acompanyar amb l'alegria dins del despatx! i també vull donar les gràcies sobretot a en Dani per tots els moments del despatx 177. Per entrar al despatx i endinsar-se en el món de les teories de LOST (això es una equivocació!) i per tots els moments APM en els que hem rigut un munt! (si, ahora ahora!, Ra Ra Ragazza! si fos veritat, seria record Guinness!!). També vull agrair a tots els que cada dijous (o com a mínim ho intentem) ens veiem les cares a la cantxa! (se va a ver un follón, que no sabe ni donde se ha metido, sa matao Paco!)

Now I want to shift to english, because I'd like to thank all people I have met in Groningen, one of the most important part of my thesis! First of all, and to start with I would like to thank to Siewert-Jan Marrink. Thanks for accepting me to come to Groningen, the first, the second and the third time I came! For me it has been a pleasure to come to Groningen not only to learn from MD GROUP and do the simulations which are one of the most important parts of this thesis!, but also because there I met a lot of great people who helped me incondicionally, specially you, that always recieved my with a big smile! Once I got in Groningen, the first crazy girl I met was Durba! Thanks Durba for ... everything! for a great scientist, for your smile and for being my friend. Also for helping me in all senses, because all the things are easy with a Mohito, aren't

they? jejejeje Together with you, I want to thank also Gemma! It has been more than a pleasure working with you girls! If all scientist could work like this, science would be no such stress!! (at least for me =)) Thanks for all the moments in Groningen, discussin and chatting about everyting! You are great! I want also to thank in general all MD group, Alex, Martti, Rennee (is NMR group, but I felt like he was in the group =)!), Kamil, Cesar, Monica, Lars, Djurre, Daniela, Marc, Andrej, Xavier, Tsjerk, Manel, Frans, Marcelo and Zofie. All of you make MD group nicer and nicer!

And last, and not less important are all people I met out from university, the *PLUTOLANNERS*!! Thanks to Jeremy, Johnnatan (Chinese commettee), Shyamal and Santanu (Indian commetee) and Ivan and Jozef (Slovaquian commettee)! Also want to thank the "Spanish Inquisition" that are present in the University!

Ara tornem al catala! En el temps passat a Groningen, també vaig tenir la oportunitat de conviure amb dos catalanets Gironins, alies *The CHILDRENNN*!(That's Durba's fault, not me). Gràcies Gemma (Jiemmaaaa) i Edu (cunyaoooo) per tot. Gemma tu per ser com ets, tant energètica, i que sempre portes alegria a tots els llocs! Per no parlar de lo treballadora que ets! Gracies per ajudar-me en moments dificils de la Tesi. I no m'oblido de tu Edu!!!! Gràcies, primer de tot per ser com ets (ja entenc perquè esteu junts!) i per dissenyar aquesta super-portada de la meva Tesi! (www.dsign-ed.com, aqui publicitat tu, que ets un crack).

No m'agradaria oblidar-me de totes les persones que vaig conèixer en els cursos de Doctorat a Santander! M'agradaria agrair a en Zamorano (Presidente! Ojala!), la Mireia (xunguinator! 0 Newtons of force!!), Laia (Playa), Ceila (mi entrenadora personal! hay que recuperar el tiempo xunga!), Ramon (el palangana, lo sabe todo el mundo!) i Juanjo (el galego xungo). En especial vull donar les gràcies a en Miquel Huix! Moltes gràcies palangana per tots moments passats, no només en els aspectes professionals, sinó que en els aspectes mes personals has sigut una persona molt important (perdoneu, pero algu ho havia de dir!). També vull donar les gràcies a les meves ex-companyes de pis (alies Dachs i Niquita), que tot i que ara visc sola (per fiii!!! jejejeje és broma poma), la major part del meu doctorat l'he passat amb vosaltres. En especial vull agrair a la Dachs per tot en general. Per ser companya de doctorat (tu i jo sabem que combinar les coses aporta un estrés extra! ànims que queda poc!!) i per tot el temps que hem viscut juntes.

Com la vida mateixa, tot es cíclic!! (com els pèptids ciclics, equilicuaaa!), i com he comenat al principi per els meus inicis, acabare les agraïments agraint

persones que han sigut presents dels dels principis dels principis (fins i tot abans del doctorat ehhhh!). Primer de tot, a tota la *PENYA DE L'ESPARDENYA*!!! Gràcies a tots, Santi, Alba, Maira, Monica F, Monica B, Marta C, Carla, Naiara, Quim, Xevi, Ferram, Ferran, Pilarin i Dachs (Dachs, el burro va al davant, ja veus que he guardat posiciò important per tu! jejeje, perdó Santi!). Gràcies per tots els boixos moments que podria anar citant, pero millor que no ho fagi, i per seguir podent fer les quedades anuals i mantenir la essencia que ens va unir! Sobretot vull agrair a en Santi, per compartir moltes de les sensacions que ens han aportat el doctorat, i per ser una persona tal qual! Tambe vull agrair en especial a l'Alba i la Maira per ser com son, no canvieu mai si us plau! i la Naiara per tota l'ajuda ja que tu i jo sabem que les coses no son fàcils, pero quan un s'ho proposa, es poden tirar endavant!(Ànims que queda poc!).

Tambe vull agrair, a tots els meus amics de Granollers. A l'Oriol (camarero, una de Nesquik!) i en Valls (ahhaaaaa!), gràcies per tots els moments amb una bona cervesa a la mà, sou genials! la Silke i la Pey (les guitarreres!! Gràcies per tots els moments tocant la guitarra ... i no tocant-la tant!! m'encanta parlar amb vosaltres, Guapes!), la Vinyo (la pet, gràcies per tots els moments passats!), en Rufes, en Xamfrà, que gràcies a tu he conegut tot el món de les xapes, en Martí (piripiiii que t'has convertit en un gran pare!), la Neus (la mare jejeje), i els petitons del grup, en Jan, l'Aleix i l'Arlet! Sou petits, però aporteu molta alegria! Gràcies a tots per tenir sempre el detall de preguntar-me ... Que és un peptid??? Tambe agrair a la Sandra Camenforte per tots els moments passat plegades (i futura dona d'un Gironiii!! ueee) i la Núria Baqué que tot i passar el temps, sembla que tot sigui igual que quan anavem a l'Institut! Moltes Gràcies.

Per últim, i no menys important, vull agrair la meva familia. Sobretot als meus tiets Jordi i Alicia, i en petit Samuel, el meu pare, el meu germà i sobretot sobretot, a la meva mare, la Mercé, a qui dedico aquesta Tesi. Perquè sense ella no hagués sigut possible, per ser com es, i per donar fins i tot quan no es possible, Moltes Gràcies!

List of Publications

1. Feliu, L., Oliveras, G., Cirac, A. D., Besalú, E., Rosés, C., Colomer, R., Bardají, E., Planas, M., Puig, T. 2010. Antimicrobial cyclic decapeptides with anticancer activity *Peptides* 31:2017-2026.

2. Cirac, A. D., Moiset, G., Mika, J. T., Koçer, A., Salvador, P., Poolman, B., Marrink, S. J., Sengupta, D. 2011. The molecular basis for antimicrobial activity of pore-forming cyclic peptides *Biophys. J.* 100:1-10

3. Mika, J. T., Moiset, G., Cirac, A. D., Feliu, L., Bardají, E., Planas, M., Sengupta, D., Marrink, S. J., Poolman, B. 2011. Structural basis for the enhanced activity of cyclic antimicrobial peptides: the case of BPC194 *BBA-Membranes In Press.*

List of Acronyms

Abbreviation	Description
Å	Angstrom
AcOH	Acetic Acid
Al	Allyl
AMP	Antimicrobial Peptide
Bn	Benzyl
Boc	*tert*-Butyloxycarbonyl
BPC	Bioactive Cyclic Peptide
CD	Circular Dichroism
CH_3CN	Acetonitril
CH_2Cl_2	Dicoloromethane
COMU	1-[(1-(Ciano-2-etoxi-2-oxoetilidenaminooxi)-dimetilaminomorfolino)] uronio hexafluorofosfato
DCC	Dicyclohexylcarbodiimide
DIC	N,N'-diisopropylcarbodiimide
DIEA	N,N-diisopropyletylamine
DMF	N,N-dimethylformamide
DMPC	Dimyristoylphosphatidylcholine
DNA	Deoxyribonicleic Acid
DOE	Design of Experiments
DPC	Dodecylphosphocholine
DOPC	Dioleoylphosphatidylcholine
DPPC	Dipalmitoylphosphatidylcholine
DPPG	Dipalmitoylphosphatidylglycerol
DSSP	Dictionary Secondary Structure Protein
DTP	Disordered Toroidal Pore
ESI-MS	Electrospray Ionization Mass Spectrometry
eq	equivalent
Fmoc	9-Fluorenylmethoxycarbonyl
G-	Gram negative

G+	Gram positive
GS	Gramicidin S
h	hour
HATU	O-(7-azabenzotriazol-1-yl)-1,1,3,3-tetramethyluronium
HBTU	O-(1H-benzotriazol-1-yl)-1,1,3,3-tetramethyluronium
HMFA	9-(hydroxymethyl)-2-fluorenenacetic acid
HND	Human Neutrophil Defensin
HPLC	High Pressure Liquid Chromatography
IC_{50}	50% Inhibition Concentration
LPS	Lipopolysacharide Phospholipid molecules
LPE	Lysophosphatidylethanolamine
μs	microsecond
MALDI-TOF	Matrix-Assisted Laser Desorption Ionization with Time-Of-Flight
MAP	Membrane Active Peptide
MBHA	4-Methylbenzhydrylamine
MD	Molecular Dynamics
M_H	Hydrophobic Moment
M_l	Linear Mass
M_c	Cyclic Mass
M_d	Dimer Mass
MIC	Minimum Inhibitory Concentration
MM	Molecular Mechanics
NMM	N-Methylmorfoline
ns	nanosecond
NMR	Nuclear Magnetic Ressonance
Nonb	3-Nitro-4-aminomethylbenzoic acid
NRP	Non-Ribosomally Synthesised Peptide
NPT	Constant number of Particles, Pressure and Temperature
NVT	Constant number of Particles, Volume and Temperature
oxyma	Ethyl 2-cyano-2-(hydroxyimino)acetate
PBC	Periodic Boundary Conditions
PEG	Polyethylenglycol
PC	Phosphatidylcholine
PE	Phosphatidylethanolamine
PG	Phosphatidyl-Glycerol

POPC	1-Palmitoyl-2-oleoyl-3-phosphatidylcholine
POPG	1-Palmitoyl-2-oleoyl-3-phosphatidylglycerol
PPII	Polyproline-II helix
PS	Polystyrene
ps	picosecond
PLP	Protrusion-Lile Point
PME	Particle-Mesh Ewald
PyBOP	Benzotriazol-1-yloxytri(pyrrolidino)- -phosphonium hexafluorophosphate
PyBrOP	Bromo-tris-pyrrolidino phosphoniumhexafluorophosphate
Rink	4-[(2,4-Dimethoxyphenyl)aminomethyl]- -phenoxyacetic acid
RF	Reaction Field
RP	Ribosomally Synthesised Peptide
SDS	Sodium Dodecyl Sulfate
SM	Sphingomyelin
SPPS	Solid-Phase Peptide Synthesis
^{t}Bu	*tert*-Butyl
TFA	Trifluoroacetic Acid
VMD	Visual Molecular Dynamics

List of Figures

List of Tables

Contents

Chapter 1

Introduction

1.1 Peptides: General Structure

Peptides are widespread in nature and represent one of the most important products of interest in a wide range of fields like chemistry, biology, pharmacology and medicine. Formally, peptides are polymers of amino acids connected by amide bonds (peptide bonds) between the carboxy group of one residue and the amino group of the following amino acid. According to the currently accepted nomenclature rules, "oligopeptides" are composed of less than 15 amino acids whereas "polypeptides" are defined to contain approximately 15-50 amino acid residues. The term "protein" is used for sequences containing more than 50 amino acids (IUPAC-IUB 1984).

The diversity of peptides and their biological function depends on the nature of the amino acids present in the sequence, the lengh of the peptide and the spatial arrangement to a specific three-dimensional structure. Owing to that, understanding the basic properties of the amino acids present in nature is important to relate the peptide folding with the biological function.

1.1.1 Amino Acids as Building Blocks: Classification, Properties and Nomenclature

In nature, different types of amino acids exist, namely the "protein amino acids" and the "non-protein amino acids", (see Figure 1.1). The former are the most important class of amino acids, which are part of the proteins and peptides encoded by DNA. The latter, rather unusual amino acids, are mostly found in prokaryote cells and lower eukaryotes like algae, sponges and fungi. These amino acids are introduced into the peptide chain by enzymatic synthesis rather that ribosomaly, since they are not coded by DNA. The "protein amino acids" are α-amino acids

composed by an amino group (-NH_2) and a carboxy group (-COOH) bound to the same carbon atom (α-carbon, C_α). A hydrogen atom and a side chain (R) are also bound to the α-carbon, which is (with the exception of glycine where R=H) an asymmetric center. Therefore, the α-amino acids are chiral molecules, meaning that each of them has two optical isomers, the L-enantiomer and D-enantiomer (Figure 1.1 B). In an absolute nomenclature, the L-enantiomers are expressed as S-forms, except for cysteine, for which this configuration is defined as R-form. On the other hand, D-enantiomers are found in some ribosomally synthesized peptides of eukaryotic origine and in peptidoglycan wall cells of bacteria (Nagata 1999).

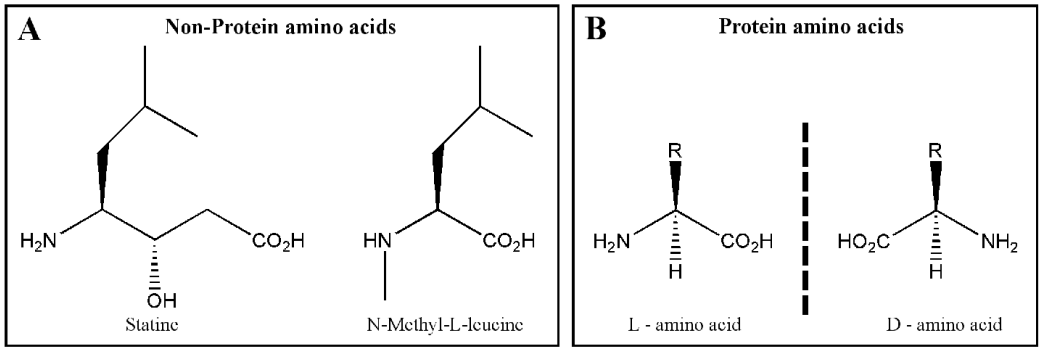

Figure 1.1: *Different types of amino acids.* **A**. Some representative non-protein amino acids. In statine (left) the amino group is not directly bound to C_α, and N-methyl-L-leucine (right) deviates from the natural α-amino acids having a methylated group in its amine function. **B**. General structure of α-amino acids. Two optical isomers, L and D are shown, being the L the isomer present in natural proteins.

Amongst the wide range of amino acids, 20 standard amino acids occurring in natural proteins exist. To identify them, a three-letter code and one-letter code abbreviation is given to each of them. A summary of the classification and properties of all protein amino acids is given in Figure 1.2. Each amino acid is characterized by its side chain R, that contributes to its biochemical properties. Due to their particular chemical features, the standard amino acids can be classified into two main groups: polar and non-polar (Figure 1.2, blue and green, respectively).

Further classification can be made inside each main group. These subgroups are listed and described below:

POLAR AMINO ACIDS

i) Neutral charged residues at physiological pH. This class comprises serine and threonine, which have a hydroxyl group, and asparagine and glutamine,

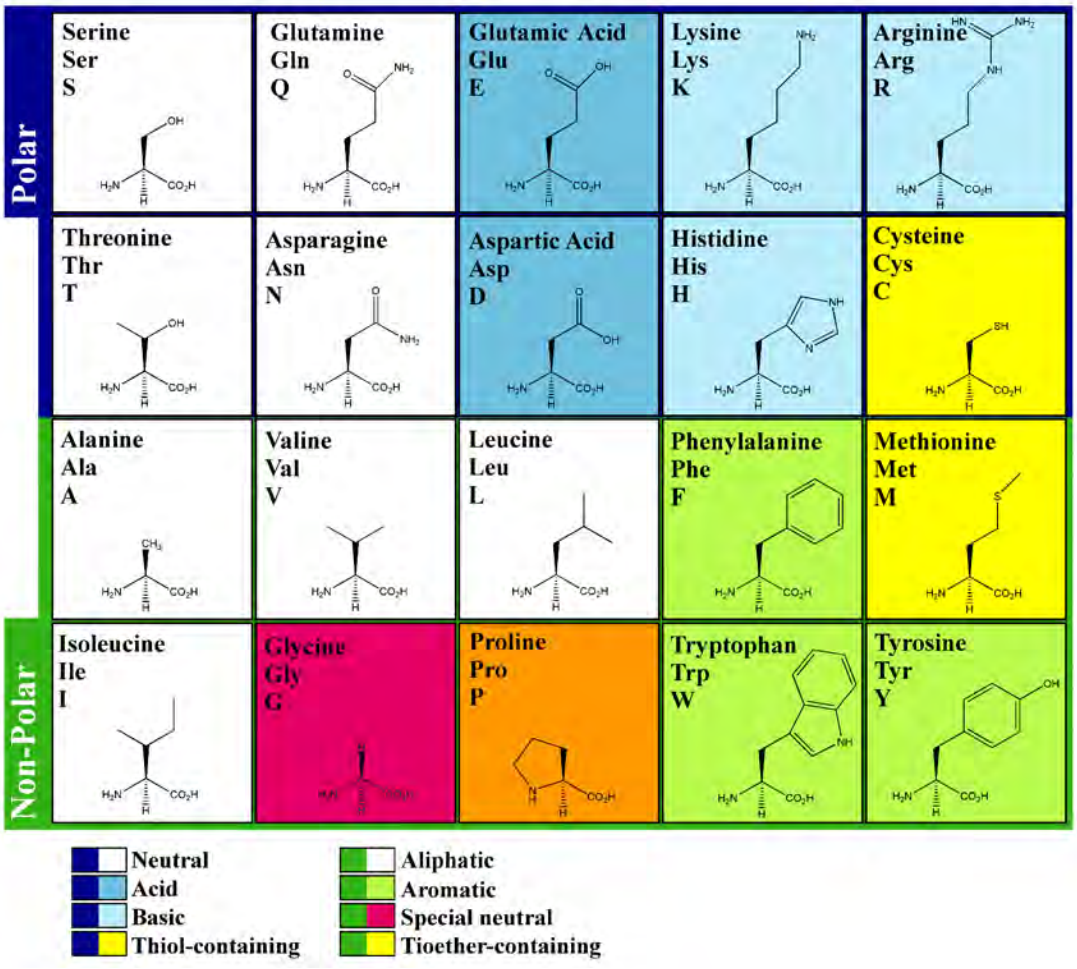

Figure 1.2: *Structure and classification of DNA-encoded 20 amino acids.* The polar amino acids (dark blue) can be subclassified by the global charge of the side chain: the neutral (white), the acid (blue) and basic amino acids (cyan). Cysteine is shown as a special polar amino acid for the presence of a sulfur atom (yellow). The non-polar residues (green), are subdivided in aliphatic (white) and aromatic (light green). Three special amino acids are methionine, with a thioeter group (yellow), proline (orange) with a cyclic residue in its side chain and glycine (fuchsia) having as a residue a hydrogen atom.

which have an amide group. In both cases, the small differences in their properties come out from an additional carbon in their side chain. For threonine, the extra methyl group in the C_β atom gives an extra asymmetric center which causes chirality to the amino acid, compared to serine. For glutamine, the extra methylene group gives a longer side chain displaying more flexibility and less interaction within the atoms of the peptide chain.

ii) Charged residues at physiological pH, such as aspartic acid and glu-

tamic acid, which are negatively charged residues, and lysine, arginine and histidine, which are basic and usually positively charged residues. The former have the same differences as their neutral analogues, asparagine and glutamine. The latter, have long and flexible side chains that can take part in internal salt bridges, whereas histidine has a heterocyclic aromatic side chain that can be charged or uncharged. These two states have been found to be important in the active sites of enzymes.

iii) The special residue cysteine, which has a thiol functional group, can play a special role by forming disulfide bond cross-bridges within other cysteine residues.

Non-polar amino acids

i) Aliphatic residues such as alanine, valine, isoleucine and leucine. Alanine is the smallest, and the remaining ones show different arrangement of their branched aliphatic side chain, hindering the main peptide chain becoming more stiff.

ii) Aromatic residues such as phenylalanine, tyrosine and tryptophan. They present an aromatic ring attached at the end of a short side chain consisting of a single methylene group. Even so, different polarity is exhibited amongst them depending on the nature of the aromatic ring. Tyrosine is the most polar aromatic one due to the presence of a phenol group. Tryptophan, with the presence of a indole heterocyclic ring is slightly polar and in the case of phenylalanine essentially non-polar character is expected with the benzyl group.

iii) The special residues glycine, proline and methionine. Glycine is the simplest amino acid having as a side chain a hydrogen atom. This gives them the highest flexibility amongst all residues. Moreover, it does not have chirality in the C_α atom. Proline is a more complex amino acid whose side chain curls back to the main chain and gives more rigidity. And methyonine, together with cysteine, is one of the two sulfur-containing amino acids. Their thioeter functional group is rather flexible and introduces some local dipole moment.

1.1.2 General Rules for Peptide Conformation Preferences

The structure of peptides and proteins can be rationalized at different hierarchical levels of increasing structural complexity.[1] The basic level is the primary structure or sequence of amino acids present in the polypeptide chain (Figure 1.3

[1]Linderstrøm-Lang, was a Danish scientist (1896-1959) who studied protein structure and function and coined the definitions of protein's primary, secondary, tertiary and quaternary structure.

A). In that level, the backbone is defined as the set of atoms present in the peptide chain, ignoring the side chains of the amino acid residues. The three dimensional arrangement of the primary structure due to the intramolecular interactions between the backbone atoms gives rise to the secondary structure (Figure 1.3 B). Higher levels of organization can be formed named as tertiary and quaternary structure. As it is depicted in Figure 1.3 C, tertiary structure is characterized by the intramolecular interactions between different secondary structure elements of the same polypeptide chain. Quaternary structure (Figure 1.3 D) is determined by non-covalent interactions between two or more polypeptide chains to form multi-unit proteins.

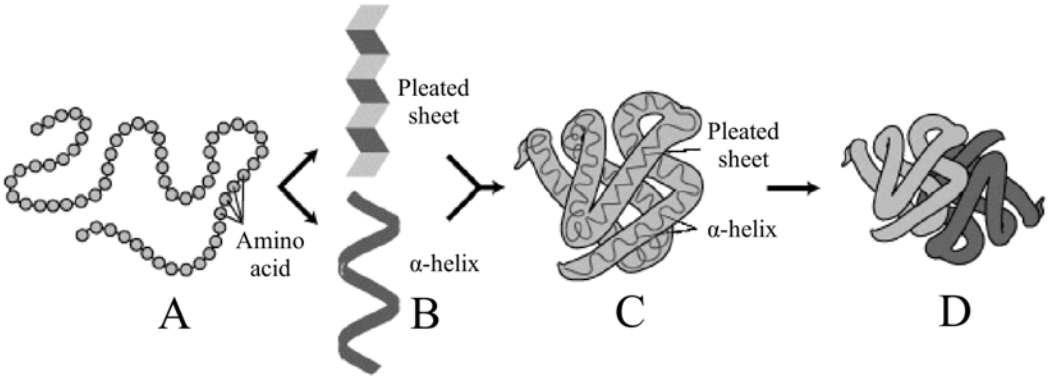

Figure 1.3: *Hierarchial levels in protein folding.* **A.** These sequence of a chain of amino acids determines the Primary protein structure. **B.** Secondary protein structure occurs when the sequence of amino acids interact via intramolecular hydrogen bonds between backbone atoms. **C.** Tertiary protein structure characterized by certain intramolecular interactions between different secondary structures. **D.** Quaternary protein structure is arranged by two or more polypeptide chains connected via non-covalent interaction. Picture adapted and modified from http://eduframe.net/andc/biology/Ravi-Bio/Ravi20proteinsODL.htm

Despite this seemingly complex ordering, the protein folding pathways for the three-dimensional arrangement mainly depend on the nature of the primary structure (Anfinsen 1972). For instance, hydrophobic amino acids will tend to interact with each other and hide inside the protein structure away from the environment, whereas polar or charged amino acids will be often exposed to solvent. So, favorable intramolecular interactions between certain amino acids can give the clues of the structure of a particular sequence. However, conformational constraints of the torsion angles involving the backbone atoms (around amide bond and bonds involving C_α atom) ultimately determine the conformational preferences of the polypeptide chain, as first observed by Linus Pauling (Pauling

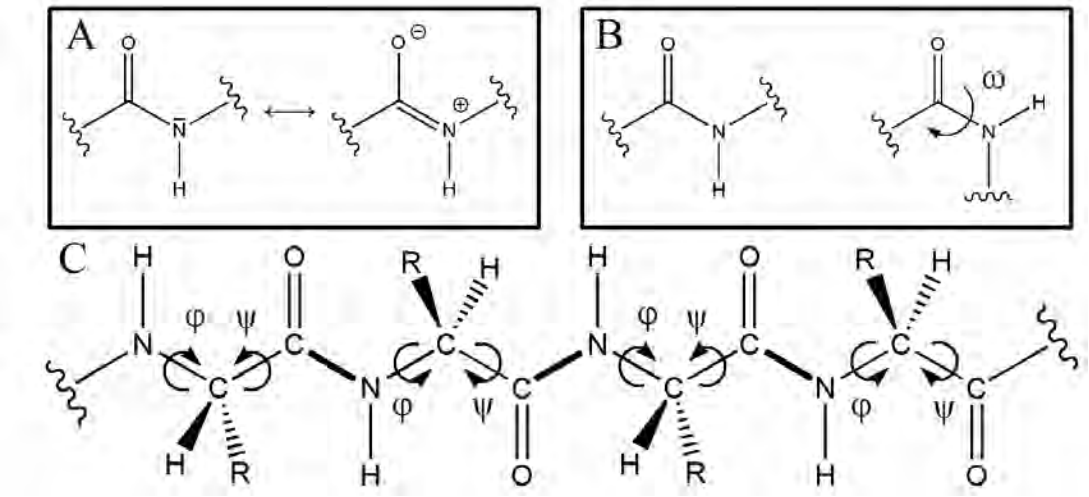

Figure 1.4: *Torsion angles around backbone atoms.* **A.** Resonant forms of the peptide bond. On the left, C'-N bond contains only axial symmetric σ-electrons allowing free rotation, whereas on the right, the bond have σ- and π-electrons inhibiting the rotation. **B.** cis/trans rotamers (right and left, respectively). The dihedral angle ω exhibits values of 0^o and 180^o for the ideal cis and trans rotamers, respectively. **C.** ϕ and ψ torsion angles involving backbone's C_α atom. The dihedral angles ϕ and ψ measure the rotation around the N-C_α and C_α-C' bonds, respectively.

1950, Pauling 1951).

1.1.2.1 Amide bond nature

The peptide bond has a quite polar character, which makes the amide carbonyl oxygen and the nitrogen of the amide group particularly good hydrogen bond acceptors and donors, respectively. The hydrogen bonds involving backbone atoms are important to stabilize the secondary structure of the polypeptide chains. However, the rotation around the peptide bond (defined by the dihedral angle ω) is highly limited by resonance[2] effects, as shown in Figure 1.4 A (Pauling 1951). Owing to its partial double-bond character, the rotation around the peptide bond leads to essentially two rotamers, a *trans*-configured peptide bond (ω=180^o), typically more stable, which is favored by 8 $kJ \cdot mol^{-1}$ (Sewald 2002), and the *cis*-configured peptide bond (ω=0^o)(Figure 1.4 B).

[2]From crystal structures of molecules containing peptide bond, Pauling and Corey found that C'-N distance was 10% shorter of a simple bond and C'-C_α was 0.02 Å longer compared to ketones. This effect was interpreted as being caused by the partial double bond character of the peptide bond.

1.1.2.2 ϕ and ψ torsion angles determine secondary structure

The flexibility of the polypeptide chain depends on the two backbone bonds involving the C_α which exhibit essentially free rotation. The rotation around these bonds is characterized by two dihedral angles that are defined for each amino acid and that determine the local secondary structure of the residue. A schematic view of these dihedral angles is depicted in Figure 1.4 C. The ϕ dihedral angle corresponds to the angle between the planes formed by atoms $C_{\alpha,n-1}$-C'_{n-1}-N_n and N_n-$C_{\alpha,n}$-C'_n atoms. The ψ angle is that defined between the planes formed by the N_n-$C_{\alpha,n}$-C'_n and $C_{\alpha,n}$-C'_n- N_{n+1} atoms (IUPAC-IUB 1969). The rotation around these dihedral angles is basically free, as compared to that around the ω dihedral angles, and is only controlled by the steric repulsions involving the methylene group at the α position, as first noted by Ramachandran (Ramachandran 1968). In 1963, before protein structures at atomic resolution were determined, G. N. Ramachandran established the foundations of the analysis conformations of peptide chains by using simple hard sphere models for the atoms. Based on this model, a given conformation is "disallowed" if it results in an atomic clash as in Figure 1.5 A. The so-called Ramachandran maps are 2D representations of the allowed regions of the ϕ,ψ space. In Figure 1.5 B, the highlighted regions correspond to allowed local conformations of the amino acid. Other regions of the map are prohibited due to steric hindrance and therefore are not energetically favorable conformations for peptide structure. It is worth to say that the shape of the Ramachandran plots do not depend dramatically on the nature of the residue, except for Glycine. In this case, a hydrogen atom is placed instead of the methyl group in α position and the allowable area is considerably larger (Bosco 2009).

1.1.3 Secondary Structure Patterns: Helices, Sheets and Turns

Based on the basic rules of conformational preferences of peptide's backbone, peptides and proteins can fold into several types of regular structures that are stabilized by intramolecular interactions between amide and carbonyl groups of the amino acids.

1.1.3.1 Helices

Helices are one of the most common secondary structures in peptides and proteins. The amino acid sequence is wrapped around a central axis by a regular pattern. The basic motif that is repeated along the axis is a turn stabilized by a

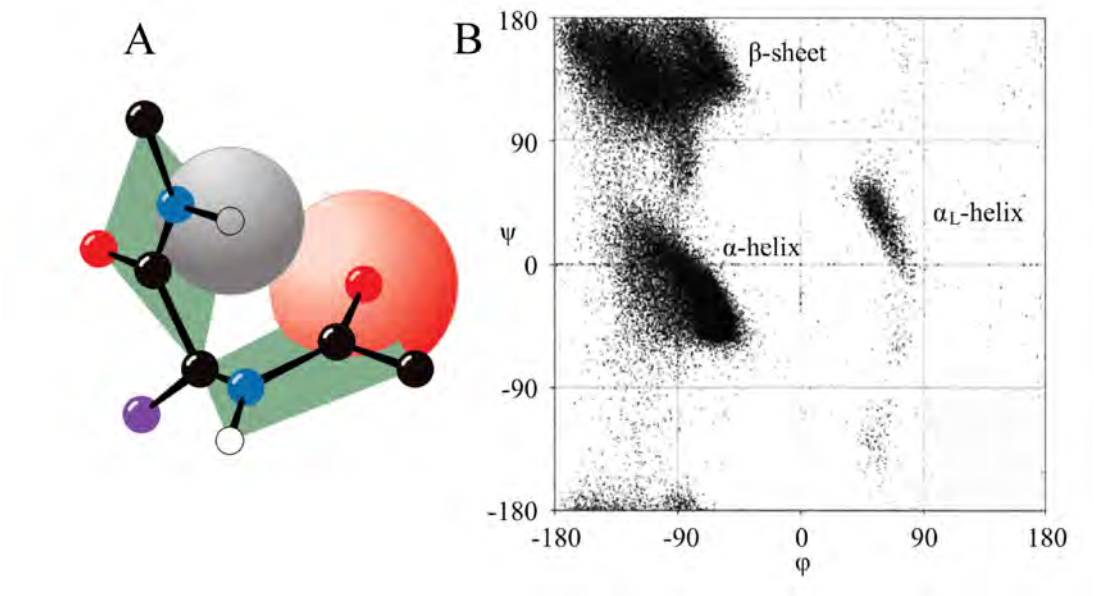

Figure 1.5: *Ramachandran plot* **A.** Steric interference between the amide hydrogen of one residue (grey sphere) and the carboxyl oxygen of the next residue (red sphere). **B.** Ramachandran plot. The dotted grey regions indicate the sterically allowed ϕ and ψ angles for all residues, excluding Gly and Pro. The allowed regions are related to α-right handed, α-helix and β-sheet secondary structure.

hydrogen bond between the oxygen atom of the carbonyl group of the amino acid in the i th position of the sequence and the hydrogen atom of the amide group on the i+n th position, where n is an integer number that determines, together with specific values of the associated dihedral angles, the type of helix. All types of helices with their characteristic dihedral angles and n values are summarized in Table 1.1.

The so-called α-helix is a 3.6_{13}-helix, meaning that it has 3.6 residues per turn and 13 atoms included in the closed loop formed by the hydrogen bond and the peptide backbone, is the most frequent helix in proteins. In this case n=4, and hence the helix is stabilized by three chains of hydrogen bonds involving residues located three amino acids away (see Figure 1.6 A). This stable secondary structure motif is characterized by dihedral angles ϕ and ψ of the residues involved with values close to -57^o and -47^o, respectively.

Other helical structures are possible, such as the 3_{10}-helix. In this case n=3, which leads to the formation of two chains of hydrogen bonds along the helix involving 10 atoms each and a somewhat tighter structure. The π-helix, characterized by 4.4 residues per turn with 16 atoms involved in each hydrogen bond and a value of n=5 is the thickest helix that can be formed involving a

Table 1.1: Types and features of helices[a]

Name	ϕ	ψ	**n**
α-helix (right-handed)	-57^o	-47^o	4
α_L-helix (left-handed)	57^o	47^o	4
3_{10}-helix	-60^o	-30^o	3
π-helix	-57^o	-70^o	5
	-51^o	153^o	-
Collagen helix	-76^o	127^o	-
	-45^o	148^o	-
Polyproline II	-78^o	149^o	-

[a] Ideal dihedral angles taken from the IUPAC-IUB 1970.

single chain of amino acids.

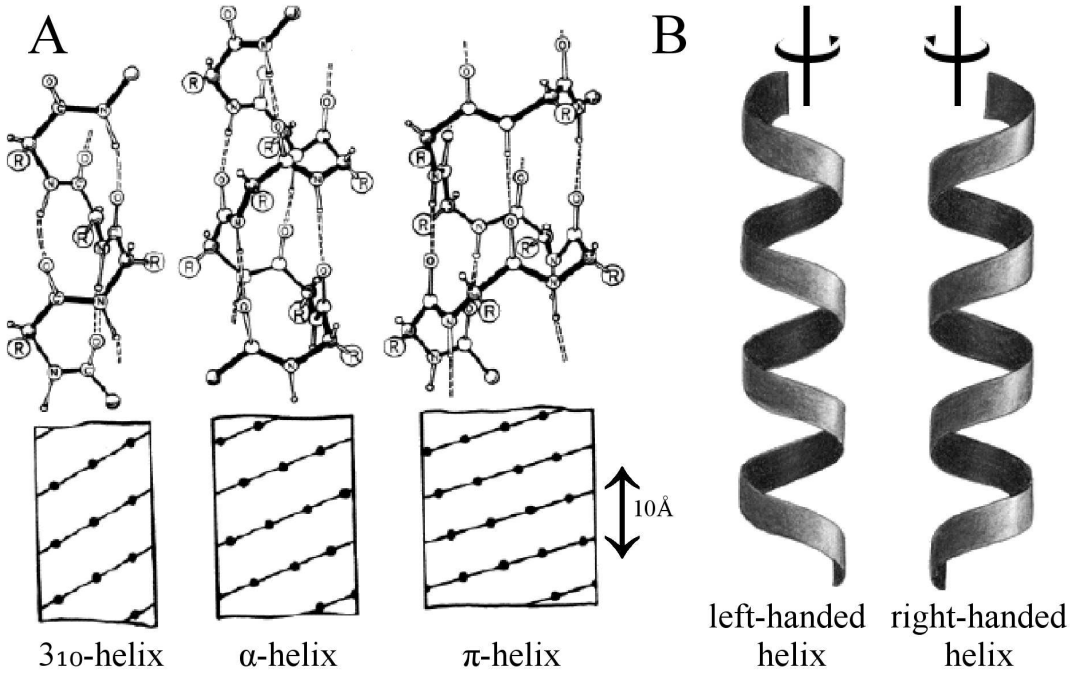

Figure 1.6: *Types and features of helices.* **A.** Different types of helices. **B.** Handness (chirality) of helices

In addition, handness or chirality is also present in some helical structures, which is defined by the screw sense of the helix. The most common α-helix present in proteins is right-handed, meaning that if we look down the helical axis from the amino terminal end, the backbone is folded from NH-terminal to C-terminal in a clockwise sense (Figure 1.6 B). The left-handed (α_L-helix) structure

is present in nature, with same but negative dihedral angles (see Table 1.1), but is much less frequent than its right-handed counterpart. For instance, so far it has never been observed in globular proteins.

Lastly, some special cases of helices are also present in nature, namely collagen-helix and polyproline-II helix (PPII). The former is build of a triple left-handed helix with the repeating amino acid sequence Gly-Pro-hydroxyproline on each of the three polypeptide chains. The latter is an helix typically consisting of proline amino acids, with no hydrogen-bonding present to stabilize the structure. It is worth to mention that the ideal PPII backbone dihedral angles (-75^o, 150^o) are frequently observed in proteins, even for amino acids other than proline, as stated by the high population of the PPII region of the Ramachandran map.

1.1.3.2 β-Sheets

β-Sheets are, together with α-helices, one of the most frequent secondary structure motifs present in nature. They are regular secondary structures composed of sequences of residues with a repeating pattern of ϕ and ψ dihedral angles. In contrast to helices, β-sheets are formed by at least two extended strands connected between them by inter-chain hydrogen bonds (Pauling 1951). Depending on the direction of the strands, β-sheets can be defined as parallel, antiparallel or mixed β-sheets (Figure 1.7 A).

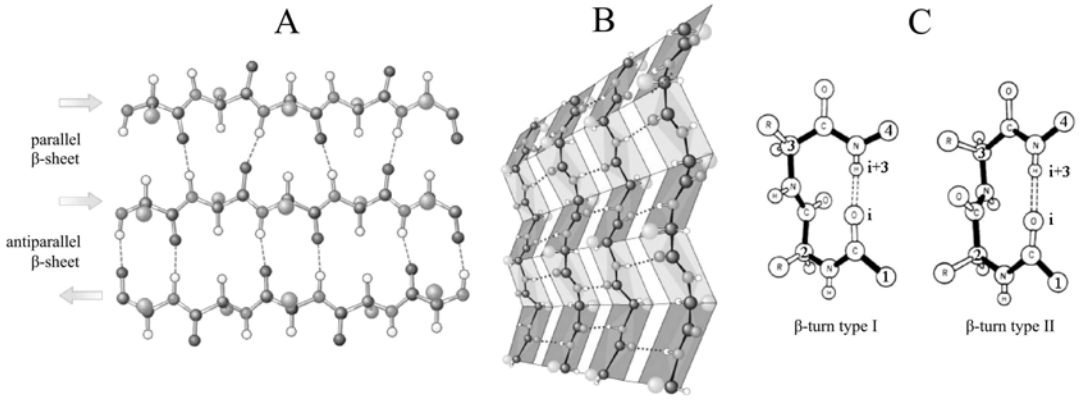

Figure 1.7: *β-Sheet and β-turn structures.* **A.** Different types of β-sheet being the parallel the stands in the same direction, and the antiparallel the ones that the stands goes to opposite directions. **B.** Rippled or pleated edge-on apparence of β-sheets. **C.** β-turn types I and II

The strands of parallel β-sheets run in the same direction (the standard criterion is from the N-terminus to C-terminus of the sequence). Contrarily, in anti parallel sheets the two interacting strands run in opposite direction. Structures

containing mixtures of parallel and antiparallel strands frequently occur. In both cases, the neighbouring strands do not present a fully extended polypeptide conformation, as it can be seen from the dihedral angles of the backbone atoms (Table 1.2). Instead the β-sheets have a rippled or pleated edge-on appearance, and for this reason, sometimes are called "pleated sheets" (Figure 1.7 B).

Table 1.2: Torsional angles for ideal β-structures

Name	ϕ	ψ
Parallel β-sheet	-119^o	113^o
Antiparallel β-sheet	-139^o	135^o

1.1.3.3 Reverse turns

Reverse turns are irregular secondary structures that have a key role on the folding back of other regular patterns such as α-helices and β-sheets. These regular structures do not show conformational stability as they extend along the peptide chain. For this reason, turns are important since they are involved in change of the direction of the polypeptide chain, in order to build more compact structures with higher stability.

Turns can be classified by the number of residues that are involved in the geometric motif. The most common turns are named β-turns formed by 4 consecutive amino acids (Figure 1.7 C).

Usually, their stabilization is due to the presence of hydrogen bonds between the oxygen atom of the i th amino acid and the hydrogen atom of the NH group of the *i+3* th position. This turn is also known as a C_{10} turn, indicating the number of atoms involved in the ring structure formed by the hydrogen bond (a 10-membered ring). It has been found with a frequency of about 25% that this hydrogen bond is not formed, leading to so-called non-standard reverse turns (Lewis 1973). Nowadays, the most accepted criterion for considering a particular motif a β-turns is that the distance between the C_α of the amino acids in position i and *i+3* must be less than 7 Å (Venkatachalam 1968, Chou 2000).

Different types of β-turns exist. They are defined by the dihedral angles of the internal residues *i+1* and *i+2*, which do not present hydrogen bonding (see Table 1.3). The most important ones are the type I and II turns for parallel interaction, and I' and II" for antiparallel one. Other turns such as α-turns and γ-turns are present in the folding of proteins, but are less common. The former

involve 5 amino acids (C_{13}) and the latter contain 3 amino acid residues (C_7).

One of the most interesting features of turns resides in their biological function. It has been found that β-turns are specially present in the surface of the proteins. Since the amide groups of the internal residues of the turn have no hydrogen bonding, they might be more available for interacting with solvent molecules. For instance, for small peptides such as vasopressin and somatostatin, it has been postulated that the turn induced by their cyclic nature is implicated in their biological activity (Rivier 1976, Smith 1978.) Moreover, turns are also considered determinant motifs for protein-protein and protein-substrate interactions (Pavone 1996).

Table 1.3: Ideal torsional angles of the residues involved in β-turns[a] and α-turns[b]

Name	ϕ_{i+1}	ψ_{i+1}	ϕ_{i+2}	ψ_{i+2}	ϕ_{i+3}	ψ_{i+3}
Type I β	-60^o	-30^o	-90^o	0^o	-	-
Type I' β	60^o	30^o	90^o	0^o	-	-
Type II β	-60^o	120^o	80^o	0^o	-	-
Type II' β	60^o	120^o	-80^o	0^o	-	-
Type I α_{RS}	-60^o	-29^o	-72^o	-29^o	-96^o	-20^o
Type I α_{LS}	48^o	42^o	67^o	33^o	70^o	32^o
Type I α_{LS}	48^o	42^o	67^o	33^o	70^o	32^o
Type II α_{RS}	-59^o	129^o	88^o	-16^o	-91^o	-32^o
Type II α_{LS}	53^o	-137^o	-95^o	81^o	57^o	38^o
Type I α_C	-103^o	143^o	-85^o	2^o	-54^o	-39^o

[a] Angles taken from Smith 1980.

[b] Angles taken from Chou 2000.

1.2 Antimicrobial Peptides: Biological Function, Activity and Mechanism of Action

Antimicrobial Peptides (AMPs) are ancient components of the innate immune system of most living organism and have become the most effective defensive weapons to protect the host organism against microbial invasion (Hwang 98). AMPs have been widely reported to be present in the living organism such as vertebrates, (Ganz 98) including mammals (Brogden 2003, Gudmundsson 1996, Lehrer 1999) or amphibians (Boland 2006); invertebrates, (Dimarcq 1998) such as insects (Bulet 1999, Lehrer 1999); plants (Broekaert 1995); and prokaryote microorganisms such as bacteria (Gause 1944, Hancock 1999).

1.2.1 Classification of Antimicrobial Peptides

Amongst the literature, several classifications have been proposed in order to sort out the large number of AMPs. They have been categorized according to their biosynthetic pathway (non-ribosomally or ribosomally synthesized), source, secondary structure elements and predominant amino acids. Here, different classifications are shown to reflect the broad nature of these AMPs.

1.2.1.1 Classification according to the Biosynthetic pathway

In line to how AMPs are produced in nature, they can fall into two classes, non-ribosomally synthesised peptides (NRP) and ribosomally synthesised peptides (RP). The former are largely produced by microorganisms like bacteria and fungi, and their synthesis occurs without predetermination of the amino acid sequence by nucleic acids. Instead, the synthesis is catalyzed by large proteins termed peptide synthetases (Konz 1999, Mootz 1997). An important feature of NRPs is that they contain not only standart amino acids but also non-proteinogenic (unusual) amino acids.

The RP include the large majority of AMPs and are produced by a wide range of multicellular organims (Nissen-Meyer 1997). They are gene encoded peptides and their synthesis involves first the transcription of one DNA strand into the complementary RNA copy (mRNA) and second the translation into the corresponding peptide by amino acid polymerization as specified in the nucleotide sequence of the mRNA.

1.2.1.2 Classification according to the primary structure: predominant amino acids

1. AMPs WITH AN UNUSUAL PROPORTION OF PROTEINOGENIC AMINO ACIDS. The presence of unusually high proportions of certain regular amino acids, leads to the folding of structures which are rather different from the regular helices and sheets discussed below.

i) Defensins are a family of cysteine rich antimicrobial peptides, which can form disulfide bonds that help to maintain their structural integrity. One of the most important families that fall in this category are defensins. They are composed of 29 to 40 amino acids and have a characteristic β-sheet fold stabilized by three disulphide-linked cysteins (Ganz 2003). There are three main defensins subfamilies, α, β and θ-defensins that differ mainly in the lenght of the peptide segments between the cystein-links and the connectivity of the terminal residues.

α-defensins. Six known α-defensins exist, four of which are found in polymorphonuclear neutrophils (HND 1-4; human neutrophil defensin, see Figure 1.8 A), and the remaining two (HD5-6) are produced by the secretory paneth cell, found in the small intestinal crypts.

β-defensins are larger and differ in the placement and connectivity of their six conserved cystein residues. In this subfamily two peptides are known in humans HβD1-2 (Ganz 1998).

θ-defensin has been found recently in rhesus monkey leukocytes. Its particular characteristic is that is a cyclic peptide from two of the nine amino acid segments of the α-defensin-like precursor (RTD-1) (Tang 1999).

other defensins have been isolated from non-mamalian sources, such as plant and insect defensins. The former comprise the γ-thionins, first isolated from barley and wheat (Mendez 1990, Colilla 1990), and the latter drosomycin, an antifungal peptide isolated from *Drosophila melanogaster* (Landon 1997). Although they possess a structure similar to that of the above defensins, they have four disulfide bonds instead of three. The overall secondary structure is made up by a single sheet of three antiparallel β-strands, with an additional α-helix inserted between the first two strands (Hwang 1998, Figure 1.8 B).

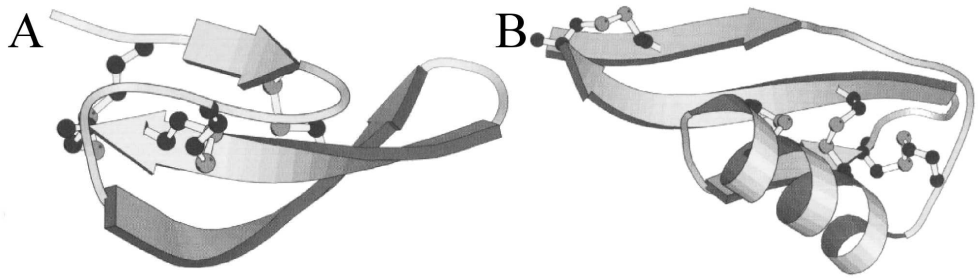

Figure 1.8: *Structure of defensins-like peptides.* **A**. α-defensin HNP-3 with a secondary structure composed by three-stranded antiparallel β-sheets **B**. δ1-Purothionin with a single sheet made up of three antiparallel β-strands and an additional α-helix inserted between the two first strands. Disulfide bridges are shown in ball-and-stick representation, and the illustrations have been taken from Hwang 1998.

ii) Histatins comprise a group of neutral and basic histidine-rich peptides present in human salivary secretions and in serum. They are unstructured in aqueous solution, but in polar aprotic solutions they adopt largely and an α-

helical conformation (Raj 1998). Their low amphipathicity structure probably accounts for the non-toxic nature of histatins, compared to other AMPs.

iii) Cathelicidins are a large well known family of AMPs with two main specific domains. They have a 100 amino acid conserved N-terminal preproregion that is called cathelin domain. As it is shown in Figure 1.9 A, this domain is followed by a C-terminal region which can have a highly heterogeneous structure, depending on the attached peptide (Zanetti 2004). These AMPs become active when the C-terminus domain is cleaved from the cathelin domain. Cathelin-associated AMPs are remarkably variable in structure. For example, indolicidin, a cationic AMP isolated from bovine neutrophils that has 13 amino acids and a high content of tryptophan residues (around 39%, Figure 1.9 B) (Falla 1996, Subbalakshmi 1998). Another example is bactenicin, a highly cationic polypeptide from the large granules of bovine neutrophils. It is composed of around 45% of proline and 23% of arginine residues and it adopts an extended secondary structure with turns and coils.

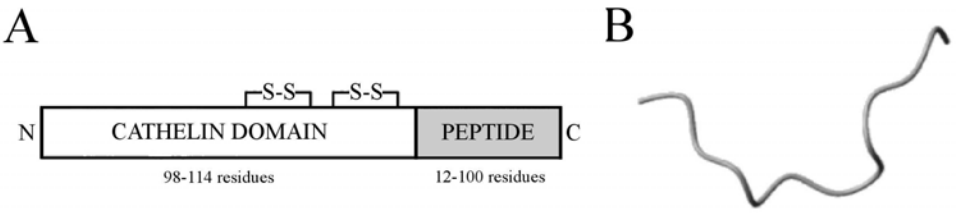

Figure 1.9: *Structure of AMPs with unusual proportion of regular amino acids.* **A**. Cathelicidins **B**. Indolicidin. The illustrations have been taken from Zanetti 2004.

2. Peptides with an uncommon modified amino acid, are isolated from bacteria and fungi and show characteristics which are more similar to those of conventional antibiotics than to those of AMPs produced by higher organisms (Klaenhammer 1993).

i) Lantibiotics are those peptides which contain "uncommon" modified amino acids with small ring structures enclosed by a thio-ether bond. One peptide of this family is nisin, which is nowadays used as an antimicrobial agent for food preservation. This AMP is produced by the bacteria *Lactococcus lactis*. NMR studies have revealed that nisin is flexible and unstructured in water but adopts several β-turn structures once bound to micelles. However, regular secondary structures such as helices and sheets have not been associated to its activity (see Figure 1.10)(van den Hooven 1996, Hwang 1998).

ii) Peptaibols are a family of AMPs with a high proportion of α-amino

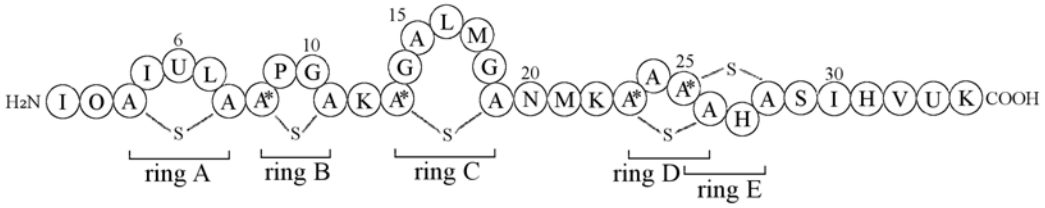

Figure 1.10: *Primary structure of nisin.* The unusual amino acids presents in the primary structure are "U" for dehydroalanine, "O" for dehydrobutyrine, "A-S-A" for lanthionine and "A*-S-A" for 3-methyllanthionine. The illustrations have been taken from Van Den Hooven 1996.

isobutyric acid (Aib) residues. This conformationally restricted amino acid, favours the adoption of an α-helical structure. A well known example is alamethicin, a 20 amino acid peptaibol, that has been isolated from the fungus *Trichoderma viride*, which adopts a largely α-helical conformation in nonaqueous solvents as well as in the presence of lipid bilayers (Franklin 1994).

1.2.1.3 Classification according to the secondary structure

1. α-Helix AMPs were the first to be identified and characterized. These peptides are unstructured in water phase, but upon membrane interaction they adopt a α-helix conformation that helps their insertion and permeabilization of the bacterial membrane (Marion 1988, Matsuzaki 1989, Williams 1990, Bechinger 1993). Amongst them, cecropins, magainins and melittins are some of the most important and better studied α-helical AMPs.

i) Cecropins are a family of peptides composed of 31-39 amino acids with antibacterial activity against both gram positive and negative bacteria. Although they do not show cytotoxic effect against eukaryotic cells, they are susceptible to protease degradation (Ultmark 1982, Andreu 1983, Steiner 1981). They are widespread throught the animal kingdom, being isolated from different sources: cecropin A and B from the giant silkworm month (*Hyalaphora cecropia*), and cecropin P1 from the pig intestine.

ii) Magainins are polypeptides of around 21-26 amino acids and have been isolated from the skin of the African clawed frog (*Xenopus laevis*) (Zasloff 1987). They show a broad-spectrum antibacterial, antifungal and tumoricidal action, but they are non-hemolytic (see Figure 1.11 A).

iii) Melittin comprises 26 amino acids. It is the most abundant AMP of the European honey bee (*Apis mellifera*) venom, and displays antimicrobial activity and a high hemolytic activity (see Figure 1.11 B).

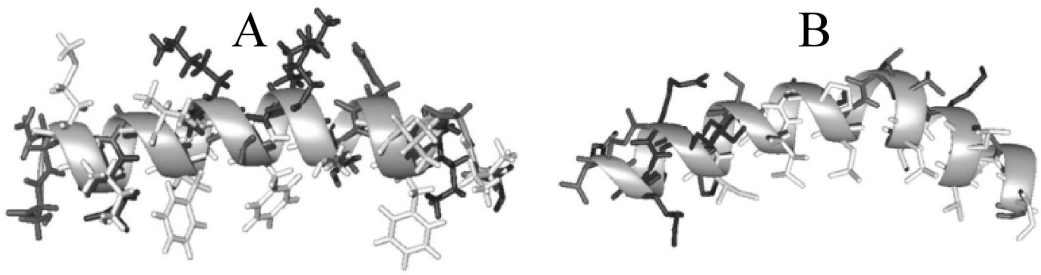

Figure 1.11: *Structure of selected α-helix peptides.* **A**. Magainin. **B**. Melittin. The hydrophobic residues are shown in white color and hydrophilic residues in black. The picture has been taken from Bechinger 2004.

2. β-Sheet AMPs comprise peptides displaying a single β-hairpin. In contrast to defensins which are cystein-rich peptides, β-sheet AMPs present no more than one or two disuflide bridges having a more simple secondary structure. Commonly, β-sheet conformations have already been detected in aqueous solution, but are further stabilized upon the peptide interaction with the bacterial cell membrane. Examples of β-sheet AMPs are tachyplesin and protegrins.

i) Tachyplesin, is a 17 amino acids cationic peptide isolated from acid extracts of horseshoe crab (*Tachypleus tridentatus*). In water phase, it displays a rigid antiparallel β-sheet structure with a type I β-turn and two disulfide bonds (Oishi 1997, Kawano 1990).

ii) Protegrins, (PG-1), are a family of cationic peptides isolated from porcine leukocytes (Kokryakov 1993), containing four cysteins which form two disulfide bridges (Fahrner 1996). Two examples of β-sheet peptides are shown Figure 1.12 A and B.

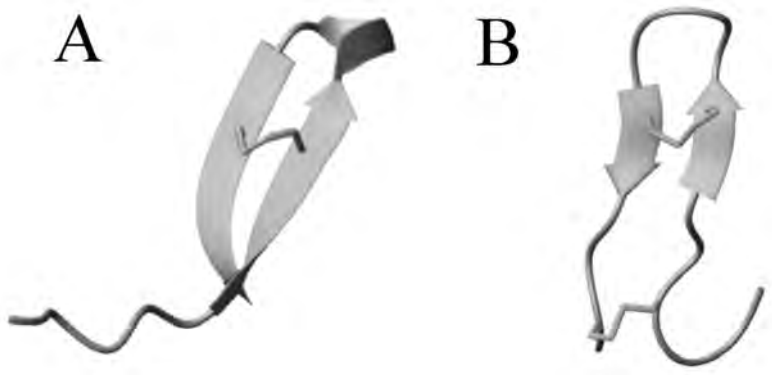

Figure 1.12: *Structure of β-sheet peptides.* **A**. looped thanatin with as an example of AMPs with one disulfide intermolecular bond within the strands **B**. β-sheet polyphemusin with a β-harpin-like structure as Tachyplesin, with two disulfide bonds within the strands. The illustrations have been taken from Jenssen 2006.

1.2.2 Structural Parameters Important for Antimicrobial Peptide's Activity

Although AMPs display a great diversity of primary and secondary structures, most of them share several common properties that are relevant for their activity. These structural and physicochemical parameters are the secondary structure, the charge, the amphipathicity and the hydrophobicity.

1.2.2.1 Secondary structure

Many AMPs are believed to adopt a non-structured/extended conformation in water environment, (Dathe 1996) while others attain specific configurations due to the presence of intermolecular hydrogen bonds, as for instance β-sheet peptides (Oishi 1997). In both cases, peptides undergo significant conformational changes upon binding to the target cell.

The importance of the secondary structure in the activity of AMPs has been widely studied in order to extract a structure-function relationship. For instance, pardaxin is an α-helix peptide that shows lytic activity to both microbial and mamalian cells. When D-amino acids were incorporated in its sequence, the α-helix conformation was converted to a β-structure. This modification gave rise to a loss of hemolytic activity but the antimicrobial activity was retained (Oren 1999). Similarly, the cyclic peptide θ-defensin, showed a three-fold greater activity compared to the open-chain analogue (Tang 1999).

Both cases indicate that i) altering the secondary structure the activity can be selectively modulated showing dissociation of the antimicrobial and hemolytic activity and ii) the loss of a rigid and stable conformation can drop the activity of an active peptide.

1.2.2.2 Charge

Cationicity is one of the indispensable features for the antimicrobial activity of AMPs. The bacterial membrane has a negative charged surface and it is believed that the first step for AMPs activity is the electrostatic interaction between the positive charge of some of the amino acids present in the sequence and this negative charge. Owing to that, the presence of positivevly charged residues such as arginine and lysine is a basic feature in the primary structure of AMPs.

Several studies have shown that there is a strong relationship amongst the cationicity and the antimicrobial activity of the peptides. As a consequence, it seems like that the number of positively charged residues is an important feature to bear in mind. However, this relationship is not linear, and the lack of a direct

correlation has been supported by investigations in model membranes (Yeaman 2003, Toke 2005, Tossi 2000). Studies with the peptide magainin 2 showed that increasing the charge from +3 to +5, the antimicrobial activity was increased. However, when the charge was further increased to +6 and +7, the hemolytic activity increased but the antimicrobial activity was lost (Dathe 2001). The optimal charge that accounted for the highest activity was +4, corresponding to the net charge of the naturally occuring magainin (Matsuzaki 1997). The rationale behind the decrease of activity above a certain peptide charge has been associated to i) the instability and reduced lifetime of the membrane permeabilization by the peptide and ii) the relationship between the excessive charge and the rearrangement of the secondary structure (Toke 2005, Tossi 2000).

Even so, the presence of the positive charge is not the only issue that has to be taken into account for antimicrobial activity. The arrangement or the pattern of the charged amino acid residues along the sequence (density of charge) is also important for the action of the AMPs. It was shown that cyclic magainin 2 displayed a reduced activity, while the activity of melittin was preserved upon cyclization. The loss or gain of activity was in direct relationship with the final charge density of the peptides. The cyclic magainin analogue had a reduced charge density because it was distributed along the entire structure. In contrast, for the cyclic melittin analogue the charge density was not modified, comprising a small portion of the ring (Unger 2001).

1.2.2.3 Amphipathicity

Amphipathicity is the ability of a peptide to arrange all hydrophobic residues in one side and all the hydrophilic residues to the opposite side. Due to the amphipathic nature of the membrane (see section 1.2.4), peptide amphipathicity has been revealed as an important parameter for AMP activity. Upon peptide interaction with the membrane bilayer and insertion, the hydrophobic residues of the peptide interact with the apolar membrane lipid tails and cluster together whereas the hydrophilic residues of the peptide interact with the polar head groups of the membrane and the aqueous environment.

The difficulty in quantifying the amphipathicity has hampered the determination of a relationship between the activity and the peptide amphipathicity. Eisenberg *et al.* proposed the hydrophobic moment (M_H), being the vectorial sum of individual amino acid hydrophobicities normalized to an ideal α-helix as a quantitative measure for peptide amphipathicity. In this study an increase of the M_H (amphipathicity) resulted in a significant increase of the hemolytic activity of the model peptide (Eisenberg 1984). This result was later corroborated with

magainin analogues where a strong relationship between amphypathicity and activity was observed. As the amphypathic character increased, peptide selectivity decreased, since both antimicrobial and hemolytic activity increased (Wieprecht 1997). This result pointed out that an increase of the peptide amphypathicity increases the affinity towards all types of cell membranes, thereby reducing the selectivity.

1.2.2.4 Hydrophobicity

The hydrophobicity is the percentage of hydrophobic residues within the peptide. Indeed, it is an elemental feature that indicates the degree of peptide interaction with the core of the bilayer. Different studies on the modulation of peptide hydrophobicity have shown that as the peptide hydrophobicity increases, the binding affinity to all types of cell membranes increases, reducing the selectivity between membrane types (Wieprecht 1997). Therefore AMPs usually have a moderate number of hydrophobic residues, and show higher affinity towards microbial cell membranes.

1.2.3 Mechanism of Action of Antimicrobial Peptides

The mechanism of action of AMPs is still an issue of study. Up to now, two different mechanisms for bacterial death have been proposed, receptor and a non-receptor mediated mechanism. However, it is clear that the interaction with the membrane target is crucial for both modes of action.

1. **The receptor-mediated mechanism** has been proposed for a few AMPs, which are active at nanomolar concentrations. These peptides are mainly produced by bacteria and are composed of two regions: a receptor-binding domain and a pore-forming domain. One of the most well charactherized examples of a receptor-mediated peptide is nisin, a small peptide which has been used in food industry for several decades. Its mechanism of action is based on the peptide interaction with the membrane-anchored cell wall precursor Lipid II (a membrane bound component involved in peptidoglycan synthesis) as a receptor. Once bound to the receptor, nisin permeabilizes the membrane by forming a pore (Breukink 1999).

2. **The non-receptor-mediated mechanism** has been postulated for most of the known AMPs, which are active in vitro at micromolar concentrations and it is believed to play the major role in the mechanism of action of most membrane-lytic peptides. This has been widely demostrated from

studies where the activity of enantiomers of pore-forming AMPs was compared. The D-enantiomer of native and model peptides exhibited the same antimicrobial activity than that of the L-enantiomer. Therefore, these results suggested a non-receptor type interaction of AMPs with membranes (Bessalle 1990, Wade 1990, Bechinger 1997, Yeaman 03).

1.2.3.1 Mechanism of action for nonreceptor-mediated Antimicrobial Peptide: fundamental steps

The mechanism of action of AMPs against bacteria has to be explained taking into account the morphology of the bacterial cell. Bacteria have a cell wall which forms a rigid structure providing strength, rigidity and shape. This wall also protects the cell from changes in water pressure. Depending on the composition of the cell wall, bacteria can be classified as Gram-positive (G^+) and Gram-negative (G^-). As it is depicted in Figure 1.13, G^+ bacteria are composed by a peptido-

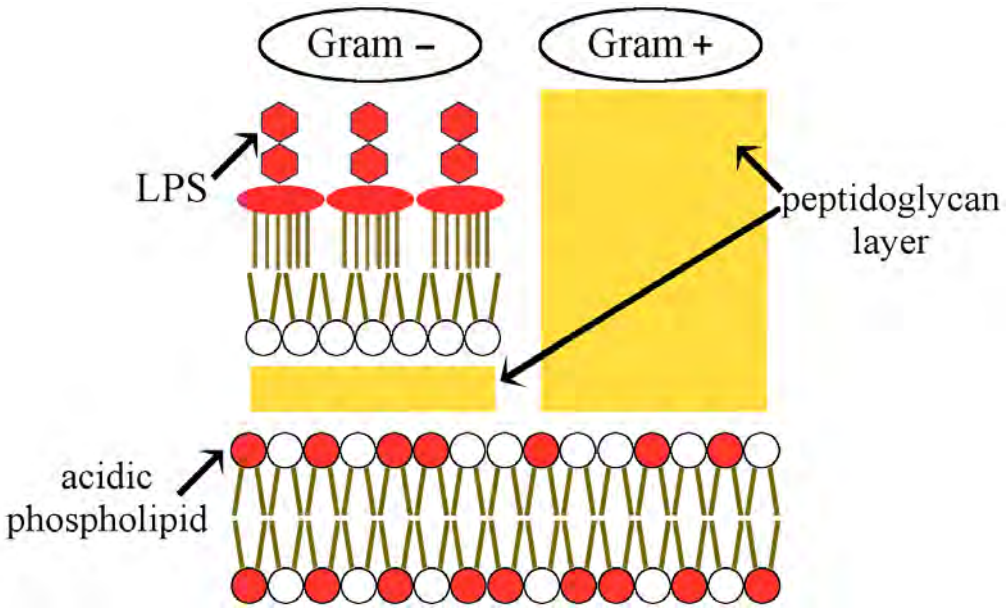

Figure 1.13: *Main architecture of G^+ and G^- bacteria.*

glycan layer and a single cytoplasmic bilayer. By contrast, (G^-) are composed by two bilayers, the outer one is composed by lipopolysaccharide-phospholipid molecules (LPS), which are negatively charged components stabilized by divalent cations like Ca^{2+} and Mg^+, and the inner one is a single cytoplasmic membrane.

For G^- bacteria, peptides first need to traverse the outer bilayer. To accomplish this, Hancock and co-workers (Hancock 1995, 1997) suggested a mechanism termed "self-promoted uptake" which involves the electrostatic interaction of the cationic peptide with the highly charged LPS molecules. This action prompts the

competitive displacement of the LPS-associated divalent cations. This displacement is likely to be energetically favorable since the affinity of the peptide-LPS has been shown to be ∼3 orders of magnitude greater than that of divalent cations (Yeaman 03). Then, peptides insert into and translocate across this outer bilayer as it is shown in Figure 1.14 A-B.

Once the first extra envelope for G^- bacteria is overcome, peptides approach the cytoplasmic membrane, interact and consequently exert their disruptive effect. This step is common for G^+ and G^- bacteria. The mechanism that explains

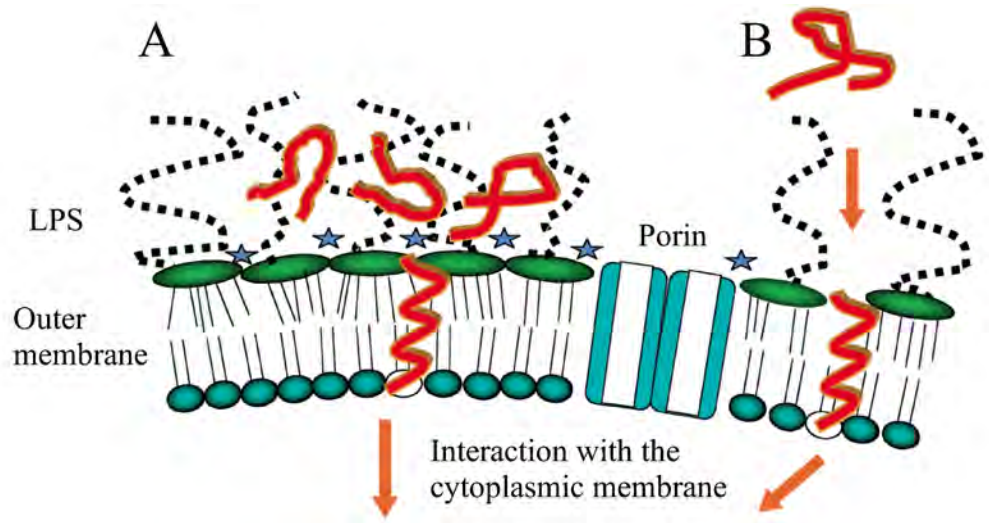

.

Figure 1.14: *Self-promoted uptake of cationic peptides across the outer membrane in G^-*. Unfolded cationic peptides are proposed to associate with the negatively charged (LPS) surface. **A.** The peptides neutralise the membrane and creates cracks through which the peptides can cross the outer bilayer. **B.** The peptides bind to the divalent cation binding sites on LPS, and disrubt the membrane. The illustrations have been taken from Hancock 2001.

the activity of most antimicrobial peptides as a consequence of the interaction with the cytoplasmic membrane is the so called "Shai-Matsuzaki-Huang" (SMH) model. This model proposes the following steps for membrane permeabilization.

1. An **initial peptide interaction with the membrane surface** mainly due to the electrostatic interaction between positively charged AMPs and the negatively charged bacterial membrane, and the hydrophobic interaction between the non-polar amino acids and the hydrophobic core of the membrane.

2. **Peptide folding at the membrane interface** helped by the amphypathic nature of the membrane bilayer. Intramolecular interactions within the peptide primary structure are favoured by the insertion of the hydrophobic

residues into the hydrophobic core of the bilayer. The hydrophilic residues remain hydrogen bonded to the charged head-groups of the lipid bilayer and to the polar enviroment. During this interaction and folding, AMPs accumulate facing parallel to the membrane surface and remain bound at the interface (see Figure 1.15, **1** and **2**).

3. **As a threshold concentration** is reached, the AMPs reorient from the surface-bound, S-state to an inserted I-state (Two-State Model, Huang 2006, Yeaman 2003) causing membrane permeabilization (see Figure 1.15, **3**). Depending on the nature of the AMPs, different models of permeabilization have been proposed including pore formation (see next section "Pore models"). However, pore formation is not the only way to permeabilize the membrane. For instance, buforin II, a 21-amino acid AMP which kill *Escherichia coli* acts without forming pores. This peptide translocates across the lipid bilayer without affecting the membrane barrier (Park 2000).

4. **Bacterial death** follows as a consequence of the permeabilization of the cytoplasmic bacterial membrane or of the insertion of the peptide into the interior of the bacteria. Several hypotheses have been proposed to explain further possible causes of bacterial death once AMPs are inserted in the bacterial membrane, including: membrane depolarization; leakage of essential metabolites; loss of compositional specificity in the membrane due to an increased rate of phospholipid flip-flopping; for G^- bacteria, exchange with the inner leaflet of the outer membrane; peptide translocation into the cytoplasmic side of the membrane where they can interfere with important cellular mechanisms; and, triggering of enzymes that cause peptidoglycan autolysis (Figure 1.15, **4**).(Tossi 2000, Zasloff 2002).

1.2.3.2 Membrane permeabilization via pore formation

Membrane permeabilization via pore formation has been widely reviewed along the last decade. All mechanisms start with the insertion of the peptide, which leads to a lateral expansion of the membrane lipids and to a thinning of the hydrophobic lipid core. However, the final shape of the pore depends on the nature of the peptide, and on the dominating interactions within the lipids and the peptide. The currently most accepted models for pore formation are depicted in Figure 1.15 A-D and can be summarized as follows.

A. **Aggregate model.** Peptides reorient to span the membrane forming micelle-like complexes composed of peptides and lipids with no particular orientation and organization. Membrane permeabilization is characterized by the formation of informal channels with a variety of sizes and lifetimes, accompained

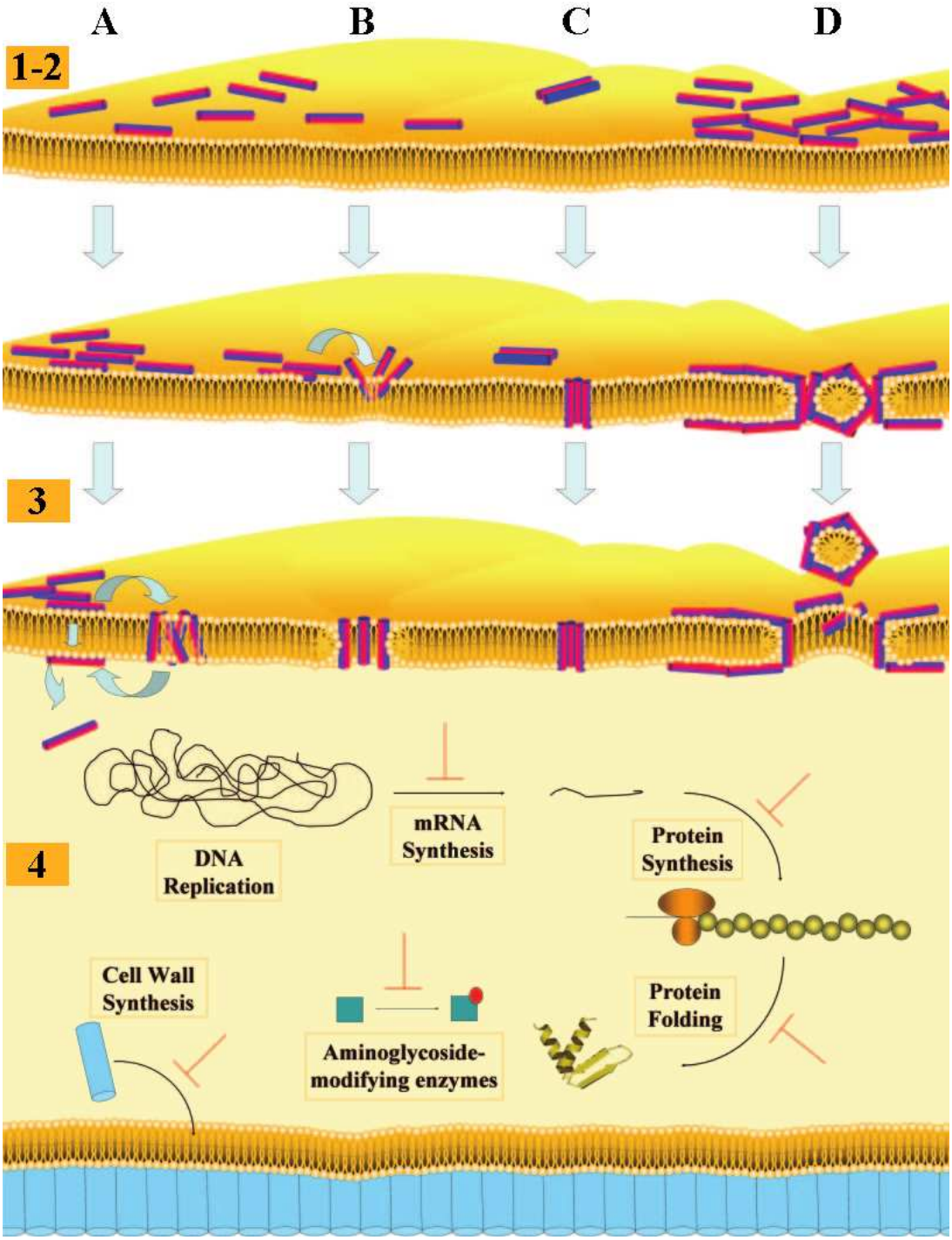

Figure 1.15: *General Mechanism of action of antibacterial peptides.* The bacterial membrane is represented as a yellow lipid bilayer with the peptides shown as cylinders, where the hydrophilic regions are colored red and the hydrophobic regions are blue. The SMH model (1-4) and the pore models (A-D) are both indicated and correlated in an schematic way. The illustrations have been taken from Jenssen 2006.

by the peptide translocation accross the bilayer to inside the bacterial cell.

B. **Toroidal model** or wormhole model. In that case, the shorter peptides bind to the lipid head-groups causing the binding of the phospholipid layers from one leaflet to the other. Hydrophilic residues of the peptide that were laying on the membrane surface, insert in the core of the membrane by pulling together the lipid molecules, resulting in a pore structure in which the peptide chains and the lipid head-groups line the wall of the pore. This model has been suggested for magainin 2 (Matsuzaki 1996, Huang 2000; Ludtke 1996), melittin (Yang 2001) and β-protegrin (Yang 2000).

C. **Barrel-stave model.** In this model, a variable number of peptides insert into the bilayer in a perpendicular manner, either as monomers or as small aggregates in a "barrel-like" ring around an aqueous pore. In that case, hydrophobic interactions play the main role in the formation of the pore. The hydrophobic residues of the peptide are facing the non-polar lipid acyl chains whereas its hydrophilic surface forms the lining of a water-filled pore and the lipid head-groups remain located at the membrane/water interface. This pore formation requires peptides sufficiently long to traverse the hydrophobic core of the membrane, without inserting the polar groups of the lipids. An example of this mechanism has been proposed for alamethicin (Sansom 1991, Beven 1999, Yang 2001), pardaxin (Rapaport 1991) and ceratotoxin A (Saint 2003).

D. **Carpet-like model.** This model includes peptides that act against microorganism through a relatively diffuse manner. Peptides accumulate on the membrane surface forming a localized carpet. Peptide chains orient themselves parallel with respect to the membrane surface and become trapped in the head-group region. As they accumulate, they create tension between the two leaflets of the bilayer, which leads to disintegration or rupture of the membrane. The formation of transient holes in the bilayer may be an intermediate step before the collapse of the membrane. This model appears to be the most general permeabilization mechanism. AMPs that follow this model include cecropins (Gazit 1994) and dermaseptins (Strahilevitz 1994), among others.

1.2.4 Selectivity of Antimicrobial Peptides

The cell membrane is mainly composed of lipids but it also contain other molecules such as cholesterol, sugars, peptides and proteins (see Figure 1.16). The membrane composition varies significally between the different species, which gives selectivity towards molecules they may interact with. In particular, many AMPs have shown a considerable selectivity amongst microbial and host cells. Factors that govern AMPs membrane selectivity are based on the dif-

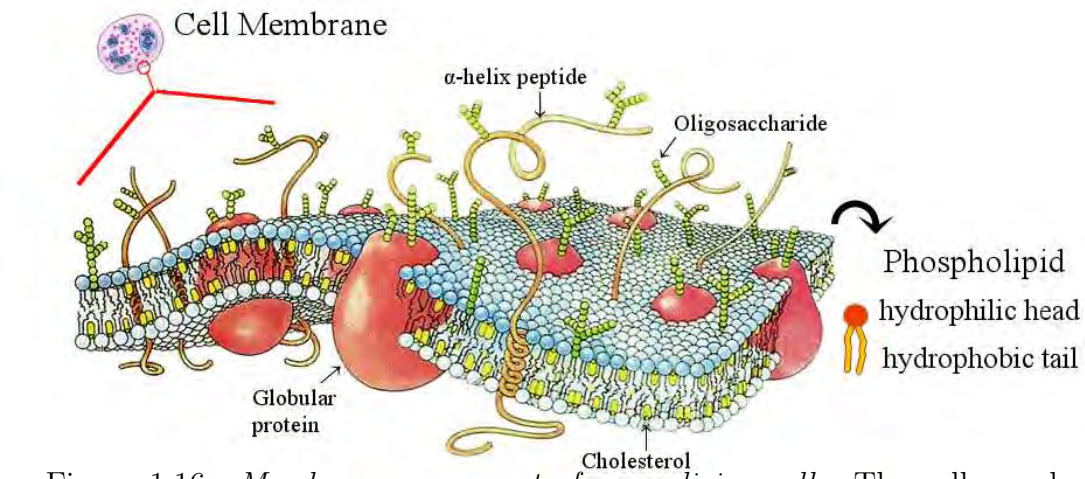

Figure 1.16: *Membrane components from a living cell.* The cell membrane, also called the plasma membrane, is a semipermeable lipid bilayer. It contains a variety of lipids, cholesterol, sugar, peptides and proteins, which are involved in a vast array of cellular processes. Picture adapted from http://docencia.izt.uam.mx/acbc/imagenes.htm

ferences in the cytoplasmic membrane between prokaryotic and eukaryotic cells. Among these factors, the difference between the lipid composition of the two cell membranes seems to be the most important one (Dathe 1999), as it is shown in Figure 1.17 A. The outer leaflet of mammalian cell membranes is exclusively composed of electronically neutral, zwitterionic phospholipids like phosphatidylcholine (PC), phosphatidylethanolamine (PE) and sphingomyelin (SM). In contrast, bacterial membranes contain large amounts of negatively charged phospholipids like phosphatidylglycerol (PG), cardiolipin (CL) and phopsphatidylserine (PS). Hence, as it is schematized in the Figure 1.17 B, AMPs which are cationic, preferentially bind to the negatively charged surface of bacterial membranes by the aid of electrostatic interaction (Devaux 1991, Dolis 1997).

Another factor also important for the selectivity of AMPs is the absence or the presence of cholesterol in cell membranes. Bacterial cell membranes, in contrast to eukaryotic cell membranes, do not have cholesterol, being more flexible and an easier target for AMP permeabilization (Turner 1970, Toke 2005, Bechinger 1999). Moreover, the large negative transmembrane potential ($\Delta\psi$) of bacterial cell may also facilitate the permeabilization by formation of ion channels (de Kroon 1991; Vaz Gomes 1993, Toke 2005, Yeaman 2003). Furthermore, the selectivity of some AMPs towards tumor cells has been suggested to be due to their higher negative membrane potential as compared to the cytoplasmic membranes (Utsugi 1991). For an interesting review about the differences amongst

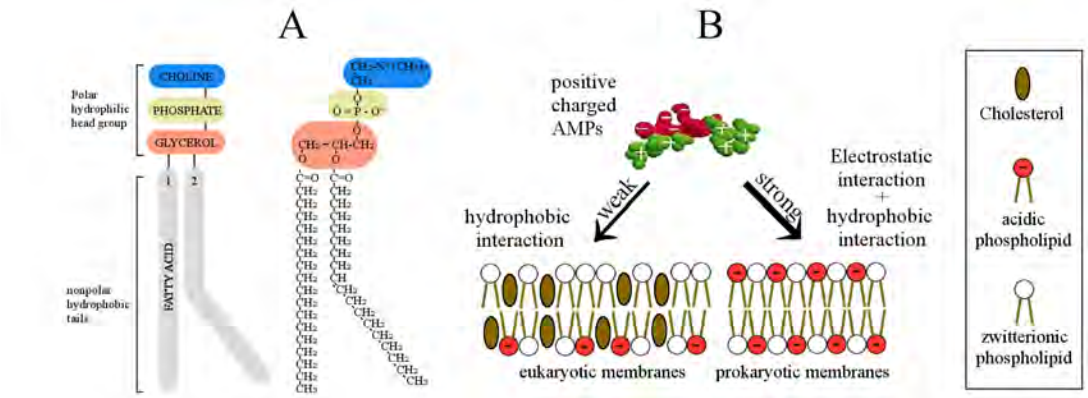

Figure 1.17: *Membrane selectivity of AMPs* **A**. Example of a phospholipid molecule (PC). The amphipathic structure of the lipid is characterized by a hydrophobic part (grey, lipid tails) and a hydrophilic part that contain a negative charged group (ocre, phosphate) connected to the variable polar group (blue, choline). **B**. Cationic peptides binds stronger to acidic lipids (prokaryotic membranes) by the aid of electrostatic interactions. The outer leaflets of the mammalian cells membranes (eukaryotic) are exclusively composed of zwitterionic phospholipids, for which the peptides show low affinity. Picture (A) modified from www.ncbi.nlm.nih.gov and the cartoon is a modified version of Zasloff 2002.

bacteria and host cells see Matsuzaki *et al.* (Matsuzaki 2009).

1.2.5 Bacterial Resistance: Development of New Drugs

Bacteria have been shown to resist antibiotics, as a result of chromosomal mutation or inductive expression of a latent chromosomal gene or by exchange of genetic material through transformation, transduction or conjugation by plasmids (Neu 1992). The rapidly increase in the frequency of appearance of bacterial resistance to conventional antibiotics has estimulated the interest for new agents. One class of antibiotics that has become the focus of attention are AMPs. Their wide variety of sequence and structures and the non-specificity of their mechanism make more difficult for the bacteria to become resistant. Bacteria would have to redesign their membrane, by changing the composition and organization of lipids (Zasloff 2002).

However, it has to be noted that several bacterial species have developed resistance to AMPs. Some of the resistance mechanisms are based in the modification of the bacterial cell envelope (like incorporating Lys in LPS), other ones employ outer membrane proteases or efflux pumps to inactivate or expel the

peptides (Toke 2003). Even so, numerous AMPs show excellent activity and selectivity towards bacteria being promising candidates as novel antibiotics (Zasloff 2002, Perron 2006, Bishop 2006).

1.3 Cyclic Antimicrobial Peptides

The spatial conformation of linear peptides can be determined by the torsional angles along the backbone conformation. Although the number of conformations is limited by the steric hindrances of the side-chains and the allowed torsional angles, the overall number of conformations for linear sequences is still large due to the flexibility of the peptide chain. The main consequence of this large diversity of conformations is the low selectivity and specificity of linear peptides for their receptors. One strategy to constrain the conformations of the linear peptides is by cyclization.

There are four main ways to obtain a cyclic peptide. In all the cases the cyclization is performed by the formation of a covalent bond, mainly an amide or a disulfide. This bond can be formed between the side chain functional groups of the two amino acids (Figure 1.18 A) or between the N- and C-terminal of the peptides (Figure 1.18 B), which is termed as "head-to-tail" cyclization. Alternatively, the cyclization can involve one amino acid side-chain and the N- or C-terminus of the peptide (Figure 1.18 C). Moreover, a cyclic peptide can also be obtained by linking the N atoms of the backbone (Figure 1.18 D). Cyclic peptides have been demonstrated to possess potential to i) withstand proteolytic degradation ii) increase receptor selectivity iii) enhance bioavailability and iv) provide conformational insight for receptor binding (Rizo 1992). Moreover, in the particular case of head-to-tail cyclic peptides, the lack of the N- and C-terminal ionization helps them to go through the membrane easily. For these reasons, cyclic peptides have attracted considerable attention as new bioactive agents.

1.3.1 Cyclic Antimicrobial Peptides in Nature

There have been isolated a variety of cyclic peptides from natural sources, such as bactenecin, gramicidin S, tachyplesin or RTD-1. These cyclic peptides have interesting antibacterial activities.

i) **Bactenicin**, is a 12 amino acid cationic cyclic AMP isolated from bovine neutrophils. The primary structure, RLCRIVVIRVCR, is constrained by a disulfide bond between the two cysteine side chains. The secondary structure is characterized by a type I β-turn even in water, while its linear counterpart adopts

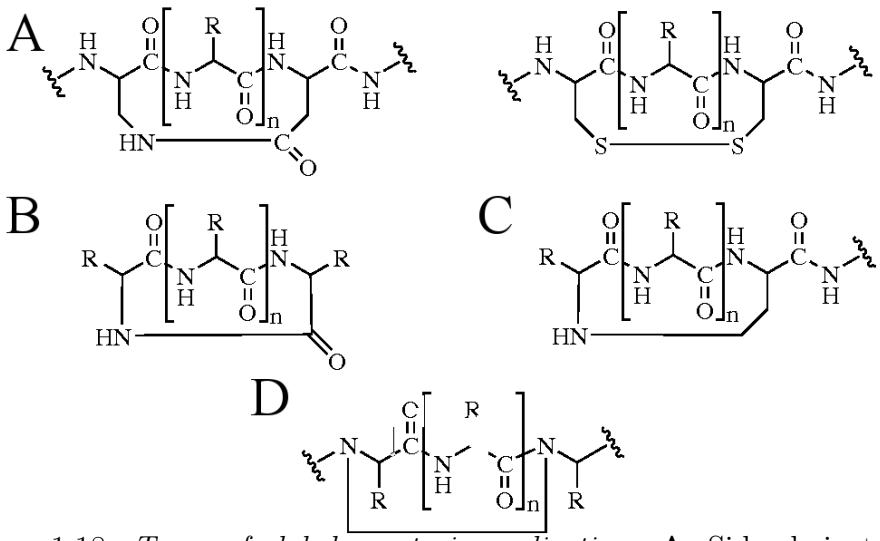

Figure 1.18: *Types of global constrain cyclization.* **A.** Side chain to side chain cyclization. **B.** Head-to-tail cyclization. **C.** Side chain to N- or C-terminus cyclization. **D.** Backbone cyclization. The illustrations have been taken from Fung 2005.

different conformations according to the lipophilicity of the environment (Wu 1999). Bactenicin showed a higher activity against gram-negative bacteria than its linear derivative, which underwent a dramatic decrease in activity associated to the loss of the cyclic structure.

ii) **Gramicidin S** (GS) is an example of a head-to-tail cyclic cationic decapeptide, produced by gram-positive bacterium *Bacillus brevis*. Its primary structure is c[(LfPVOL)$_2$], where f is a D-phenylalanine. As depicted in Figure 1.19 A on top, its secondary structure is characterized by an antiparallel β-sheet stabilized by backbone hydrogen bonds and two type II' β-turns. Moreover, the arrangement of the residues gives rise to a global amphypathic structure, with valine and leucine distributed in one side and the ornithine residues in the other side (Figure 1.19 A, bottom). GS displays a powerful antibiotic activity against a broad spectrum of gram-negative and gram-positive bacteria. However, its high hemolytic activity restricts its use to topical applications (Waki 1990, Xu 1995, Mogi 2009).

iii) **Tachyplesin** is a 17 amino acid cationic peptide isolated from acid extracts of horseshoe crab (*Tachypleus tridentatus*) hemocyte debris. Its primary structure is depicted in Figure 1.19 B, and the cyclic structure is constrained by two disulfide bridges between two pairs of cysteine residues. The high stability of this peptide has been attributed to the rigid structure imposed by the global cyclic constraint. Furthermore, this cyclic structure is amphipathic, which has

been associated to its antimicrobial activity (Nakamura 1988).

iv) **RTD-1** is a θ-defensin peptide isolated from rhesus macaque leukocytes. It is composed of 18 amino acids (see Figure 1.19 C) including six cysteines linked by three intramolecular disulfide bonds. Some recent studies revealed that the peptide backbone is cyclized through amide bonds. It has been speculated that the compact structure and the lack of N- and C-terminal functional groups of RTD-1 confers resistance to proteases and eliminates its susceptibility to exopeptidases. Furthermore, it was observed that the cyclic conformation is crucial for the activity, since the linear analogue was not active (Tang 1999).

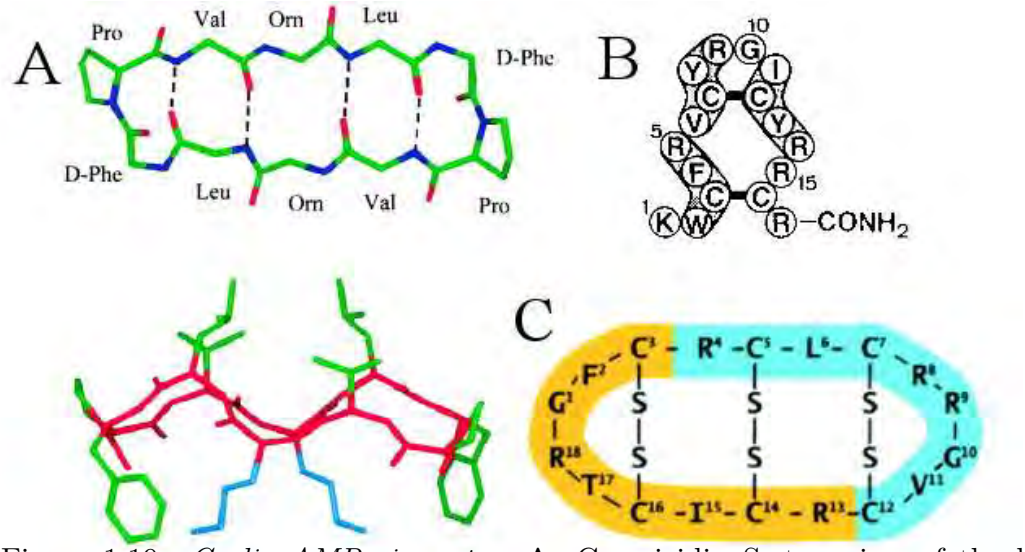

Figure 1.19: *Cyclic AMPs in nature.***A.** Gramicidin S, top view of the backbone atoms (top) and amphypatic structure (bottom) **B.** primary structure of tachyplesin **C.** cyclic peptide θ-defensin. The illustrations have been taken from Kondejewski 1999 and Tang 1999.

1.3.2 Rational Design of Cyclic Antimicrobial Peptides

Rational design of AMPs maintaining the crucial features of native antibacterial peptides has lead to the development of compounds with remarkable activity. For instance, synthetic cationic peptides (V1) were designed structurally similar to cyclic β-sheet peptides, such as protegrin 1, thanatin and androctonin (see Figure 1.20 A). To enhance the antimicrobial activity and selectivity towards bacteria, the common features of AMPs were modulated strategically while preserving the size, symmetry and amphypathic structure. The design showed that the residues forming the hydrophobic face influenced the hemolytic activity probably

by the enhanced penetration of more hydrophobic peptides into the phospholipid membrane. The introduction of less hydrophobic residues in the non-polar face resulted on a good strategy to reduce the hemolytic activity, while preserving the antimicrobial activity (Frecer 2004).

Similar conclusions were proposed by Lee *et al*. In their study, the cyclic peptide Gramicidin S was taken as the structural framework for the design of biologically active peptides. They studied the effect of the ring size, and the alteration of the amphipathicity and hydrophobicity. These investigation resulted in the identification of the peptide GS14K4, which displayed the highest terapeutic index of all the peptides designed. As depicted in Figure 1.20 B, the structure of the GS14K4 was obtained by reducing the amphypathicity of GS14. This study demonstrates that the dissociation of antimicrobial and hemolytic activities can be achieved by modulating the amphypathicity (Lee 2003).

Hence, the rational design starting from a native AMP seems to be a good strategy in order to improve the antimicrobial activity and the peptide selectivity.

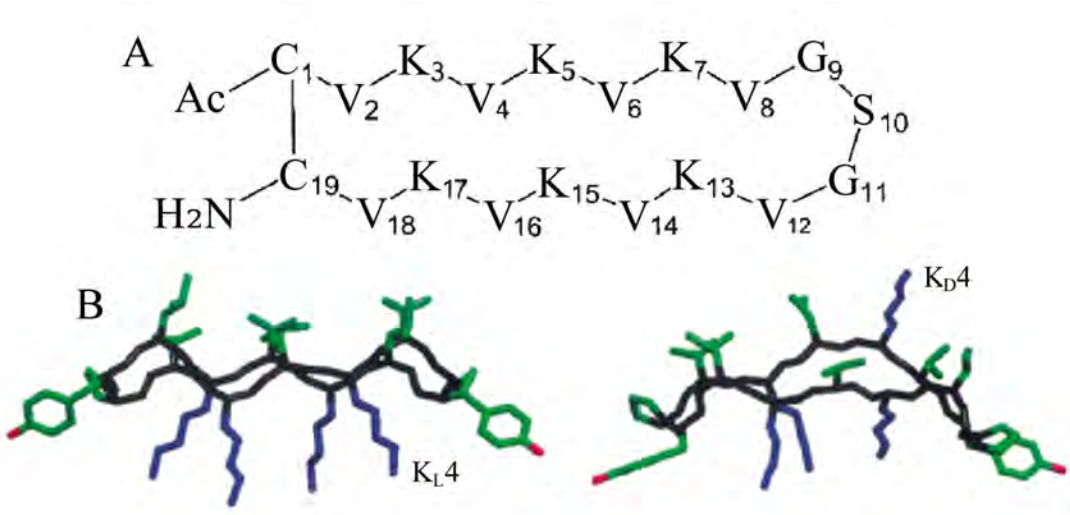

Figure 1.20: *Rational design of cyclic AMPs.* **A.** Sequence and chemical structure of *de novo* designed cyclic cationic peptide V1. **B.** NMR structures of GS14 and GS14K4. The backbone is colored in black, oxygen atoms in red, hydrophobic side-chains in green and basic residues are shown in blue. The illustrations have been taken from Lee 2003 and Frecer 2004.

1.4 Antecedents: Phe-Containing Library of Cyclic Peptides

1.4.1 First Generation of Cyclic Peptides

The LIPPSO group, in collaboration with the Plant Pathology group of the University of Girona, is interested in finding new agents to control plant diseases caused by bacteria such as *Erwinia amylovora*, *Pseudomonas syringae* and *Xanthomonas vesicatoria*. These diseases are responsible for important economic costes and, up to now, there are no effective treatments to control them. During the last years, the LIPPSO group has designed and synthesized a family of head-to-tail cyclic peptides and has tested them against those bacteria.

These cyclic peptides were *de novo* designed and consisted of alternating cationic (lysine) and hydrophobic (leucine and phenylalanine) amino acids. Their general formula was c(X_n-Y-X_m-Gln) where X is a lysine or leucine residue, and Y is a L- or D-phenylalanine (m=n=1, or m=3 and n=0-5). The most active sequence of these first generation of cyclic peptides of 4-10 residues was the cyclodeca-peptide BPC16 (c(KLKLKFKLKQ) and named as BPC10L in the original publication), with a Minimal Inhibitory Concentration (MIC) of 6.2-12.5 μM against *P. syringae* and *X. vesicatoria*)(Monroc 2006a). However, BPC16 did not show activity against *E. amylovora* and displayed a considerable hemolysis (81% at 360 μM).

1.4.2 Second Generation of Cyclic Peptides

In order to improve the biological properties of BPC16, a library of 56 cyclic decapeptides was prepared and screened for antibacterial and hemolytic activities (Monroc 2006b). The sequences incorporated a phenylalanine and a glutamine residue at positions 6 and 10, respectively. The other positions consisted of all the possible combinations of three leucines and five lysines. The second generation of cyclic peptides showed higher activity than BPC16 against *P. syringae* (MIC of 3.1-6.2 μM) and *X. vesicatoria* (MIC of 1.6-3.1 μM). Notably, peptides active against *E. amylovora* (MIC of 12.5-25 μM) were found, constituting the first report of cyclic peptide active against this bacteria. Moreover, peptides less hemolytic than BPC16 were also identified.

It was performed a frequency analysis of the most occurring residues at each position of peptides of this library displaying the highest antibacterial activity. This study revealed that the dominant sustitution obeyed to the general structure c($X^1X^2X^3X^4$KFKKLQ). A second library was synthesized in order to check for

the influence on antibacterial and hemolytic activities of residues at positions 1-4 by using design of experiments (DOE). It comprised 16 cyclopeptides with all possible combination of leucines and lysines at positions 1-4. This library was screened for antibacterial activity against the aforementioned pathogens and for hemolytic activity. Results showed that the activity against *E. amylovora* was further improved (MIC of 6.2-12.5 μM) and the best peptides displayed a low eukaryotic cytotoxicity at concentrations 30-120 times higher than the MIC. The DOE analysis permitted to define rules for high antibacterial activity and low cytotoxicity, being the main rule $X^2 \neq X^3$, and the secondary rule X^4=lysine.

The analogues with the best biological activity profile were BPC194, c(KKLKKFKKLQ), and BPC198, c(KLKKKFKKLQ), which can be considered as good cantidates for the development of effective antibacterial agents in plant protection.

1.4.2.1 Evaluation of the anticancer activity

Antimicrobial peptides have emerged as potential candidates for cancer therapy. This selectivity amongst eukaryotic cells is due to the fact that cancer cell membranes have typically a net negative charge due to a higher than normal expression of anionic molecules such as PS and O-glycosylated mucins (Hoskin 2008).

Based on these properties, the anticancer activity of the second generation library of *de novo* cyclic AMPs was evaluated (Feliu 2010). In the study, the cytotoxicity on human carcinoma cell lines, and their effects on apoptosis and cell signaling proteins in cultured human cervical carcinoma cells was performed. From all the study, eight peptides were identified with IC_{50} values ranging from 18.5 to 57.5 μM against the five cell lines tested. This indicated that these peptides exhibit a potential anticancer effect. The detailed examination of the primary structure of these eight peptides showed that a common substructure characterized by $K^5F^6K^7K^8L^9Q^{10}$ amino acids was present (see Table 1.4).

The importance of this substructure sequence was already suggested to be a structural requirement that could lead to improved activity (Monroc 2006b). Consecutively, the eight candidates were further used to determine the IC_{50} against a panel of human cancer cells and the hemolysis activity. The overall analysis of the selected peptides pointed out to the six best candidates which displayed the combination of high cytotoxic activity and low hemolytic activity (Feliu 2010). In this thesis, we report the analysis of the stability of those active cyclic peptides to proteases in human serum.

Table 1.4: Sequences of the cyclic peptides with best anticancer activity profile.

Code	1	2	3	4	5	6	7	8	9	10
BPC88	c(K	K	L	L	K	F	K	K	L	Q)
BPC94	c(K	L	L	K	K	F	K	K	L	Q)
BPC96	c(L	K	L	K	K	F	K	K	L	Q)
BPC98	c(L	L	K	K	K	F	K	K	L	Q)
BPC184	c(K	L	L	L	K	F	K	K	L	Q)
BPC194	c(K	K	L	K	K	F	K	K	L	Q)
BPC198	c(K	L	K	K	K	F	K	K	L	Q)
BPC202	c(K	K	K	K	K	F	K	K	L	Q)

1.5 Molecular Modeling of Biological Systems

Most experiments give direct insight into the macroscopic world. Their limitation in displaying the submolecular scale is known, and even though biophysical experiments have evolved in the last years, alternative methodologies are needed to study in much more detail the molecular interaction between biological molecules with membranes.

Molecular modeling in general embraces theoretical models and computational strategies devised to mimic the behaviour of molecules and molecular systems.(Leach 2001) This discipline includes all methodologies used in computational chemistry, from electronic structure methods (solution of the electronic Schrödinger equation) to simplest classical Molecular Mechanics (MM) models, and from static structure determination to Molecular Dynamics (MD) simulations. In particular, MD simulations have become in the last decades one of the most powerful methods to describe molecular motion at the atomic scale, and have been a key tool for studying the structural properties and dynamical behaviour of biological systems, from peptides to proteins and lipid membranes.

1.5.1 Molecular Dynamics and Molecular Modeling Background

It has been more than 30 years since the first MD simulation of a system with biological interest was published in Nature. (McCammon 1977) In that seminal work, a simulation of the atomic motion of a folded globular protein, bovine pancreatic trypsin inhibitor (BPTI), was performed in vaccum, covering only 9.2 ps. Despite the short time scale, this simulation higlighted that proteins were

not as rigid molecules as assumed, and that the motions of such systems could play a major role in their function.

Nowadays, a lot of work has been carried out in the field and MD simulations are widely and routinedly applied. The continuous increase in computer power and the improvement of algorithms over the last years has also allowed for simulations on a much larger timescales than that considered in the first simulation. For instance, the first μs MD simulation was already reported back in 1998 (Duan 1998). In addition, the first recorded simulation included only about 500 atoms, whereas thousands of atoms are commonly treated these days. This allows for modeling not just larger biomolecules but also for a more realistic simulation of their environment and conditions.

In the particular case of peptide research, computer simulations have become a well-established tool to complement experimental data concerning all properties and features of the peptides described in the first section. In the following section we will briefly review the relevant literature covering the use of MM models and MD simulations to address some of the main issues this thesis is devoted to, namely conformational analysis of peptides, peptide folding and unfolding, the partition of peptides upon membrane interface and the atomistic details of their mechanism of action for antimicrobial activity.

1.5.2 Conformational Space of Peptides

The physical, chemical and biological properties of peptides depend critically upon the different three-dimensional structures or conformations that can adopt (see section 1.1.2). The conformational space or the potential energy surface of a peptide is qualitatively characterized by the presence of a large number of valleys separated by high mountains and ridges. Each valley corresponds to a possible stable conformation (energy minima), which differs in energy and structure.

However, peptides have a high conformational flexibility, specially in solution. For this reason, their potential energy surface is composed by a large number of minima, which represents the main difficulty for the structural characterization of a peptide. This is known as the multiple minima problem (Ripoll 1988, Scheraga 1991), and represents the main barrier for the structural characterization of a peptide (see Figure 1.21).

Furthermore, most peptides exist in physiological conditions in thermal equilibirum as a mixture of interchangeable conformations with similar energies populated according to the Boltzmann distribution. Under such circumstances, it is often assumed that the native conformation is the one with the lowest energy, which is usually referred as the global minimum. However, we should be

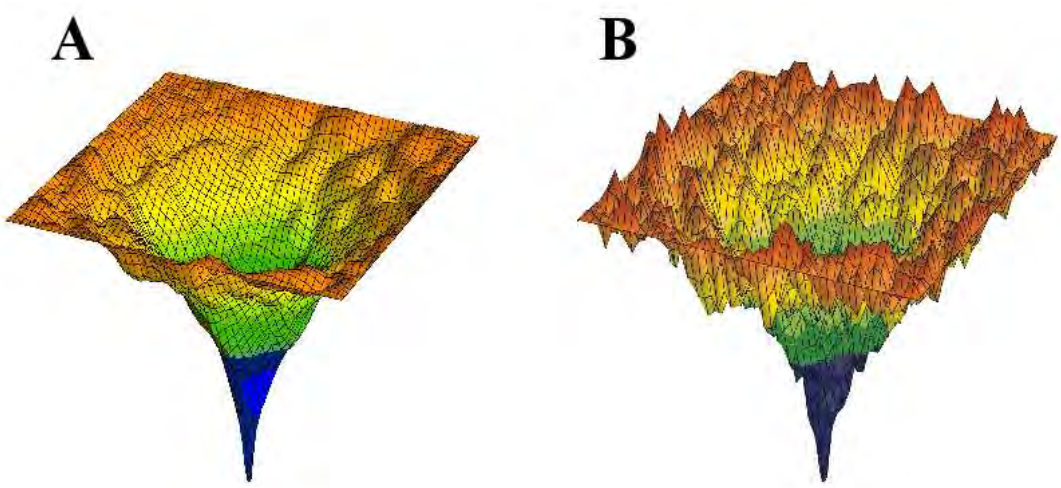

Figure 1.21: *Multiple minima problem.* **A.** Smooth potential energy surface for peptide and protein conformation. **B.** more realistic potential energy surface composed by a large number of minima. This picture has been taken from http://www.btinternet.com/martin.chaplin/protein2.html

cautious in the methodology that only finds a single conformation. The lowest energy conformation may not be the most populated one because of the contribution of the vibrational entropy to the statistical weight of each structure. Also, the entropic effect of environment should be properly taken into consideration. It must be noted that the global minimum energy conformation may not be the active structure (Leach 2001).

Despite these difficulties, in computer science conformational analysis methods are good tools to study the behaviour of peptides. This methodology requires the location of stable conformations, that occur at minimum stationary points on the multidimensional potential energy surface. Hence, energy minimisation methods play a crucial role in conformational analysis. Even so, one of the obstacles of energy minimisation is that they move to the minimum point closest to the starting structure. For this reason, different algorithms are needed to generate different initial structures in order to explore all conformational space for subsequent minimisation. Below, some of the most used in the peptide field are discussed.

1.5.2.1 Methods for conformational analysis.

A large number of studies about conformational analysis have been described and reviewed in the literature (Howards 1988, van Gunsteren 1990). There are different conformational search methods based on Molecular Mechanics and MD

simulations. Some of them are listed below.

i) **Systematic search algorithm** explores the energy surface of a molecule in a predictable fashion, such as making regular and predictable changes to the peptide conformation. For instance, the conformation segments of a polypeptide chain in globular proteins was determined by this approach. The conformations were generated by using representative sets of ϕ and ψ dihedral angles that were derived from the distribution of these angles in refined protein structures (Moult 1986).

ii) **Model-building** approaches construct conformations of a molecule by joining together three-dimensional structures of molecular fragments. This means that the efficiency compared to the systematic search algorithms is higher, since the number of combinations of structures is less than the combinations, for instance, of torsion angles. However, this algorithm presents some limitations. The analyzed molecule must have available fragments and they must be conformationally independent of each other. Each fragment must be conformationally independent to the other fragments and that the analyzed molecule should have fragments available (Leach 2001).

iii) **Random search methods** move from one region of the potencial energy surface to another unconnected region in a single step. The conformational space is explored by changing atomic Cartesian coordinates or the torsion angles of rotatable bonds.

iv) In **Distance geometry** the conformation is described by terms of distances between all pairs of atoms. Then, the molecule can be represented using an N $\times$ N symmetric matrix. Hence, the method explores the conformational space by randomly generating many distances matrices, which are then converted into conformations in Cartesian space. One of the most important uses of this methodology is for deriving conformations that are consistent with experimental distance information, such as distances from NMR experiments.

v) **Molecular Dynamics** are also used for exploring conformational space. In this case, the methodology does not generate different conformations which are directly minimized. Contrary, the performance is realized at very high temperatures (physically unrealistic), what gives to the system additional kinetic energy enhancing the ability of the molecule to explore further the conformational space preventing the molecule getting stuck in a localized region of the potential energy surface. From the trajectory, the structures are selected at regular intervals for subsequent energy minimization.

vi) **Simulated Annealing (SA)** was first described in 1983 by Kirkpatrick *et al.* (Kirkpatrick 1984). The name and idea of method originate from the

annealing process in metallurgy, a controlled heating and cooling process devoted to reduce the defects of the crystal growing of materials. With the heating process the atoms are allowed to explore large regions of the phase space, scaping thus from their original positions. The controled slow cooling allows the system to achive a set structures with the lowest energy. These ideas can be applied to the problem of finding global minimum structures by making use of MD simulations to account for the heating and cooling processes. All studies where the SA method has been used demonstrated that, although the cooling scheme is not sufficiently slow to always find the global minimum structure, it is able to find deep local energy minima of the regions explored. Several comparative studies of different protocols of the SA procedure with other methods have been carried out (Corcho 2000, Bisetty 2006). A particular example of SA protocol taken from Corcho 2003 is described in Figure 1.22.

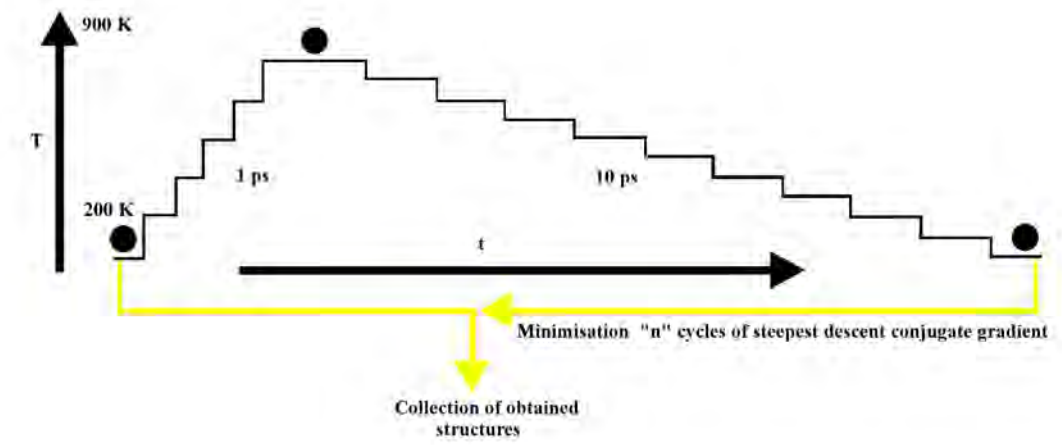

Figure 1.22: *Example of a scheme of iterative simulated annealing protocol.* A cycle comprehends the heating from 0 till 900 K in 1 ps followed by a slow cooling during 10 ps. The structure is minimized and saved as a collection of obtained structures. The illustration has been modified from Corcho 2003.

1.5.3 Peptide Folding

The protein or peptide folding is the physical process by which the molecule folds into its characteristic functional three-dimensional structure, presumably from a non-structured or random coil unfolded configuration. It was speculated that the mechanism by which a protein is able to fold into its unique fold could not be via a systematic enumeration of all possible conformations (Leach 2001).

Different computational models have been used to investigate protein folding, such as simple lattice models and atomistic models. However, considering

that the interactions at atomic level play a crucial role in the equilibria between folded and unfolded state, MD simulations should be, in principle, a valuable tool to describe the folding of a peptide or protein.

The problem of peptide folding has been extensively studied at the molecular level. One of the first simulation is the 1 μs simulation of a 36-residue peptide from an extended conformation (Duan 1998, the calculation took four months of computing time!). The final folded state was not the known experimental structure, but showed significant resemblance to its native conformation.

More advanced simulations started to shed light in the governing factors of folding pathways. One of them came out from the simulations of a variety of peptides in different solvents showing that folding into distinct native folds was a reversible process (Daura 1998, Daura 1999, Bürgi 2001, van Gunsteren 2001). In addition to this concept, the folding of a charged-21-amino acid peptide (con-T) showed a multi-step folding pathway, where hydrophobic interactions were not the major driving force of the folding process. Instead, charged-charged interactions and salt-bridge interactions amongst the peptide structure produced different local peptide shapes leading the peptide to its folded state (Wei 2005).

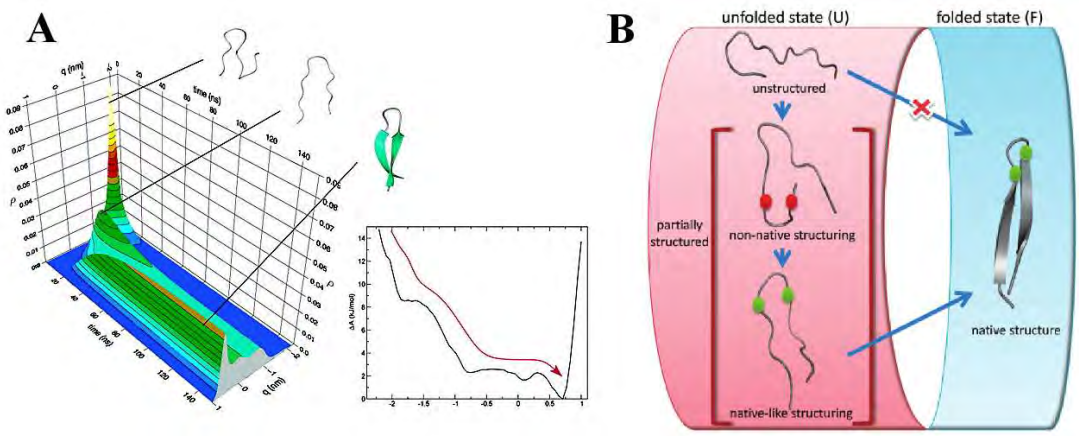

Figure 1.23: *Representation of a folding process by MD simulations.* **A.** Kinetics of the folding of a β-structure. **B.** The folded state is not reached directly from fully unstructured conformations. Instead, it is formed via partially structured-unfolded conformation to β-hairpin .The illustrations have been taken from Thukral 2009 and Daidone 2005.

In the last five years, new findings about folding process came out. Daidone and co-workers showed comprehensively that the folding kinetics behaves like a diffusive process over the free potential energy surface, exhibiting a funnel-like almost barrierless free energy profile (Daidone 2005). Besides, it was showed for

the first time the thermodynamic equilibrium of a complex system, namely a β-hairpin, for a timespan of more than 1 μs. The peptide was initially considered in an α-helix conformation and after many unfolding/refolding events, the β-hairpin was observed, with an average time of folding around 200 ns. The free energy profile describing the main conformational transitions showed the characteristic features of a funneled free energy landscape, with a downhill surface towards the β-hairpin folded basin (see Figure 1.23 A) (Daidone 2005). One of the most recent simulations study has concluded that the transition to the folded state never occurs directly from a fully unstructured conformation (see Figure 1.23 B). Instead, the peptide follows a stepwise pathway through partially structured-unfolded conformation that finally triggers the transition state to the final folded harpin structure (Thukral 2009).

1.5.4 Antimicrobial Peptides: From Water Phase to Membrane Interface

MD simulations have proven also to be valuable in describing elements of the mechanism of action of these AMPs at the atomic level, such as i) the binding of the peptides to the bilayer surface ii) the properties of such surface-bound complexes iii) the steps of peptide insertion into the bilayer iv) the structural modifications undergone by the bilayers and v) the details of the structure of stable pores induced by the AMPs.

There are several possible levels of detail with fully atomistic MD simulations. The implicit membrane models, where the lipids and solvent are not modeled explicitly as atoms, which are especially useful for studies of long time scale processes (Mottamal 2006, Ulmschneider 2008, Ulmschneider 2009), and explicit systems where bilayer models and detergent micelles are modeled (see Figure 1.24). The latter is a more realistic approach of the peptide-lipid interaction (Matyus 2007). Some of the recent simulations in different membrane lipid types, are exposed below.

1.5.4.1 Micelle simulation

Micelles are formed by lipids arranged with their hydrophilic head-groups in contact with the surrounding solvent and all the hydrophobic tails in the centre of the micelle. They represent the simplest head-tail monolayer, which is commonly used in biological/biochemical applications to mimic a lipid bilayer environment. The first MD simulation of a pure lysophosphatidylethanolamine (LPE) micelle was carried out by Wendolosky and co-workers (Wendoloski 1989). Since then,

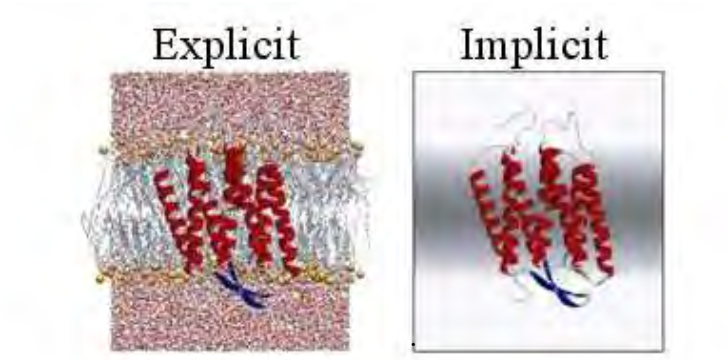

Figure 1.24: *Different levels of detail for membranes in MD simulations.* Explicit and Implicit membrane models. Picture taken from http://spider.iwr.uni-heidelberg.de/∼julmschn/

several works have tackled the interaction of antimicrobial peptides upon micelles, as simple examples of the behaviour of AMPs in lipidic environment. To relate this interaction to the antimicrobial activity two types of micelles formed from sodium dodecyl sulfate (SDS) and dodecylphosphocholine (DPC) were used. The use of these micelles are crucial to mimic the features of prokaryotic and eukariotic membranes, respectively. Below some examples of MD studies to analyze the interactions of specific AMPs with micelles are exposed.

i) **Ovispirin** has been shown by NMR experiments to interact fast to lipid membranes. MD simulations confirmed the fast interaction by placing the peptide in the water phase, close to the micelles. The preference for micelle interface was also confirmed when the peptide was placed in the simulation at the center of a SDS micelle. It showed a fast shift from the center to the water interface, in about 8-12 ns (see Figure 1.25 A). On the other hand, in the interaction with eukaryotic mimic micelles (DPC) different binding modes were seen. One of the ovispin analogues with high cytotoxic activity was found to present high content of helical structure when inserting deeply in the micelle. On the contrary, a less toxic analogue showed lesser binding depth and also a loss of helicity (Khandelia 2006).

ii) The MD simulations of **Protegrin-1** (PG-1) showed similar interaction modes as Ovispirin (see Figure 1.25 B). Once placed in the center of the membrane, the simulation showed a movement from inside the micelle to the water phase. However, this movement in DPC was 3.5 times slower than in SDS, showing a higher affinity of this peptide to the charged head-groups of the SDS micelle. Even though PG1 showed toxicity to both eukaryotic and prokaryotic

membranes, the deformation of the micelle was found to be more pronounced in the case of the SDS models (Langham 2006).

iii) Simulations with **Indolicidin** upon DPC micelles showed that a cation-π interaction between tryptophan (11 th position) and arginine (13 th position) was important in the stabilization of the defined structure near the interface. When a mutant was simulated (where the tryptophan residue was replaced by an alanine), the structure was lost. This simulations were in excellent agreement with experimental data, since the backbone of the peptide was more ordered in DPC than in SDS (Khandelia 2007).

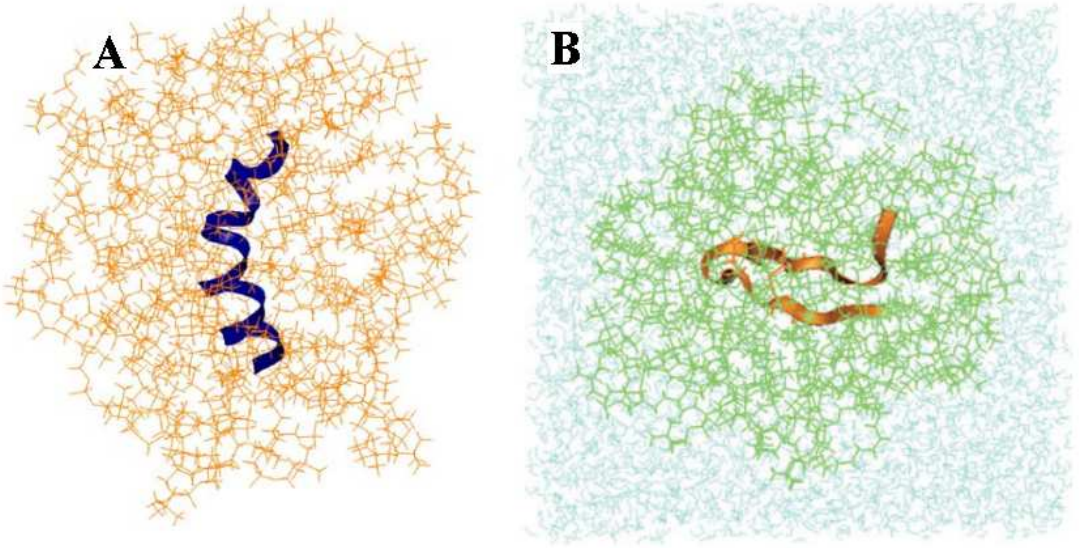

Figure 1.25: *Representation of micelle lipids with AMPs by MD simulations.* **A.** Initial conformation of the ovispin peptide in DPC micelle **B.** Initial views of PG-1 (in orange) in DPC system (green) with water molecules (light blue). The illustrations have been taken from Khandelia 2006 and Langham 2006.

These early results using micelles to mimic lipid bilayer environment were promising. Besides, the results were directly comparable to NMR structural mesurements on peptides (Matyus 2007). However, several important differences must be taken into account, like the large degree of curvature, the short single-chain surfactants, the higher deformation degree and different chain structure of the micelles compared to that of the lipid bilayers.

1.5.4.2 Lipid bilayer simulation

The first MD simulation work on a lipid bilayer with explicit solvent was carried out by Egberts in 1988 (Egberts 1988). Over the past 20 years, computer simulations of lipids have made great progress. Unlike micelles, lipid bilayers are made

of two layers of lipid molecules forming a lamellar structure, therefore leading to bigger and more complex structures to deal with.

Advances in computer simulation techniques have made possible the modeling of a broad palette of pure lipid bilayers, such as dioleoyl phosphatidylcholine (DOPC, Benz 2005), dipalmitoyl phosphatidylcholine (DPPC, Pastor 2002), dimyristoyl phosphatidylcholine (DMPC, Nagle 2000) and 1-stearoyl-2-docosahexaenoyl-sn-glycero-3-phosphocholine (SDPC, Saiz 2002). The accurate representation of lipid bilayers is of great interest since it can influence the description of the peptide-lipid interactions, a key part of the mechanism of action of active peptides. In the last few years, a large number of publications have been focused on the study of the lipid-peptide interactions, the partioning of the peptides between water-lipid phases and the mechanism of action of the AMPs upon membrane target. A review of the literature in MD studies about the interaction of AMPs with lipid bilayers is described below.

i) The secondary structure of **Dermaseptin** was seen to be stabilized upon a 1-palmitoyl-2-oleoyl-sn-glycero-3-phosphatidylcholine (POPC) bilayer by the formation of a hydrogen bond between the side chain of third residue and the phosphate group of the lipid head-group (La Rocca 1999). Due to this interaction, the insertion of the peptide into the hydrophobic region helped concluding that the presence of these amino acids may have a fundamental biophysical basis for the activity of the peptides (Chan 2006). Furthermore, the associated increase of the area per lipid associated to the decrease in the bilayer thickness was seen as a crucial step for membrane perturbation (Shepherd 2003).

ii) The **c-RW** is an amphypathic antimicrobial cyclic peptide from a synthetic combinatorial library. A series of MD simulations in membranes at various peptide:lipid (P:L) ratios were carried out upon POPC membranes by Appelt *et al.* (Appelt 2005). As predicted by several modes of action, when a threshold concentration of peptide is reached ,the membrane is more affected by the action of the peptide. In these simulations, at low P:L (2:128, Figure 1.26 A), the membrane was barely affected compared to the pure POPC bilayer. However, at higher ratios (12:128) the water molecules can be dragged in the hydrophobic core, decreasing the area per lipid. This phenomenon was, at the same time, followed by the insertion of the aromatic side-chains (Figure 1.26 B) of the cyclic peptide into the aliphatic region of the membrane, whereas the polar face of the peptide backbone and the arginine residues pointed towards the bulk of water.

iii) **Protegrin-1** was simulated as monomers on POPC and POPC/POPG (4:1) (Jang 2006, Jang 2007). The simulations showed the preferences of the peptide towards charged lipid surfaces. The PG-1 was seen to interact strongly with

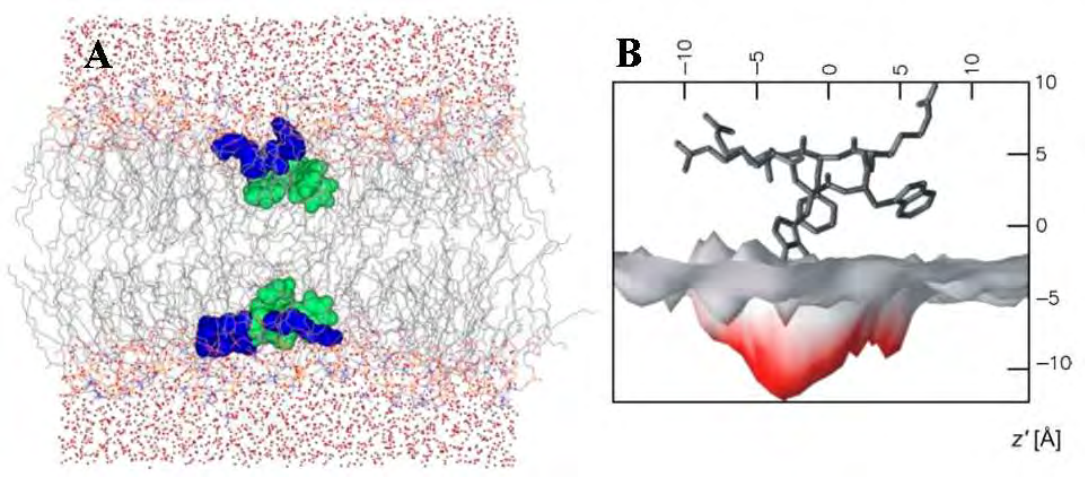

Figure 1.26: *Simulations results from c-RW peptide upon membrane.* **A.** Picture of the 2:128 simulations, where the aromatic amino acids are shown in green and the arginines in dark blue **B.** Cavity in the bilayer formed by the peptide, where the side view of the surface is shown. It can be seen that the packing of the lipids are affected, creating a cavity in the hydrophobic core by the Trp amino acid. Figures taken from Appelt 2005.

the merged POPC/POPG bilayer, confirming that the first step of its mechanism of action is the electrostatic interaction between the AMP and the bilayer. Recently, the structure of a pore caused by PG-1 in a mixed POPE:POPG bilayer predicted from NMR experiments was used as a starting configuration for MD simulations (see Figure 1.27). In the simulation, even though the lipids tilted somewhat towards the peptides, the structure of the pore was closer to a barrel-stave model, rather than a toroidal one. The movement of ions across the pore was also investigated in detail. This study showed that the pore could selectively allow ions to go through the membrane, corroborating the biological function of peptide PG-1 in bacteria. The exchange of ions through the pore was proposed to compromise the integrity of the transmembrane potential, leading the bacteria eventually to death (Langham 2008).

iv) **Indolicidin** was placed in random orientation upon different types of lipid membranes, and simulated up to 50 ns (Hsu 2007). Similarly to the case of PG-1, the authors suggested that the larger affinity for the anionic lipid bilayers was associated to electrostatic interactions. However, once the peptide was bound to the surface of the membrane, hydrophobic interactions take over and seem to be the driving force for the insertion of the peptide into the lipid membrane. These findings, were in line with previous experimental evidence from mutation studies.

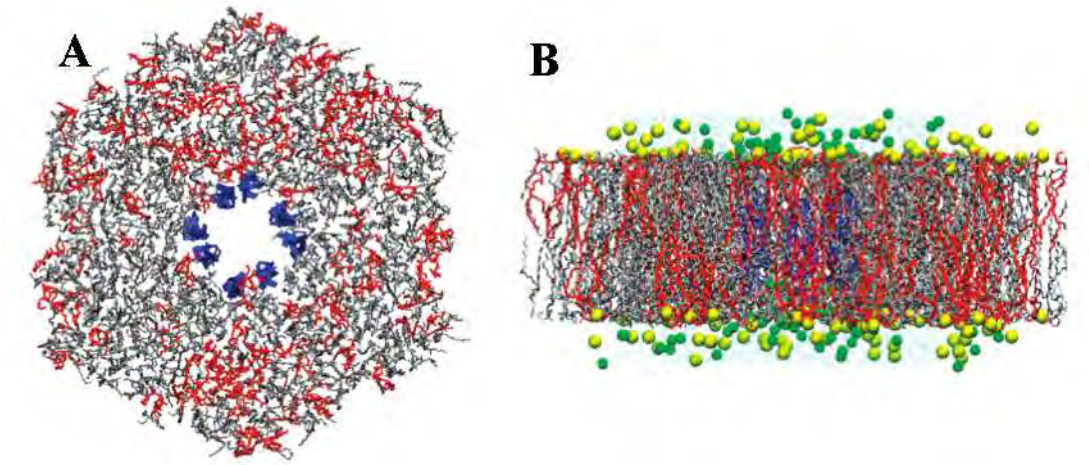

Figure 1.27: *Initial views of Protegrin-1 peptide simulated in bilayer membrane.* **A.** PG-1 in the pore seen from a top view, with the peptide in blue, POPE lipids in grey and POPG in red **B.** A side view with the water molecules in cyan, and chloride and sodium ions in yellow and green, respectively. Figures taken from Langham 2008.

v) **Magainin** was first simulated upon POPC bilayers by Kandasamy *et al.* (Kandasamy 2004). These simulations were performed with two analogue magainin peptides (magainin2 and MSI-7, a synthetic analogue), starting with several initial positions and orientations of the peptides upon the membrane. The authors found a strong specific interaction between the lysine residues and the lipid head-groups, leading to a destabilisation of the bilayer environment by increasing the lipid tail disorder and the induction of local curvature on the lipid head-groups. This hydrogen bonding interaction was found to play the main role for the peptide binding.

The antimicrobial action of this peptide was rationalized for the first time by Leontiadou *et al.* (Leontiadou 2006). The spontaneous formation of a pore-like defect in a DPPG membrane is depicted in Figure 1.28 A, where as the peptides inserted deeper in the bilayer, the lysine residues remained hydrogen bonded to the head-groups of the lipids, resulting in the introduction of some of the lipid head groups into the hydrophobic core of the membrane. This work lead to a reconsideration of the modes of action of the AMPs, proposed by experimental data, and a novel disordered toroidal pore model (DTP, see Figure 1.28 B)) was proposed, opposing to the standard and accepted toroidal pore model.

vi) **Melittin.** A series of MD simulations by Sengupta *et al.* confirmed the spontaneous formation of a disordered toroidal pore on DPPC membranes on a sub-microsecond time scale (Figure 1.28 C) (Sengupta 2008). Likewise magainin

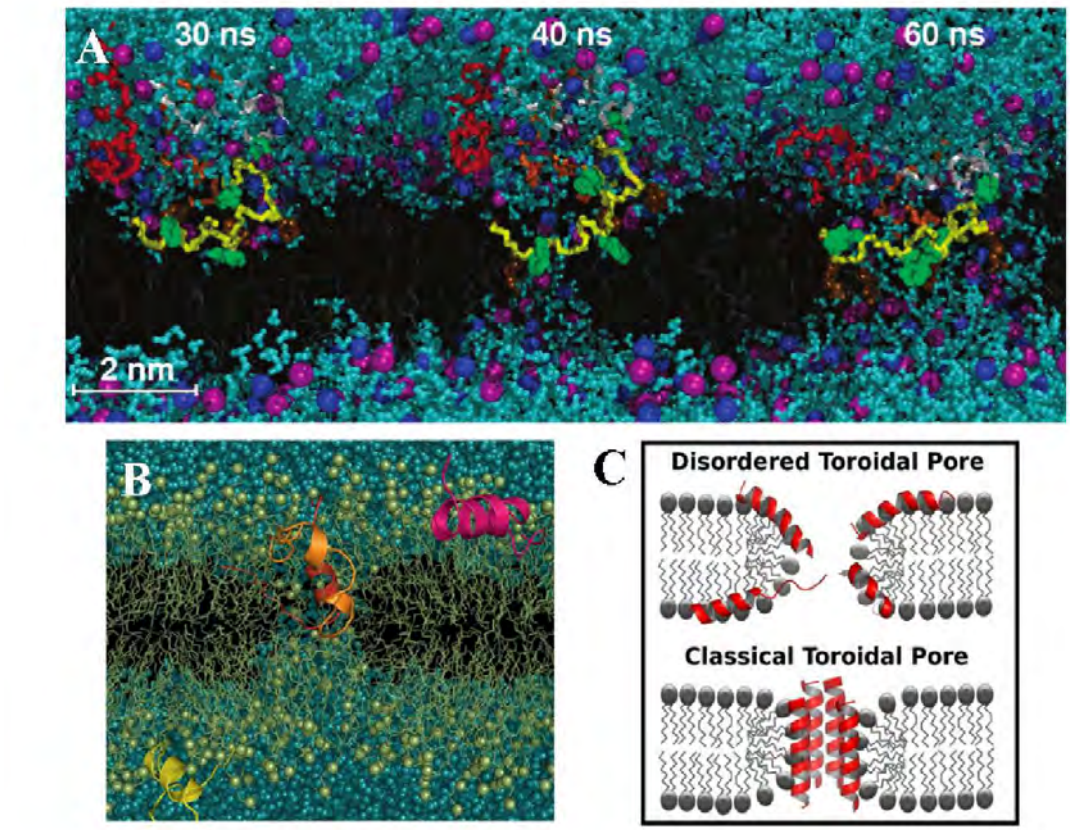

Figure 1.28: *AMPs in action by means of MD simulations.* **A.** Snapshots of the pore formation by magainin AMPs peptide. At 30 ns, one peptide moves toward the bilayer interior. Consequently it induces stress in the membrane, resulting in the sudden formation of a pore at 40 ns. And afterwards, at 60 ns the pore rapidaly adopts a toroidal-shaped pore **B.** A snapshot of the pore formed by melittin. **C.** A cartoon image comparing the disordered toroidal pore state to the traditional view proposed by experiments. Figures taken from Leontiadou 2006 and Sengupta 2008.

simulations, membrane binding of the peptide lead to asymmetric changes in the lipid tail order, with the lipid molecules bound to the peptides showing less order than those moieties located further away. Moreover, only one or two peptides were found to insert into the pore and interact with the lipid head-groups and water molecules, verifying thus the DTP model as a general mechanism by which small peptides can form stable pores. Several independent simulations proved that i) after blocking lysine and arginine side chains the pores were not formed, indicating the importance of the charged residues in pore formation and ii) under the same conditions, other peptides like WALP and KALP that do not exhibit antimicrobial activity did not lead to pore formation.

vii) **Cathelicidins.** The interaction and the penetration of these family peptides have also been studied. A combined MD and fluorescence experiments exhibited that PMAP-23 associated with membrane interface causing a severe perturbation. As a result of that, the peptide induced membrane permeability reminiscent of the carpet model (Orioni 2009, Bocchinfuso 2009) (Figure 1.29 A). On the other hand, cateslytin, a β-sheet peptide was simulated upon a DMPC bilayer (Jean François 2008). The analysis of the average normal component of the electric field (E_z) upon binding the peptides showed that the electric gradient on the peptide-bound side was decreased, creating a constant electric field in the hydrophobic interior of the bilayer. This study explained why water defects are formed previous to pore formation, which had already been shown in other simulations (Gurtovenko 2010, Tarek 2005). Positively charged AMPs are believed to induce an electric field that is, on average, normal to the membrane. Therefore, the existance of mechanical stress upon peptide binding may induce pore formation through electroporation mechanism. A picture of the pore formation induced by this peptide is shown in Figure 1.29 B (Jean François 2008).

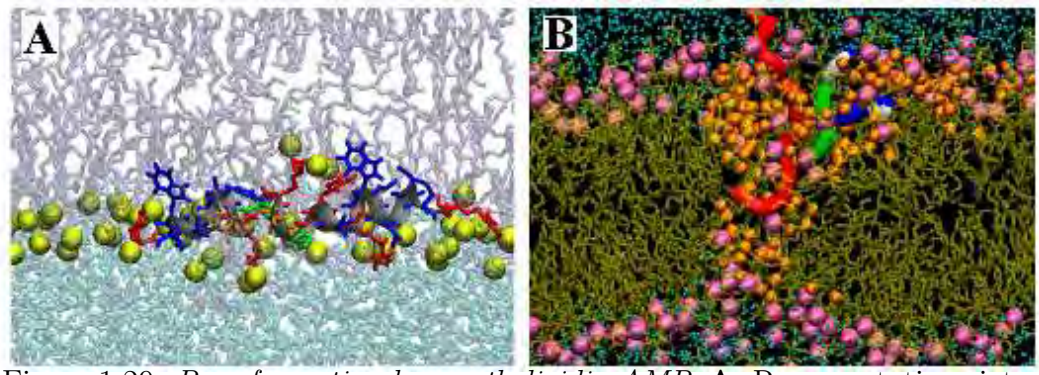

Figure 1.29: *Pore formation by a cathelicidin AMP.* **A.** Representative picture of the interaction of PMAP-23 inside the bilayer. **B.** Side view of the pore formed. The peptides that participate in the pore are depicted as ribbons, where basic residues are in dark blue, polar in green and non-polar in white. The ilustration is taken from Orioni 2009 and Jean François 2008.

To conclude, the MD simulations described here have helped in the interpretation of the basics of the activity of AMPs upon membrane surface. It is clear that the MD methodology has proved to be a very useful tool to provide atomistic details of the action of these peptides, and therefore it has extensively used in the research carried out in this thesis.

Chapter 2

Methodology

2.1 Solid-Phase Peptide Synthesis

Solid-phase synthesis is a simple and convenient methodology for the preparation of peptides. While synthesis in involves a time-consuming and labor-intensive process, solid-phase synthesis is much easier and has even been automatized.

The solid-phase peptide synthesis (SPPS) was conceived and elaborated by R. B. Merrifield in 1963, who was awarded with the Nobel Prize in 1984 (Merrifield 1963, Merrifield 1986). Nowadays, SPPS is the most applied methodology for the preparation of peptides. The main concept of SPPS is that suitably N^{α} and side-chain protected amino acids are added stepwise in the C $\rightarrow$ N direction onto a solid support. As shown in Figure 2.1, SPPS involves 4 main steps:

1. **Covalent attachment of the first amino acid** onto the insoluble polymeric support. The solid support usually incorporates a linker to facilitate the peptide cleavage after the synthesis (see further features in section 2.1.2). The amino acids are incorporated with the α-amino group conveniently protected. The side-chain functional group of trifunctional amino acids also requires the adequate protection.

2. **Selective deprotection** of the α-amino group of the first amino acid (aa_i, where $i = 1$).

3. **Consecutive cycles of coupling and α-amino group deprotection** are performed until the desired peptide sequence is achieved.

4. **Final deprotection and cleavage of the peptide from the support**. Once the chain elongation has been accomplished, it is necessary to remove the α-amino protecting group of the last amino acid incorporated. Then, the peptide is cleaved from the support.

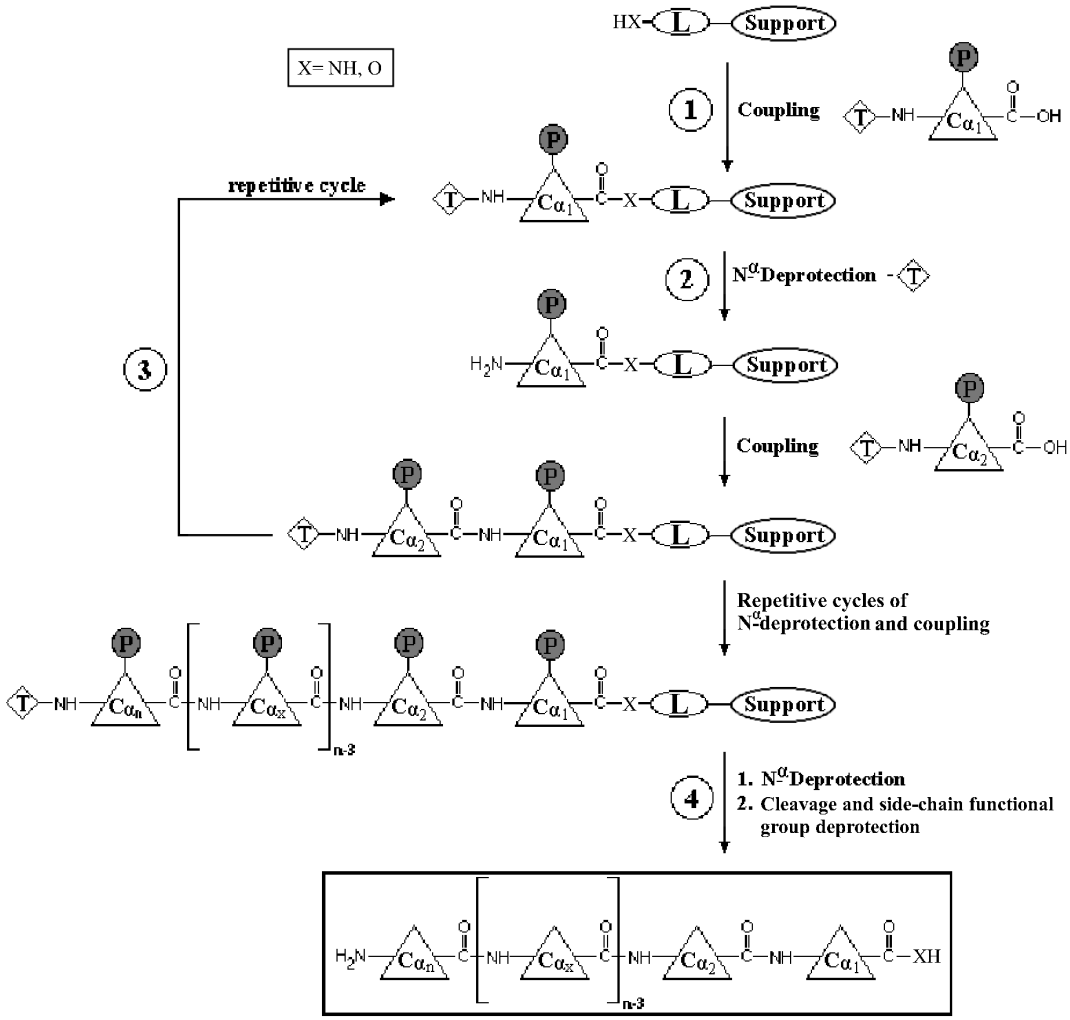

Figure 2.1: *Stepwise solid-phase synthesis of linear peptides.* **Support**: insoluble polymeric matrix; **L**: linker or spacer; $\mathbf{C}_\alpha$: α-carbon; **P**: side-chain protecting group; **T**: N^α-amino protecting group.

2.1.1 Polymeric Support

The solid support consists of an insoluble filterable polymer with an adequate mechanical stability and with desirable physicochemical properties to facilitate solid-phase synthesis. In particular, a solid support must i) be composed of mechanically robust particles of consistent and convenient shape and size; ii) be inert to all reagents and reactions conditions; iii) allow fast solvent and reagent diffusion; iv) have good swelling properties in the solvents used; and v) be conventiently functionalized to enable the anchoring of the linker or the first amino acid (Miranda 2000). In this thesis we have used two supports, resin and SynPhase® lanterns.

2.1.1.1 Resin

Resins are one of the most used solid supports for SPPS. They are composed of small polymeric beads, being cross-linked polystyrene (PS, see Figure 2.2 A), polyacrylamide, and polyethylene glycol (PEG) grafted onto a cross-linked polystyrene the most common ones (Kates 2000). These resin beads have a loading typically around 0.2-1.0 mmol/g. These dry polymer beads have an average diameter of about 50 μm, but they swell up to 2.5 to 6.2 fold in volume in the solvents used (Sarin 1980). Thus, the chemistry takes place within a well-solvated gel containing a mobile and reagent-accessible chain.

In this work, 4-methylbenzhydrylamine (MBHA) resin has been used for the synthesis of the peptides (Figure 2.2 B). This resin is made of polystyrene crosslinked with 1% of divinylbenzene (DVB). It shows excellent swelling properties with aprotic polar solvents, such as acetone, CH_3CN, CH_2Cl_2 or *N,N*-dimethylformamide (DMF).

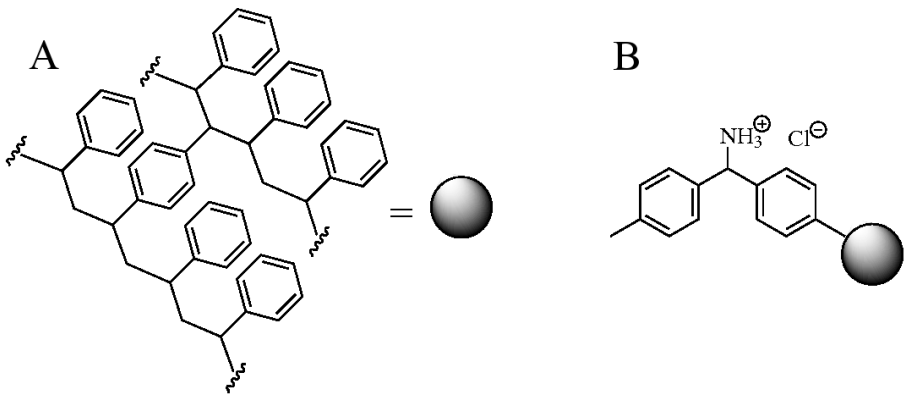

Figure 2.2: *MBHA resin.* **A.** Copolymer matrix made of polystyrene cross-linked with 1% of DVB. **B.** MBHA resin.

2.1.1.2 SynPhase® lanterns

SynPhase® lanterns are macroscopic solid support (Parson 2003), which have been found to be a practical alternative to conventional polystyrene resins because they offer the advantage of easy handling and simple washing (Ryba 2009). As depicted in Figure 2.3 A, they are made of a mobile surface polymer grafted onto a rigid unreactive polyethylene polymer. The mobile surface polymer may consist of polystyrene or polyamide. Polystyrene lanterns are hydrophobic and solvate well in most solvents used in organic synthesis except in low molecular weight alcohols. They are available in three different sizes, L-series, D-series and A-series, with a loading of 15, 35 and 75 μmol, respectively (Figure 2.3 B). On the other hand, polyamide lanterns are preferable for hydrophilic applications due to their compatibility with solvents such as water and polar alcohols. In this case, only D-series are available with a loading of 8 and 18 μmol. SynPhase® lanterns can be easily attached to stems and arranged into a standard 96-well plate for parallel synthesis or/and cleavage. This makes them a convenient support for the solid-phase synthesis of peptide libraries.

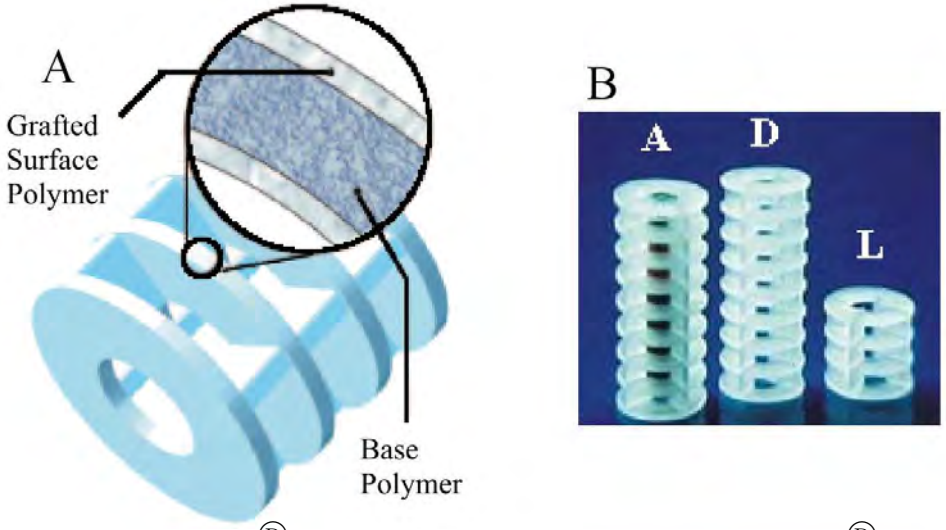

Figure 2.3: *SynPhase® lanterns.* **A.** Composition of SynPhase® lanterns **B.** Available polystyrene lanterns: A-series (75 μmol), D-series (35 μmol) and L-series (15 μmol).

2.1.2 Linker

The linker is a bifunctional molecule that plays a key role in a solid-phase synthesis strategy. One side of the molecule is irreversibly anchored to the solid support, while the other side serves as attachment point for the first amino acid.

The latter behaves as a cleavable protecting group facilitating the final release of the peptide (Kates 2000). Owing to the fact that it temporary links the peptide to the solid-phase, it must be stable to the synthesis conditions and it has to allow the peptide cleavage under mild conditions. There have been reported a wide variety of linkers that can be classified according to the cleavage conditions. Some of them are exposed in Figure 2.4 and their respective conditions in Table 2.1. In this thesis the Rink amide linker was used for the synthesis of the peptides.

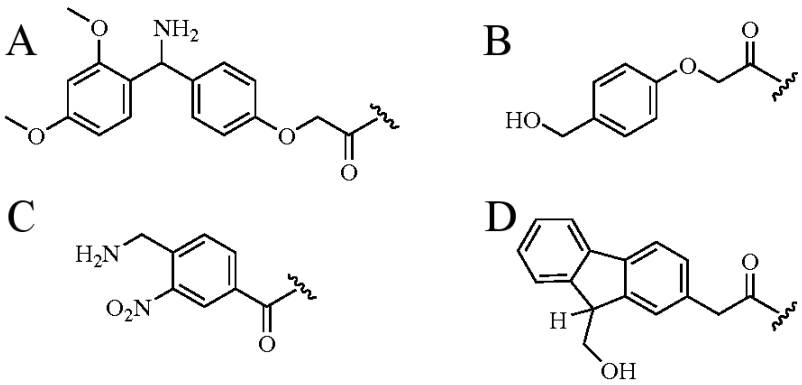

Figure 2.4: *Types of linkers.* **A.** Rink amide **B.** PAC **C.** Nonb and **D.** HMFA.

Table 2.1: Representative linkers used for SPPS.

Figure	Name	Cleavage Conditions	Resulting C-terminus
A	Rink	TFA	Amide
B	PAC	TFA	Acid
C	Nonb	ν (350 nm)	Amide
D	HMFA	Piperidine	Acid

2.1.3 Protection Schemes

The protection of amino acid functional groups that are not involved in the reaction is crucial for SPPS. The protecting groups must be easily introduced, stable to the reaction conditions, not add any additional reactivity, and safely removed (Isidro-Llobet 2009).

At least two levels of protecting-group stability are required for SPPS: "temporary" and "permanent". "Temporary" protecting groups are used for the N^{α}-amino group. Once the amino acid is anchored to the support, the temporary

protecting group is removed to attach the following amino acid (see step 2-3 in Figure 2.1, T). "Permanent" protecting groups, are used fo the side-chain functionality of trifunctional amino acids. They are present along the peptide synthesis to prevent branching or other side reactions and are usually removed during the cleavage step (see step 4 in Figure 2.1, P).

"Temporary" and "Permanent" protecting groups are usually orthogonal. This allows the removal of a specific protecting group in the presence of the other classes and in any order. Orthogonal protection schemes offer the possibility of using substantially milder overall conditions, because selectivity can be attained on the basis of differences in chemistry rather than in reaction times. The most common orthogonal strategy for SPPS is the Fmoc/^{t}Bu (Carpino 1970) (see Figure 2.5 and Table 2.2. For a further protecting group read Grant 2002).

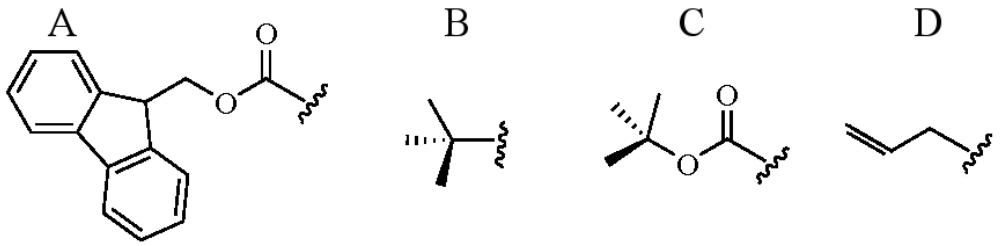

Figure 2.5: *Types of protecting groups.* **A.** Fmoc **B.** tBu and **C.** Boc.

Table 2.2: Representative orthogonal protection strategies and removal conditions.

Figure	**Name**	**Removal**
A	9-fluorenylmethoxycarbonyl (Fmoc)	Piperidine or DBU
B	*tert*-Butyl (tBu)	95 % TFA
C	*tert*-Butyloxycarbonyl (Boc)	95 % TFA
D	Allil	$Pd(PPh_3)_4$

2.1.4 Formation of the Peptide Bond; Coupling Reagents

Coupling reagents are necessary to allow the formation of the amide bond under mild conditions. In a typical amino acid coupling, the carboxylic acid moiety of the residue *i* is first activated by an appropiate coupling reagent, and then reacted with the amine moiety of the residue *i+1* to produce a desired peptide. A wide

palette of coupling reagents exists, being the most commonly used carbodiimides, phosphonium and amminium salts (Figure 2.6 A-C).

For the couplings performed with phosphonium or amminium salts, the presence of a base to deprotonate the carboxylic acid is necessary. The most common are tertiary amines such as *N,N*-diisopropylethylamine (DIEA) and *N*-methylmorpholine (NMM) (Figure 2.6 D). Moreover, additives such as HOBt or HOAT are used to minimize undesired racemisation and other side reactions (Figure 2.6 E).

Typically, in solid phase synthesis the formation of the peptide bond can be monitored by the Kaiser test. This colorimetric test is based on the detection of free primary and secondary amines. If the test is positive (blue colour) indicates the presence of free α-amino groups and that the reaction was not completed. On the other hand, if the test is negative (yellow colour) the coupling is completed and the synthesis can be continued.

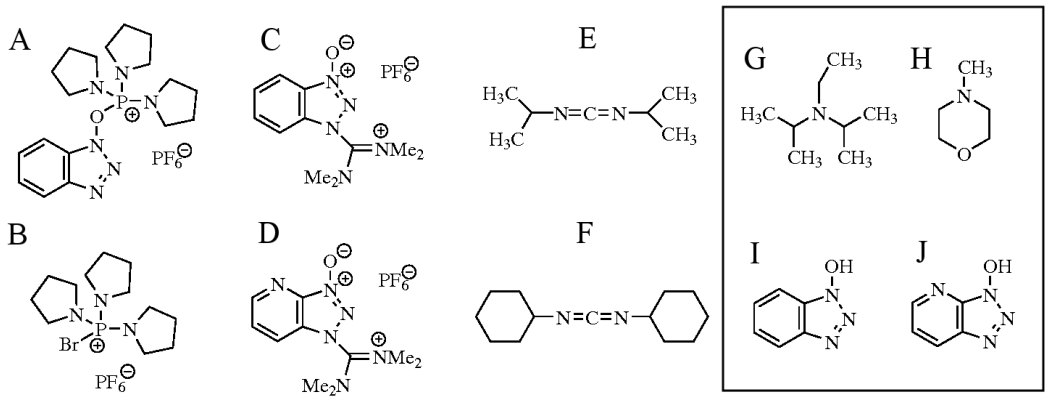

Figure 2.6: *Representative coupling reagents and additives for SPPS.* **A-B** Phosphonium salts, PyBOP and PyBrOP. **C-D.** Amminium salts, HBTU and HATU. **E-F.** Carbodiimides, DIC and DCC. **G-H.** Bases, DIEA and NMM. **I-J.** Additives, HOBt and HOAt.

2.2 Molecular Modeling

The field of Molecular Modeling comprehends all methodologies and techniques devoted to mimic the behavior of molecular systems. There is a plethora of models to describe the molecules at the atomistic level, from the first drawn representations of chemical structures of 19^{th} century to the most accurate electronic structure methods. Which one is more appropriate essentially depends on the size of the system to be considered, the required accuracy and particularly

on the kind of physicochemical phenomenon to be modeled (a photochemical process, a chemical reaction, a physical event such as a protein folding, etc...).

The most accurate methods are rooted on the laws of quantum mechanics and deal with all electrons and nuclei of the molecular system. By solving the corresponding Schrödinger equation of the system, a detailed picture of the electronic motion can be obtained. However, the computational cost of these methods often prevents their use for the modeling of large systems, especially when the environment is also included in the system. For large systems consisting of hundreds to thousands of atoms where no chemical reactions take place the most efficient methods used in Molecular Modeling studies are those based upon Classical (Newtonian) Mechanics. Since the scope of this thesis is the study of the behavior of cyclic antimicrobial peptides upon lipid membranes in water phase, we will focus solely on Molecular Mechanics models.

2.2.1 Basis of Molecular Mechanics

Molecular Mechanics (MM) models describe atoms as (fractional) point charges with an associated mass, therefore ignoring the electrons and their quantum nature. The chemical bonds are explicitly introduced (hence can not be broken) by spring-like models and the atomic interactions are described by classical electrostatic and van der Waals forces. By ignoring the electronic motion, the Potential Energy, E_{tot}, of the system is obtained as a simple analytical function that depends on all 3N nuclear coordinates, ($\vec{R}$), of the system.

$$E \equiv E_{tot}(\vec{R}), \tag{2.1}$$

This function is built from a set of parameters that typically include equilibrium bond lengths and angles, their associated force constants, partial atomic charges and van der waals radii. The values of these parameters are chosen in order to reproduce either experimental or theoretical data (often derived from more accurate electronic structure methods). The set of parameters and the corresponding functions that describe the bonded and non bonded interactions is known as Force Field, a concept borrowed from vibrational spectroscopy, which considered the forces acting between every pair of atoms in the molecule.

2.2.1.1 Force field

The force field defines the potential energy (E_{tot}) as a sum of different terms

$$E_{tot}(\vec{R}) = E_{str}(\vec{R}) + E_{bend}(\vec{R}) + E_{tors}(\vec{R}) + E_{vdW}(\vec{R}) + E_{elec}(\vec{R}), \tag{2.2}$$

that account for the deviation of the bond lengths and angles from their equilibrium values (stretching and bending, E_{str} and E_{bend}, respectively), the energy change upon rotation of the bonds (torsion, E_{tors}). Furthermore, there are energy contributions associated to non-bonded interactions in terms of electrostatic (E_{elec}) and van der Waals (E_{vdW}) interactions. See Figure 2.7 for a pictorial representation of all terms on eq.2.2.

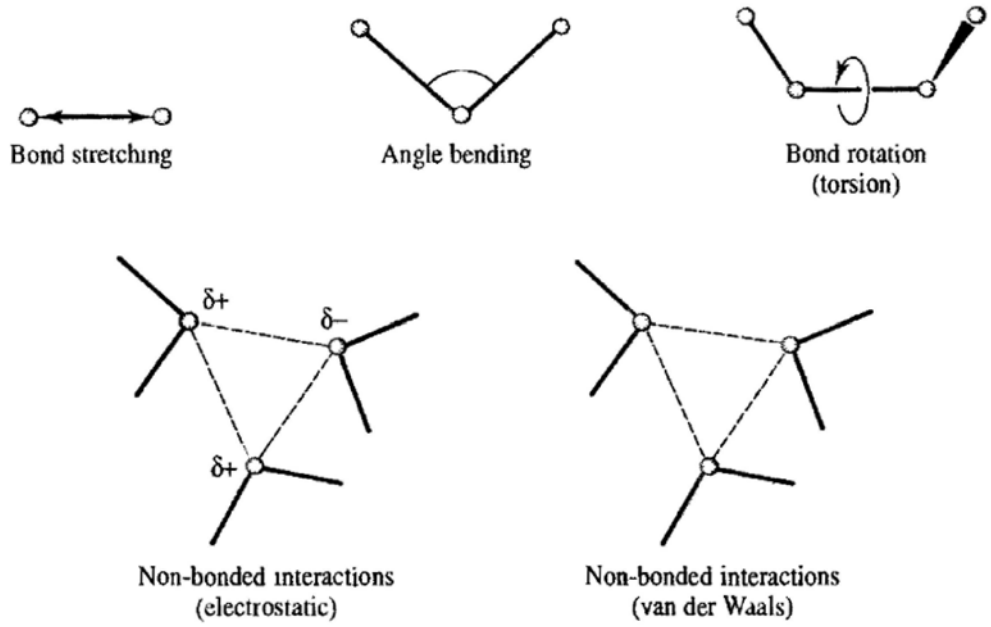

Figure 2.7: *Schematic representation of the five key contributions to a molecular mechanics force field.* On top, bond stretching, angle bending and torsional terms. On the bottom, non-bonded interactions, electrostatic and van der Waals. The picture has been taken from Leach 2001.

Stretching energy is the energy contribution associated to the deviation of the internuclear distances of all bonded atoms pairs away from their equilibrium distances. For each bonded atom pair, this energy is typically described by a quadratic function of the internuclear distance (harmonic approximation), even though quartic equations or other functions such as Morse potential[1] can also be used. As mentioned, the simplest expressions originate from a harmonic potential, which for a pair of bonded atoms A and B depends solely on the interatomic distance R_{AB} and reads

$$E_{harm}(R_{AB}) = k^{AB}(R_{AB} - R^0_{AB})^2, \tag{2.3}$$

[1]Morse potential seldom used in molecular mechanics force field. This is partly because it is not particulary amenable for efficient computation, but also because it requires three parametres to be specified for each bond (further discussion see Leach 2001)

where the parametres R^0_{AB} and k^{AB} represent the equilibrium internuclear distance and the force constant of the bond, respectively. The overall streching energy is obtained by summing over all pairs of bonded atoms of the system

$$E_{str} = \sum_{A,B}^{bonded} E_{AB} = \sum_{A,B}^{bonded} k^{AB}(R_{AB} - R^0_{AB})^2. \tag{2.4}$$

Bending energy is associated to the deviation of the angle (θ_{ABC}) between three bonded atoms A-B-C from their reference value. Similarly to the stretching, the bending energy is typically described by a quadratic function of the bond angle

$$E_{ABC}(\theta_{ABC}) = k^{ABC}(\theta_{ABC} - \theta^0_{ABC})^2, \tag{2.5}$$

where θ_{ABC} and k^{ABC} represent the equilibrium bond angle and the associated force constant. The overall bending energy is again obtained by summing over all triads of bonded atoms of the system

$$E_{bend} = \sum_{A,B,C}^{bonded} E_{ABC} = \sum_{A,B,C}^{bonded} k^{ABC}(\theta_{ABC} - \theta^0_{ABC})^2. \tag{2.6}$$

Torsional energy. For a quartet of consecutively bonded atoms A-B-C-D, there is an energy change associated to the rotation around their torsion or dihedral angle ω_{ABCD}. The dihedral angle (see Figure 2.8, left), is defined as the angle between the planes that contain atoms A,B,C and B,C,D. The function that describes this energy contribution must be periodic, and its shape must also depend on the type and multiplicity of the central B-C bond,

$$E_{ABCD}(\omega_{ABCD}) = V^{ABCD}(1 + cos(n\omega_{ABCD})), \tag{2.7}$$

where V^{ABCD} and n account for the force constant and the (integer) multiplicity associated to this particular torsion.

Furthermore, in some cases a different torsion contribution can be included to keep the planarity around a certain atom. In this case, a central atom B is bonded to the three remaining atoms as depicted in the right side of Figure 2.8. The angle that measures the deviation from planarity is defined in the force field as an "improper" torsion angle. These energy terms are typically included in the force field in order to keep planarity of aromatic rings or to prevent molecules from flipping over their mirror images. This additional term can be described by a harmonic potential depending on the dihedral angle in form

$$E^{imp}_{B,ACD}(\xi_{B,ACD}) = k^{B,ACD}(\xi_{B,ACD} - \xi^0_{B,ACD})^2, \tag{2.8}$$

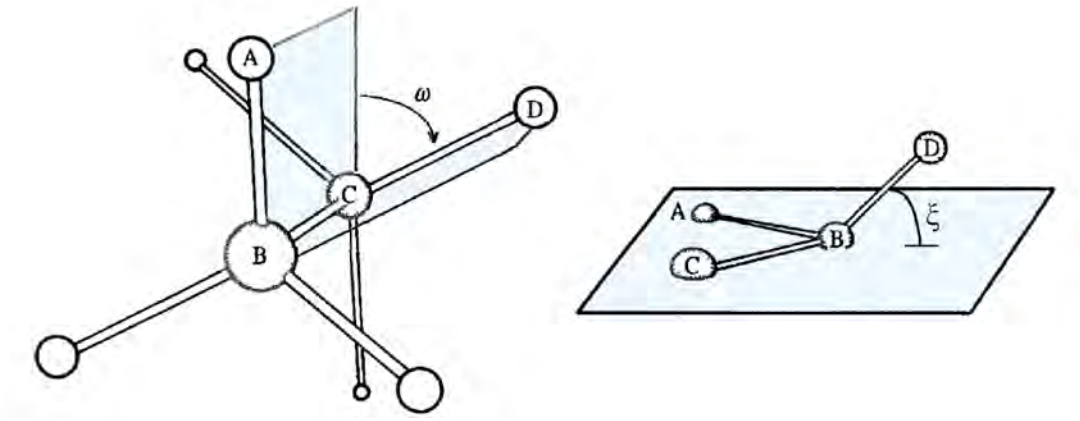

Figure 2.8: *Models to torsion contribution.* On the left the torsion angle, or dihedral angle, amongst four consecutive atoms. On the right, improper dihedral angle.

The total torsional energy is achieved by summing up the energy terms associated to all dihedral and improper angles defined in the system.

$$E_{tors} = \sum_{A,B,C,D}^{bonded} E_{ABCD}(\omega_{ABCD}) + \sum_{A,B,C,D}^{improper} E^{imp}_{B,ACD}(\xi_{B,ACD}). \tag{2.9}$$

Non-bonded energy contributions do not depend upon an explicit bonding relationship between the atoms. Instead, they are "through-space" interactions and are usually modeled as a function of some inverse power of the interatomic distance, as derived from the classical multipole expansion of a charge distribution. The electrostatic interactions are between the atoms originate from their fractional charges and are calculated using the classical pairwise-additive Coulomb's Law

$$E_{el} = \sum_{A,B}^{atoms} \frac{1}{4\pi\varepsilon_0} \frac{q_A q_B}{R_{AB}}, \tag{2.10}$$

where q_A and q_B represent the partial charges of the atoms A and B, R_{AB} the respective interatomic distance and ε_0 the vaccum permitivity or dielectric constant.

On the other hand, van der Waals interactions account for the the attractive or repulsive forces between non-bonded atoms which have no electrostatic origin. These include interactions between two permanent dipoles, between a permanent dipole and a induced dipole, and between two instantaneously induced dipoles, the so-called London dispersion. The isotropic part of the energy associated to these interactions is typically described by pairwise-additive Lennard-Jones

potentials between all pairs of non-bonded atoms of the system as

$$E_{vdW} = \sum_{A,B}^{non-bonded} \varepsilon_{AB} \left[\left(\frac{R^0_{AB}}{R_{AB}} \right)^{12} - 2 \left(\frac{R^0_{AB}}{R_{AB}} \right)^{6} \right], \tag{2.11}$$

where ε_{AB} is the depth of the potential well, R^0_{AB} the van der Waals distance and R_{AB} the distance between non-bonded atoms. Van der Waals forces are relatively weak compared to the electrostatic or those originating from covalent chemical bonds but they play a key role in accounting for hydrophobic interactions, for instance, so they are an essential part of the force field.

All these functions and their corresponding adjusted parameters constitute the "force field" by which the potential energy of a system is calculated. The parametrization of the force fields is based on experimental or theoretical data, with the aim of reproducing the real properties of the molecules. For this reason, specific force fields for different types of molecules exist, such as hydrocarbons, proteins, nucleic acids or carbohydrates, amongst others. Furthermore, in the case of peptides it is worth to note that each amino acid is typically described with different parameters for every atom, bond, bond angle, torsion, etc.

2.2.2 Molecular Dynamics

Molecular mechanics allows the study of the potential energy surface of the system. The main application is the location of stationary points (local minima) by means of geometry optimization methods. These structures can be put into correspondence with stable conformers/configurations of the system, that are assumed to be in equilibrium with each other.

The conformational analysis is useful for obtaining a "static picture" of the system while Molecular Dynamics (MD) technique provides information about the dynamic behavior of the system, giving insight into molecular motion on an atomic scale, with the inclusion of temperature or pressure effects. MD is rooted on the principles of statistical mechanics and on the ergodic hypothesis, by which ensemble averages, connected with the macroscopic properties, are estimated from time averages of the system. The time evolution of the particles of the system can be derived from Newton's mechanics or from the time-dependent Schrödinger equation, fully accounting for quantum effects. In the so-called classical Molecular Dynamics simulations, the motion of the atoms are determined by integrating Newton's Law of motion. The result is a "trajectory" that describes how the positions and velocities of the particles of the system vary with time.

The Newton's law establishes the relationship between the exerted force on a given particle i and its acceleration through its inertial mass

$$F_i = m_i \cdot a_i = m_i \frac{d^2 r_i(t)}{dt^2}, \tag{2.12}$$

The force can be then derived from the gradient of the potential energy, which in the case of classical MD simulations is readily obtained from the force field

$$F_i = -\frac{dV(r_1 ... r_N)}{dr_i}, \tag{2.13}$$

2.2.2.1 Integration methods

In a system of N particles, the force exterted on a given particle, depends upon the position of all particles of the system. The force, and hence its acceleration, will change whenever the particle changes its position, or whenever any of the other particles of the system with which it interacts moves. Under such influence, the motion of all particles is coupled, giving rise to a complex system of differential equations that can not be solved analyticaly. Therefore, the eq.2.12 for every particle of the system is integrated numerically over an interval of time to obtain the corresponding velocities and position of the particles. All integration algorithms approximate the time evolution of the position and velocities of the particles by Taylor series expansion around an initial set of atomic coordinates and distribution of velocities.

$$\vec{x}(t + \delta t) = \vec{x}(t) + \vec{v}(t)\delta t + \frac{1}{2}\vec{a}(t)\delta t^2 + ... \tag{2.14}$$

$$\vec{v}(t + \delta t) = \vec{v}(t) + \vec{a}(t)\delta t + ... \tag{2.15}$$

where

$$\vec{x}(t) = (x_1(t), x_2(t), ..., x_n(t)) \tag{2.16}$$

and

$$\vec{v}(t) = (v_1(t), v_2(t), ..., v_n(t)) \tag{2.17}$$

represent the positions and velocities of all the particles of the system at time t. The set of equations are discretized and numerically solved by choosing a time step $\Delta t > 0$ and a sampling point sequence $t_n = n \cdot \Delta t$ with the aim of constructing a sequence of points $\vec{x}_n$ and $\vec{v}_n$ that follow as close as possible the respective points $x_n(t_n)$ and $v_i(t_n)$ on the trajectory of the exact solution.

A number of different algorithms to integrate the equations of motion exist. Some typically used are Verlet and Leap-frog algorithm. The former uses the

position and the acceleration at a time t, and the positions of t - Δt to calculate the new positions at time $t + \Delta t$

$$\vec{x}(t + \Delta t) = 2\vec{x}(t) - \vec{x}(t - \Delta t) + \vec{a}(t)\Delta t^2, \tag{2.18}$$

Therefore, the Verlet algorithm makes no explicit use of the velocities. Since they are often necessary, for instance for the calcualtion of kinetic energy, they can be derived for the position terms or obtained using a Velocity Verlet algorithm.

On the other hand, in the leap-frog algorithm, the velocities are first calculated at time $t + \frac{1}{2}\Delta t$, and these are used to calculate then the positions at time $t + \Delta t$

$$\vec{x}(t + \Delta t) = \vec{x}(t) + \vec{v}\left(t + \frac{\Delta t}{2}\right) \cdot \Delta t, \tag{2.19}$$

$$\vec{v}\left(t + \frac{\Delta t}{2}\right) = \vec{v}\left(t - \frac{\Delta t}{2}\right) + \vec{a}(t)\Delta t, \tag{2.20}$$

In this algorithm the velocities leap over positions and then the positions over velocities and so on. The velocities at a given time t can be approximated by

$$\vec{v}(t) = \frac{1}{2}\left[\vec{v}\left(t - \frac{\Delta t}{2}\right) + \vec{v}\left(t + \frac{\Delta t}{2}\right)\right], \tag{2.21}$$

A critical parameter of the trajectory is the integration time step, Δ t. It affects both actual time scale the simulation is able to reach (large enough to effectively sample the whole phase space of the system), but also the accuracy of the integration (short enough to ensure the conservation of the total energy). In the case of atomistic simulations, the time step is typically chosen around 1-2 fs (1 fs=10^{-15} s). This value may be increased by using algorithms such as SHAKE (Ryckaert 1977) or LINCS (Hess 1997) which restrict the oscillatory motion of the fastest atoms.

2.2.3 Design Constraints in Molecular Dynamics Simulations

The conditions applied in the system play a key role in the results of a MD simulation. In order to achieve a realistic behaviour of the model system, different conditions must be taken into account. Some of them are listed below

2.2.3.1 Periodic boundary conditions

Periodic Boundary Conditions (PBC) are applied to minimize the edge effects in a finite system. The atoms of the system to be simulated are placed into a space-filling box, which is surrounded by translated copies of itself (see Figure 2.9) in

the three dimensions. Thus, a particle leaving the simulation cell through one side re-enters through the opposite face. In molecular dynamics simulations of biological systems PBC are usually applied to simulate solvated molecules in a bath of explicit solvent.

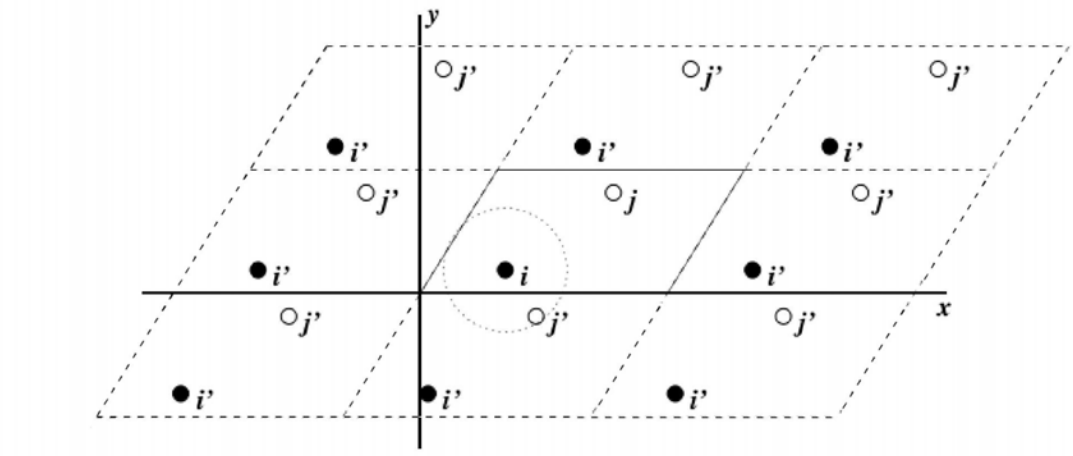

Figure 2.9: *Periodic Boundary Conditions in two dimensions.*

An important factor to take into account is the size of the simulation box. It must be large enough to prevent artifacts such as a macromolecule interacting with its own image in a neighboring box, that can lead to highly unphysical dynamics. Also, a minimum image convention is usually applied so that the actual distance between two particles is taken as the shortest distance between their periodic images. When computing short-range intermolecular energy contributions, a cutoff distance is introduced used that must not exceed half the lengh of the simulation box. Therefore, only particles separated by a distance less than the cut-off distance contribute to the calculated energy or forces.

$$R_c < \frac{1}{2} min(\| a \|, \| b \|, \| c \|), \tag{2.22}$$

2.2.3.2 Electrostatic interactions

The long-range electrostatic interactions play a dominant role in protein structural stability and are also crucial determinants in the initial encounter of many association processes. Usually in MD a huge number of atoms are present in the simulation so that the evaluation of their electrostatic interactions are often the most time-consuming part of the simulation. Since the strength of the electrostatic interaction decreases slowly with r^{-1}, special techniques such as the Ewald sum, reaction field, or particle-mesh methods need to be applied, as the interaction extends well past half the length of the simulation box . The goal of

these truncation methods is to calculate the interactions only between the atoms that reside closer to each other than a predefined cut-off distance.

2.2.3.3 Temperature and pressure coupling

The control of the temperature and/or pressure during the time course of a MD simulation is essential to ensure proper and stable fulfillment of the conditions of the appropriate statistical ensemble. There are different statistical ensemble that require different macroscopic environmental constraints of thermodynamic parameters of the system, such as the total energy (E), the number of particles (N), the volume (V), pressure (P) or temperature (T). For instance, the so-called NVE or microcanonical ensemble represents a system thermodynamically isolated with a constant number of particles, volume and energy. Unfortunately, the microcanonical ensemble does not correspond to the conditions under which most experiments are carried out so if one is interested simulating the system at specific temperature, an appropriate thermostat is required.

In MD simulations, the constant pressure and temperature ensemble (NPT or isothermal-isobaric ensemble) has been considered suitable for a variety of physical systems (Tieleman 1996, Tobias 1997), including biomolecules and biomembranes. Since the instantaneous value of the temperature is related to the kinetic energy of the particles, in order to achieve constant temperature during the time course of the simulation, the velocities of the particles need to be re-scaled. This is the idea behind the algorithm of Berendsen.

Berendsen temperature coupling mimics weak coupling with first-order kinetics to an external heat bath with a given temperature T_0. The velocities of the particles are scaled at each step, such that the rate of change of temperature is proportional to the difference between the instantaneous temperature and that of the bath as

$$\frac{dT}{dt} = \frac{T_0 - T}{\tau}, \tag{2.23}$$

where τ is a time constant or coupling parameter, that determines the strength of the coupling of the system and the bath. This method gives an exponential decay of the system towards the desired temperature (for further details see Berendsen 84).

Berendsen pressure coupling algorithm uses the same strategy to scale the instantaneous pressure of the system with a given reference pressure P_0

$$\frac{dP}{dt} = \frac{P_0 - P}{\tau_P}, \tag{2.24}$$

2.2.3.4 Solvation

A correct representation of the biomolecule's environment is important for modeling its properties. The solvent, typically water, plays a fundamental role in the structure and dynamics of proteins in the nature. The solvation effects can be simulated either implicitly or explicitly. The explicit inclusion of water molecules in the system gives a more realistic description of the hydrogen bonding interactions of the solvent with the biomolecule, for instance, but requires the inclusion of typically ten times more particles in the simulation, which translates in a much higher computational cost. There is a wide range of explicit water models available, being the so-called TIP3P, TIP4P, SPC and SPC/E the most popular ones.

It is important to note that when simulating a biomolecule surrounded by water in a large box, a considerable portion of the computation time will be spent evaluating the solvent-solvent interaction, which is not too relevant for the biomolecule itself. To avoid this the explicit molecules of solvent can be replaced by a continuous medium by modifying the dielectric constant of the media. One of the most used methods of implicit solvent is the Generalized Born model. It is worth to note that, besides the lack of explicit hydrogen bonding interactions, implicit solvent models do not account for entropic effects of the solvent (fail to describe the hydrophobic effect), and typically tend to overestimate the electrostatic energy of charged groups in nonpolar environments.

Chapter 3

Objectives

The antecedents of the present work have been detailed in section 1.4. The starting point of this thesis was a first-generation library of *de novo* cyclic peptides of 4 to 10 residues, which showed high antimicrobial activity against two plant pathogenic bacteria (*P. syringae* and *X. vesicatoria*). The most active peptide of this library was the decapeptide BPC16 (Monroc 2006a). The first part of this work focused on this cyclic peptide.

The first objective was the **optimization of the synthesis of BPC16 in different solid supports**. In particular the use of SynPhase lanters would be of special interest for handy solid-phase synthesis of peptide libraries. This organic synthetic work was carried out in the laboratory of the LIPPSO group of the University of Girona.

At the same time, at the Institute of Computational Chemistry of the University of Girona we undertook our first computer simulations, with the aim of **establishing the conformational preferences of peptide BPC16, and evaluating its dynamic stability in different environments**. For this first computational project we applied MM and MD techniques and used AMBER software.

Subsequently, a second-generation library of cyclic decapeptides was designed and prepared by the LIPPSO group (Monroc 2006b). In this improved library several peptides also exhibited antimicrobial activiy against another bacteria (*E. amylovora*), as well as a hemolitic activity lower than that of BPC16. Moreover, the anticancer activity of the library was also evaluated. Several peptides displayed high cytotoxic activity and low hemolytic activity (Feliu 2010).

As a part of the anticancer assays it was of particular interest **to evaluate the stability in human serum of several cyclic antimicrobial peptides with anticancer activty**.

After this second library was available, more ambitious objectives were proposed, with the ultimate goal of conceiving a general strategy for designing new cyclic antimicrobial peptides with improved activity. The main question to be answered was: **how the active peptides interact and permeabilize anionic membranes?**.

From the experimental point of view, the techniques based on fluorescence spectroscopy are very useful for mechanistic studies, and in particular to explore the interaction of the peptides upon membranes. This motivated the **synthesis of a Trp-containing analogue library, and the evaluation of the effect of the replacement of the phenylalanine for tryptophan amino acid on the activity and stability of the peptides**.

From a computational point of view, the first goal was to **shed light on the molecular basis at atomistic resolution of the mechanism of action of active cyclic peptides upon single lipid membrane models**. To this end, extensive MD simulations were carried out in collaboration with the MD Group of the University of Groningen, using in this case GROMACS software. All studies focused on the most active peptide of all libraries, namely the cyclic decapeptide BPC194.

At the same time, research performed by Poolman's group of the University of Groningen provided experimental evidence that the BPC194 peptide was able to induce both poration and fusion of vesicles. Thus, another major goal of this Thesis was the **computational confirmation of this dual action of the peptide upon anionic membranes by the examination of its ability to induce fusion on double bilayer membrane models**.

It is manifest that this Thesis combines both experiment and computer simulations and benefits from both. After the milestones enumerated above were achieved, we were in position to undertake the final ambition of this Thesis which was the **rational design and synthesis of new BPC194 analogues with improved antimicrobial activity**.

Chapter 4

Synthesis of Cyclic Peptides and Evaluation of their Biological Activity

This part of the thesis has been carried out at the LIPPSO group of the University of Girona. The work was centered on the family of cyclodecapeptides with general structure c(X_5-K-X_3-Q), being X= lysine or leucine, previously described in the group (Monroc 2006a and Monroc 2006b).

First, this thesis focused on the optimization of the synthesis of the cyclic peptide BPC16 (c(KLKLKFKLKQ)), the best candidate from the first generation of cyclic peptides (Monroc 2006a). Then, a library of cyclodecapeptides with general structure c(X_5-W-X_3-Q), with X=lysine or leucine, was synthesized and screened for antibacterial and hemolytic activities[1]. The influence of replacing the phenylalanine by a tryptophan was analyzed. Finally, the stability in human serum of some selected phenylalanine-containing cyclic peptides was studied.

[1]Since the mechanism of action of AMPs consists of cell membrane disruption, toxicity to animal or plant cells (cytotoxicity) may be a problem. This cytotoxicity can be assessed with animal or plant cell model systems, with erythrocytes being more frequently used due to the easier comparison with cells used in existing reports. Thus, the toxicity of the peptides to eukaryotic cells was determined as the ability to lyse erythrocytes in comparison to the toxicity of melittin.

4.1 General Strategy for the Solid-Phase Synthesis of Cyclic Peptides

The general strategy for the solid-phase synthesis of the cyclic peptides consisted of the preparation of the linear sequence followed by head-to-tail cyclization. A three-dimensional orthogonal Fmoc/Boc/Allyl strategy was used (Albericio 2000, Kates 1993). The Fmoc was the temporary α-amino protecting group, whereas Boc and Allyl groups served as permanent protection of the ε-amino group of the lysine residues and the α-carboxylic group of the glutamic acid, respectively.

In Scheme 4.1 is exposed the general strategy used for the synthesis of the cyclic peptides. First, a conveniently protected glutamic acid residue (Fmoc-Glu-OAl, step 1) was coupled to the solid-support through its side-chain carboxylic group. The linear sequence was then elongated by sequential Fmoc removal and coupling steps (Scheme 4.1, step 2 and 3). Once the protected-linear sequence was achieved, the allyl and Fmoc groups were removed (steps 4 and 5).

Finally, the head-to-tail cyclization followed by cleavage afforded the cyclic peptide (step 6 and 7). Note that at the end of the synthesis the glutamic acid residue results in a glutamine due to the amino functionalization of the Rink linker.

4.2 Optimization of the Synthesis of the Cyclic Peptide BPC16

The key step of the synthesis of a cyclic peptide is the cyclization. Even though intramolecular reactions usually proceed faster than intermolecular bond formations, competing side reactions such as dimerization or cyclodimerization can occur (Malesevic 2004). In LIPPSO group, MBHA has been widely used as a common support phase for synthesis of cyclic peptides. On the other hand SynPhase® lanterns are more handy and makes them a convenient support for the solid-phase synthesis of peptide libraries.

For these reasons, we studied the synthesis of the cyclic peptide c(KLKLKFKLKQ) (BPC16) using MBHA resin and SynPhase® lanterns as solid supports. Moreover, different parameters were taken into account for the cyclization step such as dilution, coupling reagents or temperature.

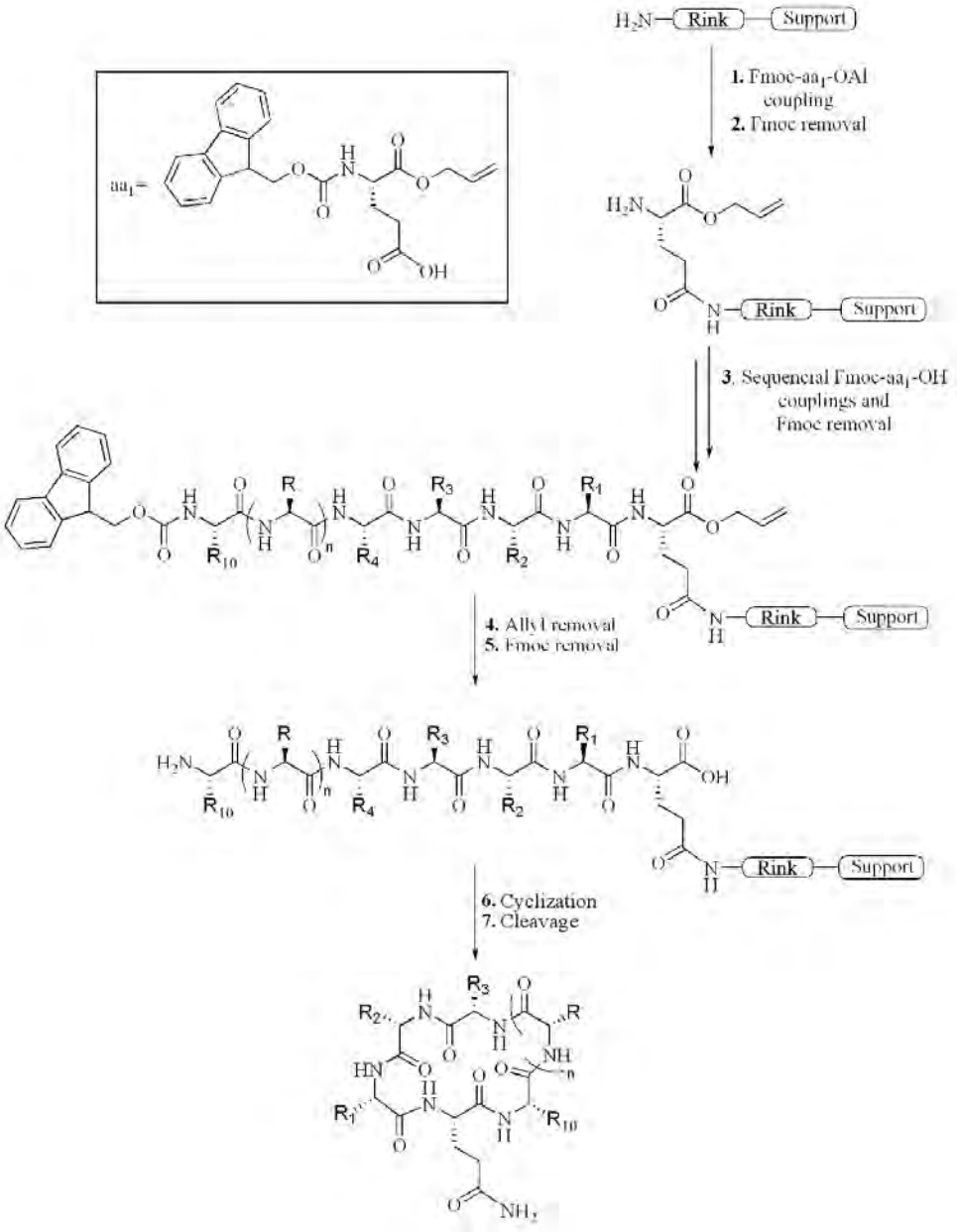

Scheme 4.1: *General strategy for the solid-phase synthesis of cyclic decapeptides on solid-phase synthesis.* **Support:** MBHA resin and SynPhase lanterns.

4.2.1 Synthesis of the linear peptide precursor

The linear precursor was synthesized on a MBHA resin (0.33 mmols/g) or on Fmoc-Rink polystyrene (35 μmol) and polyamide lanterns (18 μmol) (Scheme 4.2). For the MBHA resin, it was necessary to perform the coupling of the Rink-amide linker, which was carried out by treatment with Fmoc-Rink-OH (3 eq), HBTU (3 eq) and DIEA (3 eq) in DMF for 4 h. Then, peptide synthesis started

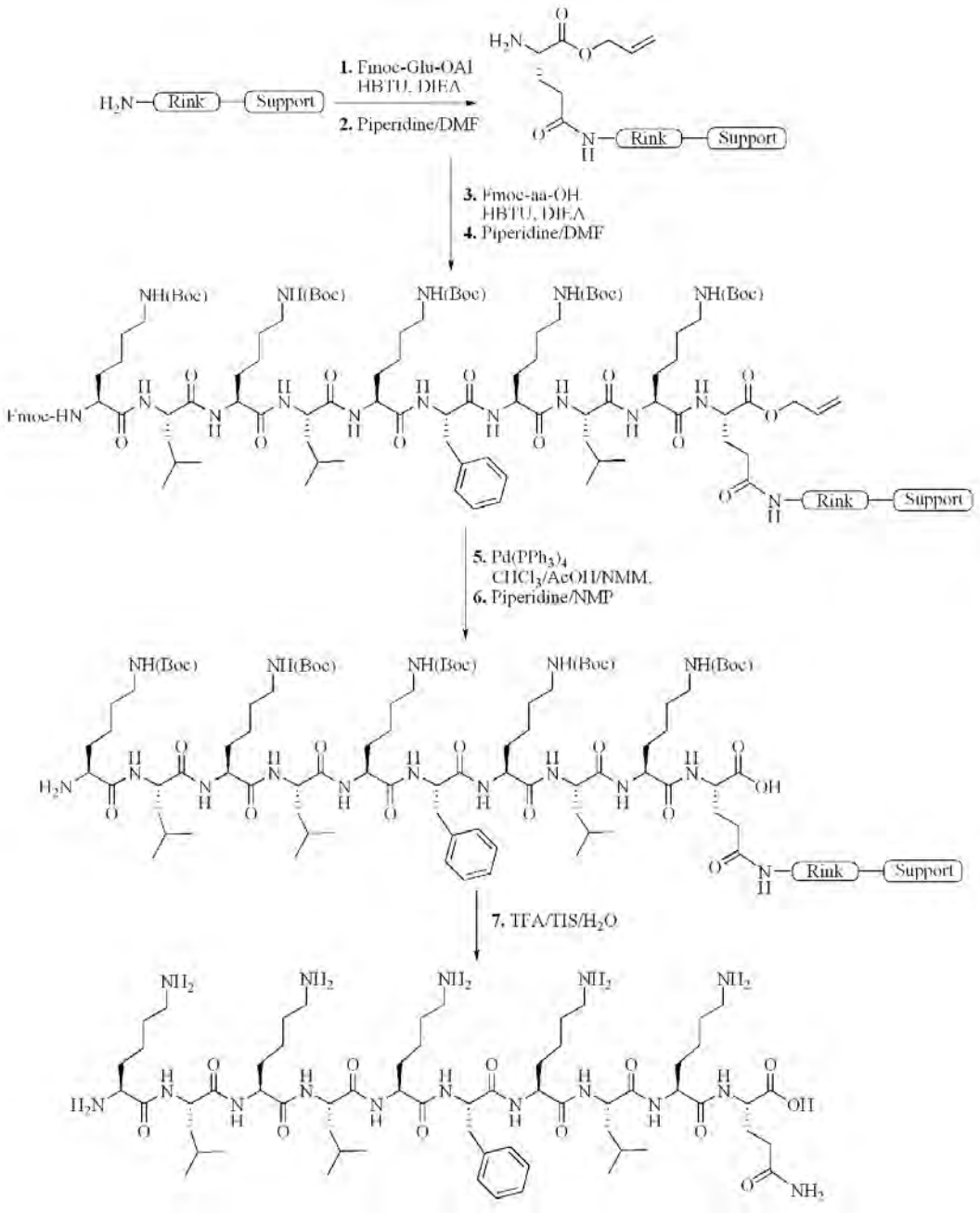

Scheme 4.2: *Solid-phase synthesis of the linear precursor of BPC16.*

with the Fmoc removal using piperidine/DMF (3:7). Fmoc-Glu-OAl was coupled onto the solid support using HBTU and DIEA in DMF (Table 4.1). Sequential Fmoc removal and couplings of the corresponding Fmoc-amino acids were performed until the linear peptide sequence was completed. It has to be pointed out that from the fifth amino acid, couplings were carried out in NMP, because this solvent decreases the peptide folding which difficults the incorporation of

the amino acids. The Kaiser test was used to monitor the completion of the reactions using MBHA resin as support.

Table 4.1: Reaction conditions for the SPS of the linear precursor of BPC16.

Stage	**MBHA resin**	**Polystyrene lanterns**	**Polyamide lanterns**
Swelling	CH_2Cl_2 (1×20 min) DMF (1×20 min)	CH_2Cl_2 (1×5 min)	CH_2Cl_2 (1×5 min)
Fmoc removal	Piperidina/DMF (3:7) 2+8 min	Piperidina/DMF (3:7) 2×40 min	Piperidina/DMF (3:7) 1×20 min
Coupling reagents	Fmoc-aa-OH[a] (3 eq) HBTU (3 eq) DIEA (3 eq)	Fmoc-aa-OH[a] (200 mM) HBTU (200 mM) DIEA (200 mM)	Fmoc-aa-OH[a] (200 mM) HBTU (200 mM) DIEA (200 mM)
Washings	DMF (10×1 min)	DMF (3×5 min) CH_2Cl_2 (2×5 min)	MeOH (3×5 min) NMP (2×5 min) CH_2Cl_2 (1×5 min)
Allyl removal	$Pd(PPh_3)_4$ (3 eq)	$Pd(PPh_3)_4$ (75 mM)	$Pd(PPh_3)_4$ (75 mM)
Cleavage	TFA/TIS/H_2O (95:2.5:2.5) (2 h)	TFA/TIS/H_2O (95:2.5:2.5) (1 h)	TFA/TIS/H_2O (95:2.5:2.5) (1 h)

[a] *aa*, stands for amino acid.

The protected linear peptidyl resin was treated with $Pd(PPh_3)_4$ in a mixture of $CHCl_3$/AcOH/NMM (92.5:5:2.5) under nitrogen to remove the allyl group. After Fmoc removal, an aliquot of the solid support was cleaved with TFA/TIS/H_2O (95:2.5:2.5). The linear precursor was then analysed by HPLC and characterized by ESI-MS. Linear peptides were obtained with high purities (>90%) and with a correct MS spectra irrespective of the solid support (see Annex II figures Figure 7.1, Figure 7.2, Figure 7.3). The reaction conditions for each step are summarized in Table 4.1.

4.2.2 Cyclization studies

4.2.2.1 Cyclization study using MBHA resin as solid support.

The linear peptidyl resin was subjected to the conditions previously described in the group (Monroc 2006), which involves the use of PyBOP (5 eq), HOBt (5 eq) and DIEA (10 eq) in NMP for 24 h at room temperature (Table 4.2,

entry **1**). The resin was then washed, and the cyclic peptide was cleaved from the solid-support by treatment with TFA/TIS/H_2O (95:2.5:2.5) for 2 h. The crude was analyzed by HPLC and characterized by ESI-MS (see Annex II figures Figure 7.4, Figure 7.5). BPC16 was obtained with a 90% purity and was used as reference for the cyclization on SynPhase® lanterns. A general scheme of the cyclization is exposed in Scheme 4.3.

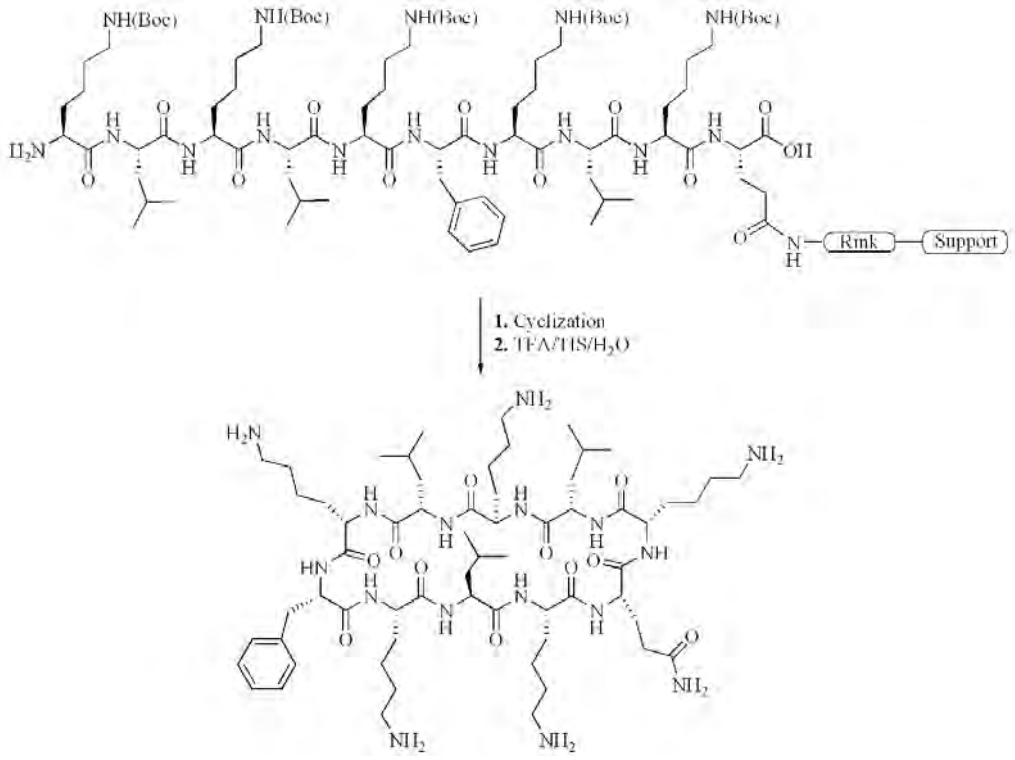

Scheme 4.3: *Solid-phase cyclization of the linear precursor of BPC16.*

4.2.2.2 Cyclization study using polystyrene lanterns as solid support.

The first attempt was carried out under similar conditions to those used with the MBHA resin. Thus, the polystyrene lanterns incorporating the linear precursor were treated with PyBOP (16 eq), HOBt (16 eq) and DIEA (32 eq) in NMP for 24 h at room temperature (Table 4.2, entry **2**). After acidolytic cleavage, the crude was analyzed by HPLC and characterized by ESI-MS. Results showed that the cyclization was not completed, only a 16% of cyclic peptide was obtained (see Annex II Figure 7.6, Figure 7.7 and Figure 7.8). In order to improve the cyclization, different conditions such as reaction time, concentration, temperature coupling reagents and influence of stirring were evaluated. Results are summarized in Table 4.2.

Table 4.2: Synthesis of BPC16 on polystyrene lanterns.

Entry	Coupling reagent (eq)	HOBt (eq)	DIEA (eq)	Time	T (^{o}C)	Cyclic (%)[a]	Annex II
1[b]	PyBOP (5)	5	10	24 h	25	90	9.4, 9.5
2	PyBOP (16)	16	32	24 h	25	16	9.6-9.8
3	PyBOP (16)	16	32	3×24 h	25	60	
4	PyBOP (16)	16	32	24 h[c]	25	25	
5	PyBOP (16)	16	32	2×15 min[d]	50	32	
6	PyBOP (16)	16	32	24 h	50	22	
7	PyBOP (32)	32	64	24 h	25	19	
8	PyBOP (24)	24	40	24 h	25	14	
9	PyBOP (16)	16	16	24 h	25	38	
10	PyBOP (16)	16	48	24 h	25	30	
11	PyBOP (16)	-	32	24 h	25	49	
12	DIC (16)	16	-	24 h	25	96[e]	9.9-9.11
13	DIC (32)	32	-	24 h	25	97[e]	

[a] Percentage obtained from HPLC analysis of the crude reaction mixture.

[b] Cyclization performed on a MBHA resin.

[c] The reaction was carried out under stirring.

[d] The reaction was carried out under MW irradiation.

[e] Cyclodimerization was observed by ESI-MS.

Using PyBOP as coupling reagent, the highest percentage of BPC16 (60%) was obtained when the above reaction conditions were repeated three times (Table 4.2, entry **3**). Stirring, conventional heating and microwave irradiation did not significantly improve the results (entry **4, 5 and 6**, respectively). The amount of coupling reagents influenced the percentage of cyclic peptide obtained (entry **7-10**), however only 38% of BPC16 was formed (entry **9**). A higher percentage of BPC16 (49%) was observed when the cyclization was performed without adding HOBt (entry **11**).

The crude reaction mixtures from the reactions carried out using DIC as coupling reagent showed by HPLC a peak of 97% purity at the same retention time as BPC16 (entry **12, 13**). Unfortunately, the ESI-MS analysis indicated that this peak corresponded to a cyclodimerization by product (see Annex II for an example Figure 7.9, Figure 7.10 and Figure 7.11). The cyclodimerization can be described as an intermolecular reaction amongst the N-terminal amino group of one linear sequence and the C-terminal carboxyl group of another one (Scheme 4.4).

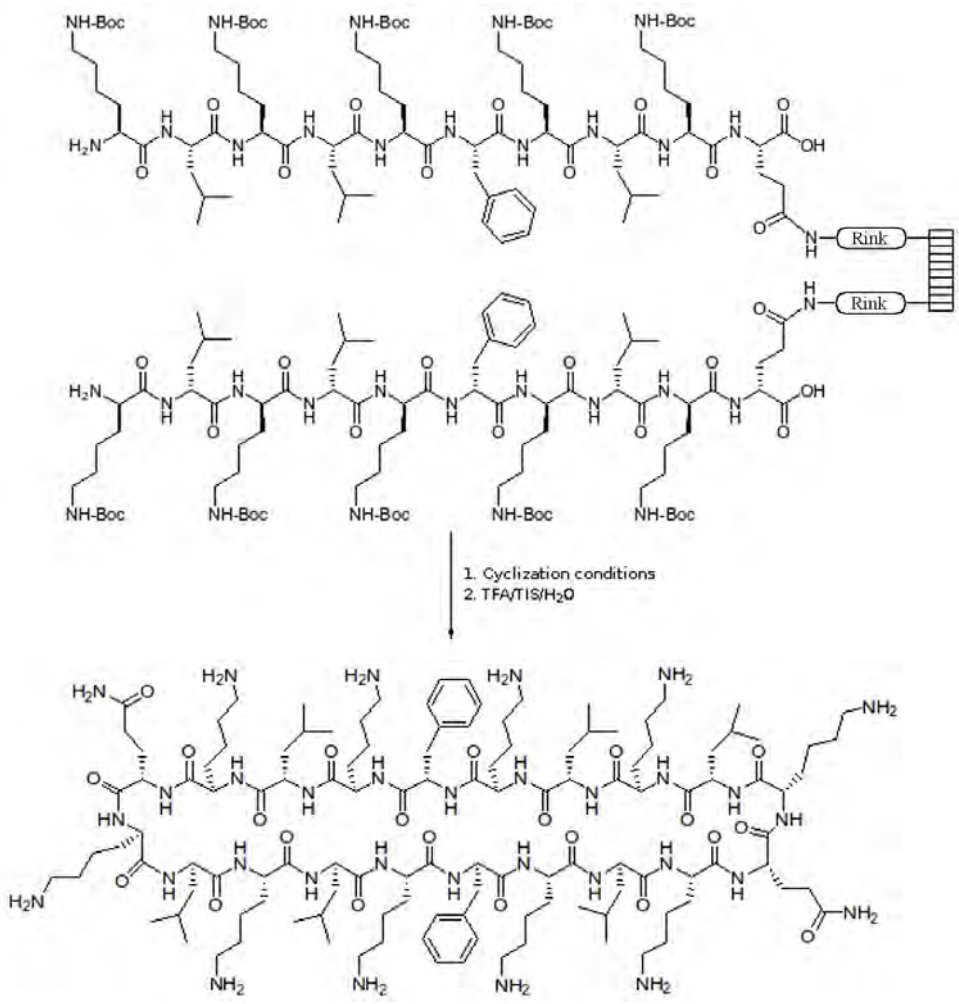

Scheme 4.4: *Formation of the cyclodimerization by product.*

4.2.2.3 Cyclization study using polyamide lanterns as solid support.

Polyamide lanterns, have a lower loading than the polystyrene ones (18 μmol compared to 35 μmol for polystyrene), which can decrease the cyclodimeritzation.

First, the cyclization was studied using PyBOP, HOBt and DIEA. Different conditions were evaluated such as the number of equivalents, the reaction time, the temperature and the solvent (Table 4.3). Results showed that the percentage of the cyclic peptide BPC16 was higher than for the polystyrene lanterns and ranged from 41-74%. However, the linear precursor was detected (26-56%) and a few amount of cyclodimer was also observed by ESI-MS (Annex II Figure 7.12, Figure 7.13, Figure 7.14, Figure 7.15 and Figure 7.16). Further cyclization studies were carried out by using different coupling conditions, including PyBOP, DIC and HATU as coupling reagents, HOAt as additive and collidine as base (Table 4.4).

Table 4.3: Synthesis of BPC16 on polyamide lanterns using PyBOP as coupling reagent.

Entry	PyBOP (eq)	HOBt (eq)	DIEA (eq)	Time	T (^{o}C)	Solvent	Cyclic (%)[a]	Annex II
1[c]	5	5	10	24 h	25	NMP	90[b]	9.4, 9.5
2	16	16	32	2×15 min[d]	50[b]	NMP	50	9.12
3	16	16	32	24 h	25	DMF	45[b]	9.13
4	5	5	10	24 h	25	NMP	41[b]	9.14
5	5	5	10	12 h	50	NMP	74[b]	
6	5	5	10	24 h	50	NMP	54[b]	
7	32	32	64	12 h	25	NMP	45[b]	9.15
8	32	32	64	24 h	25	NMP	71[b]	9.16

[a] Percentage obtained from HPLC analysis of the crude reaction mixture.

[b] Cyclodimerization was observed by ESI-MS.

[c] Cyclization was performed on a MBHA resin.

[d] The reaction was carried out under MW irradiation.

Best results were obtained using PyBOP, HOBt and collidine, yielding BPC16 in 92% HPLC purity (Table 4.4, entry **2**). Reactions performed using HATU, HOAt and DIEA or collidine, or using DIC and HOBt gave the cyclodimer as the major product, as shown by ESI-MS (entry **7-11**). When the cyclization was carried out using PyBrOP, the formation of peptide pyrrolidines was observed. These compounds resulted from the presence of pyrrolidine impurities in the PyBrOP which was used, and prevented the cyclization (see all ESI-MS in Annex II from Figure 7.17 to Figure 7.29).

In summary, conventient conditions for the synthesis of BPC16 on MBHA resin and on polyamide lanterns have been established. Lanterns are specially suited for the synthesis of peptide libraries.

Table 4.4: Syntesis of BPC16 on polyamide lanterns[a].

Entry	Coupling reagent (eq)	Additive (eq)	Base (eq)	Time	Solvent	Cyclic (%)[b]	Annex II
1[c]	PyBOP (5)	HOBt (5)	DIEA (10)	24 h	NMP	90	9.4, 9.5
2	PyBOP (16)	HOBt (16)	collidine (32)	24 h	NMP	92	9.17
3	PyBOP (16)	HOAt (16)	DIEA (32)	24 h	NMP	79[d]	9.18
4	PyBOP (16)	HOAt (16)	collidine (32)	24 h	NMP	100[d]	9.19
5	PyBrOP (16)	HOBt (16)	DIEA (32)	24 h	NMP	69[e]	9.20
6	PyBrOP (16)	HOAt (16)	DIEA (32)	24 h	NMP	82[e]	9.21
7	PyBrOP (16)	HOAt (16)	collidine (32)	24 h	NMP	100	9.22
8	HATU (16)	HOAt (16)	DIEA (32)	24 h	NMP	79[d]	9.23
9	HATU (16)	HOAt (16)	collidine (32)	24 h	NMP	100[d]	9.24
10	DIC (16)	HOBt (16)	-	12 h	NMP	78[d]	9.25
11	DIC (16)	HOBt (16)	-	24 h	DMF	93[d]	9.26
12	DIC (8)	HOBt (8)	-	24 h	NMP	72[d]	9.27
13	DIC (16)	HOAt (16)	-	24 h	NMP	95[d]	9.28
14	DIC (8)	HOAt (8)	-	12 h	NMP	73[d]	9.29

[a] All reactions were performed at 25^{o}C. Best conditions are highlighted in orange.

[b] Percentage obtained from HPLC analysis of the crude reaction mixture.

[c] Cyclization was performed on a MBHA resin.

[d] The cyclodimer is the major product obrained, as shown by ESI-MS.

[e] Peptide pyrrolidides were observed by ESI-MS.

4.3 Synthesis of a Trp-Containing Library of Cyclic Peptides with Antimicrobial Activity

The synthesis of the library of cyclodecapeptides with general structure c(X_5-F-X_3-Q), being X=lysine or leucine, allowed the identification of sequences with high antibacterial activity against the phytopathogenic bacteria *E. amylovora*, *P. syringae* and *X. vesicatoria*. However, their mechanism of action has not been still elucidated. Its understanding is important for the design of new AMPs.

Nowadays, biophysical studies are used to unravel the bases of the peptide-lipid interactions at the molecular level, which are crucial for the mechanism of action of AMPs. One of the most applied techniques in the study of the peptide-membrane interactions is fluorescence spectroscopy. The incorporation of a fluorescent amino acid into a sequence would allow to study functional peptide abilities, such as the penetration depth, membrane pore formation or membrane lysis, which could be closely related with the peptide mode of action.

Based on these considerations a library of cyclodecapeptides incorporating a tryptophan with general structure c(X_5-W-X_3-Q), being X=lysine or leucine, was synthesized and screened for its antibacterial and hemolytic activities.

4.3.1 Synthesis of the Trp-Containing Cyclic Peptide Library

The library consisted of 66 cyclic decapeptides designed similarly to the library of the phenylalanine-containing cyclic peptides previously described in the introduction section. All the sequences are listed Table 7.2 in Annex II.

The synthesis was carried out following the procedure described in 7.2 (Annex I), using MBHA resin (0.4 mmol/g) as solid support[2]. The corresponding linear precursors were synthesized on an ACT Multiple Peptide Synthesizer Apex 396 S (Aapptec) (see Scheme 4.5).

Once the linear sequences were completed, the cyclization was performed manually in 66 polypropylene syringes fitted with a polyethylene porous disk. The C-terminal allyl ester and the N-terminal Fmoc group were removed by treatment with $Pd(PPh_3)_4$ and piperidine/DMF, respectively. Cyclization was then carried out with PyBOP (5 eq), HOBt (5 eq) and DIEA (10 eq) in NMP at 25 ^{o}C for 24 h. Following washes, cyclodecapeptides were cleaved from the resin

[2]The synthesis of the full library was carried out together with Gemma Moiset Coll

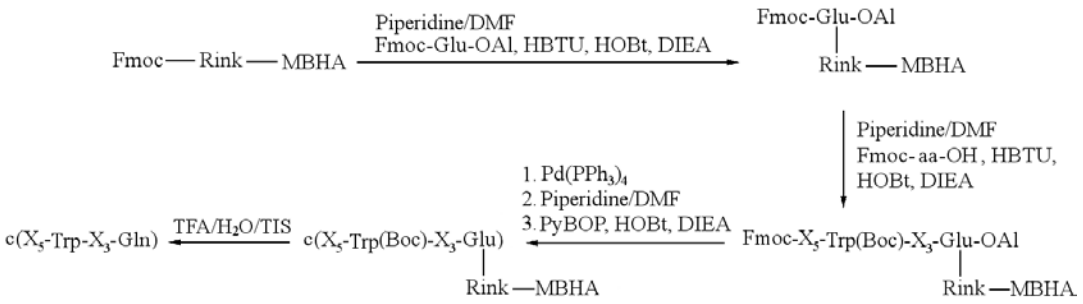

Scheme 4.5: *General strategy for the synthesis of the cyclic peptide library.*

by acid treatment. The cyclic peptides were precipitated with Et_2O, dissolved in H_2O, and analysed by analytical RP-HPLC. Final products were obtained in around 90% purity in HPLC and their structure was confirmed by ESI-MS (see section 7.5.5 in Annex II for HPLC and MALDI-TOF examples of BPC312, BPC326, BPC338, BPC354, BPC356, BPC372 and BPC360).

4.3.2 Antibacterial Activity

The analysis of the antibacterial activity of the Trp-containing cyclic peptide library showed that 33% of the sequences displayed improved activity against the three pathogens compared to the phenylalanine analogues. *X. vesicatoria* was the most sensitive pathogen to these peptides, 42 sequences showed MIC < 6.2 μM. In the case of *P. syringae*, 21 peptides exhibited activity with MIC < 6.2 μM. Against *E. amylovora*, 6 analogues displayed MIC < 12.5 μM. Even though this is the least sensitive pathogen, the introduction of a tryptophan significantly improved the results. In fact, for the phenylalanine-containing library, 39 sequences were not active (MIC >100 μM) while in the case of the tryptophan library, only 13 analogues did not display activity.

It is worth mentioning that the lead peptides identified from the phenylalanine library (BPC194 and BPC198) were not the best sequences for the tryptophan set. The most active peptides for the Trp-containing library were BPC326 and BPC348, which displayed the lowest MIC values obtained against the three pathogens. In Table 4.5 is summaryzed the antibacterial activity[3] for the entire library exposed together with their corresponding phenylalanine analogue activities.

The hemolytic activity was also checked to contrast the results of both amino

[3]The antibacterial activity was carried out by Ester Badosa from Laboratori de Patologia Vegetal, Institut de Tecnologia Agroalimentària (CIDSAV-CeRTA)

acids. As it was expected, the hemolytic activity was increased considerably. In fact, this can be explained by the high affinity of tryptophan residue with cholesterol molecules of mammalian cells (Blondelle 2000). So, the selectivity between cell membranes was lost as the phenylalanine was replaced by tryptophan. But, since the antimicrobial activity was slightly decreased, kept or highly improved, the use of the tryptophan residue as a method for mechanistic studies by fluorescence analysis of this library, seems acceptable.

Table 4.5: Antibacterial activity (MIC) of the Trp-containing cyclic peptides library[a]. The Code stands for tryptophan peptides. For further details on phenylalanine code and the corresponding sequences see Annex II.

Code	MIC (μM)						Hemolysis (%)[e]	
	Ps[b]		Ea[c]		Xv[d]			
	Trp	Phe	Trp	Phe	Trp	Phe	Trp	Phe
BPC296	12.5-25	12.5-25	>100	>100	3.1-6.2	6.2-12.5	67.3	84
BPC298	12.5-25	25-50	50-75	>100	25-50	25-50	92.7	6
BPC300	3.1-6.2	6.2-12.5	12.5-25	12.5-25	6.2-12.5	6.2-12.5	55	72
BPC302	3.1-6.2	12.5-25	12.5-25	>100	6.2-12.5	6.2-12.5	97	6
BPC304	3.1-6.2	12.5-25	<12.5	25-50	6.2-12.5	6.2-12.5	97	10
BPC306	6.2-12.5	6.2-12.5	<12.5	25-50	6.2-12.5	6.2-12.5	73	22
BPC308	6.2-12.5	25-50	25-50	>100	<3.1	25-50	77	0
BPC310	6.2-12.5	12.5-25	12.5-25	>100	<3.1	6.2-12.5	81.4	19
BPC312	3.1-6.2	6.2-12.5	12.5-25	25-50	<3.1	6.2-12.5	25	7
BPC314	6.2-12.5	6.2-12.5	12.5-25	12.5-25	3.1-6.2	6.2-12.5	86	36
BPC316	6.2-12.5	6.2-12.5	<12.5	25-50	<3.1	6.2-12.5	42	13
BPC318	6.2-12.5	12.5-25	25-50	>100	<3.1	6.2-12.5	63.6	0
BPC320	6.2-12.5	6.2-12.5	12.5-25	>100	<3.1	12.5-50	66.5	19
BPC322	6.2-12.5	12.5-25	12.5-25	25-50	<3.1	6.2-12.5	62	36
BPC324	12.5-25	12.5-25	12.5-25	12.5-25	<3.1	12.5-25	83	45
BPC326	3.1-6.2	6.2-12.5	<12.5	25-50	<3.1	25-50	62.2	8
BPC328	6.2-12.5	6.2-12.5	12.5-25	25-50	<3.1	1.6-3.1	44	33
BPC330	6.2-12.5	6.2-12.5	12.5-25	25-50	<3.1	3.1-6.2	28	35
BPC332	6.2-12.5	6.2-12.5	50-75	>100	3.1-6.2	3.1-6.2	70.5	9
BPC334	6.2-12.5	6.2-12.5	25-50	25-50	3.1-6.2	6.2-12.5	69	73
BPC336	6.2-12.5	6.2-12.5	12.5-25	12.5-25	<3.1	3.1-6.2	82.7	32
BPC338	3.1-6.2	6.2-12.5	12.5-25	12.5-25	<3.1	1.6-3.1	32	36
BPC340	12.5-25	25-50	>100	>100	6.2-12.5	25-50	64.1	2
BPC342	3.1-6.2	6.2-12.5	12.5-25	12.5-25	6.2-12.5	25-50	96.1	26
BPC344	6.2-12.5	3.1-6.2	12.5-25	>100	6.2-12.5	6.2-12.5	96	15
BPC346	3.1-6.2	12.5-25	25-50	>100	3.1-6.2	25-50	76	0
BPC348	<3.1	6.2-12.5	<12.5	>100	<3.1	12.5-25	92	2
BPC350	3.1-6.2	12.5-25	12.5-25	>100	6.2-12.5	12.5-25	96	9
BPC352	3.1-6.2	25-50	50-75	>100	6.2-12.5	25-50	92	1
BPC354	3.1-6.2	6.2-12.5	12.5-25	>100	<3.1	6.1-12.5	100	24
BPC356	3.1-6.2	6.2-12.5	12.5-25	25-50	3.1-6.2	6.1-12.5	92.9	13
BPC358	6.2-12.5	12.5-25	12.5-25	>100	12.5-25	12.5-25	94.9	6
BPC360	3.1-6.2	12.5-25	12.5-25	>100	<3.1	6.2-12.5	99.5	8

[a] Improved MICs compared to those of the phenylalaine library are highlighted in orange. Phenylalanine MICs were taken from Monroc *et al.*

[b] *Ps* stands for *Pseudomonas syringae*, [c] *Ea* stands for *Erwinia amylovora*, [d] *Xv* stands for *Xanthomonas vesicatoria*

[e] Percentage of hemolysis at 375 μM

Code	MIC (μM)						Hemolysis (%)[e]	
	Ps[b]		Ea[c]		Xv[d]			
	Trp	Phe	Trp	Phe	Trp	Phe	Trp	Phe
BPC362	3.1-6.2	6.2-12.5	12.5-25	>100	6.2-12.5	6.2-12.5	100	4
BPC364	6.2-12.5	12.5-25	50-75	>100	3.1-6.2	12.5-25	100	3
BPC366	6.2-12.5	12.5-25	25-50	>100	<3.1	6.2-12.5	22	4
BPC368	6.2-12.5	12.5-25	12.5-25	>100	<3.1	25-50	100	1
BPC370	6.2-12.5	12.5-25	12.5-25	>100	<3.1	25-50	100	6
BPC372	3.1-6.2	6.2-12.5	12.5-25	>100	<3.1	12.5-25	100	4
BPC374	6.2-12.5	12.5-25	25-50	>100	3.1-6.2	12.5-25	27	2
BPC376	6.2-12.5	6.2-12.5	<12.5	>100	3.1-6.2	6.2-12.5	63	41
BPC378	6.2-12.5	12.5-25	25-50	>100	3.1-6.2	25-50	91.3	5
BPC380	6.2-12.5	6.2-12.5	12.5-25	25-50	3.1-6.2	6.2-12.5	93.7	23
BPC382	6.2-12.5	6.2-12.5	12.5-25	25-50	3.1-6.2	6.2-12.5	99.4	14
BPC384	3.1-6.2	3.1-6.2	12.5-25	50-75	<3.1	6.2-12.5	41	9
BPC386	3.1-6.2	6.2-12.5	25-50	75-100	3.1-6.2	12.5-25	67.8	3
BPC388	12.5-25	25-50	>100	>100	12.5-25	25-50	58.1	1
BPC390	12.5-25	12.5-25	>100	>100	6.2-12.5	6.2-12.5	75.5	4
BPC392	6.2-12.5	12.5-25	75-100	>100	6.2-12.5	6.2-12.5	84.8	2
BPC394	3.1-6.2	6.2-12.5	25-50	25-50	<3.1	6.2-12.5	93.5	11
BPC396	6.2-12.5	12.5-25	>100	>100	3.1-6.2	12.5-25	82.6	3
BPC398	12.5-25	6.2-12.5	12.5-25	50-75	<3.1	6.2-12.5	50	9
BPC400	6.2-12.5	6.2-12.5	>100	>100	6.2-12.5	12.5-25	81.1	3
BPC402	6.2-12.5	12.5-25	>100	>100	3.1-6.2	12.5-25	85.6	2
BPC404	6.2-12.5	12.5-25	>100	>100	6.2-12.5	12.5-25	63.1	4
BPC406	6.2-12.5	12.5-25	>100	>100	6.2-12.5	12.5-25	34.2	0
BPC408	3.1-6.2	12.5-25	25-50	50-75	<3.1	3.1-6.2	86.9	89
BPC410	12.5-25	6.2-12.5	>100	>100	6.2-12.5	6.2-12.5	31.4	0
BPC412	6.2-12.5	12.5-25	50-75	25-50	12.5-25	6.2-12.5	93.8	87
BPC414	25-50	6.2-12.5	>100	>100	12.5-25	6.2-12.5	13.9	0
BPC416	12.5-25	12.5-25	25-50	25-50	6.2-12.5	3.1-6.2	85.2	49
BPC418	12.5-25	3.1-6.2	12.5-25	6.1-12.5	6.2-12.5	3.1-6.2	8	17
BPC420	3.1-6.2	12.5-25	>100	>100	<3.1	6.2-12.5	85	47
BPC422	25-50	3.1-6.2	25-50	12.5-25	3.1-6.2	3.1-6.2	88.9	14
BPC424	>50	25-50	75-100	>100	3.1-6.2	12.5-25	85.6	71
BPC426	25-50	12.5-25	>100	>100	12.5-25	6.2-12.5	5	2

[a] Improved MICs compared to those of the phenylalaine library are highlighted in orange. Phenylalanine MICs were taken from Monroc *et al.*

[b] *Ps* stands for *Pseudomonas syringae*, [c] *Ea* stands for *Erwinia amylovora*, [d] *Xv* stands for *Xanthomonas vesicatoria*

[e] Percentage of hemolysis at 375 μM

4.4 Evaluation of the Stability of Cyclic Peptides in Human Serum

The library of phenylalanine-containing peptides was also evaluated as antitumor agents (Feliu 2010). In order to study their potential therapeutic application, the stability of human serum of the most active peptides was analysed: BPC88, BPC94, BPC96, BPC98, BPC184, BPC194, BPC198 and BPC202 (Table 4.6). Moreover, the stability of the linear counterpart BPC87 (H-KKLLKFKKLQ-OH) was also checked.

Table 4.6: Sequences of the cyclic peptides evaluated for their stability in human serum.

Code	1	2	3	4	5	6	7	8	9	10
BPC88	c(K	K	L	L	K	F	K	K	L	Q)
BPC94	c(K	L	L	K	K	F	K	K	L	Q)
BPC96	c(L	K	L	K	K	F	K	K	L	Q)
BPC98	c(L	L	K	K	K	F	K	K	L	Q)
BPC184	c(K	L	L	L	K	F	K	K	L	Q)
BPC194	c(K	K	L	K	K	F	K	K	L	Q)
BPC198	c(K	L	K	K	K	F	K	K	L	Q)
BPC202	c(K	K	K	K	K	F	K	K	L	Q)

Each peptide was exposed to 25% aqueous filtered human serum and left at different time intervals. The presence of the peptide was analyzed by MALDI-TOF (Figure 4.1).

Results showed that all five cyclic peptides were significantly more stable in human serum than the linear counterpart BPC87. While the linear analogue was not detected after 30 min of exposure (Figure 4.1 A, expected mass; $[M+H]^+$=1272.86, $[M+Na]^+$=1295.84), the cyclic peptides were observed at longer time intervals. BPC88 was the least stable, which was detected up to 30 min (Figure 4.1 B, $[M+H]^+$=1254.85, $[M+Na]^+$=1277.85). In contrast, BPC96 and BPC98 were still detected up to 1.5 and 1 h, respectively (Figure 4.1 C-D), and the most stable peptides were BPC194 and BPC198 which were observed after 2 h (Figure 4.1 E-F).

It is remarkable that cyclization confers to peptides a high stability against metabolic degradation, which suggests that cyclic peptides are good candidates as anticancer agents.

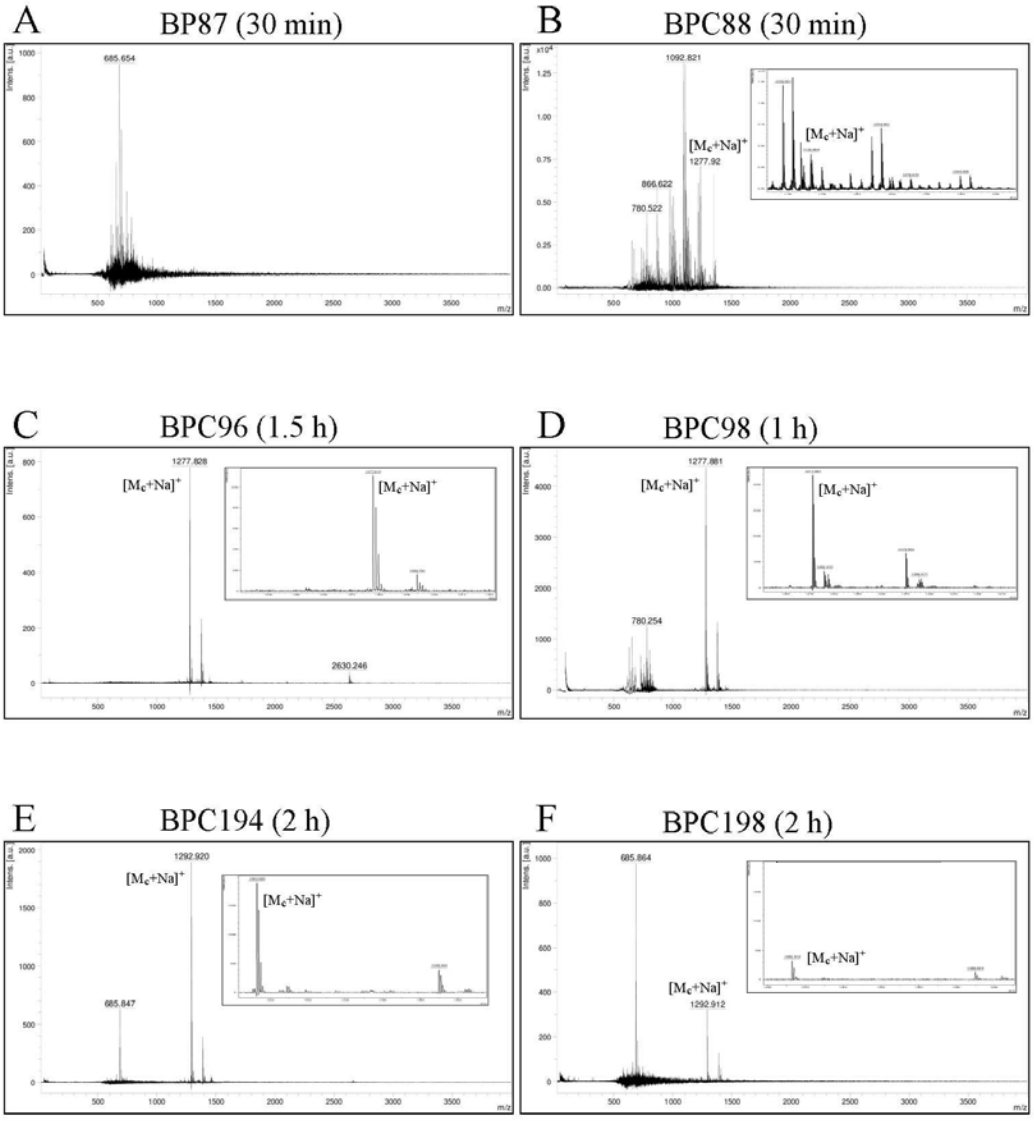

Figure 4.1: *MALDI spectra after peptide exposure to human serum.* **A.** BPC87. **B.** BPC88. **C.** BPC96. **D.** BPC98. **E** BPC194 and **D** BPC198. Inset plots shows an enlargement of the signal of the mass of the cyclic peptide (M_c).

4.5 Remarks and Conclusions

Cyclization is the key step in the synthesis of cyclic peptides. Even though this intramolecular reaction is favoured on solid support due to the pseudo-dilution phenomena (Malesevic 2004), other side reactions such as cyclodimerization can compete.

In this thesis, cyclization on a MBHA resin gave the best results, yielding the cyclic peptide BPC16 with 90% purity. Cyclization on SynPhase® lanterns needed to be optimized, since substantial cyclodimerization was observed when this reaction was conducted under the same conditions as for on resin cyclization (PyBOP, HOBt, DIEA). The use of collidine improved the reaction and BPC16 was obtained in 92% purity using polyamide lanterns. It was already described that some reagents derived from HOAt (Carpino 1995, Carpino 1993), showed advantages over the corresponding HOBt-based reagents, and that also exhibited significatly improved head-to-tail cyclization of all L-aa-penta and hexapeptides (Ehrlich 1996).

On the other hand, in general, the tryptophan library exhibited higher antimicrobial activity against *Pseudomonas syringae*, *Erwinia amylovora* and *Xanthomonas vesicatoria* than the phenylalanine library. However, these Trp-containing peptides displayed higher hemolytic activity. In fact, tryptophan has been described to be involved in the interaction of peptides to the cholesterol present in the membrane of eukaryotic cells through the indole moiety (Blondelle 1993, Subbalakshmi 1998). Moreover, higher hemolysis has been correlated to higher peptide hydrophobicity character. In this case, the tryptophan analogues showed higher HPLC retention times than phenylalanine counterparts confirming their higher hydrophobicity.

Enzymatic degradation is one of the limitations of using peptides as therapeutic agents. Cyclization has been applied to improve peptide stability against metabolic degradation. This was observed in a previous study carried out by Monroc et al. (Monroc 2006a) that showed that the cyclic peptide BPC16 was degraded significantly slower than its linear counterpart. In the present study BPC96 and BPC194 with an optimal biological profile in terms of anticancer activity, hemolysis and cytotoxicity against non-malignant fibroblast also showed good stability in human serum.

Chapter 5

Molecular Modelling of Cyclic Peptides

The second part of this thesis was carried out in collaboration with the Molecular Dynamics group of the University of Groningen. In this chapter we discuss a different prespective of the action of antimicrobial peptides. In this case, Molecular Dynamics (MD) simulations were used to see at a molecular level the structure and basis of the action of several cyclic AMPs. The observations that will be described here will hopefully bring the possibility of designing new cyclic peptides with improved antimicrobial activity.

In the first part of this chapter we presented a conformational search study of an active cyclic antimicrobial peptide. The aim of this work was to understand the most important intramolecular interactions stabilizing a given secondary structure, as well as its dynamical stability in water environment. In a second step, MD simulations of the most active cyclic AMP of the library (BPC194) and its non-active linear analog (BPC193) upon a model bilayer were carried out in order to shed light on their mechanism of action. In the last part, a bigger system composed by two bilayers was used to simulate the dual action of peptide BPC194: namely leakage and fusion.

The overall results of this chapter provide the molecular basis of antimicrobial activity of cyclic peptides.

5.1 Conformational Study and Dynamic Stability of a Cyclic Peptide with Antimicrobial Activity

Cyclic peptides, due to their restricted conformation space have become a family of molecules characterized by their high specificity for receptors (Davies 2003). Many important cyclic peptides are present in nature, like gramicidin S or tyrocidine (Mogi 2009, Wu 1999, Tang 1999, Zhang 2000, Bu 2002). The accepted secondary structure for these cyclic AMPs is dominated by the presence of an antiparallel β-sheet stabilized by intramolecular hydrogen bonds and characterized by two β-turns. It is often claimed that these structural features are important for the activity of these cyclic peptides, and even a reduction of their activity can be achieved if such secondary structure can not be formed (Mihailescu 1999, Lee 2003).

To complement our experiments with a computational approach, the conformational space of the most active peptide from the first library, namely BPC16 with sequence c(KLKLKFKLKQ), was explored by means of molecular dynamics simulations. Circular Dichroism (CD) spectra of this peptide revealed strong similiarities to that observed for Gramicidin S-related cyclic peptides, suggesting some extent of β-sheet formation (Monroc 2006a).

In order to shed light on the conformational preferences of BPC16, in this section we present i) a conformational search study using two different sampling techniques and ii) a dynamical study of the cyclic peptide with the aim of getting some clues of its structure in different environments.

5.1.1 Methodology

5.1.1.1 Cyclic peptide conformation in gas phase.

The starting conformation was built with the *leap* module of Amber. The linear sequence H-KLKLKFKLKQ-OH was first modeled and secondly a peptide bond was created between the C-terminal of the first amino acid (glutamine) and the N-terminal of the last amino acid (lysine) in the same order as its synthetic route (see 4.1). A minimization was then performed to relax the cyclic conformation and correct for unnatural bond distances caused by the design of cyclic shape. The lysines were represented in their neutral state, with a NH_2 group at the end of the side-chain. A 100 ps of equilibration step was followed up to 300 K.

5.1.1.2 Conformational search; simulated annealing and simple sampling protocol.

Starting from the cyclic peptide conformation in gas phase after equilibration, the following Simulated Annealing (SA) protocol of 400 ps was performed. Firstly, the system was heated from 0 to 1000 K during the first 100 ps. Then, after 50 ps of constant temperature, the system was cooled to 298 K for up to 400 ps. Finally, a minimization step was performed to reach the closest local minimum. The protocol was repeated for one thousand cycles and the coordinates and energies of the local minima were stored.

A Simple Sampling (SS) protocol was also performed. In this case, a 200 ps of MD simulation was performed at constant temperature. From all the trajectory 40 snapshots were selected every 5 ps and a minimization was carried out afterwards. To sample all the conformational space, seven independent simulations were performed at different temperatures, ranging from 300 to 900 K. Again, the coordinates and energies of the local minima were stored for further analysis.

5.1.1.3 Solvated systems.

In order to investigate the dynamical stability of the low energy conformers in solution, the selected cyclic peptide structures were placed in a box with a distance of 8 Å between the wall of the box and the closest atom of the peptide, producing around 1100 water molecules for the system. The corresponding equilibration of the system was carried out in consecutive steps. The system was first minimized keeping the peptide constrained with a constant force of 500 kcal/molÅ^2 in order to relax the water molecules. Then, the entire system was minimized without any restriction. Afterwards, 20 ps of molecular dynamics were performed to heat the whole system gradually up to the desired temperature constraining the peptide with a constant force of 10 kcal/molÅ^2 (NVT ensemble). Finally a last step of 100 ps of simulation without restriction was carried out for equilibration of the whole system prior to the MD simulations (NPT ensemble). In this work, 100 ns of MD simulation in aqueous phase were produced for each starting structure.

5.1.1.4 MD simulations parameters.

All MD simulations were performed with AMBER 9 software package (Case 2006) with all-atom force field ff99SB (Hornak 2006). For all dynamics, SHAKE algorithm (Ryckaert 1977) was applied to constrain all bonds involving hydrogen atoms so as to use a time step of 2 fs. Temperature was controlled by the

Langevin dynamics algorithm (Loncharich 1992) keeping the temperature at 325 K to reduce dependence of the trajectories on the initial structure (Simmerling 2002). Electrostatic interactions were calculated without cut-off for gas phase and a cut-off of 6 Å for solvated simulations. The water molecules were modeled with the SPC/E model. Periodic boundaries conditions were used to replicate the box in all directions and Particle Mesh Ewald summation was used to account for the long-range electrostatic interactions, using AMBER's default values.

5.1.1.5 Analysis.

The simulations were analysed with Ptraj, a program included in the AMBER suite to process coordinates and trajectories. A distance between heavy donor and acceptor atoms equal or shorter than 3.5 Å and bond angle equal or bigger than 120^o was used as criterion for hydrogen bond interaction characterization giving the distances between the oxygen and nitrogen atoms. To monitor the stability of the hydrogen bond along the simulations, the distance between the oxygen atom of the donor and the hydrogen atom of the acceptor was used, therefore smaller values were achieved. In order to check for the presence of different turns, a FORTRAN program based on the analysis of consecutive dihedral angles was written. Different types of α and β turns characterized by specific values of dihedral angles of the corresponding residues were considered, according to the classification of Chou (Chou 2000). Moreover, the well-known DSSP protocol and corresponding computer program (Kabsch 1983) was employed to analyze the time evolution of local secondary structure in the sequence. The graphical interface VMD was used as a molecular visualization program (Humphrey 1996).

5.1.2 Simulated Annealing versus Simple Sampling

A collection of 988 and 274 minimum energy structures (MES) were obtained form the application of the aforementioned Simulated annealing and Simple Sampling protocols, respectively. In order to analyse any differences in the set of MES obtained from both protocols, the histogram of frequency distribution of energies from all minima is exhibited in Figure 5.1 A.

The results exhibit different shapes of the energy frequency distribution of both sets. In the case of the SA protocol the histogram exhibits a "bell-shape" with an maximum around -165 kcal/mol (relative energy), with a frequency of about 29%. On the contrary, the SS approach presents a bimodal distribution with two maxima of similar frequency (about 20%), located at -170kcal/mol and 160 kcal/mol. The overall conclusion that arises from the comparison of

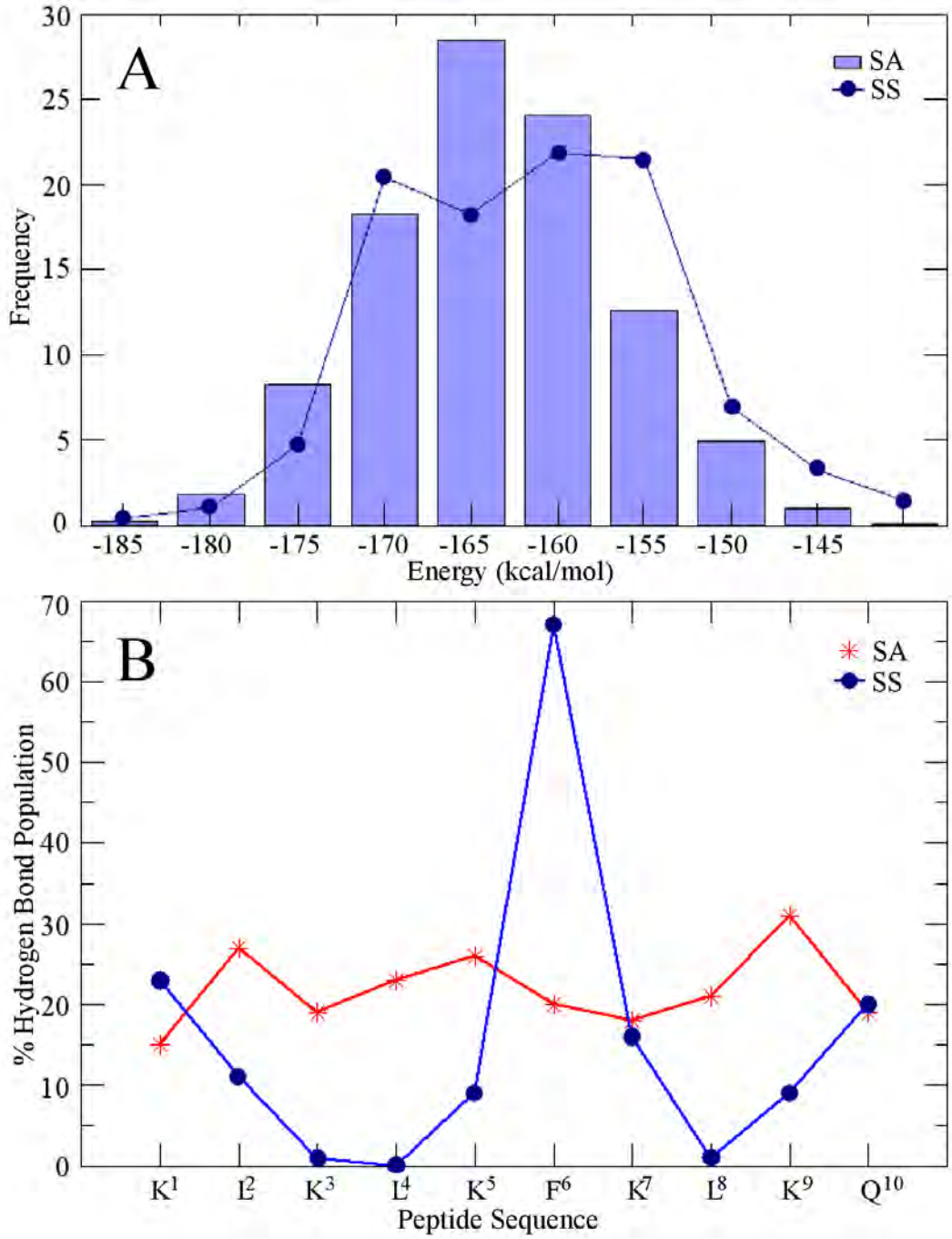

Figure 5.1: *Energy histogram and hydrogen bond populations* **A.** Histogram of the energy frequency distribution for SA (blue) and SS (doted blue line) set of minimum energy structures. **B.** Hydrogen bond population of each residue. The hydrogen bond is formed between the oxygen atom of i th residue and the hydrogen atom of $i+3$ th amino acid.

both histograms is that the SA procedure gave a slightly higher propensity for low-energy structures.

The presence of hydrogen bonds between backbone atoms separated by three residues, featuring a typical beta turn secondary structure pattern is shown for all MES in Figure 5.1 B. For a general summary of the main hydrogen bond interactions and percentage of specific local secondary structure for all MES see Table 5.1.

The set of MES obtained from the SA protocol showed very similar population of hydrogen bonds for all ten residues. A hydrogen bond involving residues 9 (lysine) and 2 (leucine) was observed in 30% of the set of minim energy structures, whereas the less populated one (16%) involved residues 1 (lysine) and 4 (leucine). For the rest of residues, the hydrogen bond occupation was about 20%. In all cases, the interaction between the oxygen atom of i th residue and the hydrogen atom of $i+3$ th amino acid gave rise to the formation of a type I β-turn. Hydrogen bonds between the same backbone's donor and acceptor atoms atoms but involving residues $i \rightarrow i+4$ th (see Table 5.1, light grey cells) were also observed in 5 to 10% of the minimum energy structures. In this case, the intramolecular interaction brought to the formation of either RS or LS type I α-turns, which stabilized the conformation of the cyclic peptide.

Finally, hydrogen bonding interactions involving at least one side-chain atom of the residues are indicated in dark grey cells. Such interactions are found again in 5 to 10% of the structures, with a somewhat higher preference for the side-chain of the only glutamine residue. No secondary structure is associated to these hydrogen bonds as it does not imply any backbone-backbone interaction. Thus, one can say that the minimum energy structures obtained from the SA protocol present, on average, about 3 hydrogen bonds, mostly involving donor and acceptor atoms of the backbone.

On the contrary, the SS protocol exhibited significant bias towards interaction involving specific amino acids. The hydrogen bond involving residues 6 (phenylalanine) and 9 (lysine) was present in 68% of the MES, whereas almost no structure was found with $i \rightarrow i+3$ hydrogen bonds originating from residues 3, 4 or 8. The phenylalanine residue also acted as hydrogen bond donor with hydrogen acceptor on residue 10 (glutamine) in 50% of the structures. In fact, careful analysis showed that in most cases the oxygen atom of the residue 6 showed a bifurcated hydrogen bond, with a somewhat higher preference for the $i \rightarrow i+3$ th, as indicated also for a larger percentage of beta turn conformation.

Table 5.1: Summary of hydrogen bond analysis of the MES found in the SA and SS conformational searches. White cells are the percentage of hydrogen bonds between the oxygen atom of the *i* th amino acid and the hydrogen atom of the *i+3* th residue and light gray cells between *i* th amino acid and *i+4* th residue. Hydrogen bonds involving side-chain atoms are shown in dark gray cells. D stands for Donor residue and A for Acceptor residue.

Simulated Annealing				**Simple Sampling**			
D	**A**	**% Hbond**[a]	**SS %**	**D**	**A**	**Hbond**[a]	**SS %**
K^{9}	L^{2}	31	13 β-turn I	F^{6}	K^{9}	68	31 β-turn I
L^{2}	K^{5}	27	9 β-turn I	K^{1}	L^{4}	23	9 β-turn I
K^{5}	L^{8}	26	10 β-turn I	Q^{10}	K^{3}	21	3 β-turn I
L^{4}	K^{7}	23	13 β-turn I	K^{7}	Q^{10}	17	8 β-turn I
L^{8}	K^{1}	21	11 β-turn I	L^{2}	K^{5}	12	5 β-turn I
F^{6}	K^{9}	21	5 β-turn I	K^{9}	L^{9}	9	1 β-turn I
Q^{10}	K^{3}	20	10 β-turn I	K^{5}	L^{8}	9	3 β-turn I
K^{3}	F^{6}	19	6 β-turn I	K^{3}	F^{6}	2	-
K^{7}	Q^{10}	18	6 β-turn I	L^{8}	K^{1}	2	-
K^{1}	L^{4}	16	4 β-turn I	L^{4}	K^{7}	1	-
K^{5}	K^{9}	10	-	F^{6}	Q^{10}	51	4 α_{RS}-turn I
L^{8}	L^{2}	9	3 α_{RS}-turn I	K^{5}	K^{9}	13	6 α_{C}-turn I
K^{9}	K^{3}	8	4 α_{RS}-turn I	K^{1}	K^{5}	12	5 α_{LS}-turn I
L^{4}	L^{8}	8	-	K^{7b}	L^{2}	29	-
K^{3}	K^{7}	7	-	Q^{10b}	K^{1}	29	-
Q^{10}	L^{4}	7	-	K^{3b}	K^{5}	23	-
K^{1}	K^{5}	5	3 α_{LS}-turn I	Q^{10b}	F^{6}	21	-
K^{7}	K^{1}	5	3 α_{LS}-turn I	K^{9b}	Q^{10}	18	-
F^{6}	Q^{10}	4	-	Q^{10}	K^{7b}	15	-
L^{2}	F^{6}	4	-	K^{5b}	Q^{10b}	15	-
L^{8}	Q^{10b}	11	-	K^{1}	K^{5b}	15	-
K^{7}	Q^{10b}	10	-	K^{5b}	K^{1b}	13	-
Q^{10b}	K^{1}	8	-	Q^{10b}	K^{5}	10	-
K^{1}	K^{3b}	7	-	K^{9b}	Q^{10b}	10	-
Q^{10b}	L^{2}	6	-	K^{1b}	Q^{10b}	9	-
Q^{10b}	K^{1}	6	-	K^{5b}	Q^{10b}	8	-
K^{1}	K^{3b}	6	-	K^{1b}	K^{3b}	8	-

[a] Hydrogen bond percentage %.

[b] A side-chain is involved in the hydrogen bond formation.

This seems to indicate that the SA protocol was a more homogeneous procedure for conformational search, whereas the applied SS protocol seems to get stuck in a specific conformation, thus avoiding the screening of the overall conformational space. This could be attributed to a too short time scale used in the SS protocol.

Furthermore, from the data on Table 5.1 it can be clearly seen that the set of MES produced by the SS protocol were mainly governed by either sidechain-backbone or sidechain-sidechain interactions. Up to eleven different hydrogen bonds involving side-chains were observed with a frequency of at least 10%, two of them observed for almost 30% of the structures. In contrast, only two different hydrogen bonds involving the sidechains displayed a frequency of occurrence over 10% in the structures obtained from the SA protocol.

So, in average, the SA protocol provided for the cyclic BPC16 peptide minimum energy structures with higher interaction within backbone atoms, resulting in specific secondary structure patters such as β and α-turns. Moreover, it showed better efficiency for the screening of the whole conformational space of the peptide. On the other hand, the SS approach provided less homogeneous set of conformations, being the most populated the one forming a bifurcated hydrogen bond between F^6-K^9 and F^6-Q^{10} residues. Besides, the MES were significatively stabilized by hydrogen bond interactions where the side-chain atoms were involved.

5.1.3 Relationship between Secondary Structure and Total Energy

The set of 998 minimum energy structures obtained from the SA protocol was further analyzed in order to find clues of the relationship between the total energy of the conformer and its 3D structure. To do so, the global minimum was taken as reference structure and the root mean square deviation (rmsd) of the backbone atoms was calculated for all MES of the set. The radius of gyration (root mean square distance of the atoms of the molecule from its center of gravity) of all structures of the set was also determined.

In Figure 5.2 A-B the energy is plotted versus the rmsd and the radius of gyration, respectively. There is no straightforward correlation between energy and structure. Although there is some linear correlation for the structures with small rmsd values (<1 Å), there is a large cluster of MES that exhibit a wide range of energies (from -150 to -185 kcal/mol) in the range 1 to 3 Å of rmsd with no correlation at all. In fact, there are up to 20 minimum energy structures

differing from the global minimum by 5 kcal/mol or less, and the second lowest minimum energy structure, just 1 kcal/mol higher, exhibits a rmsd value of almost 3 Å. We have attempted cluster analysis relative to the global minimum in order to classify the large number of MES of the set with no success. The cyclic nature of the peptide clearly restricts its conformational space and the MES seem to exhibit little structural differences.

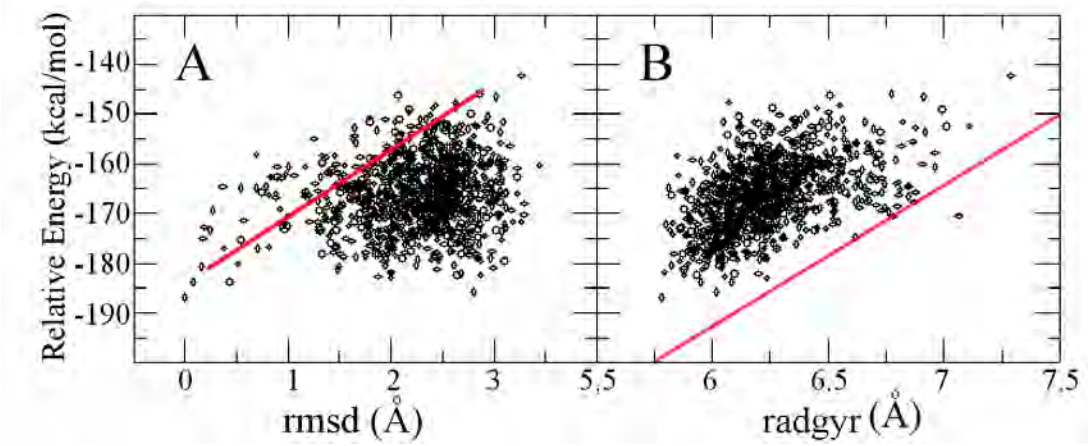

Figure 5.2: *Structure-Energy relationship for the set of MES from the SA protocol.* **A.** Energy (kcal/mol) vs rmsd (Å). **B.** Energy (kcal/mol) vs Radius of gyration (Å). The tendency of the data is indicated by the straight red line.

However, there seems to be some correlation between the energy and the radius of gyration of the MES (see Figure 5.2 B). Structures with small radius of gyration tend to be more stable. Indeed, the smallest value of radius of gyration was indeed found for the global minimum (5.7 Å), while the highest energy minimum shows the largest value (7.28 Å) of all conformations. Furthermore, the two dimensional plot can be divided by a straight line (red line in Figure 5.2 B) and all structures but one lay on the upper side of the graph. This indicates, for instance, that all structures with a radius of gyration over 6.5 Å differ in energy from the local minimum by more than 10 kcal/mol. The radius of gyration is associated to how compact is the conformation of the cyclic peptide. Hence, this suggests that the stability of the collection of MES for BPC16 is determined by the degree of favorable interactions amongst the backbone atoms.

5.1.4 Structural Characterization of Global Minima

The global minimum energy structures obtained with the SA and SS protocols were structurally quite different, yet very close in energy. The energy difference between them was less than 2 kcal/mol, being the global minimum structure

from the SA protocol (henceforth SA minimum) the most stable one. The 3D structure of both conformers is shown in Figure 5.3.

The SA minimum (Figure 5.3 A) is characterized by the presence of three loops stabilized by a number of hydrogen bonds involving backbone atoms. The strongest interaction is characterized by a bifurcated hydrogen bond between residues K^5-L^8 and K^5-K^9. The distances between the oxygen atom of lysine (K^5) and the nitrogen atoms of residues L^8 and K^9 are 2.89 and 2.77 Å, respectively (Table 5.2). These interaction were associated to type I β and type I α_{RS}-turns. The remaining two loops were stabilized by hydrogen bonds involving residues K^9-L^2, Q^{10}-K^3 and L^2-K^5, associated to a type I and type II' β-turns, respectively. The respective hydrogen bond distances are 2.94, 2.97 and 3.16 Å. The presence of these three pattern stabilizes the structure giving rise to a compact non-regular circular-shaped geometry. Besides the hydrogen bond interactions of the backbone atoms, the SA minimum also exhibits up to three relevant interactions involving side-chain atoms. The carbonyl group of residues L^4 and F^6 form hydrogen bonds of 2.84 and 2.97 Å with the amino side-chains of residues Q^{10} and K^7, respectively. Finally, the oxygen atom of the amide side-chain of the glutamine residue (Q^{10}) forms a hydrogen bond with the amino group of the side-chain of the K^1. For an overall description see Table 5.2.

On the other hand, the lowest minimum energy structure obtained from the SS protocol (henceforth SS minimum, see Figure 5.3 B) exhibits a rather different geometry, characterized by the presence of only two loops. One of them, associated mainly to a type I β turn, is stabilized by the presence of a bifurcated hydrogen bond involving the backbone atoms of residues F^6-K^9 and F^6-Q^{10} with hydrogen bond distances of 2.95 and 3.02 Å, respectively (Table 5.2). Similarly, the oxygen atom of the carbonyl group of residue K^5 is involved in another rather long-range bifurcated interaction with the amino groups of residues K^3 and L^4, that help the stabilization of the second turn. Nevertheless the hydrogen bond distances of 3.14 and 3.24 Å and also the rather large deviation of these hydrogen bond interactions from linearity indicate that this interaction should be rather weak. In this case, the hydrogen bonding pattern between residues $i \rightarrow i-2$ and $i \rightarrow i-1$ are characteristic of C11-type and C8-type interactions.

Unlike the SA minimum, the main hydrogen bond interactions present in the SS minimum involve side-chain atoms. On one hand, the spatial arrangement of the side-chains of lysines amino acids in position 1, 3 and 5 and the side-chain of the glutamine un 10th position lead to the formation of a complex net of hydrogen bonds. Some of them occur between the hydrogen atom of the amino group and the nitrogen atom of different side-chains of lysine amino acid, which

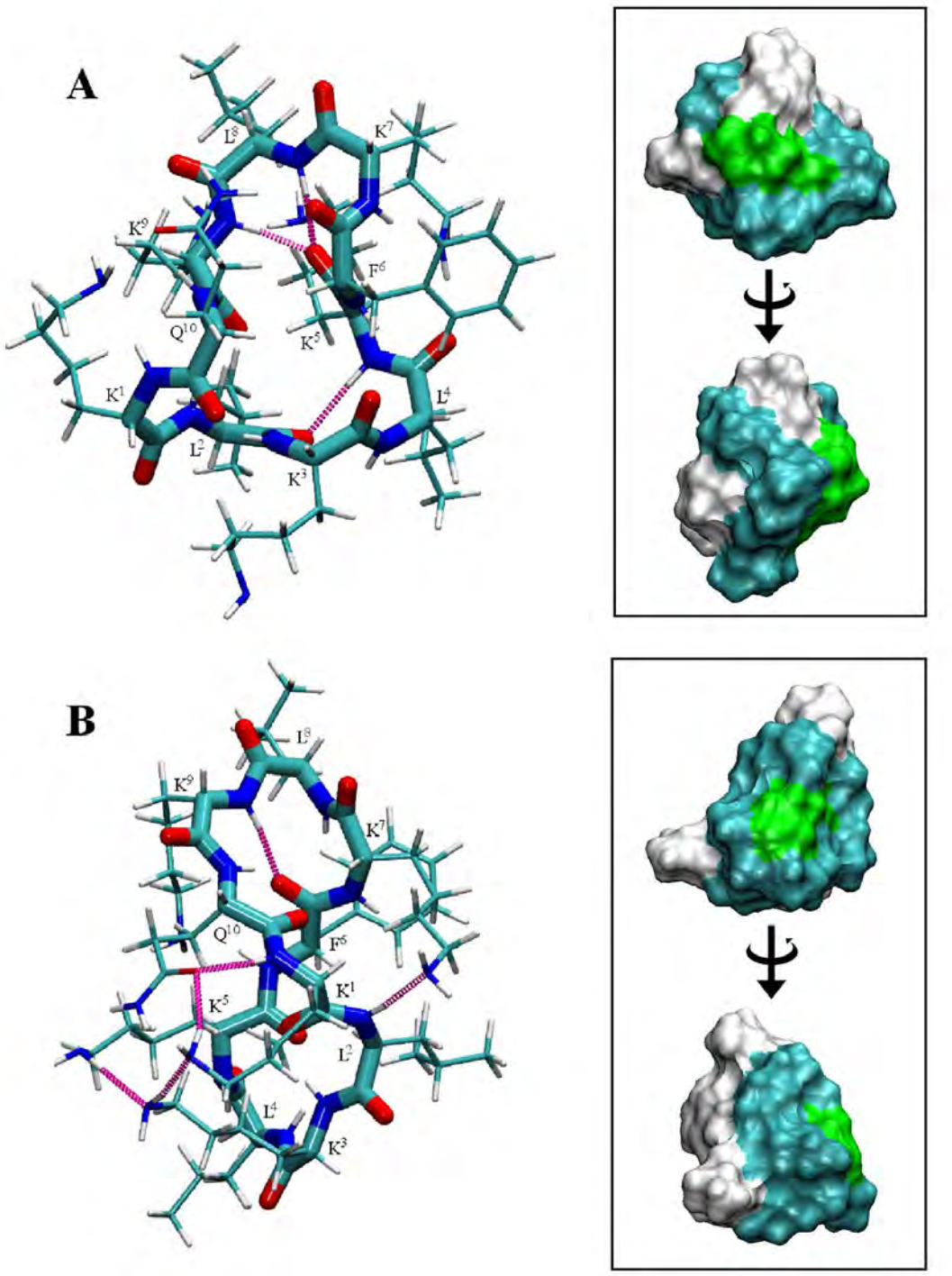

Figure 5.3: *Pictorial representation of two low energy structures* **A.** SA global minimum. **B.** SS global minimum. The backbone atoms are shown in red (oxygen), blue (nitrogen) and white (hydrogen). Small panels on the right hand side show the 3D of the accessible water surface area representation of both structures, where the hydrophilic side-chains are depicted in cyan (K), the hydrophobic in white (L and F) and the polar in green (Q). The main hydrogen bonding interactions are shown in magenta dashed lines.

would be rather weak (*e.g.* K^3-K^5 interaction). On the other hand, the presence of side-chain - backbone interactions is also observed, as exposed in Table 5.2. Even so, the network of hydrogen bonds might be the main responsible for the low energy of the structure, overcoming the apparent lack of backbone-backbone interaction.

Table 5.2: Hydrogen bond features of the global minima. Backbone - Backbone (B-B); side-chain - backbone (SS-B); side-chain - side-chain (SS-SS) interactions. D stands for donor and A for acceptor.

	Interaction	**D**	**A**	**Secondary structure**	**Hbond distance (Å)**	**Hbond angle (^{o})**
SA	B-B	K^5	L^8	β-turn I	2.89	16.61
	B-B	K^5	L^9	α_{RS}-turn I	2.77	15.37
	B-B	K^9	L^2	β-turn I	2.94	30.47
	B-B	Q^{10}	K^3	-	2.97	31.24
	B-B	L^2	K^5	β-turn II'	3.16	9.56
	B-SS	L^4	K^7	-	2.97	11.77
	B-SS	F^6	Q^{10}	-	2.84	23.30
	SS-SS	Q^{10}	K^1	-	2.93	30.74
SS	B-B	F^6	K^9	β-turn I	2.95	8.10
	B-B	F^6	Q^{10}	α_{RS}-turn I	3.02	25.10
	B-B	K^5	L^4	C8-type	3.24	38.26
	B-B	K^5	K^3	C11-type	3.14	29.30
	SS-B	K^9	F^6	-	3.07	26.91
	SS-B	K^7	L^2	-	3.02	7.38
	SS-B	Q^{10}	K^1	-	2.89	16.14
	SS-SS	Q^{10}	K^1	-	3.02	21.81
	SS-SS	K^1	Q^{10}	-	2.97	29.28
	SS-SS	K^5	Q^{10}	-	2.90	32.02
	SS-SS	K^3	K^5	-	3.07	3.74
	SS-SS	K^1	K^3	-	3.05	12.30

So, with regard to the differences on their structure, the SA minimum showed intramolecular interactions preferably between backbone atoms, whereas in the SS minimum preferential interactions involved the side-chains. In fact, the spatial arrangement of the different side-chains of the residues mainly governs the appearance of amphipatic structures, where the hydrophobic and hydrophilic side-chains are placed in opposite sides of the structure. The amphipatic character of both the SA and SS minimum structures is also illustrated in the small panels of Figure 5.3 by means of colored surface area representations. The SA

global minimum does not exhibit a clear amphipatic structure, as the hydrophobic residues do not seem to be organized. In contrast, structure of the SS minimum do shows a certain amphipatic character since all lysine side-chains are oriented towards one direction while the leucine and phenylalanine residues lay on the other side of the structure.

5.1.5 Global Minimum Stability in Gas Phase

In order to determine the strength of the different intramolecular interactions that stabilize the geometries of the two minimum energy structures discussed above, two independent MD simulations in gas phase starting from the SA and SS minimum structures were carried out. Several hydrogen bond distances were monitored along the time course of the simulations, both involving backbone and side-chain atoms. These distance fluctuations are shown in Figure 5.4. The average hydrogen bond distances and percentage of persistence along the trajectories are gathered in Table 5.3.

The results[1] indicate that the structure corresponding to the SA minimum appears to be much more stable as compared to that of the SS minimum. As it can be seen, the hydrogen bond distances of the main backbone - backbone interactions remain quite constant along the simulation. Only the hydrogen bond involving residues Q^{10}-K^3 displayed momentary disruptions (Figure 5.4, top panel A, green line). The remaining hydrogen bonds oscillated around equilibrium distance, being the bifurcated K^5/L^8-K^9 and K^9-L^2 (Figure 5.4, top panel A, black and orange lines) the ones significantly shorter than those involving residues K^3-F^6 and L^2-K^5 (Figure 5.4, top panel A, blue and red lines). In the bottom panel of Figure 5.4 A, one can see the fluctuation of the distance of two hydrogen bonds involving side-chain atoms. In this case, the one associated with the glutamine side-chain (purple line) was very stable along the simulation, whereas the one involving the side-chain of residue K^7 showed huge fluctuations.

The average data on Table 5.3 indicates that the bifurcated hydrogen bond involving residue K^5 was extremely stable (99% of persistence). Two more hydrogen bonds involving residues K^9 and F^6 were also present essentially during the whole trajectory (87% and 95% of persistences, respectively). The weakest hydrogen bond turned out to be the one involving residue L^2-K^5, showing a rather large average distance of 2.66 Å and consequently a lower persistence of 52%. This intramolecular interaction was responsible for the stabilization of the type II' β-turn present in the SA minimum.

[1]Note that the distances in this case are smaller than the exposed in the previous section. The monitoring was calculated different as it is explained in section 5.1.1.5

Table 5.3: Average distances standard deviation and persistence of the main hydrogen bonding interactions along the MD simulations in gas-phase and in water-phase.

		Vaccum Simulation		**Water Simulation**		
	Residues[a]	**Distance (Å)**	**% Hbond formation**[b]	**Distance (Å)**	**% Hbond formation**[b]	**% Solvent interaction**[c]
SA	K^5-L^8	2.02±0.06	99	2.13±0.37	95	1-2
	K^5-K^9	1.95±0.07	99	2.18±0.41	87	1-2
	K^9-L^2	2.25±0.13	87	2.75±0.60	55	1-2
	L^2-K^5	2.66±0.25	52	2.98±0.87	55	6
	F^6-Q^{10}(HE)	2.08±0.09	95	-	-	15
	L^4-K^7(HZ)	3.04±0.66	71	-	-	20
SS	F^6-K^9	2.12±0.07	98	2.93±2.40	51	51
	F^6-Q^{10}	-	97	-	44	51
	K^5-L^4	-	∼ 5	-	-	>100[d]
	K^5-K^3	-	∼ 5	-	-	
	Q^{10}-L^4	2.68±1.20	75	-	3	60
	L^2-K^5	3.12±0.95	40	-	-	>100[d]

[a] The hydrogen bond is formed between the oxygen atom of the carbonyl group of the first residue (donor) and a hydrogen atom of the second residue (acceptor).

[b] Percentage of time the hydrogen bond was formed over the trajectory.

[c] Percentage of time solvent molecules were involved in hydrogen bond formation.

[d] Values >100% indicate more than a single water molecule involved in the hydrogen bond.

On the other hand, the structure of the SS minimum manifested a quite different dynamical behaviour in gas phase. The initial structure was not stable albeit the hydrogen bond network involving the side-chains of a number of residues. One can see in the top panel of Figure 5.4 B that the bifurcated hydrogen bond involving residues F^6-K^9 and F^6-Q^{10} (black line) was very stable and exhibited little fluctuations during the simulation. On the contrary, the other bifurcated hydrogen bond involving residue K^5 that was present in the starting structure was lost within the first 10 ns of the simulation (blue line). Simultaneously, two new hydrogen bonds were formed between residues L^2-K^5 and Q^{10}-L^4. Specially the latter (green line) showed rather high stability during the rest of the simulation. Also, the network of hydrogen bonds involving the lysine and glutamine side-chains was broken within the first few ns of the simulations. In the lower panel of Figure 5.4 B one can see how some representative hydrogen

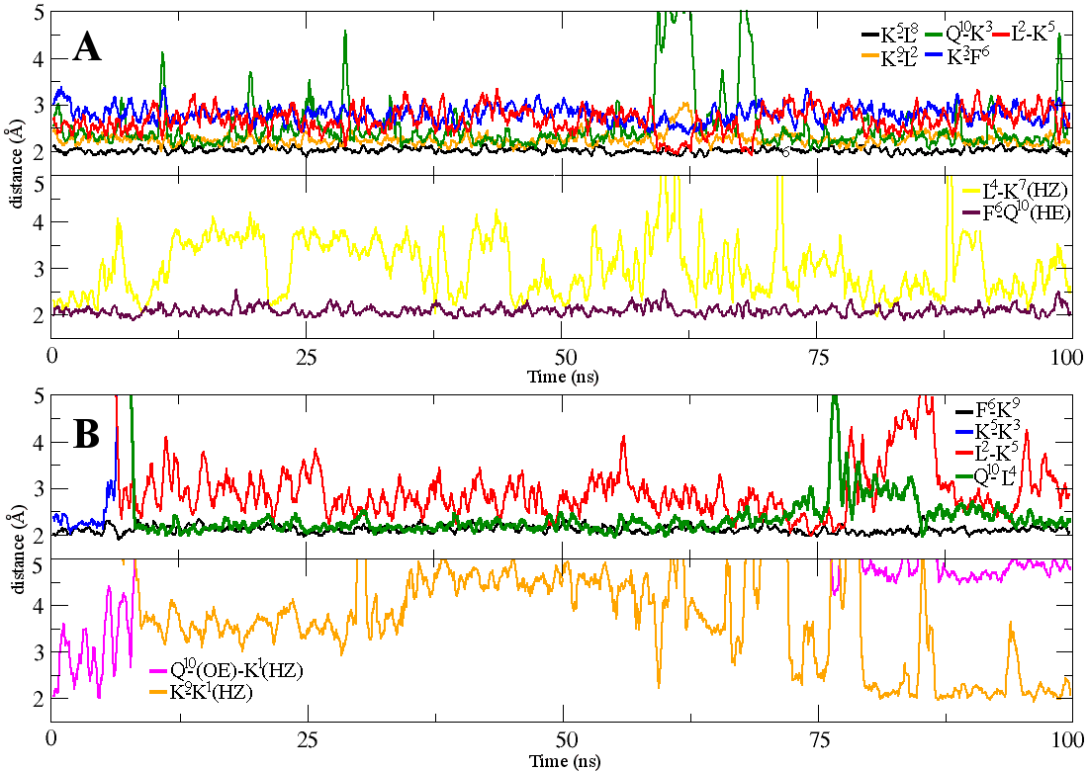

Figure 5.4: *Hydrogen bond distances as function of time* **A.** Hydrogen bond distances from MD simulation of the SA minimum. **B.** Hydrogen bond distances from MD simulation of the SS minimum. The top panel show hydrogen bonds between backbone atoms, and bottom panel show the most important interactions involving side-chain atoms. Distances are shown in Å and time in ns.

bond distances rapidly increase and oscillate around very large values.

Therefore it is clear that the SS minimum structure underwent a conformational change. The turn stabilized by the residue F^6 persisted along the simulation but the second turn, originated by C8 and C11-type interaction, was lost and two new hydrogen bonds showed up. It is worth noticing that these two new hydrogen bond interactions were observed in the static conformational analysis described in previous section. In fact, the hydrogen bond between residues L^2-K^5 was present in 27% of the set of MES obtained with the SA protocol, the second most populated one (see Table 5.1).

In Figure 5.5 two snapshots corresponding to the initial and final structure of the simulation (A and B, respectively) are compared. The superposition of the two structures (Figure 5.5 C) shows how the rather tight initial lower loop shifted towards a wider one stabilized by two hydrogen bonds, in particular a $i \rightarrow i+4$ th one.

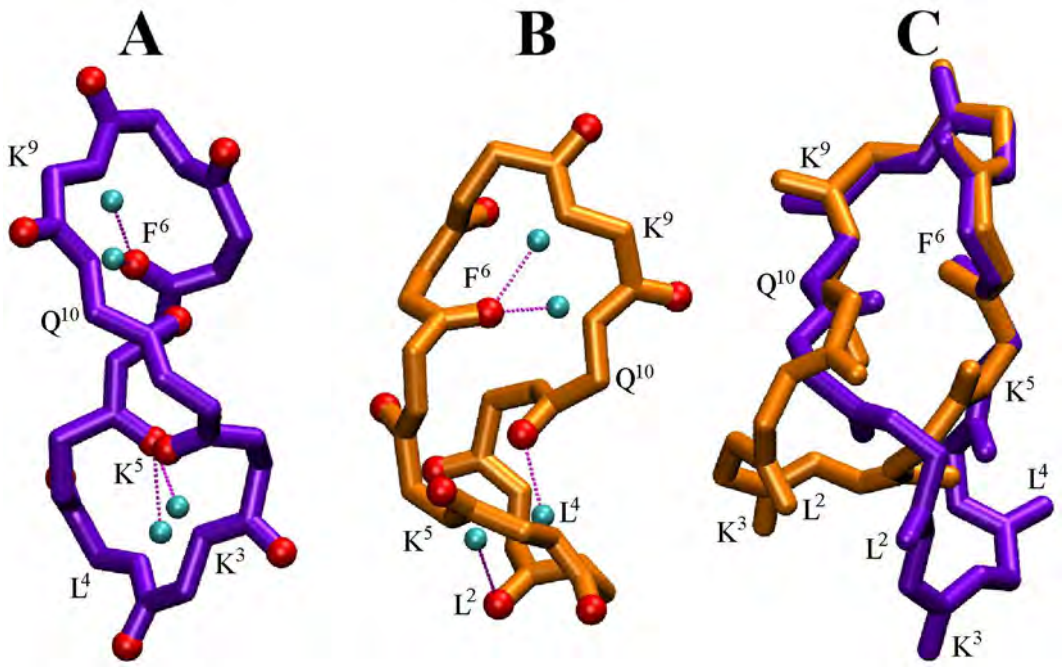

Figure 5.5: *SS global minimum stability in gas phase* **A.** Initial conformation (purple) where the two bifurcated hydrogen bonds are shown. **B.** New arrangement of the global minimum (orange) due to the formation of two new hydrogen bonds. **C.** Superposition of both structures. Oxygen atoms (red spheres) and hydrogen atoms (cyan spheres) are depicted to clarify the hydrogen bond (interaction indicated with purple line).

5.1.6 Global Minimum Stability in Water Phase

The analysis of the dynamical behaviour of the two lowest minimum energy structures in gas phase indicated that some hydrogen bonding interactions were intrinsically more stable than others. This was specially the case of the $i \rightarrow i{+}3$ th and $i \rightarrow i{+}4$ th hydrogen bonds between backbone atoms, that even appeared in the form of bifurcated hydrogen bonds of particular stability. Such analysis, however, could not take into account the possible effect of the solvent, such as water molecules, in the stability of the hydrogen bonds and hence on the conformation of the BPC16 cyclic peptide in solution. For this purpose, two independent MD simulations in water solvent were also carried out, starting again from the SA and SS minimum structures obtained in gas-phase. As expected, because of the the interaction of water molecules with the hydrogen bond donor and acceptor groups of the peptide, and the screening of the long-range interactions, the geometries of both minimum energy structures exhibited more fluctuations along the simulation compared to the gas phase case. In Table 5.3 the average hydrogen bond distances and persistence of both intramolecular and

intermolecular (solvent) hydrogen bond formation for both simulations in water phase are summarized.

Again, the structure of the SA minimum showed high dynamical stability. The most important intramolecular hydrogen bonds between backbone atoms, that were essential for the stability of the local secondary structure motifs were preserved for the time scale of the simulation. The average hydrogen bond distances were somewhat larger that in the gas-phase simulation, and their fluctuations significatively increased. For instance, the bifurcated hydrogen bonding between residues K^5-L^8 and K^5-K^9 showed occupancies of 95 and 87%, and the average hydrogen bond distances increased by roughly 0.2 Å from their values in gas-phase to 2.13 and 2.18 Å in water phase, respectively. The standard deviation of these average values (about ±0.4 Å) was also significatively larger than in gas-phase (±0.07 Å). The other two intramolecular hydrogen bonds that secured the stability of the other turns of the structure exhibited an occupation around 55% and substantial increase of their distance and fluctuation. However, even for the apparently weakest hydrogen bond, involving residues L^2-K^5, the donor and acceptor hydrogen bond sites were occupied by solvent molecules only for up to 6% of the time simulation. This indicates that the main hydrogen bond interactions in the backbone interaction showed little vulnerability in front solvation, and hence were essentially present during the simulation, yet weakened by the screening action of the solvent molecules. Conversely, the hydrogen bond interactions involving the side-chain atoms were not detected as a result of the solvation with water molecules. For instance, the carbonyl groups of residues F^6 and L^4, that were involved in hydrogen bonds with acceptor groups of the side-chains, now show occupations by solvent molecules of 15-20%. In fact the side-chains were essentially pulled apart from the backbone and the polar groups fully solvated by water molecules.

Unlike the SA minimum, the SS minimum structure was dramatically affected by the solvent and from the very beginning of the simulation all hydrogen bonds in the backbone were lost except for the bifurcated one involving residues F^6-K^9 and F^6-Q^{10}. Even for this interaction the average distance increased by more than 0.8 Å as compared to the gas-phase case, and the persistence of occupations dropped to 51% and 44%, respectively. In this case, however, the large fluctuation of the hydrogen bond distance and an occupation of 51% of the F^6 carbonyl group by solvent molecules is indicative that this hydrogen bond interaction was effectively lost for half of the simulation. Moreover, a high percentage of hydrogen bond formation between backbone donor groups and water molecules was observed through the simulation, which in some cases involved more than

one water molecule simultaneously. Similarly to the case of the SA minimum structure, the side-chains were pulled apart by the action of solvent molecules so the network of hydrogen bonds between the side-chains was again disrupted by the solvent effects.

To conclude, the application of SA and SS protocols for the conformational analysis of the antimicrobial cyclic peptide BPC16 led to a large set of minimum energy structures. Due to the cyclic nature of the peptide the structural motifs of these conformers were not too different, yet a certain predisposition towards compact structures was observed. The structural stability of the two lowest minimum energy structures was investigated by means of MD simulations in gas-phase and in solution. It was found that the global minimum, which presented three turns stabilized by a number of hydrogen bond interactions in the backbone was very stable in both environments. Even though some hydrogen bonds were shown to be energetically less stable than others, they persisted significantly at least for the time scale of the simulations. The screening effects induced by the water molecules further weakened those hydrogen bonds and pulled the side-chains away from the backbone, but the local secondary structure was preserved. In all cases the most stable structural motifs were manifested by the formation of bifurcated hydrogen bonds, giving rise to mostly type I β structures.

Another low energy conformer characterized by a large number of hydrogen bond interactions involving the side-chains and having a clear amphipatic structure exhibited little dynamical stability, even in gas-phase. This indicates that amphipaticity is not necessarily connected with lower energy or enhanced stability. On the contrary, these structures seem to be penalized by entropic effects. Whether a possible amphipatic character of a peptide can account for its antimicrobial activity or not, should be sustained by further studies where not only the peptide and the solvent is included in the system but also its target.

In this line, in the next section the interaction of several cyclic peptides with lipid membranes models are discussed in deep detail.

5.2 Study of the Interaction of a Cyclic Peptide with Lipid Membranes Models

The structural characteristics of AMPs have been extensively studied, especially for linear α-helical peptides that have been shown to be unstructured in water phase, but able to adopt a defined secondary structure upon association with a lipid membrane (Huang 2000, Ludtke 1996, Qian 2008 and van den Bogaart 2008). Though some short peptides lacking of a well defined secondary structure are also active (Houston 1998), acquiring structure upon membrane binding has been proposed to be an important feature for antimicrobial activity. Associated to the formation of secondary structure, the partitioning behaviour of the peptides, i.e. the membrane-aqueous medium partition coefficient and the membrane penetration depth may also be relevant for their function and selectivity. Hence it is clear that in order to understand the molecular basis of the activity of the AMPs, more realistic MD simulations including lipid membrane models must be considered.

In this section we describe a number of MD simulations where a model membrane was used to examine the behaviour of a cyclic peptide in such environment. We have focused our attention on the cyclic peptide BPC194, with sequence c(KKLKKFKKLQ), which was found to be the best candidate from the second generation of de novo cyclic decapeptides obtained by Monroc (Monroc 2006b). Its linear analogue (BPC193), which was found to be poorly active against the same pathogenic bacteria, was also considered in the simulations for comparasion.

We have found that the peptide BPC194 and its linear analogue exhibit significant differences in i) membrane binding properties, ii) propensity to adopt an ordered secondary structure upon membrane interaction, and iii) insertion depth in the lipid membrane. These factors appear to be the first clues for its high activity.

5.2.1 Methodology

5.2.1.1 System set-up.

MD simulations were performed with peptide BPC194, with sequence c(KKLKKFKKLQ), and its linear analogue BPC193, with sequence H-KKLKKFKKLQ-OH. For the cyclic peptide, a peptide bond was created between the N-terminal lysine residue and the C-terminal glutamine residue. The initial structure of the peptides was modeled using the *leap* module of AMBER

9 (Case 2006).

5.2.1.2 Peptide in aqueous environment.

A number of systems were prepared with either one cyclic or one linear peptide solvated by water. The cyclic peptide was initially unstructured (no hydrogen bond within the backbone atoms) in all simulations. Different starting conformations of the linear analogue were tested, namely α-helical, bend and random-coil. An overview of all simulations performed is shown in Table 5.4 (simulation codes W_a-W_k). Further details can be found in Annex II Table 7.3. All systems were simulated in a cubic box of length 4 to 5 nm and about 3000 water molecules. In several simulations, an appropriate number of Cl^- counterions were added to neutralize the system.

Table 5.4: Overview of all simulations performed on the cyclic (BPC194) and linear (BPC193) peptides.

P:L ratio	Code	Peptide	Number of Simulations
No lipid	W_a-W_c	Cyclic	3
	W_d-W_k	Linear	8
1:128	$1C_a$-$1C_g$	Cyclic	7
	$1L_a$-$1L_b$	Linear	2
2:60	$2L_a$-$2L_b$	Linear	2
4:128	$4C_a$-$4C_c$	Cyclic	3
	$4L_a$-$4L_b$	Linear	2
9:128	$9C_a$-$9C_j$	Cyclic	10
	$9L_a$-$9L_g$	Linear	7

5.2.1.3 Peptide-membrane systems.

A number of simulations were performed for a solvated 128 DPPG (1,2-dipalmitoyl-sn-glycero-3-phosphatidylglycerol) lipid membrane system and a molar peptide:lipid (P:L) ratios of 1:128, 2:60, 4:128 and 9:128 for both BPC193 and BPC193 peptides. The system included 6000-8000 water molecules and 128 K^+ as counterions for anionic lipids. For an overview of the simulations performed see Table 5.4 and Supplementary Table 7.3 in Annex II 7.6.

The peptides were initially placed in the water phase close to the membrane surface, with distances between the peptides and membrane ranging from 1.5

to 2.3 nm. The orientation of the peptides was chosen so as to minimize the size of the simulation box. The cyclic peptide units were initially unstructured and again different conformations were tested in the case of the linear analog. Multiple simulations were run from different initial random velocity distributions for each of the P:L ratios. The simulations were carried out both in the presence and in absence of counterions, as well as using different algorithms to account for the electrostatic interactions.

5.2.1.4 Simulation parameters.

The GROMACS software package (van der Spoel 2005) was used to perform all MD simulations. The GROMOS force-field 43a2 (van Gunsteren 1996) was used to describe the peptide and peptide-solvent interactions. Simulations in water were also run using GROMOS force-field 53a6 (Oostenbrink 2005). The force-field for DPPG lipids was optimized from DPPC (Aneézo 2003) and POPG (Zhao 2007) lipids, compatible with the GROMOS96 parameters. The choline head-groups were replaced by glycerol models from the POPG force-field, and the tail parameters were taken from the DPPC force-field. The parameters were then optimized to achieve an area per lipid consistent with experiment (Pabst 2007). The equilibrated DPPG bilayer had a thickness of 3.54±0.05 nm and an area per lipid of 0.69±0.01 nm^2. All force-fields were parameterized for use with a group-based twin range cut-off scheme (using cutoffs of 1.0/1.4 nm and a pair-list update frequency of once per 10 steps), including a reaction field (RF)(Tironi 1995) correction with a dielectric constant of 78 to account for the truncation of long-range electrostatic interactions. To test the effect of long-range electrostatic interactions, in some simulations the RF was replaced by the particle-mesh Ewald (PME) method. The water was modeled using the SPC model (Berendsen 1981). A time step of 2 fs was used. Bond lengths were constrained using the LINCS algorithm (Hess 1997). The simulations were performed in the $NP_{|}P_{Z}T$ ensemble using periodic boundary conditions. The temperature was weakly coupled (coupling time 0.1 ps) to T = 320 K using the Berendsen thermostat (Berendsen 84). The pressure was also weakly coupled (coupling time of 1.0 ps and compressibility of 4.5×10^{-5}), using a semi isotropic coupling scheme in which the lateral ($P_{|}$) and perpendicular (P_{Z}) pressures were coupled independently at 1 bar, corresponding to a tension-free state of the membrane. The simulation setup is similar to that used in previous studies of peptide-membrane interactions (Leontiadou 2006, Sengupta 2008, Yesylevskyy 1999).

5.2.1.5 Analysis.

The secondary structure of the peptides was calculated with the DSSP code (Kabsch 83). For the cyclic peptide, the bonded N-terminus (K^1) and C-terminus (Q^{10}), present in the turn region, were neglected when calculating the secondary structure. The structural properties were then calculated from the average number of residues involved in each secondary structural feature along the simulation. The total β-structure is reported as the sum of β-sheet and β-bridge (one hydrogen bond less than β-sheet) and the non-structured, as the sum of coil, bend and turn. To analyze the alignment of the lysine residues, the distance between the planes formed by the C_α, C_γ and N_δ atoms of the spatially-symmetric lysine residues K^1-K^8, K^2-K^7 and K^4-K^5 were calculated.

5.2.2 Linear and Cyclic Peptides are Structureless in Aqueous Solution

To analyze the structure of the peptides in aqueous solution, atomistic MD simulations in water environment were performed. In the simulations, the cyclic and the linear peptide showed no defined secondary structure in aqueous solution and appeared mainly in a non-structured conformation as it is shown in Figure 5.6.

Table 5.5: Secondary structure of the cyclic (BPC194) and linear (BPC193) peptides in the simulations. Results are averaged over all peptides present in the system and over all independent simulations. The standard errors reported are calculated from the standard deviation between all peptides in all simulations.

Peptide	P:L ratio	% Non-Structured	% β-Structure
Cyclic	Water	87±5	13±5
	1:128	79±3	21±3
	4:128	67±4	33±4
	9:128	68±2	32±2
Linear	Water	84±4	16±4
	1:128	100±0	0±0
	4:128	100±0	0±0
	9:128	99±0	1±0

On average, only 13 and 16% β-structure was adopted by the cyclic and linear peptide, respectively (see Table 5.5). Although we found that 50 ns of

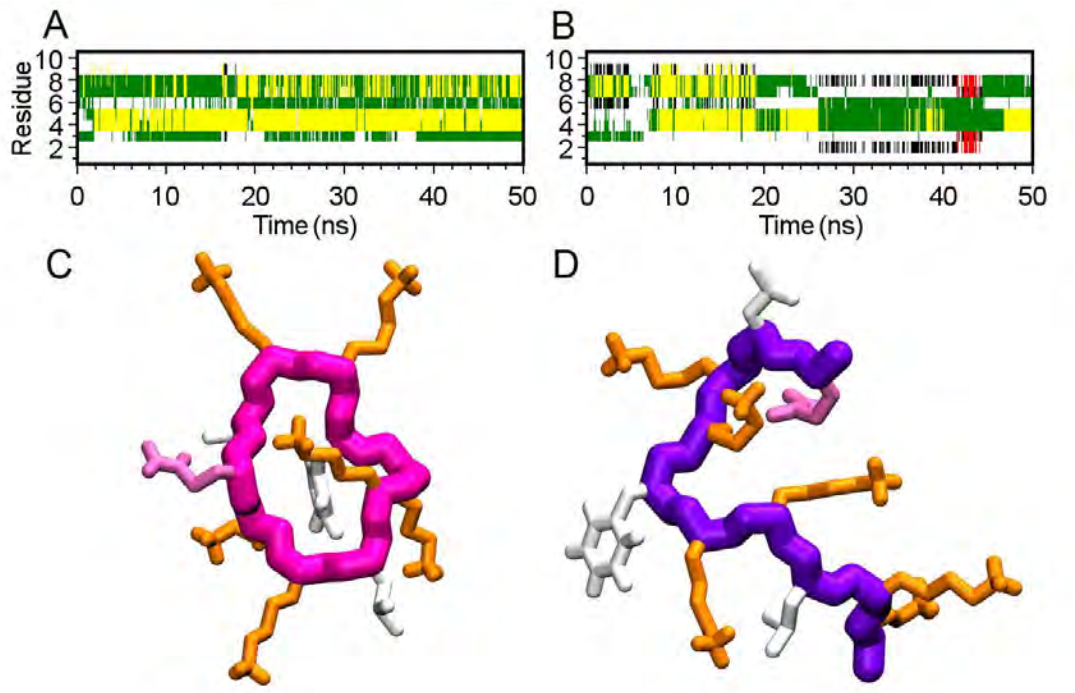

Figure 5.6: *Cyclic and linear peptides are unstructured in water.* **A-B.** Secondary structure plot of BPC194 and BPC193, respectively in water as determined by the DSSP code. The colours associated with the secondary structural elements are red (β-sheet), yellow (turn), green (bend), black (β-bridge) and white (coil). **C-D.** Representative snapshots of BPC194 and BPC193, respectively. In both cases, lysine residues are shown in orange, phenylalanine and leucine in white and glutamine in light pink.

simulation were not sufficient for the peptides to completely sample their configurational space, our data points towards an unstructured conformation of both peptides in solution. The lack of secondary structure of the peptides predicted by the MD simulations was also confirmed by CD spectroscopy measurements carried out in buffer (Figure 7.44 in Annex II 7.6). The data supported that both BPC194 and BPC193 exhibit characteristic features of disordered peptides.

5.2.3 Cyclic Peptides Adopt a β-Structure Upon Binding to Membranes.

To predict the structure of BPC194 at the membrane surface, simulations were performed with multiple copies of the peptides placed in water phase close to the membrane surface of a DPPG bilayer at P:L ratios of 1:128, 4:128 and 9:128. The cyclic peptide was bound to the membrane rather fast at nanosecond time

scale (see Figure 5.7 A). The initial binding was driven by the electrostatic interactions between the positive charge of the lysines and the negative charge of the head-group of the phospatydylglycerol moieties of the lipids. Upon interaction with the DPPG membrane surface, the secondary structure was induced within nanoseconds, and the average fraction of β-structure (both β-sheet and β-bridge) increased from 13% to 32% (Table 5.5). The increase in β-structure was more pronounced at the high P:L ratios of 4:128 and 9:128. CD measurements were consistent with these MD simulations as it can be seen in Figure 7.44 in Annex II 7.6. Upon addition of DOPG membranes, a substantial change in ellipticity of the cyclic peptide was observed, indicating that the peptides adopted a β-sheet structure in the presence of DOPG (Mika 2011).

5.2.4 Linear Peptides Remain Unstructured Upon Membrane Binding.

The linear analogue BPC193 was simulated under the same conditions as its cyclic analog. The peptide was able to bind to the membrane as fast as the cyclic peptide, as can be seen in Figure 5.7 A. However, in contrast to the cyclic analogue, the linear peptide did not adopt a particular secondary structure (Figure 5.7 B-D). It remained fully unstructured with no presence of intramolecular hydrogen bonding at the DPPG membrane interface at P:L ratios of 1:128 and 4:128 (Table 5.5). At the highest P:L ratio (9:128) a few intermolecular interactions were seen between two different peptides, which resulted in some β-sheet like structure. These interactions were mainly due to acceptor atoms of the C-terminus, the glutamine side-chain and some backbone atoms. We also performed a simulation with the linear peptide folded into an ideal α-helix structure and the rapid unfolding to a random-coil conformation was observed (Table 5.4, simulations 2La-2Lb). The simulations were again in agreement with the CD spectra. In fact, neither the addition of TFE (a secondary structure inducer for amphipathic peptides) nor DOPG-containing liposomes resulted in changes in secondary structure (Figure 7.44 in Annex II 7.6).

5.2.5 Cyclic Peptides Insert Deeper into the Membrane than the Linear Analogues.

In the simulations, the cyclic peptide and the linear analogue bound to the membrane rather fast and at similar time scales. This was due to the electrostatic interaction between the positive charge of the lysines and the negative charge of the head of the group of the DPPG membrane. Nevertheless, the way they were

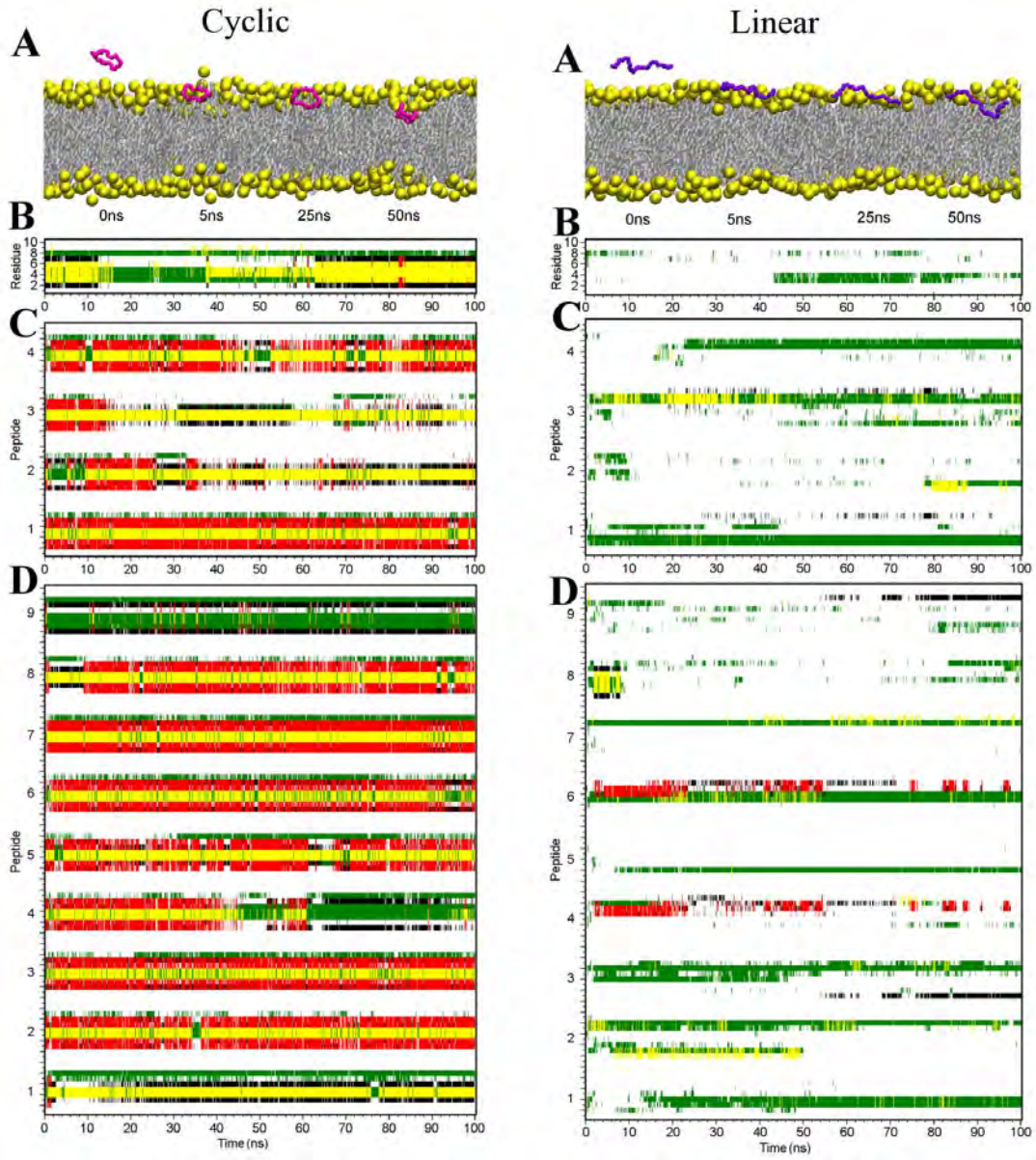

Figure 5.7: *The cyclic peptide binds and acquires secondary structure upon membrane binding, whereas the linear peptide remains unstructured* **A.** Time course of the simulations $1C_a$ (BPC194 in pink) and $1L_b$ (BPC193 in violet) interacting with DPPG membranes. The head-group phosphorus atoms are shown in yellow, the lipid tails in grey and side-chains have been removed for clarity. **B-D.** DSSP plots of the simulations at P:L ratios of 1:128, 4:128 and 9:128, respectively. The color legend is the same as in Figure 5.6.

able to bind differed. The simulation series 1C-1L, 4C-4L and 9C-9L showed that BPC194 was able to penetrate deeper into the phospholipid membrane than its linear counterpart.

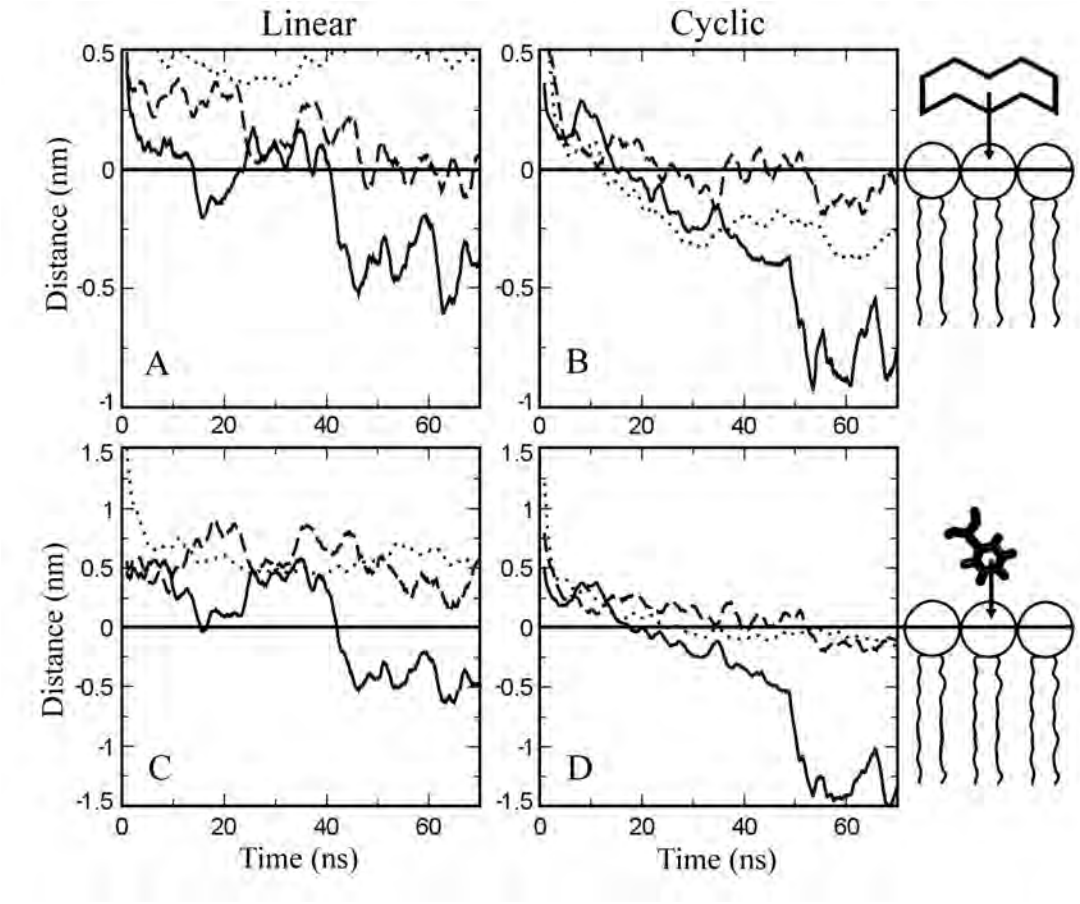

Figure 5.8: *The cyclic peptide embeds deeper into the membrane than the linear one* Time evolution of the distance between the center of mass of the peptides BPC193 **(A)** and BPC194 **(B)** and the phosphorus atoms of the DPPG bilayer at different P:L ratios; 1:128 (solid line), 4:128 (dashed line) and 9:128 (dotted line). At higher P:L ratios, the distances plotted are the averages of all peptides in the system. The sub-panels (**C** and **D**) depict the distance between the phenylalanine residue and head-group phosphorus atoms. The zero value was taken as the interface boundary (black line).

The distance between the phosphorus atoms of the outer leaflet and the center of mass of either the whole peptide or the phenylalanine side-chain were calculated as a measure of the penetration depth. The results are described in Figure 5.8. The cyclic peptide BPC194 was able to insert below the level of the phosphorus atoms even at low P:L ratios, whereas the linear peptide remained, at low P:L ratios, at the interface most of the time, and even at the highest

ratios the peptide remained above the level of the phosphorus atoms. To further compare both peptides, in Table 5.6 the average of the binding depth for all peptides present in the simulation is presented, together with the maximum insertion for individual peptides. A single cyclic peptide (P:L 1:128) appeared on average to bind deeper (-0.34 nm) compared to systems with P:L ratios of 4:128, 9:128 (-0.08 nm and -0.24 nm). However, the maximum insertion for individual peptides was at P:L ratio of 9:128 (-1.20 nm). Visual inspection of the trajectories showed that large values of insertion of the cyclic peptide were associated with high local perturbations (see section 5.3.2). In contrast to the cyclic peptide, the linear analogue BPC193 did not embed very deeply in the membrane. The maximum insertion observed was only -0.62 nm below the level of the phosphorus atoms and was not accompanied by large bilayer perturbations. Experiments confirmed the MD simulation by analysing the fluorescence emission spectra of tryptophan analogues of both peptides in different environment, such as water and hydrophobic phase. In the experiments, the tryptophan analogue of BPC194 (BPC418) showed stronger binding and deeper insertion compared to the linear peptide (BPC417) which showed low insertion and even dissociation from the membrane by addition of NaCl (Figure 7.45 in Annex II 7.6).

Table 5.6: Depth of binding of the cyclic (BPC194) and linear (BPC193) peptides in the simulations. The average binding depth as well as the maximum binding depth observed for a particular peptide are given. The standard deviation between all peptides in all simulations is also reported.

		Cyclic BPC194		**Linear BPC193**	
	P:L Ratio	**Av. Depth (nm)**	**Max. Depth (nm)**	**Av. Depth (nm)**	**Max. Depth (nm)**
Peptide[a]	1:128	-0.34±0.38	-1.16	-0.18±0.25	-0.78
	4:128	-0.08±0.23	-0.99	0.10±0.18	-0.75
	9:128	-0.24±0.25	-1.20	0.41±0.19	-0.62
Phe[b]	1:128	-0.52±0.65	-1.75	-0.10±0.41	-0.85
	4:128	-0.03±0.29	-0.86	0.50±0.23	-0.46
	9:128	-0.57±0.20	-1.40	0.52±0.19	-1.37

[a] Center of mass of the peptide.

[b] Center of mass of the phenyl ring of the phenylalanine residue.

5.2.6 Functional Relevance of the β-Structure of the Cyclic Peptide

Visual inspection of the MD simulations of BPC194 showed that the β-structure induced upon membrane binding gave rise to an amphypathic-like structure of the peptide, with a spatially-symmetric arrangement of two pairs of lysine residues on the opposite strands, namely K^1-K^8, K^2-K^7. The Figure 5.9 A and B shows how the residues K^4-K^5 were close together in space even for unstructured conformations. When the peptide adopted a β-structure, these lysine pairs aligned in a parallel manner and gave rise to a high local charge accumulation. When the intra-strand hydrogen bonds were weakened and the β-structure was lost, the lysine residues could point away from each other (see Figure 5.9 C). On average, the distances between the lysine pairs at the membrane interface were reduced to about 0.7 nm from their value above 1 nm in aqueous medium (see Table 7.4 in Annex II).

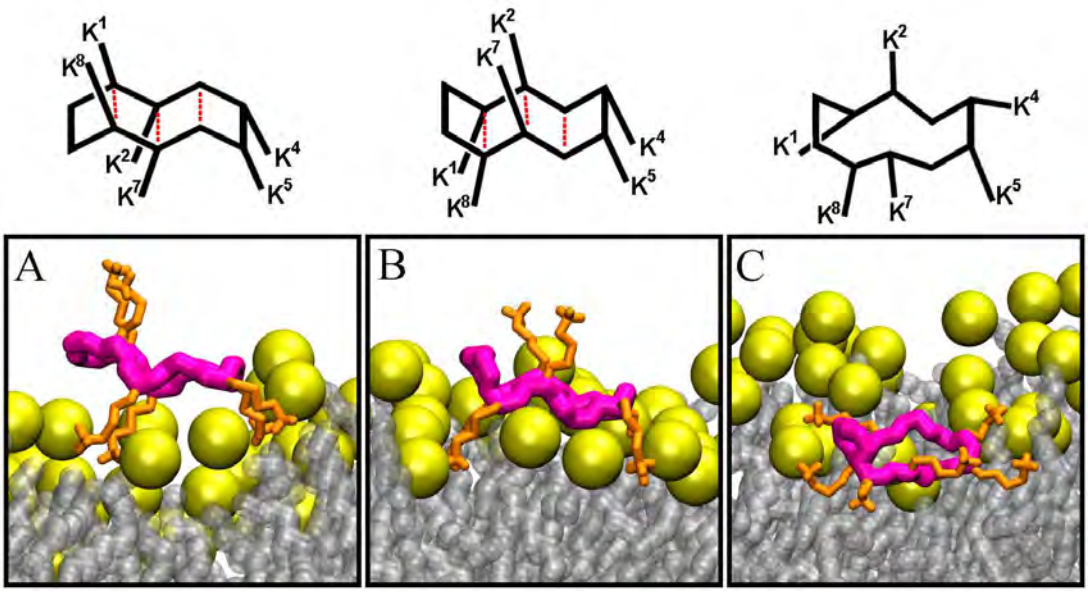

Figure 5.9: *Different binding modes of the cyclic peptide.* MD simulations of the peptides. The lysine residues are depicted in orange, the head-group phosphorus atoms as yellow spheres and the acyl tails in grey. **A-B.** In certain binding modes during the simulation, the lysine residues aligned with inter-strand hydrogen bonds (depicted in red). **C.** The lysines snorkelled out independently and the inter-strand distances increased.

5.3 Mechanism of Action of Antimicrobial Peptides: How do Cyclic Antimicrobial Peptides Form a Pore?

How antimicrobial peptides kill bacteria by interacting with the cell membrane is not fully understood. These peptides are secreted into the aqueous phase, usually in an unfolded state, and bind quickly to the target membrane, where secondary structure may be induced (Brogden 2005, Hancock 2002, Seelig 2004). At a certain threshold concentration antimicrobial peptides permeabilize the membrane, either by forming a discrete pore or by disrupting the bilayer structure (Ferre 2009, Melo 2009). For linear α-helical peptides the barrel-stave and toroidal-shaped model have been proposed as pore structures (Tossi 2000, Ludtke 1996, Qian 2008 and Subbalakshmi 1998). In addition, a disordered toroidal pore has been proposed for linear antimicrobial peptides from molecular dynamics simulations (Jean François 2008, Leontiadou 2006 and Sengupta 2008).

Cyclic AMPs have emerged as good antimicrobial candidates due to their robust secondary structure and high activity (Jelokhani-Niaraki 2002, Jelokhani-Niaraki 2008, Matsuzaki 2009). Gramicidin S, a cationic decapeptide, is one of the best studied cyclic AMPs (Jelokhani-Niaraki 2002, Jelokhani-Niaraki 2008, Gibbs 1998, Prenner 1999) and has been shown to permeabilize bilayers but not to stabilize well-defined pores (Mak 1995). MD simulations have shown that cyclic peptides such as gramicidin S (Mihailescu 1999, Mihailescu 2000) and arenicin-2 (Stavrakoudis 2009) have β-structures with a relatively rigid backbone conformation. Arginine-rich cyclic peptides have been shown to assemble into nanotubes and extrude the bilayer in MD simulations (Khalfa 2010). In general, the molecular details of the action of cyclic AMPs, such as whether these short peptides can open and stabilize pores, as well as the molecular basis for their increased activity is still unclear.

We have further extended the study of the interaction of the BPC194 cyclic peptide upon a membrane model to analyze the mode of action of this active cyclic peptide and its linear analogue. Here, we show how the cyclic peptide causes large perturbations in the bilayer increasing the penetration of water molecules through the membrane. Even though no spontaneous pore formation was seen, we could identify a transition state-like structure that was used as a starting point for further independent simulations. In most of them, the cyclic peptides were able to cooperatively open a pore, shedding light on how this peptide permeabilizes the membrane, as compared to the behaviour of the linear analog.

5.3.1 Methodology

5.3.1.1 System set-up.

MD simulations were performed for systems containing 9 peptides (BPC194 c(KKLKKFKKLQ); BPC193 H-KKLKKFKKLQ-OH) and a fully solvated DPPG (dipalmitoylphosphatidylglycerol; anionic lipid) bilayer. The simulations were carried out at a peptide:lipid (P:L) ratio of 9:128 for both cyclic and the linear analogues together with 6000-8000 water molecules and 128 K^+ as counter-ions for the anionic lipids. The peptides were initially placed in the water phase at a distance of 1.5-2.3 nm from the membrane surface. The peptides were modeled unstructured with no intramolecular hydrogen bonds, using the *leap* module of AMBER 9 (Case 2006). Multiple simulations were run from different initial random velocity distributions. In all simulations the reaction field correction was included for the truncation of long-range electrostatic interactions. See Table 5.7 for an overview of all simulations.

Table 5.7: Overview of the MD simulations performed.

Code	System	Counter-ions	Time (ns)
$9C_a$	Cyclic	-	160
$9C_b$	Cyclic	-	20
$9C_c$	Cyclic	-	30
$9C_d$	Cyclic	-	30
$9C_e$	Cyclic	$54Cl^-$	90
$9C_f$	Cyclic	$54Cl^-$	75
$9C_g$	Cyclic	$54Cl^-$	75
$9L_a$	Linear	-	140
$9L_b$	Linear	-	100
$9L_c$	Linear	-	40
$9L_d$	Linear	-	35
$9L_e$	Linear	$54Cl^-$	90
$9L_f$	Linear	$54Cl^-$	85

5.3.1.2 Set-up for transition state simulations.

As mentioned above, even though no spontaneous pore formation was observed in the simulations, a transition state-like structure was recognized and used as a starting point for further simulations. This corresponds to a snapshot at 109 ns taken from the simulation $9C_a$ (see Table 5.7). From this point, ten simulations

were performed with different initial velocity distributions. The transition state was later modified to substitute the cyclic peptide by the linear analogue, by cutting the peptide bond between N-terminal residue and the C-terminal residue, as well as adding the corresponding missing atoms. In this case, the system was simulated with the linear peptide but at the initial hairpin conformation of the cyclic peptide. Further, a harmonic potential was applied to the linear peptide to pull the N-terminal from C-terminal to obtain a random-coil conformation in the transition state. For the modified systems, a minimization was carried out followed by an equilibration with constraints on phosphorus atom and water molecules to keep the position of the transition state. Ten simulations were run for the hairpin conformation and two of the random-coil conformation by changing the starting random velocities.

5.3.1.3 Analysis.

The secondary structure of the peptides was calculated following the same procedure described in section 5.2.1.5. The persistence of structure over time was calculated as the percentage of time the β-structure was present. The estimation of the membrane perturbation was calculated by lipid tail order parameters, computed with respect to the membrane normal axis (Egberts 1994). The program calculate the order parameters using the equation

$$S_z = \frac{3}{2}\left\langle cos^2\theta_z \right\rangle - \frac{1}{2} \tag{5.1}$$

where θ_z is the angle between the z-axis of the simulation box and the average director vector of the atoms $C_i - 1$ to $C_i + 1$ being C_i a carbon atom from the lipid chain. Here we calculate the order parameter for each CH_2 segment of the lipid tail separately (named in the plot as carbon number) giving and idea of the ordering of the lipid tail (values close to 1 the more order and close to 0 the more disorder). Note that the two fatty acid chains of the lipids are denoted as Sn1 and Sn2. For the calculations in this thesis only Sn2 chain has been used. Furthermore, the fluctuations in the outer leaflet was calculated as the deviation of the phosphorus atoms of the head-groups from their center of mass.

5.3.1.4 Simulation parameters.

All MD simulations were performed using the parameters and conditions explained in section 5.2.1.4. However, in this section long-range electrostatic interaction were only computed with the reaction field method.

5.3.2 The Cyclic Peptide Causes Large Perturbations in DPPG Bilayers

In section 5.2, we showed that simulations of BPC194 interacting with DPPG bilayers at low P:L ratios showed little perturbations, in line with the notion that antimicrobial peptides require a minimum threshold concentration to function. Thus, we report here simulations at a higher 9:128 P:L ratio.

The time course of a particular simulation (Table 5.7, simulation $9C_a$) is depicted in Figure 5.10 A, but similar behaviour was observed in the remaining simulations (Table 5.7, simulations $9C_b$-C_g).

The peptides were initially placed in the water layer close to the bilayer (0 ns) and subsequently bound fast (∼5 ns) to the membrane interface. During the simulation, most of the cyclic peptides remained bound at the interface. However, a few peptides were able to cooperatively perturb the outer leaflet and consequently insert deeper (Figure 5.10 around 16-60 ns). During the perturbation, the positively-charged residues of the peptides interacted with the closest

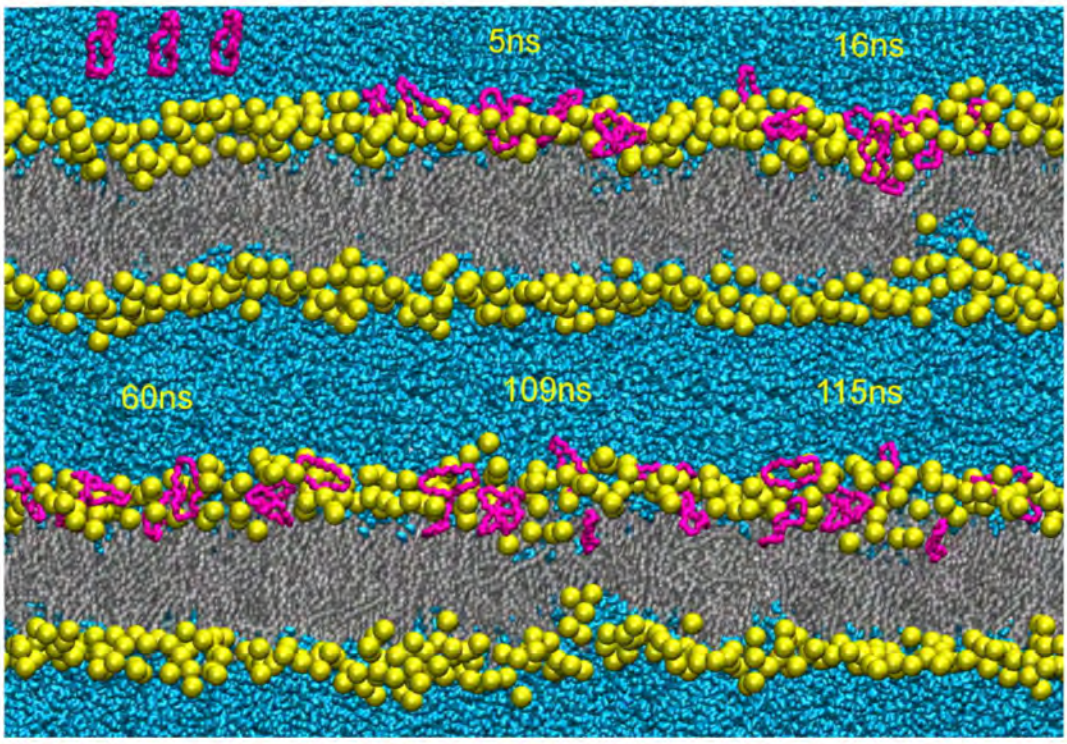

Figure 5.10: *The cyclic peptides cause large fluctuations in the membrane upon binding.* Time course of the simulation $9C_a$. The headgroups are depicted in yellow spheres. The peptide backbone is shown in pink, lipid tails in grey and water molecules in cyan.

head-group moieties and pulled them, together with some water molecules, into the core of the membrane. The peptide-free inner leaflet was also affected by the action of the cyclic peptide bound on the outer leaflet.

The first strong perturbation of the membrane was seen at 16 ns when some lipids from the inner leaflet were pulled inside the bilayer due to the peptide insertion. This behaviour was seen repetitively during the simulation and was usually followed by a relaxation of both leaflets. Occasionally, a much larger perturbation occurred (at 109 ns). The lipid-chain order of the lipids involved in this large perturbation was calculated as described in section 5.3.1.3. As the peptides bound at the interface and inserted deeper (see Figure 5.11, 0-60 ns) the lipids associated to the first large perturbation (LP, dashed-dotted line) became slightly more disordered than those not associated with the large perturbation (labeled as not LP, dotted line).

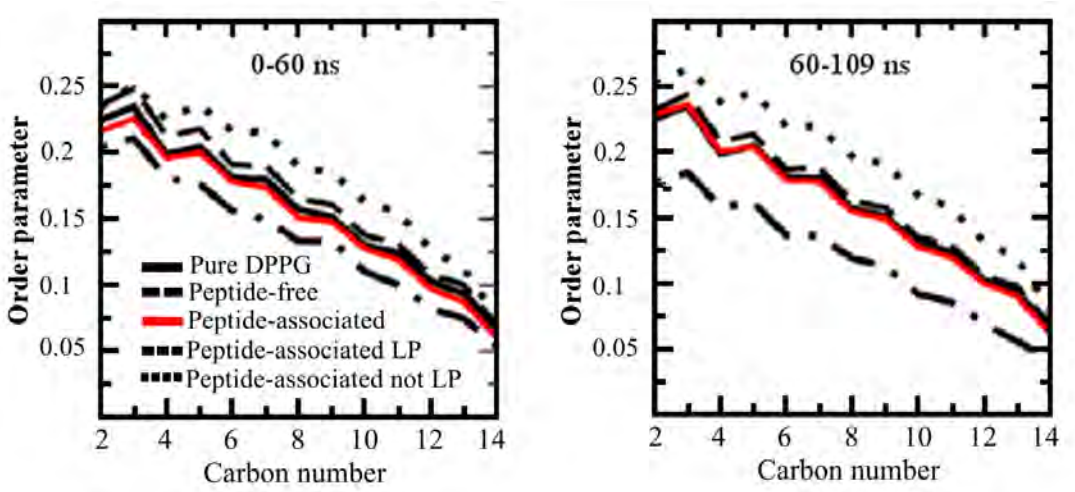

Figure 5.11: *The membrane order changes as the cyclic peptide inserts.* Lipid-tail order parameters of the Sn2 chain obtained from simulation $9C_a$. The order parameters are plotted distinguishing between the lipids involved in the large perturbation with the rest. The left plot shows the first part of the simulation between 0-60 ns, where the peptides interact and bind to membrane surface. The right plot displays the insertion process of the peptides till the largest perturbation occurs (60-190 ns).

As the system evolves towards the transition like-state (see Figure 5.11, 60-109 ns) this asymmetric behaviour was increased caused by a cooperative effect of three peptides, one of which adopted a transmembrane-orientation with its glutamine residue close to the center of the hydrophobic core. In this position, the glutamine residue interacted with some head-group atoms of the inner leaflet. During this perturbation, a few water molecules were able to cross the membrane.

However, the inner leaflet relaxed again and the orientation of the glutamine residue inserted out to the interface (Figure 5.10 at 115 ns). No further large perturbations of the membrane were observed in the remainder of the simulation.

5.3.3 The Cyclic Peptide Can Form a Disordered Toroidal Pore.

In previous simulations of AMP action on lipid membranes (Leontiadou 2006, Sengupta 2008) the first event during pore formation was the bridging of the two leaflets by a peptide. Though such an orientation of the peptides was seen in simulation $9C_a$ (Figure 5.10 at 109 ns), it did not lead to a porated state. Nevertheless, we expect this highly perturbed state to be an intermediate state close to the true transition state towards pore formation. To sample the conformational space around this point, which we will putatively call transition state from now on, ten simulations were set up changing the velocities in the system to provide a different direction on the potential energy surface that may lead to pore formation.

Indeed, a pore was formed in six out of ten simulations. The mechanism of the pore formation is depicted in Figure 5.12 A using simulation C9 as a representative of all simulations. The first time point (0 ns) is taken as the transition state from which the simulation was started (cf. Figure 5.10 at 109 ns). At once, more water molecules readily inserted into the bilayer and finally after 1$\sim$2 ns, some water molecules crossed the bilayer to open a water channel. Head-group atoms of both leaflets also moved inside the membrane core to line the water channel. From then on, the pore remained open and the lipid head-groups of both leaflets rearranged to form a disordered, toroidal-shaped pore at around 25 ns. A detailed information of the outcome of all the simulations is provided in Table 5.8, simulations C1 to C10.

Note that in all simulations, less than 5 ns were required to open a water channel, which lead to the insertion of the lipid head-groups in the hydrophobic core of the membrane and stabilized along the toroidal pore. Besides, the ones which were not able to overcome the energy barrier to pore formation, showed large perturbations afterwards with fluctations of the leaflet around ± 0.44, compared to ± 0.53 for deviations where a pore was formed.

A more detailed picture of two typical pores formed by the cyclic peptides is shown in Figure 5.12 B. The pores formed in our simulations could be characterized as disordered toroidal pores with the peptides residing in different positions and orientations. It is worth noting that in all cases, the pore was stabilized

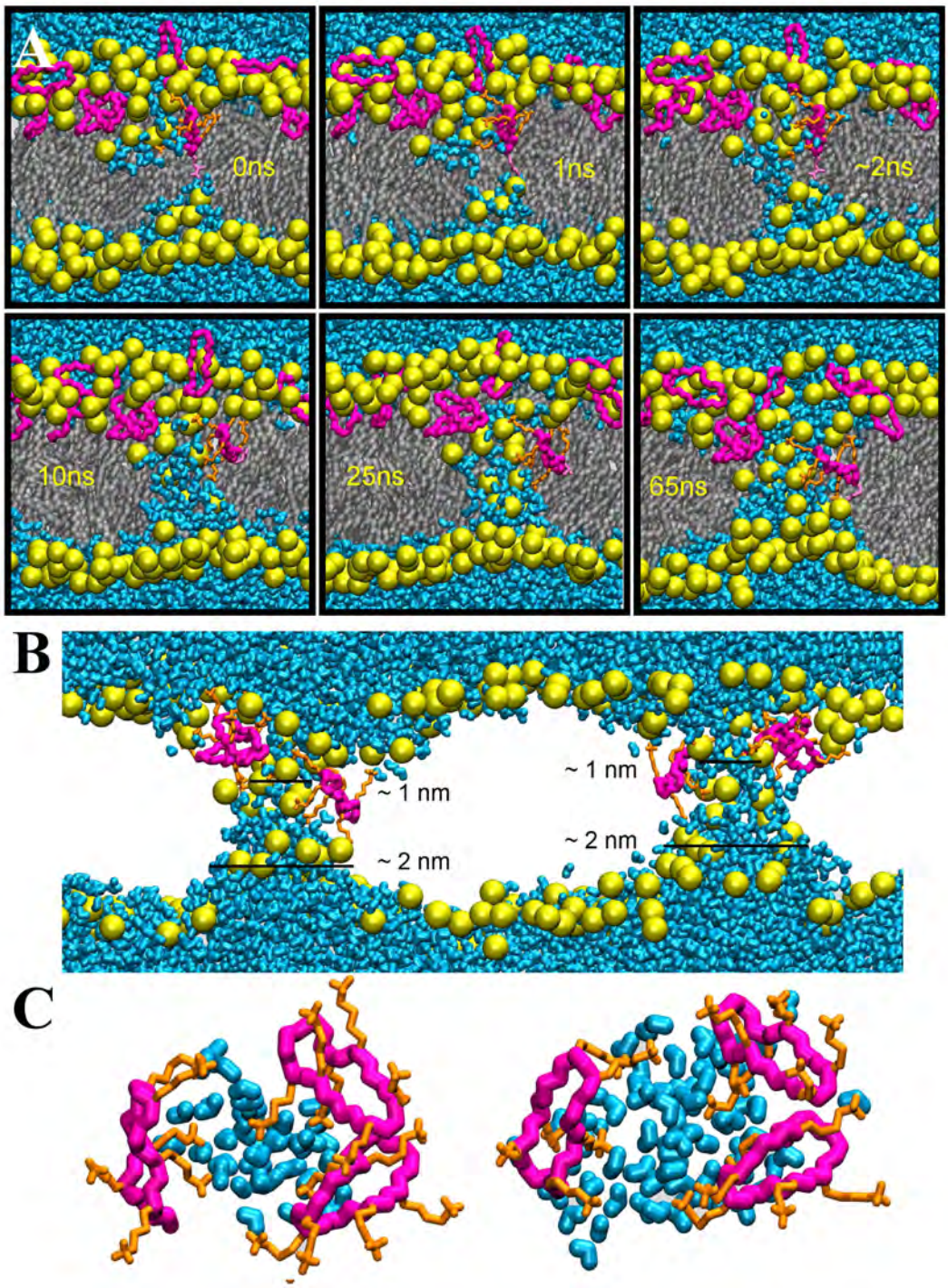

Figure 5.12: *Pore formation by cyclic peptides.* **A.** Time course of the pore formation taking the transition state as the starting structure (0 ns). **B.** Two examples of the disordered toroidal pore (simulations C9 and C10, respectively). **C.** Two independent examples of top view of the pore. The phosphorus atoms are colored in yellow spheres, the peptide backbone in pink, lysine side-chain in orange and the glutamine residue in light pink. The water molecules that are present in the channel are depicted in cyan.

by three peptides: a dimer and a monomeric peptide (Figure 5.12 C), with the remaining peptides lying close to the pore. Note, however, that the structure is biased by the starting point of these simulations, the transition state, which was formed by the same three peptides.

The nanosecond time scale of the simulations is not enough to sample the redistribution of the peptides and likewise, no peptide translocation was observed even in the longest simulations (C9 and C10). The size of the water channel fluctuated both in time as well as along the direction of the pore axis, varying between 1 and 2 nm wide.

Table 5.8: Overview of the MD simulations performed with the cyclic peptide using the transition state as the starting point. DTP stands for disordered toroidal pore and HG stands for head-group atoms.

Code	**Open Water Channel**	**Features**	**Remarks**	**Outer Leaflet Fluctuation**	**% SS**[a]	**No. of peptides in pore**	**Time (ns)**
C1	2-3 ns	DTP	Stabilization HG 20 ns	±0.50	29.9	3	40
C2	4 ns	DTP	Stabilization HG 12 ns	±0.50	34.5	3	40
C3	4 ns	DTP	Stabilization HG 17 ns	±0.52	36.7	3	40
C4	-	No pore	Perturbations afterwards	±0.46	34.2	-	40
C5	1 ns	DTP	Stabilization HG 20 ns	±0.54	34.2	3	40
C6	-	No pore	Perturbations afterwards	±0.40	34.1	-	40
C7	-	No pore	Perturbations afterwards	±0.48	32.8	-	40
C8	-	No pore	Perturbations afterwards	±0.43	33.1	-	40
C9	1-2 ns	DTP	Stabilization HG 10 ns	±0.59	33.4	3	125
C10	1-2 ns	DTP	Stabilization HG 10 ns	±0.55	36.6	3	170

[a] SS stands for secondary structure given by % of β-structure.

5.3.4 The Linear Peptide Does not Perturb DPPG Bilayers Substantially.

In a second step, we performed simulations of the linear analogue interacting with DPPG bilayers under conditions identical to the cyclic peptide (see Table 5.7, simulations $9L_a$-L_f). The same behaviour was observed in all six independent simulations, for which a typical time course is depicted in Figure 5.13.

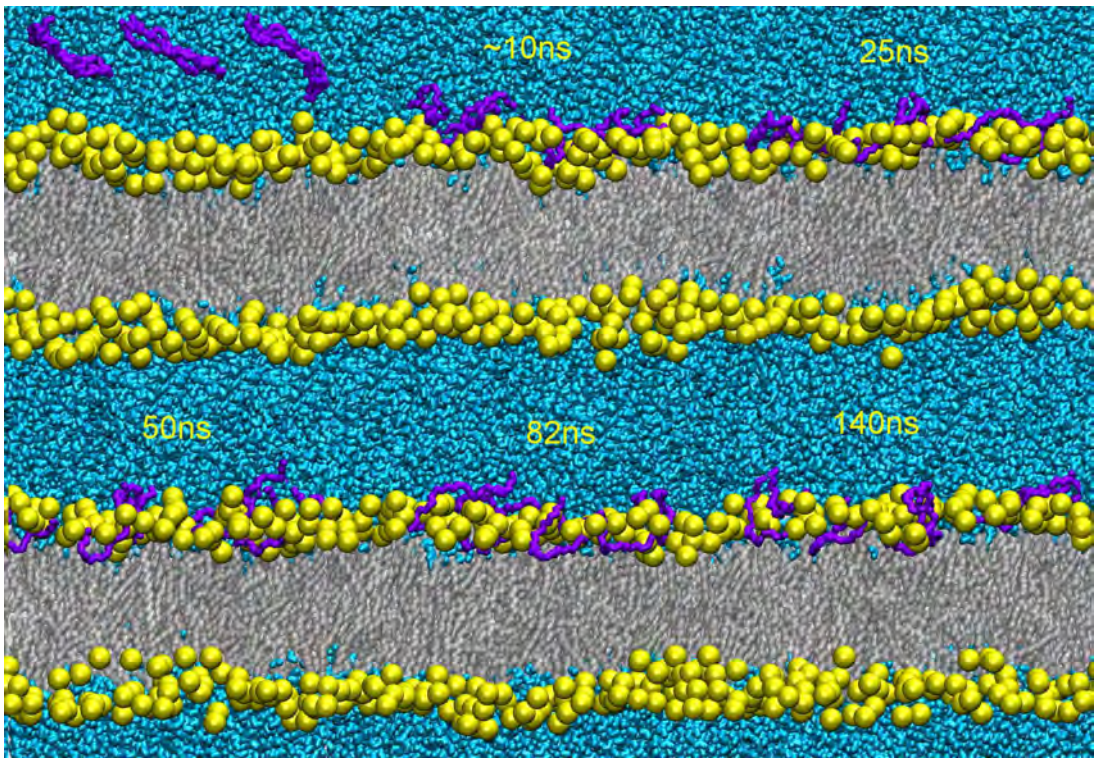

Figure 5.13: *The linear peptide does not induce fluctuations in the membrane.* Time course of the simulation $9L_a$. Initially (0 ns), all linear peptides were placed close to the outer leaflet. Within 10 ns all peptides bound and remained at the membrane interface. No large perturbations were seen along the simulation (25-104 ns). The phosphorus atoms of the head-group of DPPG are depicted in yellow spheres, the peptide backbone in violet, lipid tails in grey and water molecules in cyan.

The linear peptide bound to the outer leaflet of the bilayer, at a comparable time (within 10 ns) to the cyclic peptide. Upon binding, the peptides were able to perturb the membrane to some extent, though much less than the cyclic peptide. Larger perturbations leading to a transition state were not seen in any of the simulations with the linear peptide. Though the average thickness of the bilayer was similar for the two peptides (3.7±0.1 nm for the linear and 3.6±0.1 nm for the cyclic peptide), the perturbations in the outer leaflet were substantially

larger when the cyclic peptide was attached. The fluctuations in the outer leaflet was ±0.29 nm for the linear peptide, in comparison to ±0.44 nm for the cyclic peptide analogue (see analysis 5.3.1.3). These results were supported by the electrophysiology measurements, in which the the linear analog did not showed pore formation (see Figure 7.46 in Annex II).

5.3.5 Structure-Function Relationship: A Constrained Secondary Structure is Important for Function.

In section 5.2.3, we showed that there is a clear difference between the cyclic and linear peptide in regard to their secondary structure upon binding to anionic membranes. Therefore, we tackled the investigation of the relation between secondary structure and the ability of the peptides to stabilize a pore in the six simulations where a pore was formed. The peptides could be clustered depending on how far they lie from the pore and the role they play in stabilizing it (see Figure 5.14 A-B).

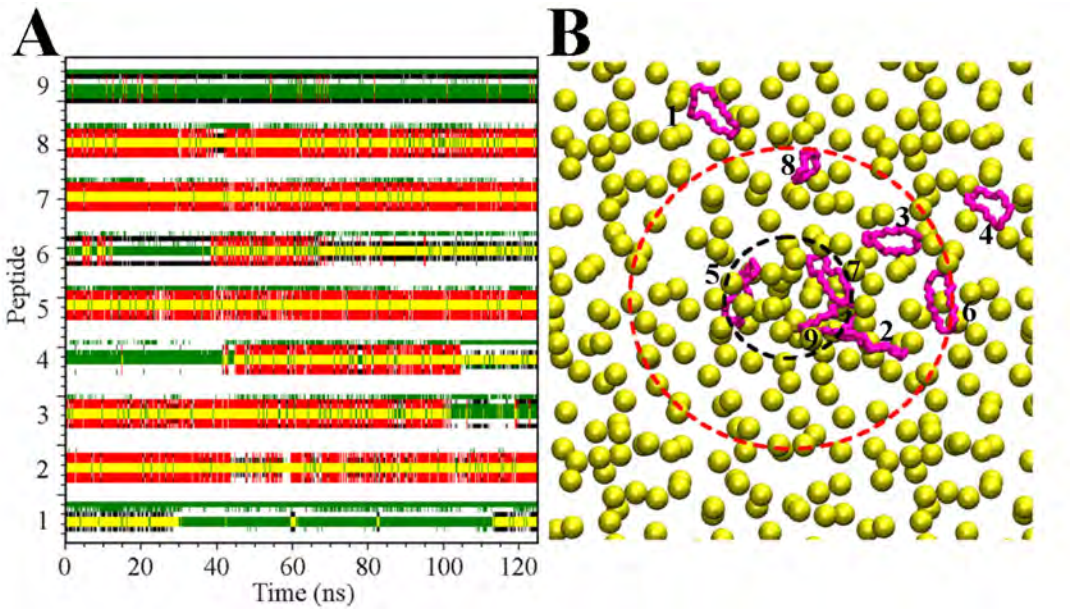

Figure 5.14: *Secondary structure related to the distance at the rim of the pore.* **A.** DSSP plot of the secondary structure of all peptides for simulation C9, taking the transition state as the 0 ns time point. **B.** Top view of the pore showing the positions of the nine peptides. The phosphorus atoms of the outer leaflet are depicted as yellow spheres and the backbone is colored in pink. Region 1 peptides are those involved in the pore (within dashed black line). The peptides that remain at the rim of the pore (region 2) are delimited by the red dashed line. The peptides furthest from the pore (region 3) are outside the circles.

In Table 5.9 the statistics of secondary structure and distance of each peptide to the center of the pore are detailed.

Table 5.9: Secondary structure and distance from the center of the pore for the peptides belonging to the three regions.[a]

Region	Peptide	Distance (nm)	% Coil	% β-Structure	% Bend	% Turn	% Time of β-structure[b]
1	5	0.09±0	20.7	45.7	10.3	23.4	94.8
	7	0.09±0	19.6	47.9	8.4	24.1	98.4
	9	0.09±0	25.2	26.2	45.4	3.4	97.7
	Average	0.09±0	22±1	40±6	31±11	17±6	97±1
2	2	0.30±0.05	29.9	43.8	2.8	23.6	92
	3	0.78±0.15	24.8	42.8	12.0	20.4	92.6
	6	1.10±0.15	36.0	32.2	14.2	16.5	91.7
	8	1.50±0.23	30.0	39.1	10.9	20.0	78.1
	Average	0.9±0.2	30±2	39±2	10±2	20±1	89±3
3	4	1.59±0.30	38.5	28.1	15.3	18.2	62.5
	1	2.07±0.25	45.4	8.6	30.9	15.1	33.6
	Average	1.8±0.2	42±2	18±7	23±6	17±1	48±10

[a] The values reported are an average calculated from all simulations where a pore was formed. The standard errors reported are calculated from the standard deviation between all peptides in all simulations.

[b] Persistence of β-structure over time (see section 5.3.1.3).

From all this data, three classes of peptides were distinguished: those within the rim of the pore (distance <0.3 nm from the center of the pore, region 1), those lying at the mouth of the pore (within 0.3-1.5 nm, region 2) and those not involved in the pore (further away than 1.5 nm, region 3). Peptides in region 1 adopted a stable secondary structure (40% β-structure). Two peptides belonging to this first region (peptide 5 and 7) were always entirely inserted into the pore and exhibited the highest content of β-structure (46% and 48%, resp.). The third (peptide 9), lying more at the rim of the pore and not inserted completely into it, showed a 26% of β-structure and 45% bend conformation with one less inter-strand hydrogen bond formed. Although the number of residues involved in secondary structure varied from the other two peptides, all three peptides showed the longest persistence of β-structure over time (97%). The peptides belonging to region 2 also exhibited a high content of β-structure (39% for peptides of this region), but it fluctuated over time and the persistence of β-structure was 89%.

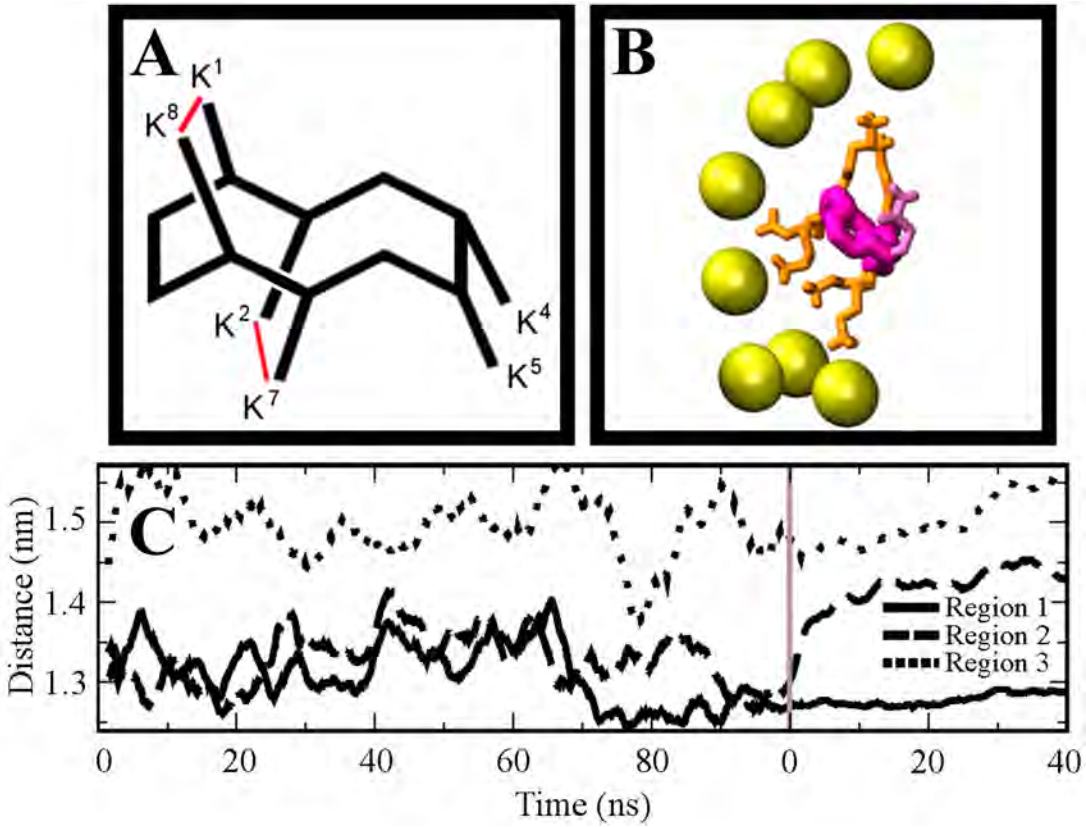

Figure 5.15: *Relationship of the folded structure to function.* **A.** Parallel arrangement of lysine residues in the β-structure. **B.** An illustrative snapshot of the aligned lysine residues stabilizing the lipid curvature in the porated state (side-view of the pore). **C.** The average distance between lysine residues K^1-K^8 and K^2-K^7 (plotted as a sum) for peptides in regions 1, 2 and 3. The time scale to the left of the grey line refers to simulation $9C_a$ (before transition state formation 0-109 ns). The time frame to the right is an average for all simulations (C1-10) where a pore was formed with the starting time 0 ns being the putative transition state.

Finally, the peptides in region 3 exhibited multiple folds and adopted different conformations showing only 18% β-structure for the individual peptides.

The apparent importance of the β-structure for stabilization of the pore can be rationalized by considering the relative orientation of the lysine side-chains. As illustrated in Figure 5.15 A, the β-structure gave rise to a parallel arrangement of the lysine pairs (K^1-K^8 and K^2-K^7) on the two strands that, presumably, facilitated the interaction of the lysines with the lipid head-groups in the curved geometry of the pore (Figure 5.15 B). The time evolution of the distances between the lysine pairs K^1-K^8 and K^2-K^7 (plotted as a sum of the two values) for the three regions of the peptides is shown in Figure 5.15 C. When

the peptides were bound to the membrane (0-109 ns, till grey line), the value fluctuated for all three clusters of peptides. However, once the transition state was reached and later when a pore was opened (beyond grey line), the distance between the lysine pairs in the peptides in region 1 remained low, consistent with their high persistence of secondary structure. The value for the peptides in region 2 was also low at the transition state but increased as the pore relaxed. The peptides in region 3, which were not involved in the pore, showed the largest distance between the lysine pairs along the simulations.

5.3.6 Transition State Alchemy: Why the Linear Peptide Cannot Stabilize Pores.

To test our hypothesis that the β-strand conformation is linked to the activity of the cyclic peptide, we repeated the simulations that were started from the transition state, however, this time with the linear rather than the cyclic peptide. To do so, a bit of alchemy was required; the peptide bond between the first and last residue was removed in silico.

In Table 5.10 the results of these simulations are summarized. In seven of out the ten simulations, the bilayer relaxed and the linear peptide moved back to the interface while the remaining three simulations, a water channel eventually opened but on average in larger time scales (around 20 ns). It is noteworthy that the simulations where the lipids were relaxed, no further perturbations were seen afterwards, presenting fluctuations of the leaflets around ± 0.42. On the other hand, once a pore was formed, the perturbations were also less important than those caused by the cyclic peptide, being ± 0.49 for the linear case.

Although we observed that the linear peptide was also able to stabilize a water pore across the membrane, the pore differed in a number of ways from the pore formed in the presence of the cyclic peptides. The time course of one of the poration events (simulation L7, Table 5.10) is depicted in Figure 5.16. In a nutshell, i) the time scale of the pore formation was markedly larger ($>$ 25 ns compared to $<$ 5 ns for linear and cyclic peptides, respectively), ii) only one of the three peptides involved in the transition state remained embedded near the central pore region; and iii) the lipid head-groups did not line the pore as clearly as in the case of the cyclic peptide. In most of the simulations, the average percentage of β-structure (see Table 5.10) dropped to a value around 20%, compared to $>$ 30% for the cyclic peptide (cf. Table 5.8). In the simulations in which a pore was formed, the peptide in closest vicinity of the pore preserved a somewhat higher percentage of β-structure ($\sim$28%).

Table 5.10: Overview of the ten simulations starting from the transition state for the in-silico modified linear peptide. DTP stands for disordered toroidal pore and HG stands for head-group atoms.

Code	Open Water Channel	Features	Remarks	Outer Leaflet Fluctuation	% β-Structure	Nr. of peptides in pore	Time (ns)
L1	25 ns	DTP	Stabilization HG 45 ns	±0.47	33.2	1	50
L2	-	No pore	Relaxation	±0.39	21.9	-	50
L3	-	No pore	Large Perturbations	±0.48	16.1	-	50
L4	-	No pore	Relaxation	±0.41	20.7	-	40
L5	-	No pore	Relaxation	±0.38	19.8	-	40
L6	-	No pore	Relaxation	±0.40	22.3	-	40
L7	20-30 ns	DTP	Stabilization HG 60 ns	±0.54	22.2	1	150
L8	-	No pore	Relaxation	±0.43	18.7	-	40
L9	-	No pore	Relaxation	±0.45	26.7	-	60
L10	3-4 ns	DTP	Stabilization HG 45 ns	±0.48	17.9	1	150

Two additional unbiased transition state simulations of the linear peptide in its native random-coil conformation were also performed. The conformation of the peptide was changed from the initial β-structure to an extended conformation representative for the linear peptide using a harmonic potential to drive the N- and C-terminal residues apart. We found that, in the extended conformation, the peptide could not stabilize even those head-groups that were already inserted into the membrane, and the bilayer recovered immediately from the large perturbations induced by the cyclic peptide.

5.3.7 Molecular Basis for the Activity of BPC194

Based on comprehensive MD simulations and corroborated by biophysical experiments carried out in University of Groningen (Cirac 2011), we propose a molecular-detailed model outlining the differences in the mode of action of the two related peptides that leads to the molecular basis for activity of the BPC194 (see Figure 5.17).

First, both peptides appear to be similar when present in the aqueous phase being mainly unstructured and having analogous propensity to bind to anionic

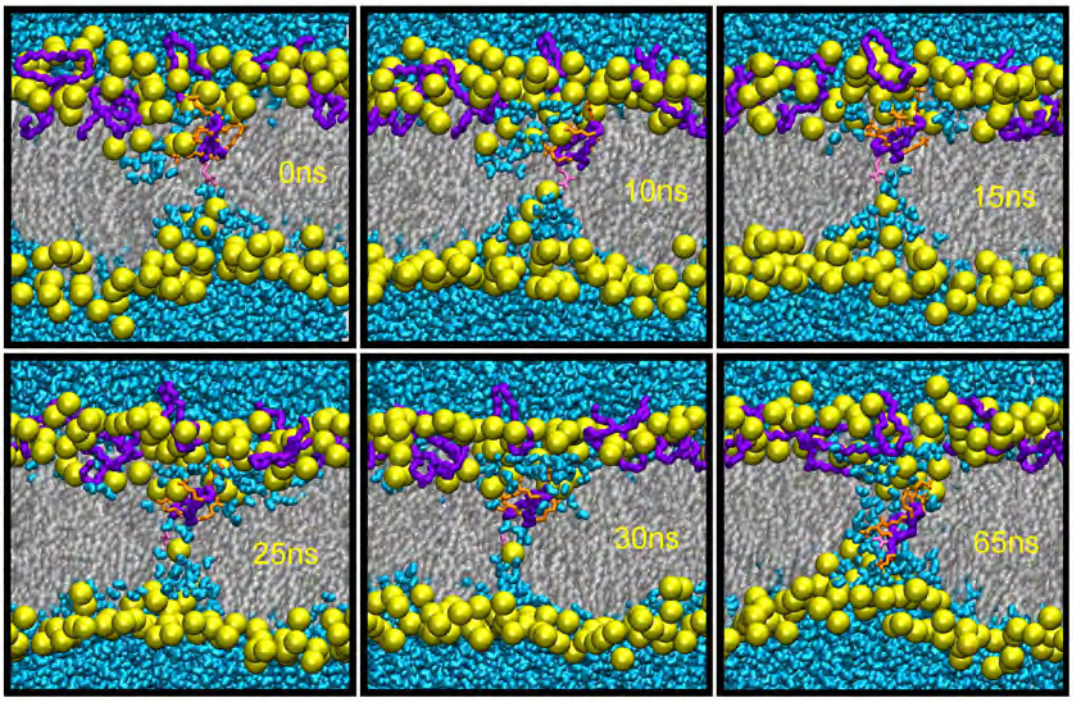

Figure 5.16: *The linear peptides cause large perturbations from the in-silico modified transition state.* Time course of a transient pore formed by a linear peptide (simulation L7). The time point 0 ns correspond to the transition state taken from the simulation with the cyclic peptide. After 10-30 ns, large perturbations were seen and a few water molecules crossed the bilayer. At longer time scales (65 ns), eventually a water channel was opened but was not completly lined by the phosphorus atoms moieties. Please note that in most simulations the bilayer relaxes and such large perturbation are not seen.

membrane surfaces (Figure 5.17, stages I-II). From this point on, the behaviour of the two peptides diverges. The cyclic peptide had a larger tendency to fold, enabling it to insert deeper into the membrane interface, while the linear one remained unfolded in the interface with no insertion (Figure 5.17, stage III). This is related to the higher energy cost of inserting a non hydrogen bonded amide bond into the membrane. Through cooperative interactions, some of these membrane embedded and folded cyclic peptides caused large perturbations which led to the formation of an intermediate or transition state characterized by a single peptide bridging the two leaflets, while the linear peptide assumed a more extended conformation and was unable to perturb the membrane substantially (Figure 5.17, stage IV).

Using the transition state as seed for many independent trajectories, the deepest-embedded peptide was able to open a water channel and as a result of

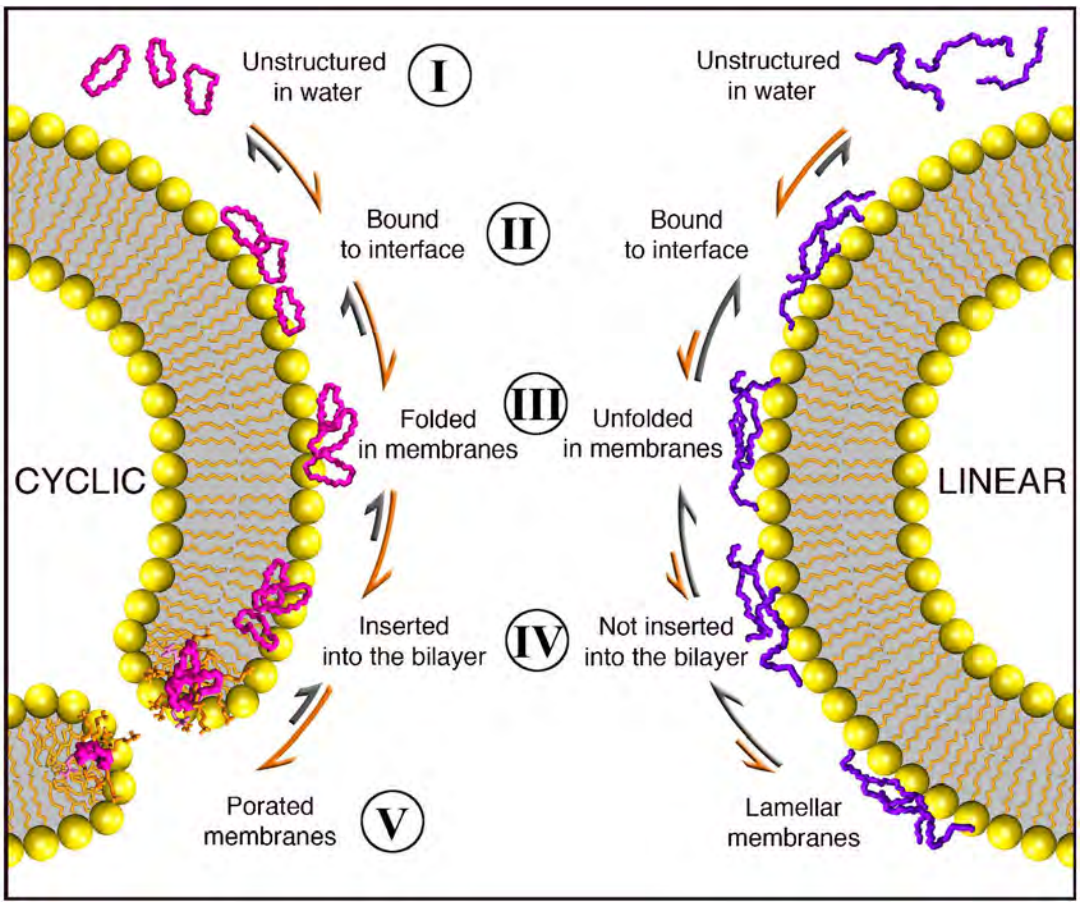

Figure 5.17: *Mode of action.* A schematic view of the mechanism of action of the cyclic peptide BPC194 (left, pink peptide) and its linear analogue BPC193 (right, violet). The five possible states (stable or metastable) are: (I) aqueous-unfolded, (II) membrane-adsorbed, (III) folded, (IV) inserted and (V) porated. The equilibrium is shifted to the right for the cyclic peptide BPC194 and the porated state is the most favorable one. For the linear analogue BPC193, the membrane-adsorbed is the most favoured state and the peptide remains unfolded at the surface of the membrane. This model has been extracted from Mika 2011.

that it stabilized a toroidal-shaped pore of 1-2 nm diameter, which is in line with the electrophysiology and pore-sizing experiments (see Figure 7.47 in Annex II, Figure 5.17, stages V). Only two/three peptides actually lied in the pore, while some of the remaining peptides lined the mouth of the pore and stabilized the membrane curvature. Unlike the cyclic peptide, the linear analog could not open a pore from the unfolded state, and could only stabilize it if the starting structure was the transition state structure obtained with the cyclic peptide. The main differences of the action of both peptides of the porated state seen in MD simulations are schematized in Table 5.11.

Table 5.11: Summary of pore features created by the cyclic and the linear peptide.

Pore features	**Cyclic Peptide**	**Linear Peptide**
Pore propensity	High	Low
Pore diameter	1-2 nm	<1 nm
Number of peptides inside	3	1
β-structure	34%	21%
Outer leaflet deviation	$\pm$0.55	$\pm$0.48
Number of porated states	6/10	3/10
Number of lipid head-groups	8-11	6-10
Number of water molecules	100-123	76-84
Formation time	1-4 ns	3-30 ns

Here, a constrained secondary structure rather than a high percentage of secondary structure was required to stabilize the pore. The importance of the secondary structure, induced on membrane binding, appeared to be the alignment of the charged residues such that they fit the toroidal shape of the pore explaining why the linear peptide is less active (for entropic reasons a folded structure is less likely to occur spontaneously). This entropic penalty is prepaid by the cyclic nature of BPC194 which showed the most stable β-structure stability as it remained close to poration events.

Even though the mechanism of pore formation by BPC194 may be related to its activity, in the next section we speculate that the origin for its high activity could be as a result of a "multi-hit" process in which poration is involved.

5.4 Dual Action of the Cyclic Antimicrobial Peptide BPC194: Fusion and Leakage

Several studies have postulated that poration events that occur at a threshold concentration are one of the possible mechanisms by which the AMPs kill bacteria (Melo 2009). However, experimental evidences are now indicating that these membrane-active peptides (MAPs) may affect the cell membrane in multiple ways: the so called multi-hit phenomenon (Zhang 2000, Shai 2002). Some AMPs have already been shown to promote fusion of anionic vesicles (Cummings 2007, Domingues 2009), but whether these multiple modes of action are a consequence of the biophysics of the protein-membrane interactions and/or are an important characteristic of its function is still unclear. Furthermore, the molecular characteristics of the multi-mode processes, as well as the common features of the peptides that allow or promote these actions, remain unknown.

In the particular case of BPC194, it has already been shown that the peptide was able to porate anionic lipid bilayers by means of biophysical studies and MD simulations. In addition, further experiments of Dual-Color Fluorescence Burst Analysis (DCFBA, van den Bogaart 2008) and Forster Resonance Energy Transfer (FRET, Struck 1981) were done and showed that the cyclic peptide was able to fuse and porate membranes simultaneously. While the molecular basis of BPC194 for pore formation has already been unraveled, the mechanism of membrane fusion by this cyclic AMP is still unclear at the molecular level.

Fusion pathways includes the rearrangement of the membrane lipids matrices. Since the bilayer is stabilized against any structural changes by a powerful hydrophobic effect, fusion requires energy which can come from fluctuations exerted by the membrane or delivered by specialized proteins (Chernomordik 2008). One of the most accepted pathways for pure membrane fusion is schematized in Figure 5.18 I-V. After establishing contact between the membranes, the formation of transient membrane discontinuities is required as a previous step for lipid mergering, what is also called “point-like protrusion” (PLP) or “prestalk” fusion intermediate (Efrat 2007)(Figure 5.18 II). Further junction of the transient intermediate of the contacting monolayers leads the membranes to form the fusion stalk, which is followed afterwards by the fusion of the membranes, as seen in Figure 5.18 IV-V.

Because the molecular details of these events remain unclear by the action of AMPs, several MD simulations were performed to model the fusiogenic activity of BPC194, in order to get insight on the peptide-membrane interactions that discriminate its poration activity from its fusiogenic activity.

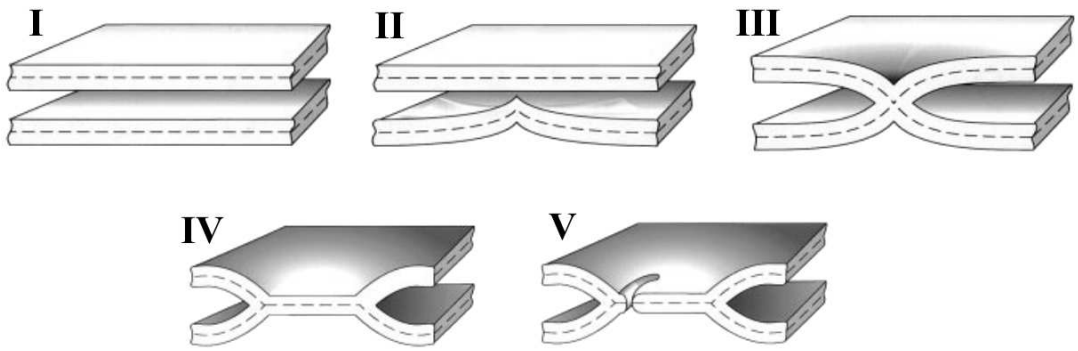

Figure 5.18: *Fusion pathways of lipid bilayers.* **I.** Establishment of membrane contact. **II.** Pointlike protrusion (pre-stalk intermediate) at the prefusion stage. **III.** Fusion stalk. **IV.** Hemifusion diaphragm. **V.** Cracklike fusion pore. This picture has been taken from Chernomordik 2008.

In this section we show in detail how the peptide is able to porate and promote fusion simultaneously. The simulations carried out provide a direct connection between the atomisitc details of the dual action of the cyclic peptides and the macroscopic properties observed from experiments.

5.4.1 Methodology

5.4.1.1 System set-up.

The starting system comprised of two solvated DPPG bilayer with consisting of 512 lipids each, and placed at a distance of about 3 nm from each other. BPC194 peptides were placed between the bilayers in the water phase at a P:L ratio of 1:15. The cyclic peptides were modeled based on the setup described in section 5.2.1.1. The system consisted of about 32000 water molecules. An appropiate number of K^+ ions were added as counter-ions for anionic lipids and Cl^- ions were added to neutralize the overall system. Multiple simulations were set up with different starting random velocities. For an overview of the simulations see Table 5.12.

5.4.1.2 Simulations parameters

All MD simulations were performed under the same conditions as those described in section 5.2.1.4.

Table 5.12: Overview of the MD simulations of the fusion process performed.

Simulation	No. Peptides	P:L	d(P-P) (nm)	Time (ns)
F1	64	1:15	∼3	360
F2	64	1:15	∼3	210
F3	64	1:15	∼3	590
F4	64	1:15	∼3	160
F5	64	1:15	∼3	230

5.4.1.3 MD analysis

Tilting and splaying of lipids An usual measure of deformation of the two contact monolayer to fuse the membranes (Figure 5.19, top) is the ability of the lipid chains to tilt and splay with respect to the lipid-water interface. The tilt of the lipid, was determined by calculating the angle between the z-axis of the simulation box (which is perpendicular to the membrane) and the average director vector of the lipid tail (taken using atoms P, C2A, C2P of the lipid). The values close to 0^o indicate no tilt whereas values closte to 90^o mean complete tilt (Figure 5.19, bottom left). The splay was calculated by the angle created between the average director vectors of the two chains of the lipids, using atoms C1A, C1P (from Sn1 tail) and C2A, C2P (from Sn2). Values of the angle close to 180^o indicate full splay of the hydrocarbons tails (Figure 5.19, bottom right).

5.4.2 Sequence of Events of the Leaky Fusogenic action of BPC194.

To study the fusion/leakage events at an atomistic level, multiple independent simulations were set up with multiple copies of the peptide placed between the bilayers (Figure 5.20 A). All five simulations showed similar behaviour: representative snapshots showing the sequence of events in a particular simulation (F1, Table 5.12) are shown in Figure 5.20. The following steps were observed: i) peptide binding leading to membrane bridging, ii) lipid perturbations leading to pre-stalk formation, and iii) peptide penetration resulting in pore formation.

Membrane bridging: An initial fast binding of the peptides was observed with most peptides binding to one of the contact monolayers, typically within 10 ns see Figure 5.20 B. The binding is driven by multiple electrostatic interactions of the positively charged lysine residues with the negatively charged head-group

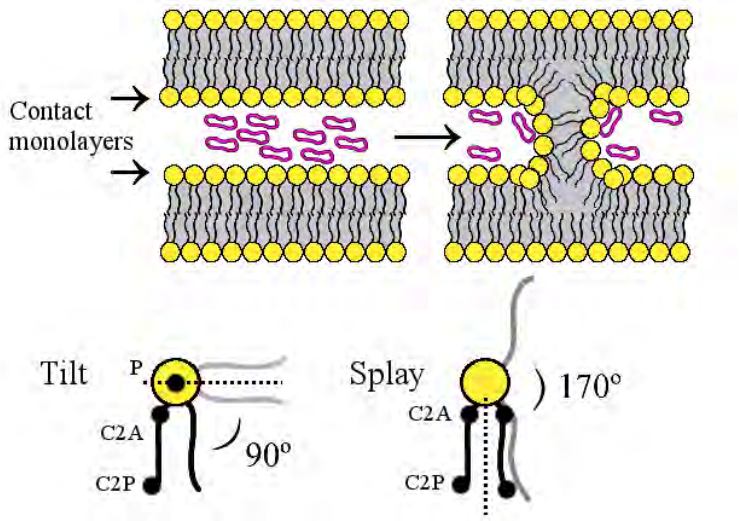

Figure 5.19: *Sketch of a model of membrane fusion of cyclic peptides.* **top** Membrane fusion scheme of two bilayers by the deformation of contact monolayers. **bottom** On the left the tilting and on the right the splaying of a lipid chain with respect to the lipid-water interface.

moieties of the PG lipids. Importantly, a few of the peptides were able to interact simultaneously with both membranes. As a result, these peptides formed a bridge between the apposing membranes and are referred to as bridging peptides. A close-up of a few bridging peptides is presented in Figure 5.20 E.

Pre-stalk formation: Due to the effect of the bridging peptides, some of the lipids were perturbed locally and protruded out of the membrane creating a stalk-like structure (Figure 5.20 C). Both an increased curvature as well as protrusions of individual lipids out of the leaflet were observed. The stalk-like intermediate remained stable during the length of the simulations. However, full contact between the hydrophobic tails of lipids from the contacting leaflets did not occur, and so we refer to this state as pre-stalk. Formation of the pre-stalk takes place on the time scale of 10-20 ns, the time required for the bridging peptides to extract the lipid tails from the contacting monolayers.

Pore formation: Subsequent to the pre-stalk formation, spontaneous pore formation was observed (Figure 5.20 D). Pore formation was triggered by a few of the peptides, not involved in stabilizing the pre-stalk, inserted deeper into the bilayer. Whether or not pores are actually formed appeared to be stochastic process, with three out of five simulations showing pore formation on the time scale of the simulation (Table 5.13). In two of the simulations even two pores were formed. In each case, the pores formed adjacent to the pre-stalk, on a time scale ranging between 10 to 150 ns. A close-up of the stalk/pore complex is shown in

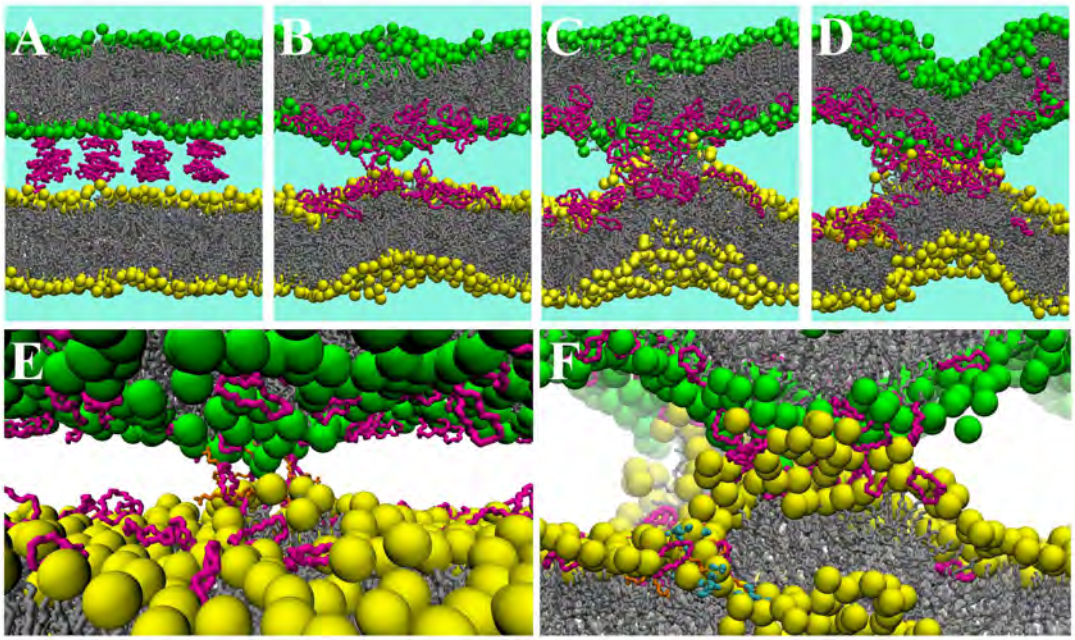

Figure 5.20: *Sequence of events of the leaky fusogenic action of cyclic peptide BPC194* **A.** Initial setup with peptides placed between two bilayers. **B.** Bridging of contact monolayers of the two bilayers by BPC194. **C.** Lipid bulging caused by the action of peptides associated with the bilayers. **D.** Pre-stalk intermediate accompained by disordered toroidal pore. **E.** Close-up of the bridging peptides. **F.** Close-up of the stalk-pore complex. The peptides are depicted in ping, the P atoms of the two bilayers in yellow and green, respectively and the lipid chains in grey. The water molecules in panel F are shown as an indicative of pore formation.

Figure 5.20 F. The pores formed are reminiscent of the disordered toroidal pores formed by other antimicrobial peptides (Leontiadou 2006 and Sengupta 2008), and also by this peptide on a single bilayer as shown in the previous section.

The MD simulations thus point to a dual role of the peptides; the peptides promote both stalk-like perturbations and are able to induce pores. To further characterize the perturbing effect of the peptides on the lipids, we quantified the splaying and tilting of the lipid tails (see analysis section). The results are given in Table 5.13. In each of the five simulations, the tilting is quite substantial compared to a pure bilayer. For example, in simulation-F3, 28% of the lipids of the contact leaflet tilted more than 85^o from their initial position at least once during the simulation. In the pure DPPG bilayer no such extensive tilting is observed. In addition, several lipids were also significantly splayed to values larger than 170^o implying a full opening of the lipids tails. Not surprisingly, the lipids that are most perturbated are the ones in direct contact with the peptides,

and especially the lipids involved in the formation of the pre-stalk, and later the pore. An example is presented in Figure 5.21 A-D, showing how a single lipid is splayed by interacting with a few neighboring peptides. In this particular example, the splayed lipid tail remains stable over 50 ns. The stabilizing contacts between the peptides and the lipids are formed between the lysine residues and the charged head-groups, and the apolar phenylalanine and leucine residues shielding the hydrophobic tails of the lipids from the water.

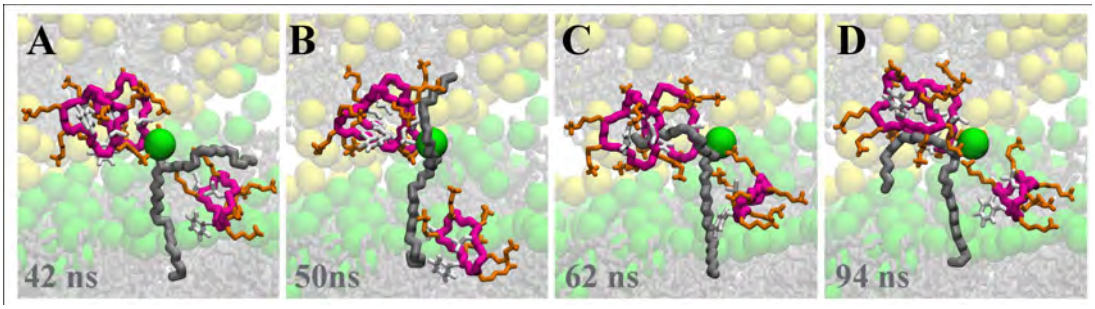

Figure 5.21: *Molecular details of the splaying of an example lipid during the course of the simulation.*

Table 5.13: Percentage of lipids in the contacting monolayers (during the simulation) tilt by more than $>85^o$ or splay by more than $>170^o$ is indicated. The standard error of the average is obtained from the standard deviation between all five simulations. The simulation length and formation of pores is also indicated.

Simulation	**Time** (ns)	**Nr. Pores**	**Time scale Pore (ns)**	**Contact monolayers**	
				% Tilt ($>85^o$)	% Splay ($>170^o$)
pure DPPG	100	-	-	0	2
F1	360	2	40/58	24	9
F2	210	-	-	18	8
F3	590	1	150	28	12
F4	160	2	10/70	10	6
F5	230	-	-	16	10
Average	-	-	-	19.2±3.1	8.9±1.1

5.4.3 Molecular Basis of "multi-hit" Processes for Antimicrobial Activity

As described in section 5.3.3, at a high P:L ratio the cyclic peptide BPC194 showed the formation of a stable disordered toroidal pore by the cooperative insertion of three cyclic peptides into the lipid membrane. However, it is worth to recall that the pore was not formed spontaneously in the time course of the simulations. Starting from a highly perturbed state (transition state) several simulations were set up changing velocities in the system and a pore was observed in six out of ten of them.

In the present simulations, two membranes are present in close proximity, and the peptides are actually able to bridge the two membranes. As a result of that a pre-stalk intermediate is identified together with the spontaneous formation of a disordered toroidal pore. Unlike the previous simulations where three peptides were required to porate, in this simulations two cyclic peptides were able to open a pore, ruling out the fact that a specific number of peptides was needed for leakage.

Adsorbing at the interface, the peptides exert considerable stress on the outer, contacting monolayers, inducing a strong disordering of the lipids in the vicinity of the peptides leading to lipid splaying, tilting, and protrusions as evidenced by our MD simulations. Poration is another way in which the excess stress can be relieved. In fact it is generally viewed as the mode of action of antimicrobial peptides, causing cell content leakage or even complete lysis of the cell membrane. For isolated membranes it is probably the only way, but under conditions where membranes are in close proximity, the stalk/pore complex can form. We believe that the multi-mode action, at least in this specific case, may also be functionally-relevant and contribute to higher potency towards bacteria killing, and that certain AMPs could act as fusiogenic peptides and vice versa.

5.5 Remarks and Conclusions

In this chapter, different types of computational methods have been used to model the structure and behaviour of cyclic peptides, providing insight on the molecular basis for the antimicrobial activity.

In the first part, the conformational space of the active peptide BPC16 was analysed by means of two different conformational search methods, namely Simulated Annealing and Simple Sampling. A simple sampling protocol applied for a range of 300 K to 900 K produced up to 274 minumum energy structures that displayed a bimodal distribution. A similar bimodal profile was already found by Corcho *et al.* (Corcho 2000). The analysis of the conformers revealed a bias towards the formation of specific hydrogen bonds in the backbone, showing that the procedure was not able to screen the overall conformational space of the cyclic peptides.

On the contrary, the Simulating Annealing protocol applied provided a more homogeneous set of 998 energy minima structures, exhibiting significant formation of hydrogen bonds between the backbone atoms of all residues. The analysis of the large set of conformers revealed that structures with smaller radius of gyration were more stable. We concluded that the SA protocol sampled more efficiently low energy conformations that the SS approach applied. The latter, however, lead to less compact low energy structures exhibiting more relevant side-chain interactions.

The lowest energy structure obtained from the SA protocol was established as the global minimum. The conformer displayed a very compact shape, with a large number of hydrogen bonds involving the backbone atoms. The lowest energy structure provided by the SS method was just 2 kcal/mol above in energy. In contrast with the global minimum, this structure was characterized by a network of hydrogen bonds involving the lysine side-chains.

The dynamical behaviour of the lowest energy structures obtained from each protocol was tested, both in gas phase and in solution. In vacuum, the structure of the global minimum was extremely stable. In the case of the lowest energy structure obtained from the SS protocol, the side-chain interactions are lost within few ns of the simulation and the structure is stabilized by the presence of new hydrogen bonds between backbone atoms, leading again to a more compact structure.

In the water phase, the entropic effect of water molecules caused more fluctuations in the secondary structure of both minima structures. The second low energy conformation considered lost completely its secondary structure and most of the hydrogen bonds formed between the backbone atoms were broken and ex-

posed to solvent. For the global minimum the bifurcated hydrogen bond involving residues K^5-K^8 and K^5-K^9 remained during the whole simulation, leading to a stable β-turn I and α-turn structure.

Albeit conformational search techniques are widely used and are assumed to be a good tool for searching the conformational preferences of peptide, one can not assume that the lowest energy conformation of the peptide is the actual bioactive form (Leach 2001). The peptide primary sequence contains all the functional groups needed to provide the biological activity, but the bioactive conformation corresponds to the spatial arrangement that favors the interaction of these functional groups with a given target. Therefore, the bioactive conformation is related to the biological activity that the peptide is able to carry out (perhaps several activities, with likely several bioactive conformations).

Accordingly, in the second part of this work we studied the secondary structure of a bioactive cyclic peptide (BPC194) in contact with a lipid bilayer that modeled the microbial membrane. Interestingly, the linear analogue of this peptide (BPC193) is not active so the analysis of the MD simulations of the interaction of both peptides upon membrane gave us useful information about the secondary structures relevant for the antimicrobial activity, as well as deep insight on the mechanism of action of the active peptide at the atomic scale.

We found that both peptides, when present in the aqueous phase, are mainly unstructured and showed a high propensity to bind to the (anionic) membrane surfaces. However, from this point on, the behaviour of the two peptides diverges. The cyclic peptide had a marked tendency to fold to a β-structure that gave rise to a spatially-symmetric arrangement of the lysine side-chains, resulting in an amphipathic-like structure. On the contrary, in the case of the linear peptide, the folding of the backbone to form a β-hairpin structure is less favorable than in the cyclic peptide, due to its larger conformational entropy.

The ability of the cyclic peptide to fold allowed it to insert deeper into the membrane interface. Through cooperative interactions, several of these membrane-embedded and folded cyclic peptides caused large perturbations in the bilayer that, eventually led to the formation of a stable transmembrane pore. The linear peptide assumed a more extended conformation and was unable to substantially perturb the membrane.

The simulations highlighted the importance of the secondary structure in stabilization of the porated state. In the simulations, a constrained secondary structure rather than a high percentage of secondary structure was required to stabilize the pore. The importance of the secondary structure, induced on membrane binding, appeared to be the alignment of the charged residues such that

they fit the toroidal shape of the pore. This explained why the linear analogue of the active peptide is less active: for entropic reasons a folded structure is less favorable, whereas in the case of the cyclic peptide this entropic penalty is prepaid by the cyclic peptide. In fact, we observed that the linear peptide could not open a pore but was able to stabilize to some extent an already formed one by the cyclic analog.

The last part of this chapter focused on the study of other modes of action of BPC194, in particular its ability to induce membrane fusion. Such multi-action of the peptide may account for its high activity towards bacteria killing. Our MD simulations demonstrated that poration and fusion occur simultaneously, which at the same time corroborated experimental evidences. One one hand, cyclic peptides were able to absorb on the outer membrane leaflets and insert deeper into the hydrophobic core opening disordered toroidal pores. At the same time, the peptides units that were not as deeply inserted, which we refer as bridging peptides, were able to protrude the lipids out from the lamellar phase. The interaction of the lysine residues with the polar head-groups of the lipids induced relevant tilt and splay of the lipids. Furthermore, the hydrophobic side-chains shielded the fatty tails, favouring the interaction of the lipids with the water phase. These factors contributed to the spontaneous formation of a prestalk phase, which has already been proposed as an intermediate for stalk and membrane fusion (Efrat 2007).

Taken as a hole story, the atomistic simulations carried out in this work have shed light in the molecular basis for antimicrobial activity of a small cationic cyclic peptide. The information gathered has helped us to endeavor the ultimate goal of this work, namely the *de novo* design of new cyclic peptides with enhanced activity. These results will be presented in the next chapter.

Chapter 6

Rational Design of Cyclic Antimicrobial Peptides

In our MD simulations described in Chapter 5 we observed that BPC194, the most active peptide of the Phe-containing library of cyclic AMPs, adopted an amphipathic β-structure with a spatially-symmetric arrangement of the lysine side-chains. We hypothesize that this distinct structural motif could play a fundamental role in the antimicrobial activity of this active peptide and hence be the key of a novel structure-function relationship.

Accordingly, we have carried out several MD simulations to check the dynamic stability of the structure of peptide BPC194, specifically the vulnerability of its backbone's hydrogen bonding patterns. Further MD simulations of another active cyclic peptide of the library (BPC198) were also performed in order to determine whether a similar symmetric arrangement was particularly stable. In this case, a different structure proved to be more stable. Thus, both conformations were considered in the process of rational design of new cyclic peptides with high antimicrobial activity for the library.

The last part of this chapter is devoted to the synthesis of a new library of nine cyclic peptides, where all peptides have the same number and type of amino acids. Finally, the high antimicrobial activity found for some of these new peptides evidence the value of our structure-activity model and illustrate the benefits of rational design versus the combinatorial approach.

6.1 Structural Factors Governing the Activity of Cyclic Peptides

Understanding the structural factors that govern the antimicrobial activity of the library of cyclic peptides is a daunting task. However, our MD simulations already highlighted the importance of peptide's secondary structure for the process of forming stable pores and inducing the fusion on lipid membranes. In the case of peptide BPC194, a stable symmetric arrangement of the lysine side-chains was observed for the peptides inserted in the pore (see previous section). The polar side-chains pairs K^1-K^8, K^2-K^7 and K^4-K^5 aligned producing a particular structure reminiscent of an *anchor* that helped to stabilize the polar head groups of the lipids and the water channel.

We believe that this structural motif could play a fundamental role in the antimicrobial activity of this active peptide. Hence, we have started by comparing the primary structure of several cyclic peptides of the library in order to find clues of their different antimicrobial and hemolytic activity.

In Table 6.1 we present the amino acid sequence of six representative peptides from the Phe-containing library, together with their activity.

Table 6.1: Amino acid sequence activity towards three bacteria and hemolytic character of six representative peptides from the Phe-containing library. Orange residues indicate amino acid substitution (BPC194 is taken as reference sequence).

Code	**X^1-X^4**	**Common Sequence**	**MIC (μM)**			**Hemolysis %**[d]
			Ps[a]	**Xv**[b]	**Ea**[c]	
BPC194	KKLK	$K^5F^6K^7K^8L^9Q^{10}$	3.1-6.2	3.1-6.2	6.2-12.5	17±1.7
BPC096	LKLK	$K^5F^6K^7K^8L^9Q^{10}$	6.2-12.5	3.1-6.2	12.5-25	24±4.3
BPC094	KLLK	$K^5F^6K^7K^8L^9Q^{10}$	6.2-12.5	6.2-12.5	25-50	75±1.6
BPC202	KKKK	$K^5F^6K^7K^8L^9Q^{10}$	12.5-25	6.2-12.5	>100	2±0.2
BPC190	LKKK	$K^5F^6K^7K^8L^9Q^{10}$	6.2-12.5	6.2-12.5	>100	0±0.0
BPC198	KLKK	$K^5F^6K^7K^8L^9Q^{10}$	3.1-6.2	3.1-6.2	12.5-25	14±1.4

[a] *Ps* stands for *Pseudomonas syringae*

[b] *Xv* stands for *Xanthomonas vesicatoria*

[c] *Ea* stands for *Erwinia amylovora*

[d] Percentage of hemolysis at 375 μM

It can be seen that minor changes in the primary structure affect the an-

timicrobial activity. Taking BPC194 as reference, in the analogues BPC096 and BPC094 a single amino acid (lysine) has been replaced by a leucine (in position 1 and 2, respectively). We speculate that the amphypatic structure of BPC194 might be lost by the substitution affecting their activity. Comparing the activities of both analogues, the breaking of the lysine pair K^2-K^7 had a major influence in the loss of activity and also in the enhancement of the hemolytic character of the peptide.

Besides the alignment of the polar side-chains, the β-structure of BPC194 peptide also induces a spatial alignment of the side-chains of amino acids in position 3 and 6, which in the case of BPC194 correspond to two hydrophobic residues (leucine and phenylalanine, respectively). Breaking this hydrophobic association by changing the third position for a lysine amino acid has a dramatic effect on the activity of analogues BPC202, BPC190. However, in the case of BPC198 the antimicrobial and hemolytic character are retained, with only a small decrease on the activity with respect to bacteria *E. amylovora*. In BPC198, both the polar K^2-K^7 and the hydrophobic L^3-F^6 pairs would be broken. So, while peptides BPC096, BPC094, BPC202 and BPC190 show lesser activity that might be caused by the mismatching of the alignments of the side-chains occurring on the β-structure, it is clear that the primary structure for BPC198 does not follow the structure-function model deduced from BPC194 structure. It is likely that BPC198 peptide might exhibit an alternative folding that could permit other polar and hydrophobic alignments to take place.

In order to understand the molecular basis for the activity of peptide BPC198, we have carried out several MD simulations in solution of this peptide and analogues with different starting conformations. The structure of BPC194 was taken as a reference since its structural motif was already characterized and associated to its function. An overview of the MD simulations carried out is summarized in Table 6.2.

It is important to note that the original conformation of BPC194 presented a cis-peptide bond at the turn region, involving residues K^4-K^5 (Table 6.2, simulation C1). This cis-peptide bond was originated during the minimization step after modelling the cyclic peptide with *leap* utility of AMBER9. So, besides the simulation of BPC194 starting from its active conformation, another simulation (C2) was carried out for an all-trans peptide bond conformation to check if the presence of the cis peptide bond was critical for the stability of the symmetric structure. Also, another simulation (C3) was performed for an analogue of BPC194 where the phenylalanine residue was replaced (in silico) by a tryptophan (peptide BPC418). Taking into account that in the experimental procedure a

Table 6.2: Overview of the simulations for BPC194 and BPC198[a].

Code	Peptide	Peptide bond configuration[b]	Time (ns)
C1	BPC194	cis	300
C2	BPC194	trans	300
C3	BPC194W	trans	300
C4	BPC198	cis	300
C5	BPC198	trans	530
C6	BPC198W	trans	300

[a] A β-structure characteristic of BPC194 is used for all simulations.

[b] Peptide bond configuration in 4-5 th position (turn region). All remaining peptide bonds have trans configuration.

Trp-containing library was synthesized and evaluated for antimicrobial activity, this simulation included to analyse the effects of the presence of tryptophan residue in the already folded state of BPC194.

Finally, three extra simulations were carried out with the same conditions as described above where the BPC194 was replaced in silico by the BPC198 peptide (simulations C4, C5 and C6).

6.1.1 Methodology

6.1.1.1 System set-up.

All MD simulations were performed for systems containing a single cyclic peptide unit solvated by water. The starting peptide structure was characterized by a β-sheet conformation taken from a snapshot of peptide BPC194 of the simulation of the pore formation (Table 5.8, simulation C1) where the polar and hydrophobic side-chains were aligned (see Figure 6.1 A). In the case of BPC198, the initial structure was initially modeled in silico using Yasara program by replacing the appropriate residues (in position 2 and 3). Then, an energy minimization step was applied in order to remove the bad contacts originating from the substitution of the side-chains.

In Figure 6.1 one can readily see how the aromatic ring of the phenylalanine side-chain in position 6 rotated to avoid the neighboring lysine side-chain, that now lies in position 3. A similar strategy was applied to generate the initial struc-

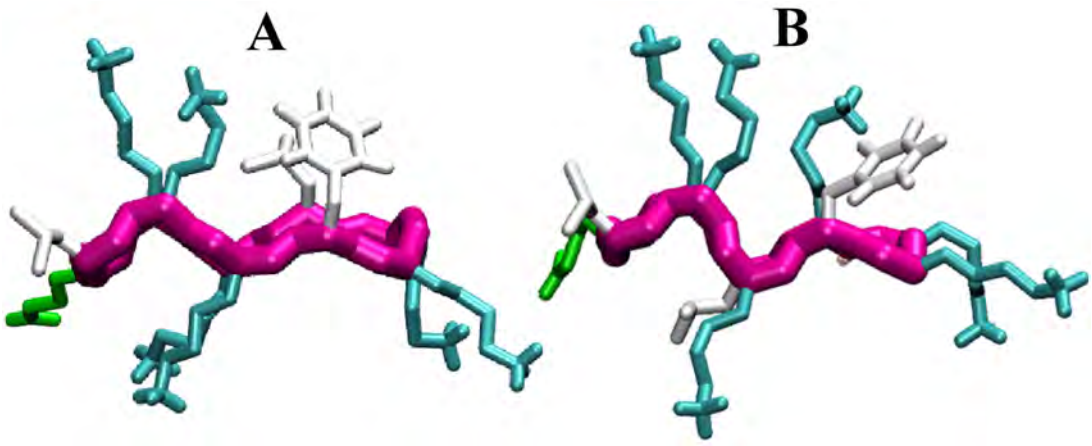

Figure 6.1: *Initial conformation.* **A.** Structure for the simulations C1 and **B.** C4 involving BPC194 and BPC198, respectively.

ture of the tryptophan analogues of both BPC194 and BCP198 peptides. The all-trans peptide bond initial conformations of peptides BPC194 and BPC198 were also generated by twisting the peptide bond between amino acids in position 4 and 5, followed by an energy minimization step.

All systems were simulated in a cubic box of length ∼4 nm and about 1600-2100 water molecules, with counterions (Cl^-) to neutralize the charged lysines.

6.1.1.2 Analysis.

The conformation of the different cyclic peptides along the simulations was characterized by the hydrogen bond distance between the oxygen donor and hydrogen acceptor of the backbone atoms. Also, the angle between the normal vector to the (approximate) planes formed by the backbone atoms and the vector representing the side-chains was used to represent the spatial arrangement of the side-chains, and as a measure of amphypathicity. The distance between the capping atoms of selected side-chains was also monitored along some of the simulations. Finally, the time evolution of the secondary structure of the peptides were also determined following the same procedure as in section 5.2.1.5.

6.1.1.3 Simulation parameters.

All MD simulations were performed using the same parameters as described in detail in section 5.2.1.4. No membrane model was used in this case.

6.1.2 The Stable 3D Structure of BPC194

The peptide BPC194 in its folded state was simulated for over 300 ns in solution to check its stability and vulnerability in water environment. First, the spatial arrangement of the side-chains was analyzed along the trajectory. For this purpose, the angle formed between the normal vector to the backbone plane and a vector representing each of the side-chains of the residues was calculated. As shown in the inset of Figure 6.2 B, small values of the angle ($<90^o$) indicate that the corresponding side-chain is arranged on the upper part of the peptide, whereas values larger than 90^o correspond to the bottom region. In Figure Figure 6.2 A we show the time evolution of the calculated angles for the simulation C1 (Table 6.2), where the initial conformation of the peptide was the active one.

The lysine side-chains K^2 and K^7 (cyan curves) are "paired", and occupy the lower side of the peptide during the whole simulation, with little fluctuation. Similarly, the pairs K^1-K^8 and L^3-F^6 appear to be also aligned, and are placed on the upper side of the peptide. A slight fluctuation of the angles seems to take place in the case of the hydrophobic pair L^3-F^6, probably due to the fact that the dispersion interactions that take place are weaker.

The side-chains of the remaining residues, which are part of the turn regions, show a more fluctuating behaviour. The values of the angles for the lysine pair K^4-K^5 often oscillate near 100^o, quite close to co-planarity with the backbone.

Finally, the side-chains of residues L^9 and Q^{10} exhibit larger fluctuations and oscillate between the upper and lower regions during the simulation. Nevertheless, the overall disposition of the side-chains gives rise to an amphypathic structure that is stable during the whole simulation.

We also determined the evolution of the secondary structure of the peptide with a typical DSSP plot, as depicted in Figure 6.3. In this figure, the time evolution for the simulations C1, C2 and C3 is represented.

In all cases, the hydrogen bonds between residues K^1-K^8 and L^3-F^6 that give rise to the β-structure were maintained during most of the simulation time, specially for the structure presenting a cis peptide bond in the turn (Figure 6.3 A, C1). The all-trans peptide bond (B) and the tryptophan derivative (C) structures showed a slightly less stable secondary structure, presenting longer distances in one of the hydrogen bonds and larger fluctuations, that are confirmed by the lower percentage of β-sheet along the simulation (see Table 6.3).

In the case of the tryptophan analogue of BPC194 (C3), the β-structure was found less stable due to the weakening of the hydrogen bonds in the backbone. This is evident from the increased average hydrogen bond distance between residues K^1-K^8 (0.29 ± 0.15 nm as compared to 0.22 ± 0.07 nm in the case of simu-

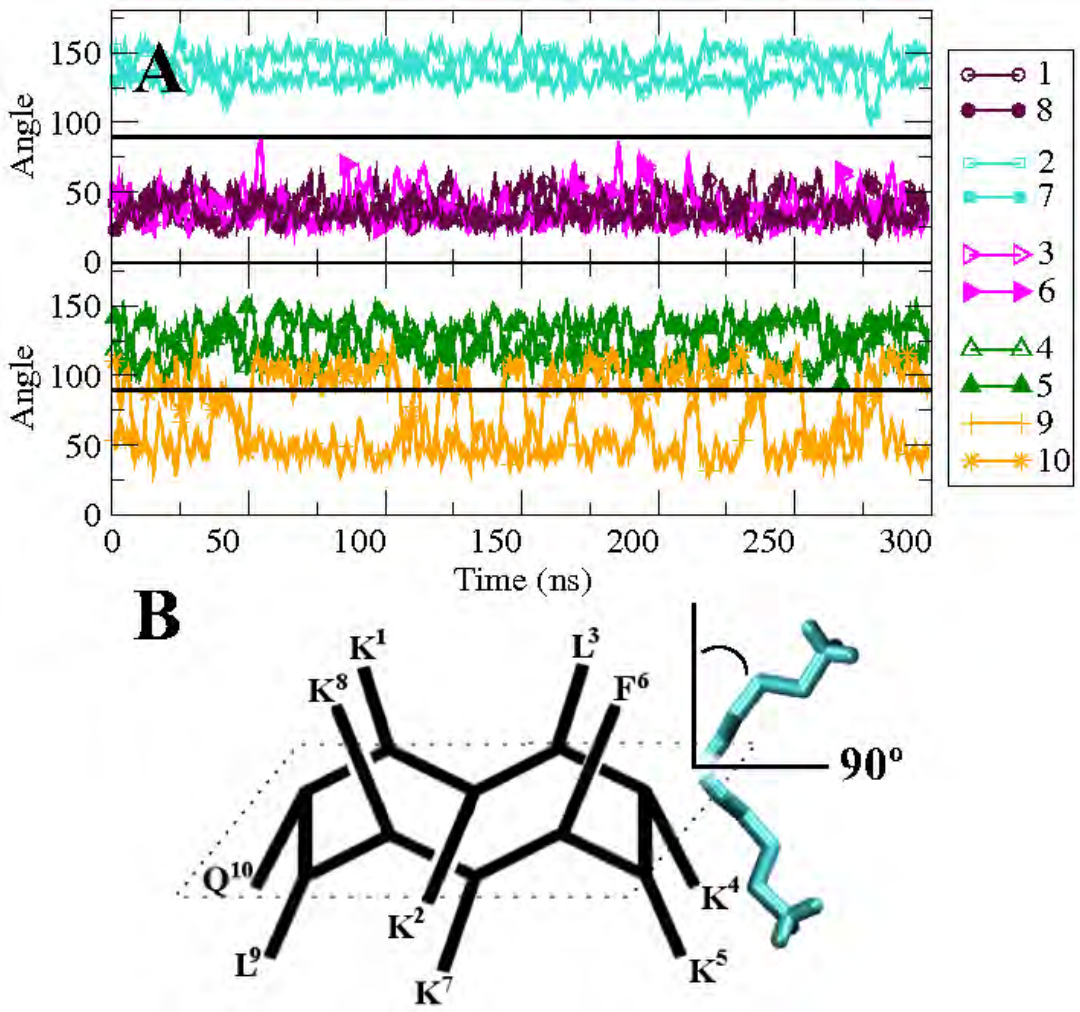

Figure 6.2: *Stable structure of BPC194.* **A.** Time evolution of the angle formed between the normal vector to the backbone plane and a vector representing each of the side-chains for simulation C1. **B.** Diagram indicating the stable amphipathic β-structure of BPC194.

lation C1). We speculate that this higher vulnerability might explain the subtle decrease in the activity observed for the tryptophan-based library described in Chapter 4. It has to be pointed out that the BPC194 was found in the MD simulations, described in Chapter 5 to be in an essentially unfolded state in water environment, prior to its interaction with the lipid membrane. The long simulations in water environment described here show a seemingly the opposite view, where "starting form a folded state", the structure was quite stable for as long as 300 ns. Only in the case of the tryptophan analogue some of the hydrogen bonds in the backbone were more vulnerable. So, the lipid membrane and possibly the presence of other peptides induce the formation of a stable specific

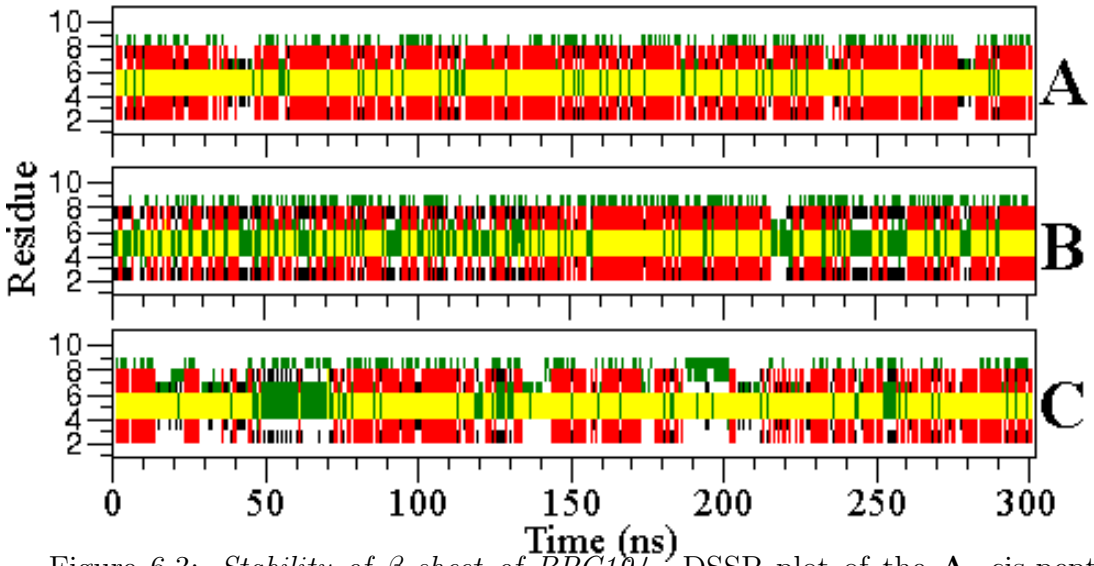

Figure 6.3: *Stability of β-sheet of BPC194.* DSSP plot of the **A.** cis-peptide bond configuration (C1), **B.** all-trans peptide bond configuration (C2) and **C.** tryptophan analogue (C3).

active structure that is less likely to be formed in solution due to entropic effects. Nevertheless, the fact that the active structure is stable in solution opens up the possibility of studying other peptides of the library in similar conformations to that of BPC194 in the same conditions.

6.1.3 Unfolding Path of BPC198 Towards an Alternative β-structure

Analogous simulations to those described in the previous sections were carried out for the active cyclic peptide BPC198. The qualitative analysis of the possible alignment of the side-chains in terms of the amino acid sequence already showed a mismatch of polar and hydrophobic residues that could indicate that the structure might not be stable. This is indeed the case and BPC198 showed a very different behavior in water phase. In Figure 6.4 the DSSP plot of the secondary structure evolution of simulations Table 6.2 C4, C5 and C6 is shown.

In all cases the peptide unfolded after about 100 ns. In the simulation C4 where the starting conformation presented a cis-peptide bond in the turn region (K^4-K^5) (Figure 6.4 A), the loss of secondary structure was not followed by any rearrangement of the residues to an alternative compact conformation. Instead, the peptide adopted an unstructured conformation presenting only turns due to the cyclic nature of the molecule. The average hydrogen bonding distance

Table 6.3: Average hydrogen bond distances and percentage of secondary structure of the simulations involving BPC194 peptide.

Code	K^1-K^8 (nm)[a]	L^3-F/W^6 (nm)[b]	β-Sheet structure (%)
C1	0.22±0.07	0.21±0.03	41.3
C2	0.20±0.03	0.28±0.06	38.7
C3	0.29±0.15	0.23±0.05	31.2

[a] The hydrogen bond is between the oxygen donor atom of K^8 and acceptor hydrogen atom of K^1

[b] The hydrogen bond is between the oxygen donor atom of F/W^6 and acceptor hydrogen atom of L^3

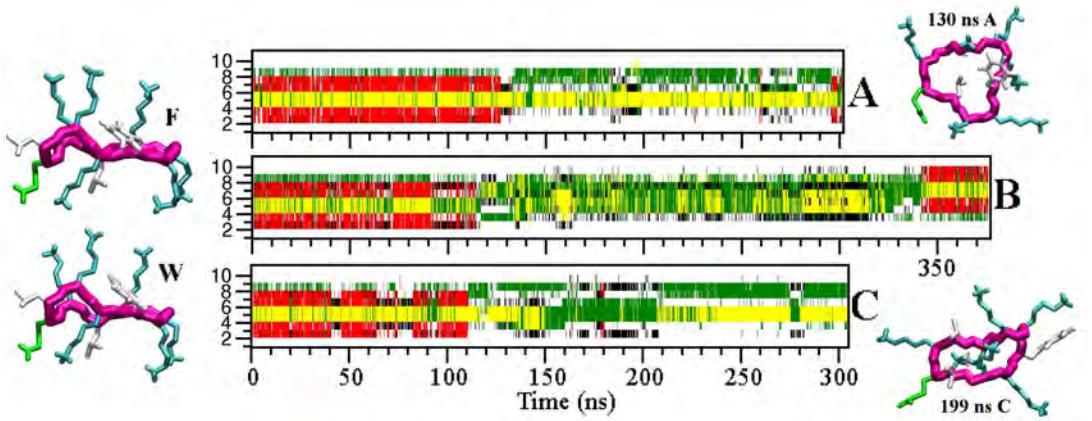

Figure 6.4: *Secondary structure of peptide BPC198.* **A.** BPC198 with a cis-peptide bond. **B.** BPC198 with all-trans peptide bond. **C.** BPC198 tryptophan analogue with a cis-peptide bond.

between the residues K^1-K^8 and L^3-F^6 were 0.46±0.18 nm and 0.23±0.04 nm, respectively, indicating that the first hydrogen bond was completely lost. It is likely that the presence of the cis-peptide bond constrained somehow the possibility of forming other hydrogen bonds in the backbone as the simulation of the tryptophan analogue (simulation C6) showed similar behaviour (see Figure 6.4 C).

However, the simulation of the all-trans peptide bond conformation (C5) exhibited different behaviour. We extended the simulation time beyond 350 ns and a new folded structure was formed and remained stable. The turn region

(yellow color in DSSP plot) shifted to the residues in position 6 and 7 and new hydrogen bonds were formed within the backbone atoms that stabilized a compact structure. For a better characterization of this unfolding/folding process several key hydrogen bond distances were monitored. These are displayed in Figure 6.5

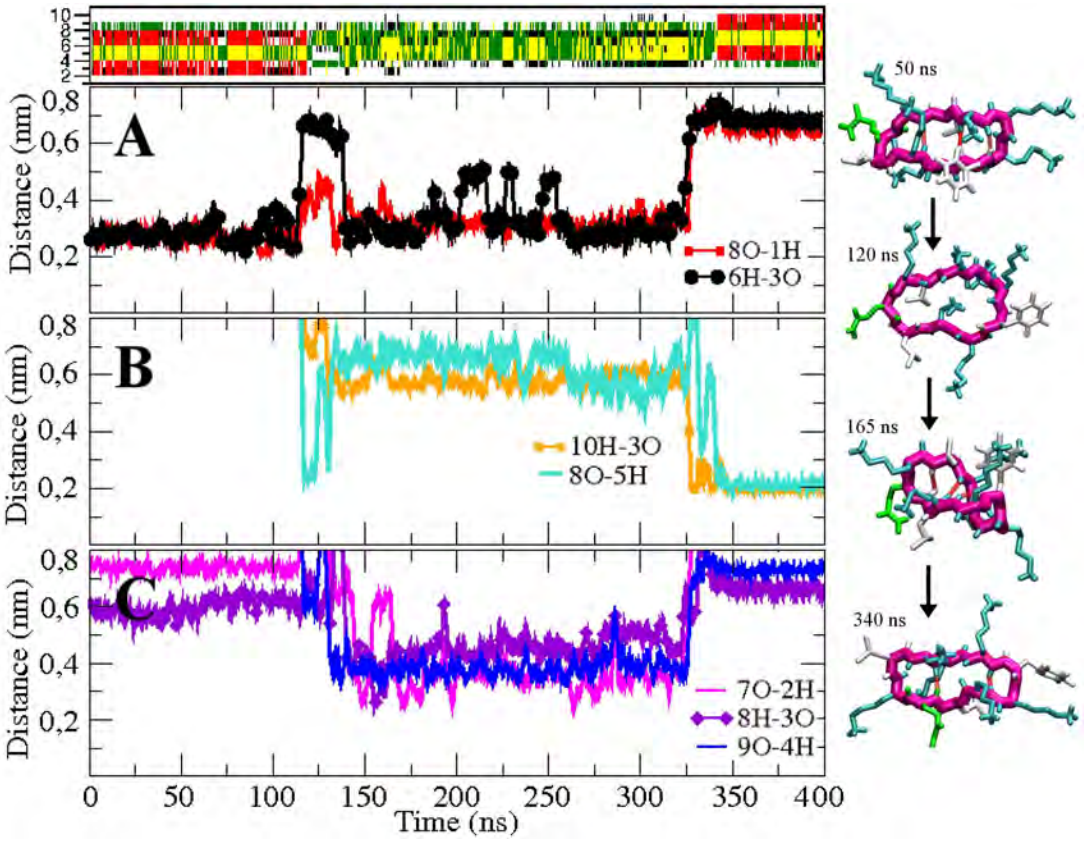

Figure 6.5: *Hydrogen bonding distances of unfolding/folding of BPC198.* **A.** Initial hydrogen bonds. **B.** Transient interactions along the unfolding/folding pathway and **C.** Hydrogen bonds of the new conformation. **righ pictures.** Snapshots along the time course of the process.

The initial hydrogen bond interactions between residues K^1-K^8 and K^3-F^6 were again stable till around 120 ns. At this point a sudden fluctuation lead to a simultaneous breaking of both hydrogen bonds and a concomitant approach of residues K^5-K^8 to hydrogen bonding distances. After this event, the structure became more compact, as indicated by the shorter distances observed between residues K^7-L^2, K^8-K^3 and L^9-K^4, which even led to the temporary formation of weak hydrogen bonds. The distances between the initial hydrogen bonds slightly increased and oscillated until approximately 340 ns where a large fluctuation lead to a new folded β-structure characterized by strong and stable hydrogen bonds

involving residues K^5-K^8 and L^3-Q^{10} (see Figure 6.5 B).

It is interesting to see how the side-chains arrange in space during the unfolding/folding process and also whether they also align in the upper and lower sides of the molecule like in the case of peptide BPC194. In Figure 6.6 we have analyzed the time evolution of the angles between the normal vector to the backbone plane a and a vector representing each of the side-chains of the residues.

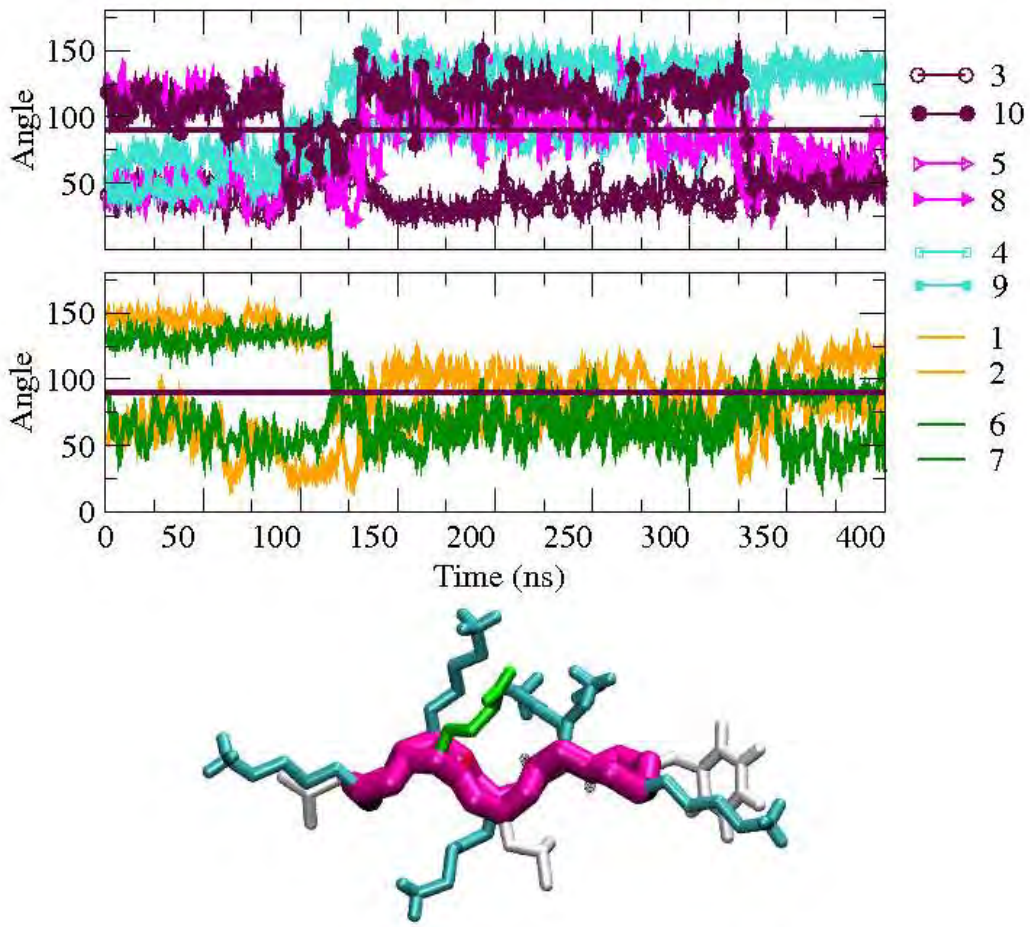

Figure 6.6: *Characterization of a new β-structure of BPC198.* Time evolution of the angle formed between the normal vector to the backbone plane and a vector representing each of the side-chains. On the bottom, a representative snapshot of the new conformation of BPC198.

It can be seen that the arrangement of the sides-chains of the initial structure remains quite constant until around 80 ns. At this point, the side-chain of residue Q^{10} suddenly migrates from the lower side of the peptide (angle $>90\ ^o$) to the upper region and temporarily aligns with the K^3 side-chain, that remains in the upper region during the whole simulation. A similar process occur at the same time for the side-chain of residue K^5. In this case, however, after aligning with

the side-chain of K^8, both start to oscillate around an angle of 90^o until the final structure is formed.

Since these events occur at a shorter time than the breaking of the intramolecular hydrogen bonds in the backbone, it is clear that the later must be somehow induced by the oscillation of the side-chains and not the opposite. After 120 ns, when β-structure is lost, the side-chains of residues K^1, L^2, F^{10} and K^7 start to oscillate around a parallel position with respect to the backbone (angle close to 90^o). These residues end up in the turn region of the new β-structure and do not align.

Finally, after 325 ns, right before the formation of the hydrogen bonds in the backbone that stabilize the new β-structure (340 ns), the side-chain of residue Q^{10} swings again to the upper region of the molecule and aligns with the lysine K^3 until the end of the simulation. The lysine pair K^5-K^8 also align to the upper part of the molecule but the angle (around 60 degrees) is somewhat larger than expected for a pairing of two polar residues.

A representative snapshot of the final β-structure is depicted at the bottom of Figure 6.6. The conformation is reminiscent of the active structure of BPC194 where two pairs of polar side-chains are spatially aligned and arranged in one side the molecule. However, in this case in the lower region a lysine (polar) and a leucine (hydrophobic) side-chains are forced to face due to the presence of tight hydrogen bonds in the backbone. So, this structure is not as amphiphatic as the one observed for the BPC194. To ensure that the new configuration was stable in solution, an extra MD simulation was performed starting from the new β-structure and was stable along the time course of the simulation (400 ns).

6.2 *De novo* Design of BPC194 Analogues

At this point, we believe we have identified the factors behind the formation of stable β-structures with certain amphypathic character. The final step and ultimate goal of this thesis is the *de novo* design of new peptides with improved activity. With the information gathered in the experiments and simulations described in the preceding chapters we will attempt a rational design that is exposed next.

6.2.1 Design of New Analogues

Based on our assumptions, nine cyclic peptides were designed in order to i) validate our structure-function model and ii) to check if we could identify a cyclic

peptide with improved antimicrobial activity. To do so, our strategy was based on the following criteria which might help to stablish the factors that influence the antimicrobial activity. The criteria are listed below.

1. Maintain the same number of hydrophobic and hydophilic residues: six lysines, two leucines, one phenylalanine and one glutamine residue.
2. Allow for a parallel arrangement of pairs of hydrophobic or hydrophilic residues that might give rise to a stable β-structure (e.g. a lysine, a leucine or a phenylalanine - leucine pair).
3. Combine different positions of the side-chain pairs along the backbone to test the influence in the activity.
4. Change the position of the phenylalanine and glutamine residues.
5. Take as a reference the conformation and secondary structure patterns found for BPC194 and BPC198 using MD simulations.

The primary structure of the nine cyclic peptides designed are listed in Table 6.4 and the speculated conformation in depicted in Figure 6.7. Peptides

Table 6.4: Primary structure of the nine cyclic peptides proposed as candidates.

Code	Sequence
BPC194[a]	c(KKLKKFKKLQ)
BPC198[a]	c(KLKKKFKKLQ)
BPC480	c(KKKLFKKKLQ)
BPC482	c(KLKKKKFKLQ)
BPC484	c(LKKKKKKFLQ)
BPC486	c(LKKKKKKLFQ)
BPC488	c(KLKKKKLKFQ)
BPC490	c(KKLKKLKKFQ)
BPC492	c(KKKLLKKKFQ)
BPC494	c(LKKKKFLKKQ)
BPC496	c(LKKFKKKKLQ)

[a] BPC194 and BPC198 have also been included for comparison purposes

BPC480, BPC482 and BPC484 differed in the position of the hydrophobic pair L-F along the backbone. On the other hand, peptides BPC486, BPC488, BPC490,

BPC492 displayed hydrophobic pairs in the same position but involving two leucine residues (L-L). In this case, the phenylalanine residue was kept at the ninth position, leaving the lysine residues paired in the rest of positions. Finally, peptides BPC494 and BPC496 based on the proposed conformation for BPC198, where the glutamine would be paired with a hydrophilic residue in the upper region of the peptide.

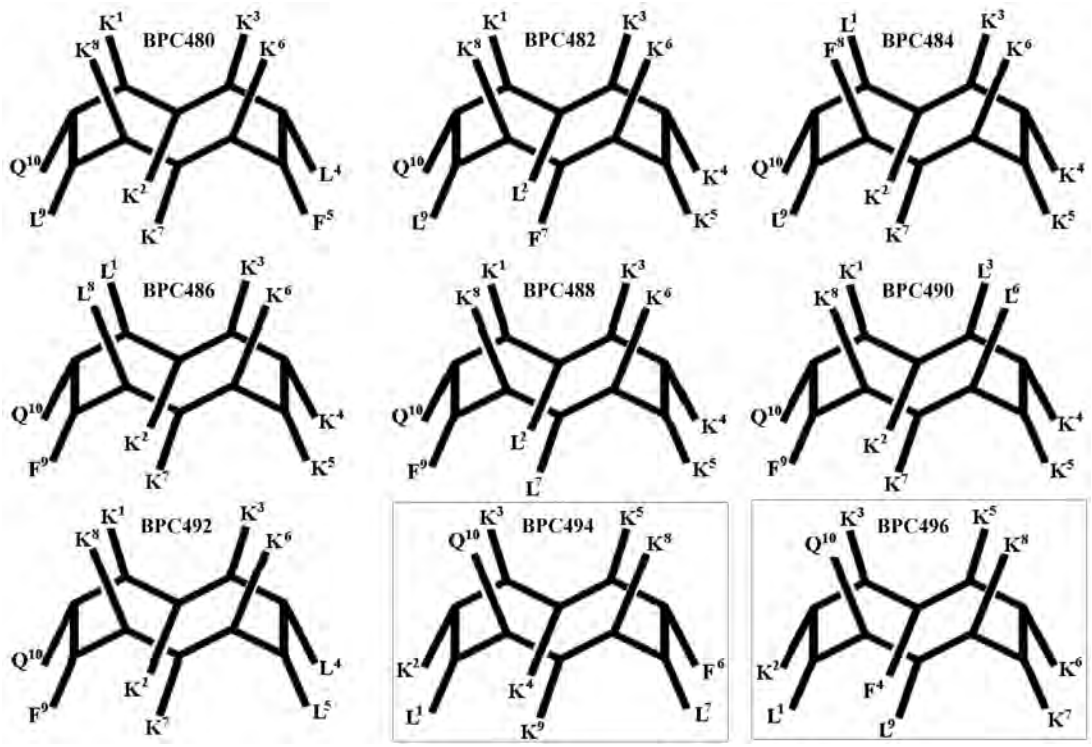

Figure 6.7: *De novo design of cyclic peptides from BPC194 and BPC198.* Ideal conformations of the nine cyclic peptides of the rational design

6.2.2 Synthesis of the *De novo* Designed Cyclic Peptides

The synthesis of the *de novo* cyclic AMPs was carried out on a MBHA resin (0.4 mmols/g) following the same strategy described in of section 4.1. However, in here different couplings were performed using COMU and oxyma as coupling reagents (El-Faham 2009, El-Faham 2010, Subiros-Funosas 2009). These reagents are a safer alternative to HBTU and HOBt, that have been described to be explosive and to cause allergic reactions. The synthesis of the lead peptide BPC194 was also carried out for comparison purposes. The final cyclic peptides were analysed by HPLC and characterized by ESI-MS. In most cases the HPLC chromatogram showed a single wide peak, however some impurities were observed in the ESI-MS spectra. Peptides were purified by reverse-phase prepar-

ative HPLC, but some small impurities remained in the peptide crude. However, cyclic peptides showed HPLC purities >90% (the corresponding HPLC are shown in Annex as it is indicated in Table 6.5).

6.2.3 Antibacterial Activity of *De novo* Designed Cyclic Peptides

The antibacterial activity of the *de novo* designed cyclic peptides against *P. syringae*, *X. vesicatoria* and *E. amylovora* were evaluated as well as the hemolysis (Table 6.5).

Table 6.5: Antibacterial activity (MIC μM) and hemolysis of *de novo* designed cyclic peptides.

Code	Sequence	MIC (μM)			Hemolysis (%)[d]	HPLC Annex
		Ps[a]	Xv[b]	Ea[c]		
BPC194	c(KKLKKFKKLQ)	6.2-12.5	3.1-6.2	25-50	11.2	Figure 7.48
BPC480	c(KKKLFKKKLQ)	25-50	>50	>50	0.57	Figure 7.49
BPC482	c(KLKKKKFKLQ)	12.5-25	12.5-25	>50	0.41	Figure 7.50
BPC484	c(LKKKKKKFLQ)	12.5-25	25-50	>50	0.17	Figure 7.51
BPC486	c(LKKKKKKLFQ)	12.5-25	25-50	>50	0.17	Figure 7.52
BPC488	c(KLKKKKLKFQ)	6.2-12.5	6.2-12.5	>50	0.17	Figure 7.53
BPC490	c(KKLKKLKKFQ)	3.1-6.2	1.6-3.1	12.5-25	13.06	Figure 7.54
BPC492	c(KKKLLKKKFQ)	12.5-25	12.5-25	>50	0.21	Figure 7.55
BPC494	c(LKKKKFLKKQ)	6.2-12.5	6.2-12.5	>50	0.00	Figure 7.56
BPC496	c(LKKFKKKKLQ)	12.5-25	6.2-12.5	>50	0.31	Figure 7.57

[a] *Ps* stands for *Pseudomonas syringae*

[b] *Xv* stands for *Xanthomonas vesicatoria*

[c] *Ea* stands for *Erwinia amylovora*

[d] Percent hemolysis at 375 μM

The results showed a slight decrease in the activity of BPC194, compared to the one previously found for this peptide (Table 4.5). This could be attributed to remaining impurities from the this synthesis. Even so, two out of three bacteria (*P. syringae* and *X. vesicatoria*) showed comparable activities and within same magnitude as in the original experiment (Monroc 2006), indicating that these new measured activities can be trusted.

The *de novo* designed cyclic peptides, except for BPC490, (MIC of 12.5-25 μM) were not active against *E. amylovora* (MIC of > 50 μM). Against *P.*

syringae, two peptides, BPC488 and BPC494 were as active as BPC194 (MIC of 6.2-12.5 μM) and one peptide, BPC490 was also the most active against *X. vesicatoria* (MIC of 1.6-3.1 μM), being more active than BPC194.

It is worth mentioning that for the best peptide, BPC490, a similar secondary structure to that of BPC194 could be proposed. Both structures only differ in the hydrophobic pair. Whereas BPC194 is suggested to fold having a parallel F-L pair, BPC490 would have preference for a parallel L-L pair. These observations point out that our hypothesis on the secondary structure of BPC194 might be correct. However, NMR studies are needed to confirm this hypothesis.

On the other hand, these *de novo* designed cyclic peptides were not hemolytic at 375 μM. Only BPC490 showed an hemolysis of 13% at this concentration, which is similar to that of BPC194.

6.3 Remarks and Conclusions

In this last Chapter, MD simulations have been used as a tool to recognize the factors that drive the formation of stable β-structures with partial amphypathic character.

First of all, the stability of the active conformation of peptide BPC194 found in Chapter 5 was tested by several independent MD simulations. The presence of a cis peptide bond in the turn region proved not to be determinant as a similar strucutre with all trans peptide bonds exhibited similar stability.

Analogous simulations for another active peptide of the library (BPC198) highlighted the key role of the parallel alignment of the side-chain of residues in the β region. At the active conformation of BPC194, the amino acid sequence of BPC198 induced the mismatch of polar and hydrophobic side-chains that eventually lead to a unfolding and a folding of the peptide to form an alternative compact and stable β-structure. The folding process has been monitored by the hydrogen bonding formation within backbone atoms and the spatial arrangement of the side-chains. It was seen that the unfolding pathway of the β-sheet formation was initiated by fluctuations of the side-chains of key residues, that lead to the breaking of the hydrogen bonds that stabilized the structure. Then, transient hydrogen bonds were established until the proper alignment of the side-chains triggered the formations of new strong hydrogen bonds and the final β-structure.

Common patterns were already been seen in the literature. The folding of a charged-21-amino acid peptide (con-T) showed a multi-step folding pathway, where hydrophobic interactions were not the major driving force of the folding process. Instead, charged-charged interactions and salt-bridge interactions amongst the peptide structure produced different local peptide shapes that, after consecutively broken-formation interactions, lead the peptide to its folded state (Wei 2005). Also it is worth mentioning that in the particular case of this β-hairpin, different mechanisms of folding were proposed. In a first "hydrophobic collapse" model, the first step corresponds to the formation of a native hydrophobic cluster followed by the interstrand hydrogen-bond formation (Pande 1999). In contrast, in a second model called "zipper" mechanism, the formation of the native β-hairpin occurs through significant populations of misregistered hairpin, which was identified as a specific folding pathway (Wei 2004).

Based on our findings, a set of nine cyclic peptides were designed and synthesized. This approach allowed the identification of the cyclic peptide BPC490, c(KKLKKLKKFQ), displaying a higher antibacterial activity than BPC194, the most active peptide of the previous libraries. Their secondary structure differs only in the hydrophobic pair of the amphypatic structure, indicating that the

leucine pair might be a favorable arrangement for the antimicrobial activity. Furthermore, it has to be noted that the second best candidate from the nine peptides was designed in light of a new β-structure of the analogue BPC198 found by MD simulations.

One of the most interesting findings was the low cytotoxic activity displayed by these peptides. Eight out of nine sequences showed less than 1% of hemolysis. These results suggest that, while the antimicrobial activity was generally maintained, the relationship between antimicrobial activity and hemolysis was dissociated.

Chapter 7

Conclusions

• We have described the synthesis of cyclic antimicrobial peptides using SPS and we have evaluated their antibacterial activity. We conclude that cyclization on a MBHA resin gives better results compared to SynPhase® lanterns cyclization, where an optimization step is needed. In this case, cyclodimerization is observed as the major product of the cyclization reaction. However, the use of collidine improves the reaction and BPC16 is obtained in 92% purity being the cyclic peptide the major product of the reaction.

• We have synthesized a Trp-containing library of cyclic peptides. In general, the antibacterial activity of the peptides is improved compared to the Phe-containing library, but the cytotoxic activity is also enhanced, ruling out the use of tryptophan analogues for new antimicrobial agents. However, due to their high activity they can still be good candidates for fluorescence studies.

• We have analyzed the stability of eight selected cyclic antimicrobial peptides with anticancer activity in human serum. Peptides BPC96 and BPC194, with optimal biological profile, are also very stable in human serum. The cyclic peptides are less vulnerable to enzymatic reactions and hence their is significatively slower than for their linear analogues.

• We have applied Simulated Annealing and Simple Sampling protocols for the conformational analysis of peptide BPC16. SA provided more homogeneous set of minimum energy structures compared to the SS protocol. We have found some correlation between the radius of gyration of the minimum energy structures and their relative energy. A very compact structure stabilized by with a large number of hydrogen bonds involving the backbone atoms has been stablished as the global minimum. A second structure close in energy is dominated by side-chain interactions.

We have performed MD simulations for the two lowest minimum energy

structures in gas and water phase. We have determined that the global minimum is very stable both in gas phase and in solution, whereas in the other conformation the side-chain interactions are lost. We have found that the structure is stabilized by the presence of a bifurcated hydrogen bond between K^5-K^8 and K^5-K^9 residues, which gives rise to β-turn I and α-turn motifs.

- We have studied at atomistic detail the interaction of the active cyclic peptide BPC194 and its non active linear analogue BPC193 upon a single anionic model membrane by MD simulations. We have established that the molecular basis for the activity of BPC194 lies in the ability to fold into an amphipathic structure, characterized by the spatially-symmetric arrangement of the lysine side-chains, which help the BPC194 to insert deeper into the membrane interface and stabilize a disordered toroidal pore. Unlike BPC194, its linear analogue BPC193 is unable to fold and to penetrate in the membrane. The MD simulations illustrate why the cyclic peptide is active while its linear analogue is not.

- We have explored the ability of peptide BPC194 to induce membrane fusion by MD simulations of a system composed by a double anionic model membrane. We have demonstrated that, as indicated by experimental evidences, poration and fusion occur simultaneously. This dual action is induced by the cyclic peptide by i) binding and inserting deeper in the membrane to form a pore, and ii) perturbing and protruding out lipids, leading to the formation of a bridge that triggers the fusion of the membranes.

- We have undertaken a rational design and synthesis of a small library of cyclic peptides based on the bioactive conformation of peptide BPC194. We have identified peptide BPC490 as the best candidate of the library, exhibiting comparable and even higher activities than BPC194. We have also recognized several non-hemolytic peptides form the library, concluding that the relationship between antimicrobial activity and hemolysis could be dissociated.

Annex I

Materials and Methods

7.1 General procedure for the solid-phase synthesis of cyclic peptides

7.1.1 Synthesis of BPC16 on a MBHA resin

The synthesis was performed on syringes (5 ml) fitted with a polyethylene porous disk to filter the excess of reagents and the solvents used in the reactions.

7.1.1.1 MHBA resin swelling

The MHBA resin (200 - 400 mesh, 0.33 mmol/g) was weighed into a syringe, was swollen with CH_2Cl_2 (1×20 min), DMF (1×20 min), treated with piperidine/DMF (3:7, (1×5 min)). The resin was then washed with DMF (6×1 min) and CH_2Cl_2 (3×1 min).

7.1.1.2 Coupling of the Fmoc-Rink linker

The resin was treated with Fmoc-Rink linker (3 eq), HBTU (3 eq) and DIEA (3 eq) in DMF under stirring overnight. After this time, the resin was washed with DMF (6×1 min) and CH_2Cl_2 (3×1 min). The Kaiser test was performed to confirm the coupling.

7.1.1.3 Fmoc group removal

The resin was treated with piperidine/DMF (3:7, 2 + 8 min) and washed with DMF (6×1 min) and CH_2Cl_2 (3×1 min).

7.1.1.4 Amino acid coupling

The resin was treated with the corresponding Fmoc-protected amino acid (3 eq), HBTU (3 eq) and DIEA (3 eq) in DMF. The mixture was stirred for 4 h. After this time the resin was then washed with DMF (6×1 min) and CH_2Cl_2 (3×1 min). The coupling was monitored with the Kaiser test.From the fifth amino acid coupling, NMP was used as solvent. The amino acids used for the synthesis of BPC16 were Fmoc-Lys(Boc)-OH, Fmoc-Glu-OAl, Fmoc-Phe-OH and Fmoc-Leu-OH.

7.1.1.5 Allyl group removal

Once the chain assembly was completed, the resin was placed under N_2 for 5 min. Afterwards, the resin was treated with $Pd(PPh_3)_4$ (3 eq) in $CHCl_3$/AcOH/NMM (92.5:5:2.5) under N_2 atmosphere for 3 h. After this time, the resin was washed following the procedure described in table Table 7.1.

Table 7.1: Washing protocol for allyl group removal on a MBHA resin.

Step	Solvent/reagent	Time
1	THF	2×10 s
2	THF	3×2 min
3	DMF	3×2 min
4	CH_2Cl_2	3×2 min
5	5% DIEA/CH_2Cl_2	3×2 min
6	0.03M $NaS_2CN(C_2H_5)_2$/DMF	3×15 min
7	DMF	10×1 min
8	CH_2Cl_2	3×2 min
9	DMF	3×2 min

7.1.1.6 Cleavage, analysis and characterization of the linear precursor

After allyl group removal, a small amount of resin (5 mg), was placed into a syringe, and was subjected to Fmoc group removal. The resin was then washed with CH_2Cl_2 (3×1 min) Et_2O (3×1 min) and air-dried. Afterwards the resin was treated with TFA/TIS/H_2O (95;2.5:2.5) for 2 h. The solution was filtered in an eppendorf and TFA was evaporated under N_2. The peptide was precipitated with Et_2O, centrifuged (11,000 rpm, 5 min) and the supernatant was removed to obtain a white solid. This was repeated three times. Then, the linear peptide was dissolved in H_2O/CH_3CN, analysed by analytical RP-HPLC and characterized by

ESI-MS. **HPLC (λ=220 nm):** t_R 5.886 min. **ESI-MS** *m/e*: 1273.9 $[M_L+H]^+$; 1295.9 $[M_L+Na]^+$; 1311.9 $[M_L+K]^+$ (Annex, figures Figure 7.1 and Figure 7.3)

7.1.1.7 Cyclization on a MBHA resin

The linear peptidyl resin completely deprotected was treated with PyBOP (5 eq), HOBt (5 eq) and DIEA (10 eq) in NMP under stirring for 24 h at room temperature. The resin was then washed with DMF (6×1 min) and CH_2Cl_2 (3×1 min). The reaction was monitored with the Kaiser test. The resin was dried with CH_2Cl_2 (3×1 min) and Et_2O (3×1 min). The cyclic peptide was then cleaved from the resin, analyzed by analytical RP-HPLC and characterized by ESI-MS. **HPLC (λ=220 nm):** t_R 6.225 min. **ESI-MS** *m/e*: 419.29 $[M_C+3H]^{+3}$; 628.43 $[M_C+2H]^{+2}$ (Annex figures Figure 7.4 and Figure 7.5).

7.1.2 Synthesis of BPC16 on polystyrene lanterns

The synthesis was performed on Fmoc-Rink polystyrene lanterns (D-series, 35 μmol) in a glass vial.

7.1.2.1 Polystyrene lanterns swelling

Lanterns were placed in a vial and swollen in CH_2Cl_2 (1×5 min).

7.1.2.2 Fmoc group removal

Lanterns were treated with piperidine/DMF/CH_2Cl_2 (20:40:40, 1×40 min) and washed with CH_2Cl_2 (1×5 min). The treatment was repeated again with piperidine/DMF/CH_2Cl_2 (20:40:40, 1×40 min) and washed with DMF (3×5 min) and CH_2Cl_2 (3×5 min).

7.1.2.3 Amino acid coupling

Lanterns were treated with the corresponding Fmoc-protected amino acid (200 mM), HBTU (200 mM) and DIEA (200 mM) in the required amount of DMF to cover the lanterns (1 ml per lantern approx.) for 4 h (no stirring was required). Then lanterns were washed with DMF (3×5 min) and CH_2Cl_2 (3×5 min). From the fifth amino acid, NMP was used as solvent.

7.1.2.4 Allyl group removal

Once the chain assembly was completed, lanterns were treated with $CHCl_3$/AcOH/NMM (92.5:5:2.5) under N_2, followed by addition of $Pd(PPh_3)_4$

(75 mM). The mixture was left under N_2 without stirring for 6 h. Then, lanterns were washed following the procedure described in Table Table 7.2.

Table 7.2: Washing protocol for allyl group removal on polystyrene lanterns.

Step	Solvent/reagent	Time
1	$CHCl_3$/AcOH/NMM (92.5:5:2.5)	3×2 min
2	5% DIEA/CH_2Cl_2	3×5 min
3	0.03M $NaS_2CN(C_2H_5)_2$/DMF	3×15 min
4	NMP	5×5 min
5	CH_2Cl_2	5×5 min

7.1.2.5 Cleavage, analysis and characterization of the linear precursor

After allyl group removal, a small piece of lantern was subjected to Fmoc group removal, washed with DMF (3×5 min) and CH_2Cl_2 (3×5 min) and air-dried. Afterwards, the piece of lantern was treated with TFA/TIS/H_2O (95;2.5:2.5) for 1 h. After this time, the piece of lantern was removed from the vial and the TFA was evaporated under N_2. Then, the peptide was precipitated with Et_2O, centrifuged (11,000 rpm, 5 min) and the supernatant was removed to obtain a white solid. This process was repeated three times. Then, the linear peptide was dissolved in H_2O/CH_3CN, analysed by analytical RP-HPLC and characterized by ESI-MS. **HPLC (λ=220 nm):** t_R 5.870 min. **ESI-MS** *m/e***:** 1273.9 $[M_L+H]^+$; 1295.9 $[M_L+Na]^+$; 1311.9 $[M_L+K]^+$ (Annex, figure Figure 7.2)

7.1.2.6 Ciylization study using polystyrene lanterns

Lanterns were solvated in NMP (1 ml) and subjected to the conditions summarized in section 4.1.1.5 (Table 4.2). Then lanterns were washed with DMF (3×5 min) and CH_2Cl_2 (3×5 min), and subjected to cleavage conditions. The crude reaction mixture was analyzed by analytical RP-HPLC and characterized by ESI-MS. **Linear peptide; HPLC (λ=220 nm):** t_R 5.902 min. **ESI-MS** *m/e***:** 425.6 $[M_L+3H]^{+3}$; 637.8 $[M_L+2H]^{+2}$, **BPC16 and cyclodimer; HPLC (λ=220 nm):** t_R 6.012 min and 6.334 min. **ESI-MS** *m/e***:** 628.68 $[M_D+4H]^{+4}$; 2533.6 $[M_D+Na]^+$, (Annex, figures Figure 7.6, Figure 7.7, Figure 7.8, Figure 7.9, Figure 7.10 and Figure 7.11).

7.1.3 Synthesis of BPC16 on polyamide lanterns

The synthesis was performed on Fmoc-Rink polyamide lanterns (D-series, 18 μmol) in a glass vial.

7.1.3.1 Polyamide lanterns swelling

Lanterns were placed in a vial and swollen in CH_2Cl_2 (1×5 min).

7.1.3.2 Fmoc protectin removal

Lanterns were treated with piperidine/DMF (3:7, 1×20 min) and washed with DMF (3×5 min), MeOH (2×5 min) and CH_2Cl_2 (1×5 min).

7.1.3.3 Amino acid coupling

Lanterns were treated with the corresponding Fmoc-protected amino acid (120 mM), HBTU (120 mM) and DIEA (240 mM) in the required amount of DMF to cover the lanterns (1 ml per lantern approx.) for 2 h (no stirring was required). Then lanterns were washed with DMF (3×5 min), MeOH (2×5 min) and CH_2Cl_2 (1×5 min). From the fifth amino acid NMP was used as a solvent.

7.1.3.4 Allyl group removal

Once the chain assembly was completed, lanterns were treated with $CHCl_3$/AcOH/NMM (92.5:5:2.5) under N_2 followed by addition of $Pd(PPh_3)_4$ (75 mM) was added to the vial. The mixture was left under N_2 without stirring for 6 h. Then, lanterns were washed following the procedure described in Table Table 7.2.

7.1.3.5 Cleavage, analysis and characterization of the linear precursor

The procedure is the same as the one described for polystyrene lanterns (section 7.1.2.5). **HPLC (λ=220 nm):** t_R 5.870 min. **ESI-MS** *m/e***:** 1273.9 $[M_L+H]^+$; 1295.9 $[M_L+Na]^+$; 1311.9 $[M_L+K]^+$ (Annex, figure Figure 7.2).

7.1.3.6 Cyclization study using polyamide lanterns

Lanterns were solvated in NMP (1 ml) and subjected to the conditions summarized in section 4.1.1.5 (Table 4.2). Then lanterns were washed with DMF (3×5 min), MeOH (2×5 min) and CH_2Cl_2 (1×5 min), and subjected to the cleavage conditions. The crude reaction mixture was analyzed by analytical RP-HPLC and characterized by ESI-MS. **ESI-MS** *m/e***:** 1273.9 $[M_L+H]^+$;

1296.0 $[M_L+Na]^+$; 1311.9 $[M_L+K]^+$; 1278.9 $[M_C+Na]^+$; 2511.8 $[M_D+H]^+$; 2533.9 $[M_D+Na]^+$; 2604.9 $[M_{DL}+Na+pirrolidine]^+$; 3861.2 $[M_{TL}+Na+pirrolidine]^+$, (Annex, figures Figure 7.17-Figure 7.29, posar els correctes)

7.2 Synthesis of a Trp-Containing Library of Cyclic Peptides

The Trp-containing cyclic peptide library was synthesized on a MBHA resin (0.4 mmol/g). The synthesis was performed using a three-dimensional orthogonal Fmoc/Boc/Allyl strategy. The side-chain protection for lysine and tryptophan residues was as *tert*-butyl carbamate (Boc). The resin was swollen with CH_2Cl_2 (1×20 min) and DMF (1×20 min), and washed with piperidine/DMF (3:7, 1×5 min), DMF (6×1 min) and CH_2Cl_2 (3×1 min). Then, the resin was treated with Fmoc-Rink linker (5 eq), HBTU (5 eq) and DIEA (10 eq) in DMF overnight. After this time, the resin was washed with DMF (6×1 min), CH_2Cl_2 (3×1 min) and Et_2O (3×1 min), and air-dried.

The linear sequences were prepared on an ACT Multiple Peptide Synthesizer Apex 396 S (Aapptec). The above resin was split into 66 wells (50 mg aprox.). Couplings were conducted using the corresponding Fmoc-protected amino acid (0.6 M) and DIEA (1.2 M) in DMF for 1 h. Fmoc removal were performed with piperidine/DMF (3:7, 5 + 10 min). After each coupling and deprotection step the resin was washed with DMF (5×1 min). Once the chain assembly was completed, next steps were performed manually in 66 polypropylene syringes fitted with a polyethylene porous disk. The C-terminal allyl ester was cleaved by treatment with $Pd(PPh_3)_4$ (3 eq) in $CHCl_3$/AcOH/NMM (37:2:1) under N_2 for 3 h, the resin was washed as described in Table Table 7.1 and Fmoc was removed with piperidine/DMF (3:7, 2 + 10 min). Then, cyclization was carried out by treating the resin with PyBOP (5 eq), HOBt (5 eq) and DIEA (10 eq) in NMP at 25^{o}C for 24 h. Following washes with NMP (6×1 min) and CH_2Cl_2 (3×1 min), cyclodecapeptides were cleaved from the resin by treatment with TFA/H_2O/TIS (95:2.5:2.5) for 1 h. The cleavage cocktail was then evaporated, and after Et_2O extractions, the cyclic peptides were dissolved in H_2O, lyophylized and analysed by analytical RP-HPLC. Final products were obtained in around 90% of purity and were confirmed by MALDI-TOF (see Annex II section 7.5.5 for HPLC and MALDI-TOF examples of BPC312, BPC326, BPC338, BPC354, BPC356, BPC372 and BPC360).

7.2.1 Synthesis of *de novo* designed cyclic peptides based on BPC194 and BPC198

The *de novo* designed cyclic peptide were synthesized on a MBHA resin (0.4 mmol/g). The synthesis was performed using a three-dimensional orthogonal Fmoc/Boc/Allyl strategy. The side-chain protection for lysine and tryptophan residues was as *tert*-butyl carbamate (Boc). The resin was swollen with CH_2Cl_2 (1×20 min) and DMF (1×20 min), and washed with piperidine/DMF (3:7, 1×5 min), DMF (6×1 min) and CH_2Cl_2 (3×1 min). Then, the resin was treated with Fmoc-Rink linker (5 eq), Oxyma (4 eq) and DIC (4 eq) in DMF for 2 h. After this time, the resin was washed with DMF (6×1 min), CH_2Cl_2 (3×1 min).

The linear sequences were prepared by sequential couplings of the corresponding Fmoc-protected amino acid (4 eq), oxyma (4 eq) and DIC (4 eq) in DMF for 2 h. Fmoc removal was performed with piperidine/DMF (3:7, 5 + 10 min). After each coupling and deprotection step the resin was washed with DMF (6×1 min), CH_2Cl_2 (3×1 min). From the fifth amino acid, NMP was used as solvent.

Once the chain assembly was completed, the C-terminal allyl ester was cleaved by treatment with $Pd(PPh_3)_4$ (3 eq) in $CHCl_3$/AcOH/NMM (37:2:1) under N_2 for 3 h, the resin was washed as described in Table Table 7.1 and the Fmoc was removed with piperidine/DMF (3:7, 2 + 10 min). Then, cyclization was carried out by treating the resin with oxyma (5 eq), COMU (5 eq) and DIEA (10 eq) in NMP at 25 ^{o}C for 24 h. Following washes with NMP (6×1 min) and CH_2Cl_2 (3×1 min), cyclodecapeptides were cleaved from the resin by treatment with TFA/H_2O/TIS (95:2.5:2.5) for 1 h. The cleavage cocktail was then evaporated, and after diehtyl ether extractions, the cyclic peptides were dissolved in H_2O, lyophylized, analysed by analytical RP-HPLC and characterized by ESI-MS (Annex Fig. Figure 7.48; Figure 7.49; Figure 7.50; Figure 7.51; Figure 7.52; Figure 7.53; Figure 7.54; Figure 7.55; Figure 7.56; Figure 7.57)

7.3 Stability of Peptides in Serum

Human serum was supplied by *Banc de Sang i Teixits of Hospital Josep Trueta* and was stored at 20 ^{o}C. The selected peptides were placed in different eppendorfs (2.5 mg) and were exposed to 25% aqueous filtered human serum (1 ml) at 37 ^{o}C. After 30 min, 1, 1.5 and 2 h exposure, aliquots (200 μl) were removed and proteins were precipitated with CH_3CN (200 μl). Samples were cooled to 0^{o}C for 15 min and centrifugued (10,000 rpm, 5 min). The supernatant was frozen,

freeze-dried and analyzed by MALDI-TOF.

A small portion of the lyophylized peptide was placed in an eppendorff and was dissolved in 0.1% aqueous TFA (20μl). In a new eppendorff, the matrix was prepared by adding α-cyano-4-hydroxycinnamic acid (HCCA) (2μl) and 0.1% aqueous TFA (2μl). Finally, 2μl of peptide solution and 2μl of matrix mixture were mixed and placed in duplicate in the sampler target. A standard was used for calibration of the spectra. Afterwards, the sampler was placed in the MALDI-TOF instrument.

7.4 Experimental Techniques

7.4.1 High-Performance Liquid Chromatography

The reverse-phase high-performance liquid chromatography (RP-HPLC) was performed using a Dionex liquid chromatography instrument composed of a P680 Dionex quaternary pump, an ASI-100 Dionex automatic injector, UV/VIS Dionex UVD170U detector and CHROMALEON® 6.60 software. Analysis were carried out at a flow rate of 1.0 ml/min using a Kromasil 100 C_{18} (4.6×40 mm; 3.5 μm particle size) column. Linear gradients of 0.1% aqueous TFA and 0.1% TFA in CH_3CN were run from 98:2 to 0:100 (H_2O:CH_3CN) over 17 min with UV detection at 220 nm.

Peptide purification was performed on a reverse-phase semipreparative HPLC using a Tracer C18 (1.0×25 cm, 5 μm) column (Teknokroma, Barcelona, Spain). Linear gradients of 0.1% aqueous TFA and 0.1% TFA in CH_3CN were run from 98:2 to 0:100 (H_2O:CH_3CN) over 35 min with UV detection at 220 nm.

7.4.2 Mass Spectrometry

7.4.2.1 Electrospray ionization mass spectrometry

ESI-MS analysis were performed with a Brucker MicroTof-Q instrument using a hybrid quadrupole-time-of-flight mass spectrometer (Univesity of Zaragoza). Samples were introduced into the mass spectrometer ion source directly through a 1100 series Agilent HPLC autosampler and were externally calibrated using sodium formiate. The instrument was operated in positive (ESI^+) and negative (ESI^-) ion mode.

7.4.2.2 Matrix-Assisted Laser Desorption Ionization with Time-Of-Flight

MALDI-TOF analysis were performed with a Bruker Daltonics, ULTRAflex TOF mass spectrometer (Serveis Tecnics de Recerca, UdG). The analysis programs were Flex Control 2.2 and Flex Analysis 2.2. α-Cyano-4-hydroxycinnamic acid (HCCA) was used as matrix and a standard was used for calibration of the spectra.

7.4.3 Microwave irradiation

Microwave-assisted (MW) reactions were performed with an Ethos SEL lab-station microwave (Milestone) equiped with a dual magnetron (1600 W). The time, temperature and power were controled by the EasyControl software. The temperature was monitored through the ATC-400FO Automatic Fiber Optic Temperature Control System immersed in a standard Milestone reference vessel. This equipement regulates the power to achieve and maintain the selected temperature (Serveis Tecnics de Recerca, UdG).

7.4.4 Monitor Peptide Synthesis

During the SPPS, it is frequently worthwhile to verify that the coupling has gone to completion by some monitoring techniques. One of the best known monitoring methods is the ninhydrin test or Kaiser test (Kaiser 1970). This is a qualitative test to detect free N^{α}-amino groups, where a positive colorimetric assay indicates the presence of unreacted N^{α}-amino groups. The reaction that takes place is a transamination-descaboxilation between the free amino group and the ninhidrine, to give a blue colour known as Ruhemann's purple.

Annex II

Supplementary Data

7.5 Spectra of Cyclic Peptides

7.5.1 Linear Peptide Precursor

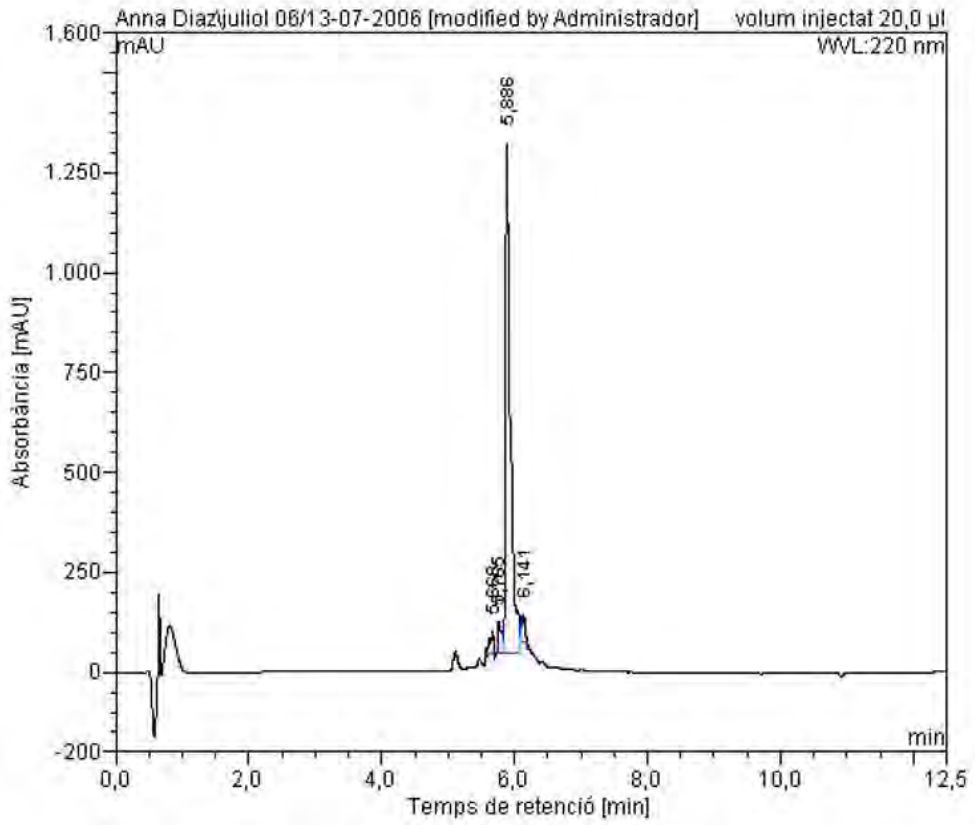

Figure 7.1: HPLC of the linear precursor synthetized on a MBHA resin.

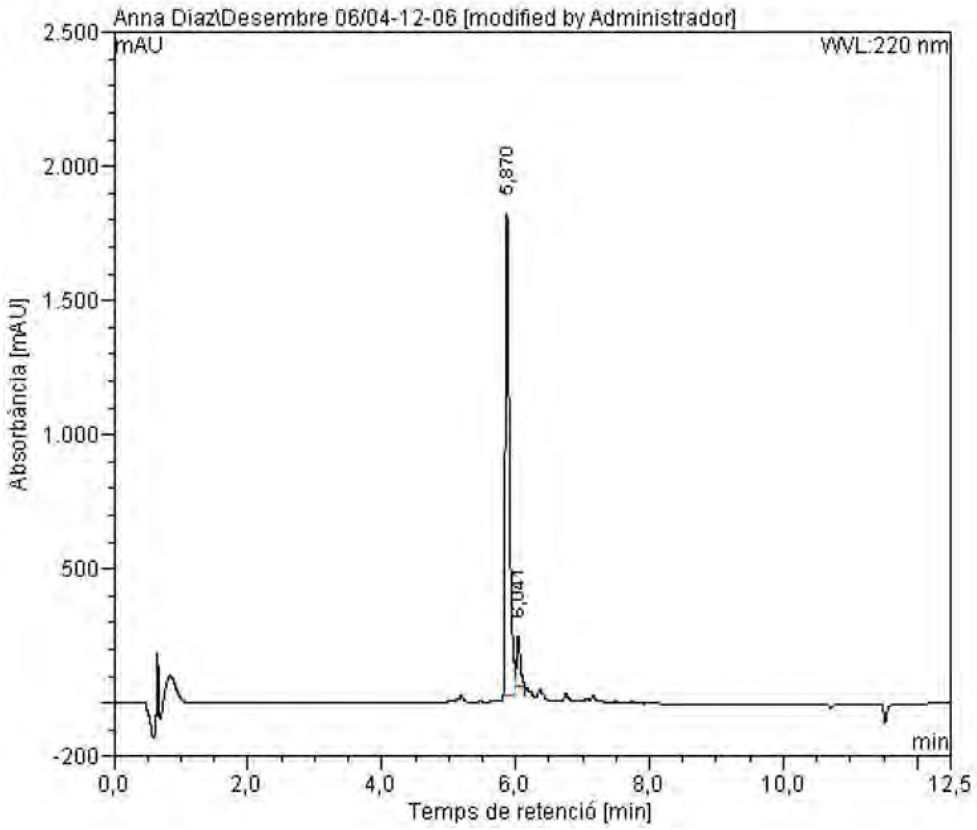

Figure 7.2: HPLC of the linear precursor synthetized on polystyrene lanterns.

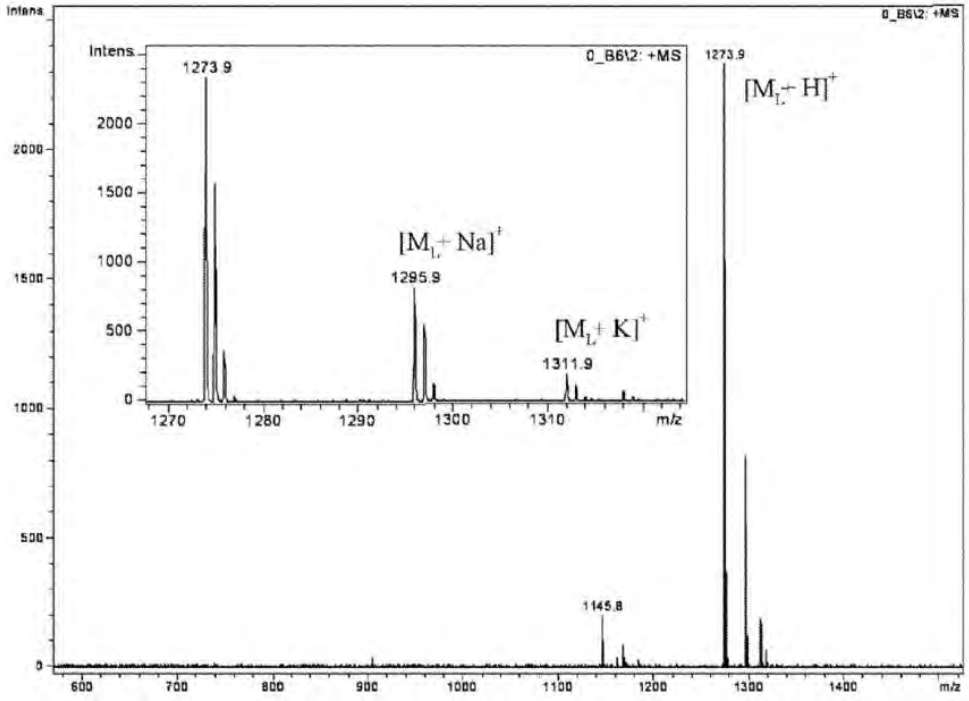

Figure 7.3: ESI-MS spectra of the linear peptide precursor synthetized on polystyrene lanterns.

7.5.2 BPC16 on a MBHA Resin

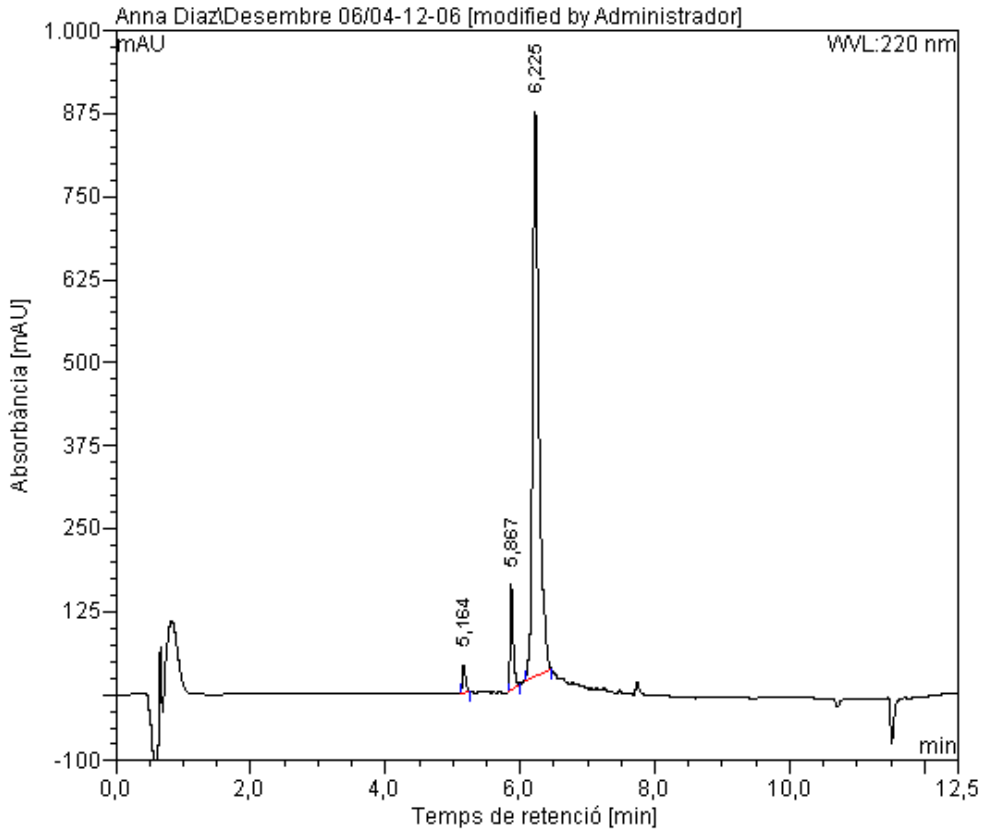

Figure 7.4: HPLC of BPC16 synthesized on a MBHA resin. conditions: PyBOP (5 eq), HOBt (5 eq), DIEA (10 eq), 24 h, room temperature.

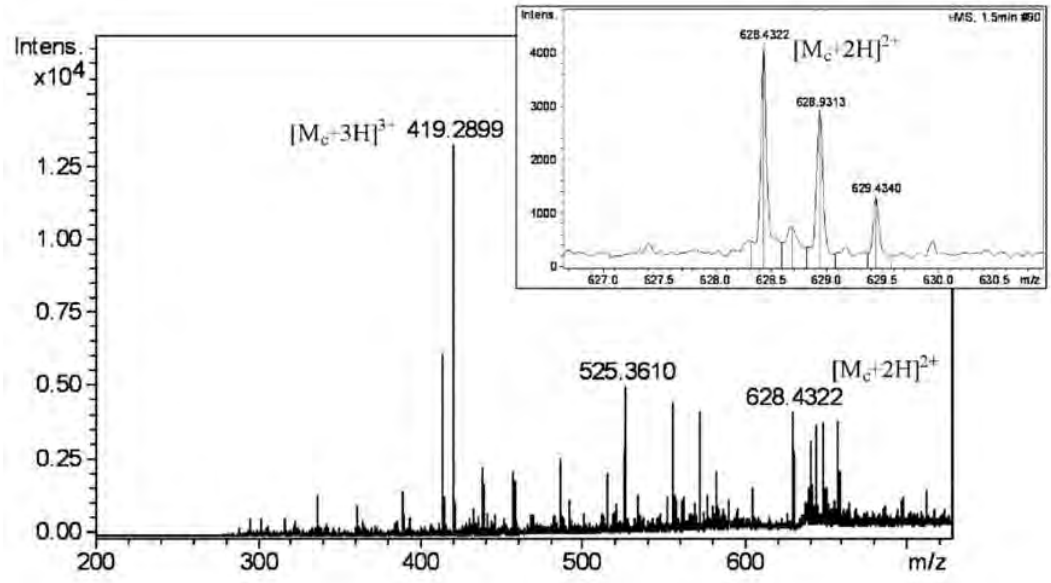

Figure 7.5: ESI-MS of BPC16 synthesized on a MBHA resin. conditions: PyBOP (5 eq), HOBt (5 eq), DIEA (10 eq), 24 h, room temperature.

7.5.3 Cyclization Study Using Polystyrene Lanterns

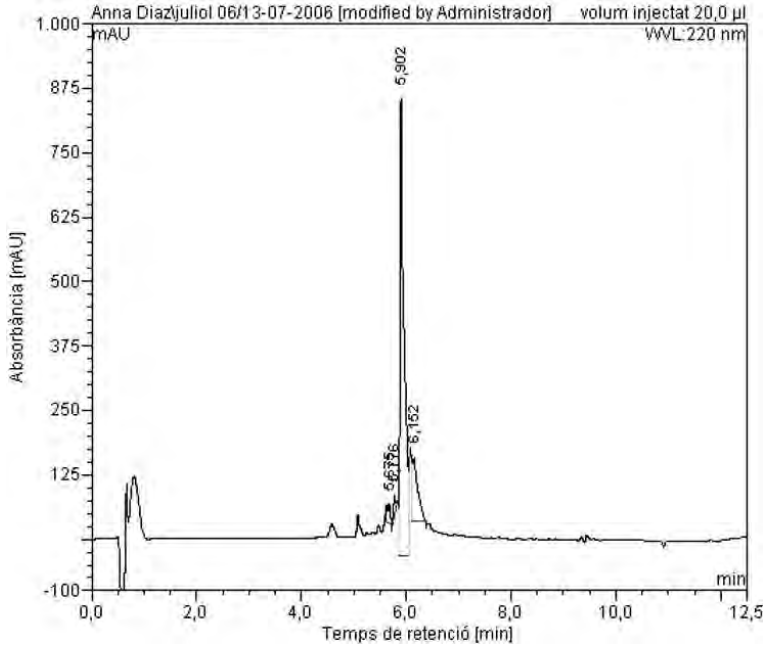

Figure 7.6: HPLC of the crude reaction mixture obtained using: PyBOP (16 eq), HOBt (16 eq), DIEA (32 eq) for 24 h at room temperature (Entry 2, Table 4.2).

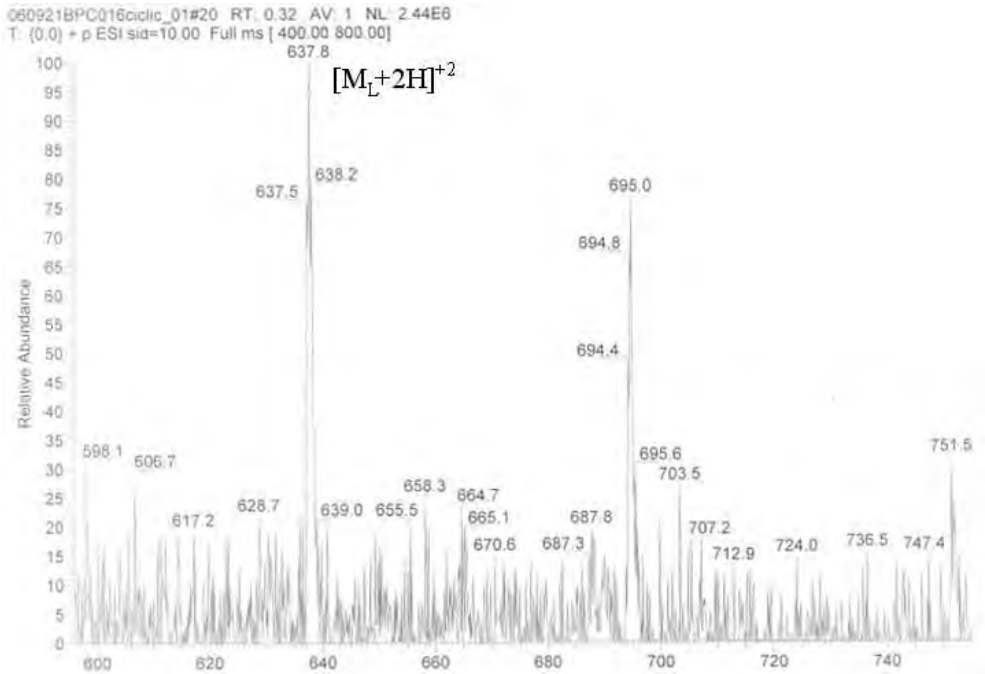

Figure 7.7: ESI-MS of the crude reaction mixture obtained using: PyBOP (16 eq), HOBt (16 eq), DIEA (32 eq) for 24 h at room temperature (Entry 2), Table 4.2).

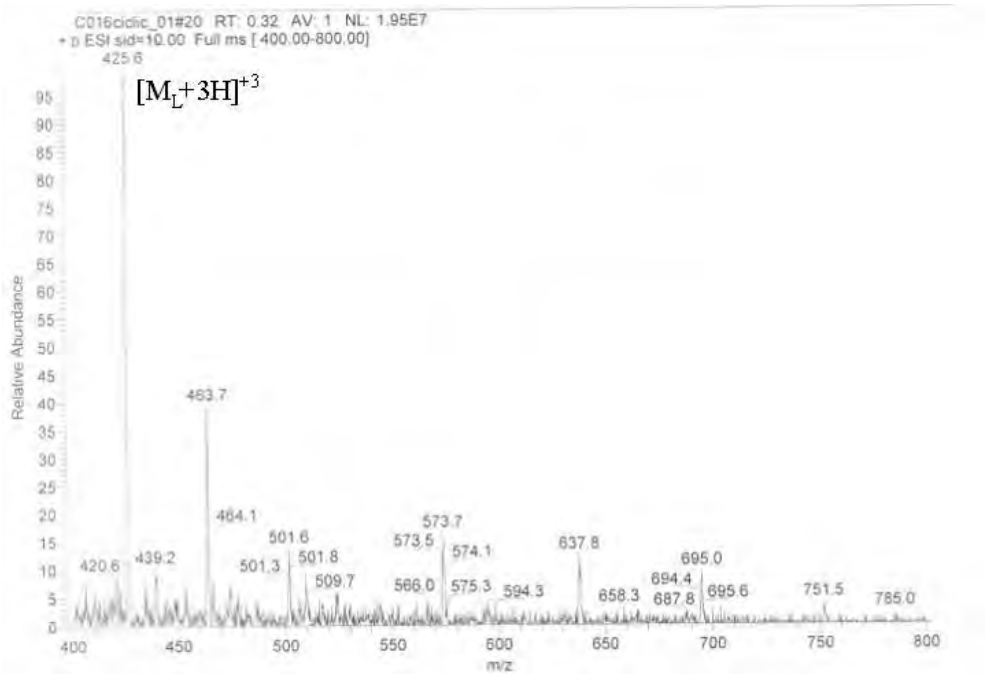

Figure 7.8: ESI-MS of the crude reaction mixture obtained using: PyBOP (16 eq), HOBt (16 eq), DIEA (32 eq) for 24 h at room temperature (Entry 2), Table 4.2).

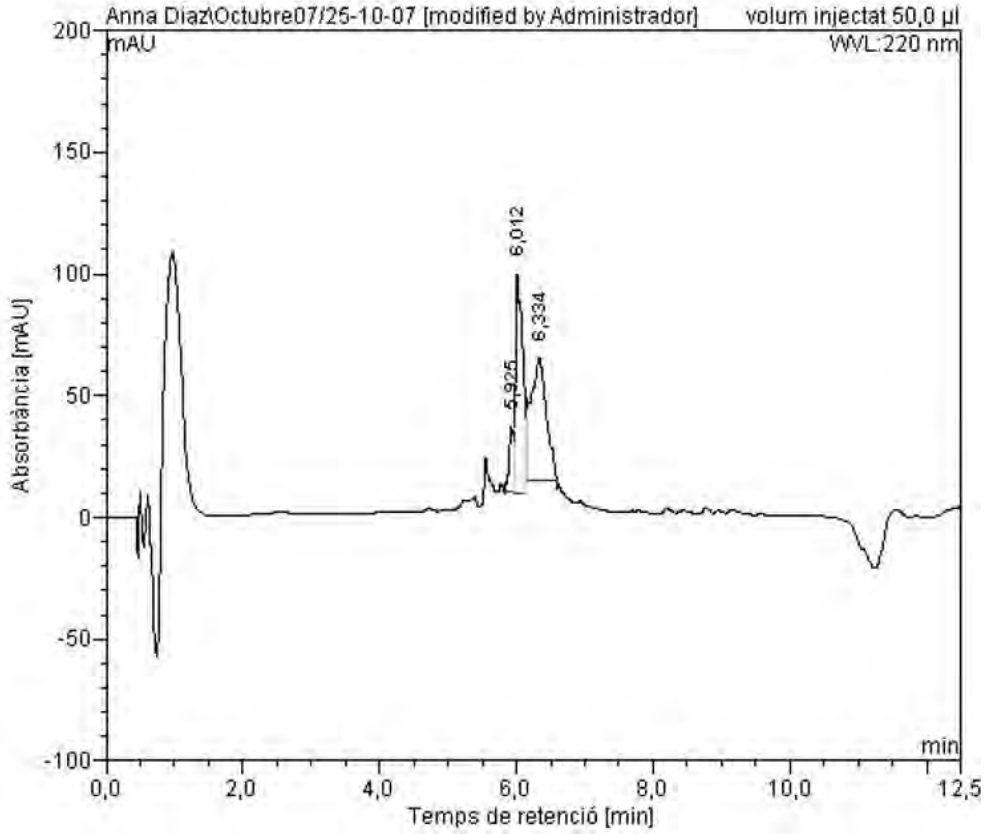

Figure 7.9: HPLC of the crude reaction mixture obtained using: DIC (16 eq), HOBt (16 eq) for 24 h at room temperature (Entry 12), Table 4.2).

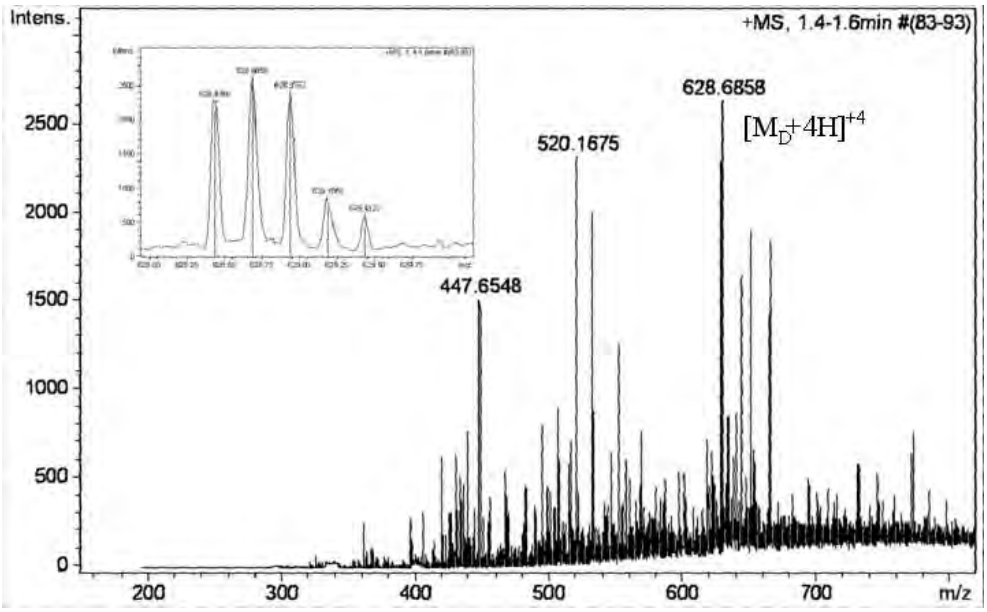

Figure 7.10: ESI-MS of the crude reaction mixture obtained using: DIC (16 eq), HOBt (16 eq) for 24 h at room temperature (Entry 12), Table 4.2).

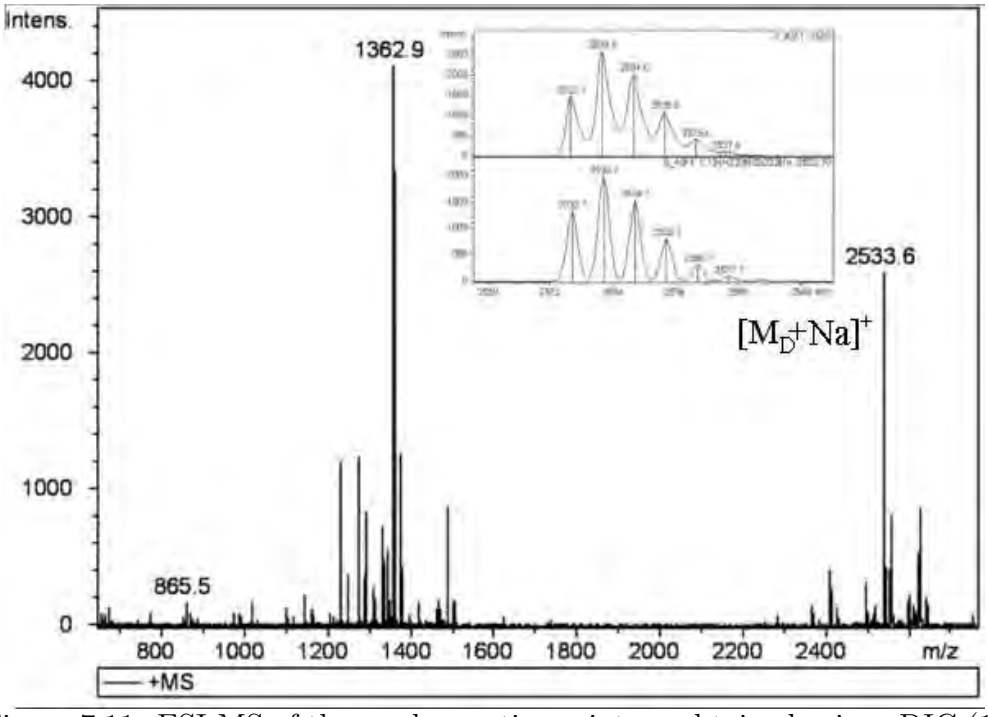

Figure 7.11: ESI-MS of the crude reaction mixture obtained using: DIC (16 eq), HOBt (16 eq) for 24 h at room temperature (Entry 12), Table 4.2).

7.5.4 Cyclization Study Using Polyamide Lanterns

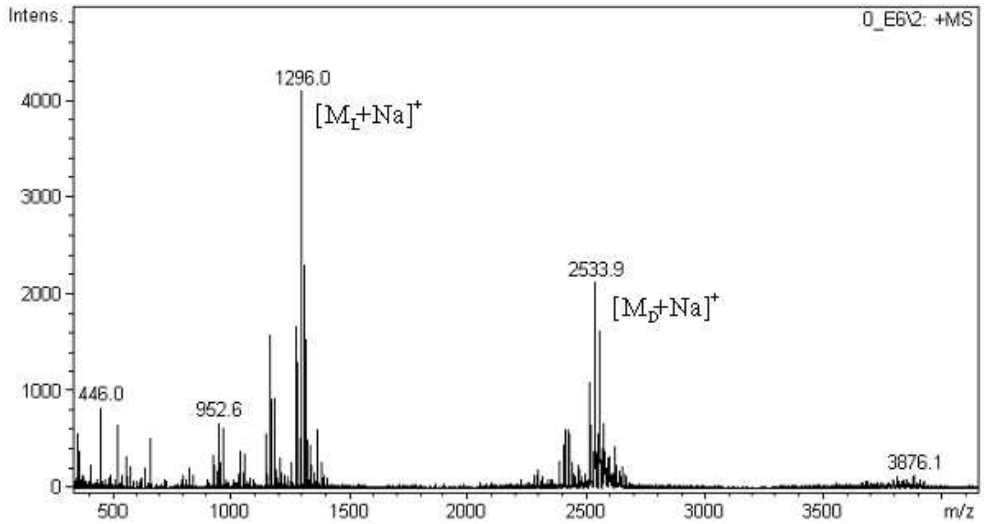

Figure 7.12: ESI-MS of the crude reaction mixture obtained using PyBOP (16 eq), HOBt (16 eq), DIEA (32 eq), 2×15 min MW, 50^{o}C (Entry 2, Table 4.3).

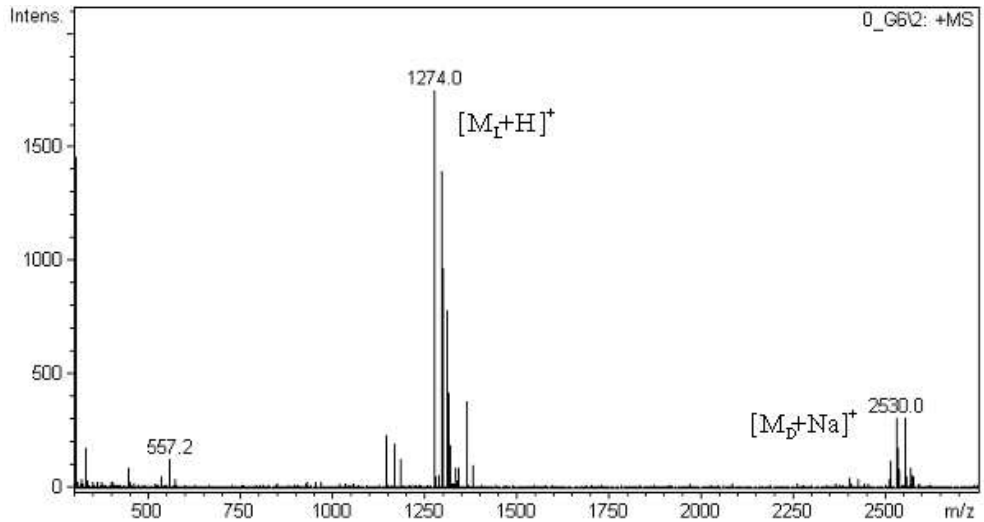

Figure 7.13: ESI-MS of the crude reaction mixture obtained using PyBOP (16 eq), HOBt (16 eq), DIEA (32 eq), DMF, 24 h, 25^{o}C (Entry 3, Table 4.3).

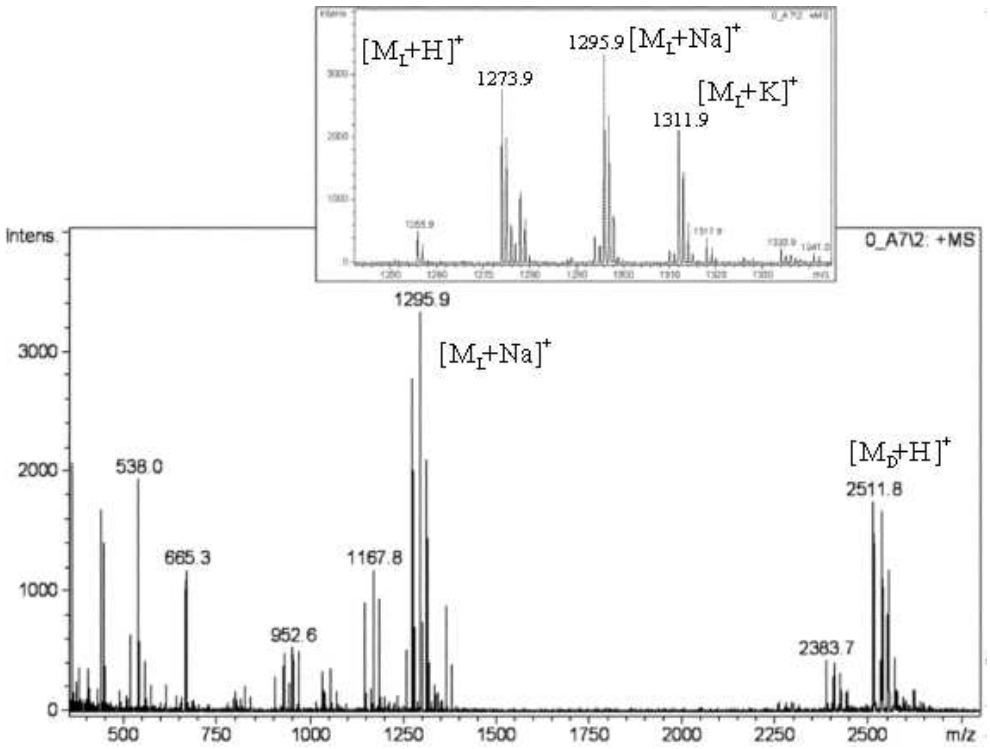

Figure 7.14: ESI-MS of the crude reaction mixture obtained using PyBOP (5 eq), HOBt (5 eq), DIEA (10 eq), 24 h, 25^{o}C (Entry 4, Table 4.3).

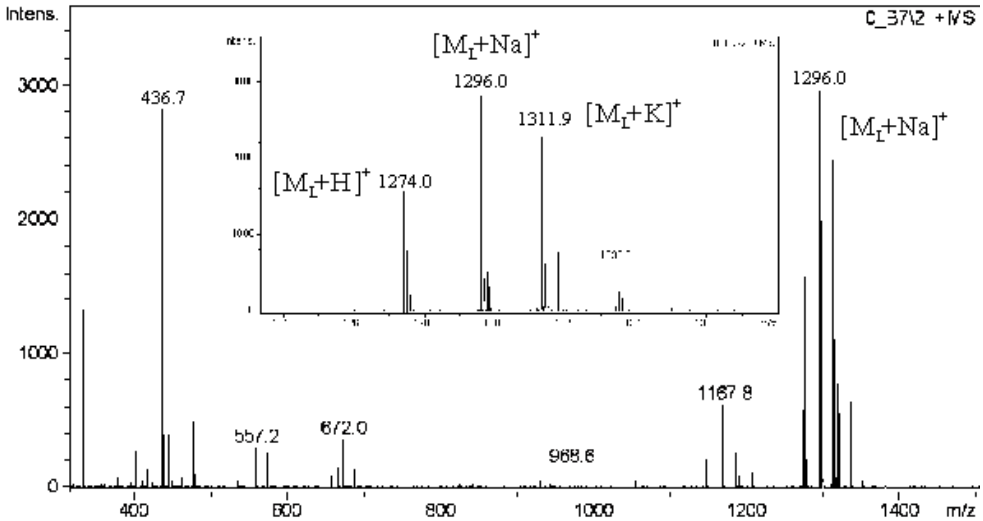

Figure 7.15: ESI-MS of the crude reaction mixture obtained using PyBOP (32 eq), HOBt (32 eq), DIEA (64 eq), 12 h, 25^{o}C (Entry 7, Table 4.3).

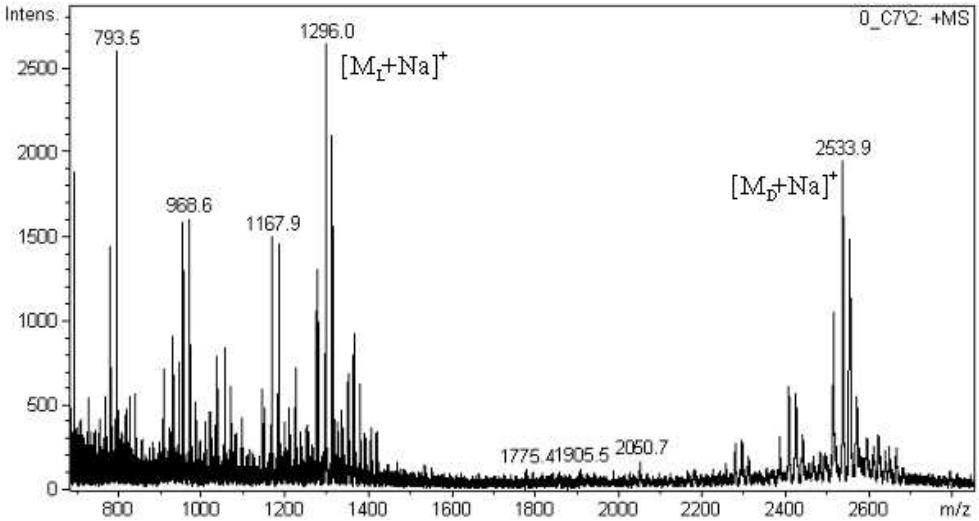

Figure 7.16: ESI-MS of the crude reaction mixture obtained using PyBOP (32 eq), HOBt (32 eq), DIEA (64 eq), 24 h, 25^{o}C (Entry 8, Table 4.3).

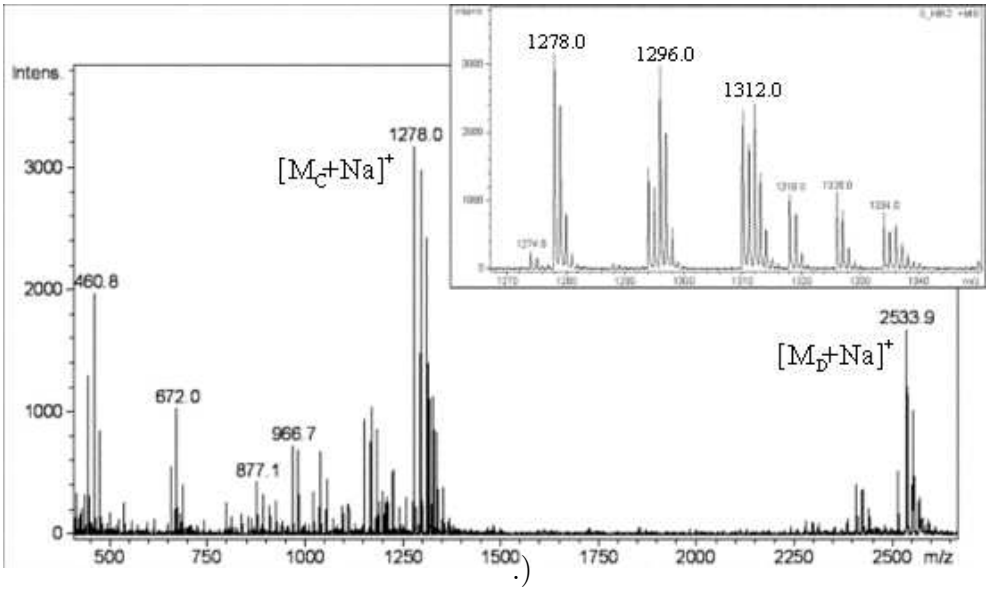

Figure 7.17: ESI-MSof the crude reaction mixture obtained using PyBOP (16 eq), HOBt (16 eq), collidina (32 eq), 24 h, 25^{o}C (Entry 2, Table 4.4

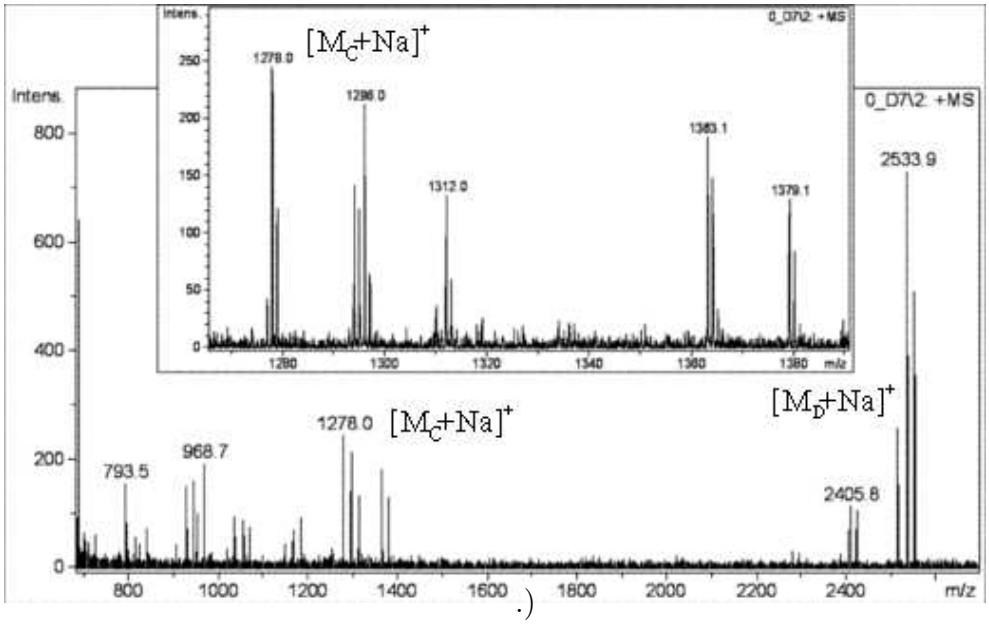

.)

Figure 7.18: ESI-MS of the crude reaction mixture obtained using PyBOP (16 eq), HOAt (16 eq), DIEA (32 eq), 24 h, 25^{o}C (Entry 3, Table 4.4

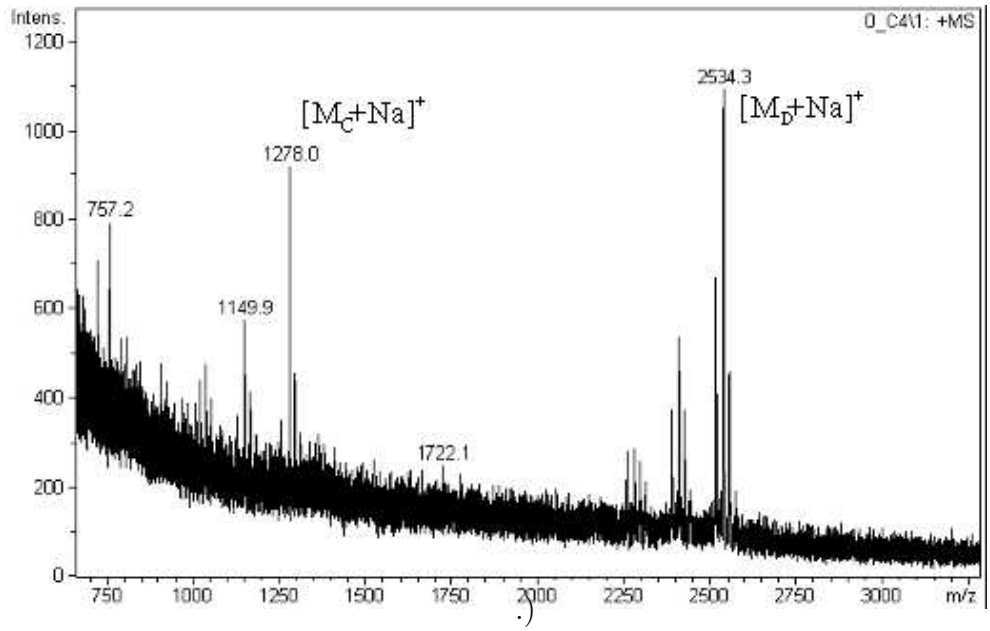

.)

Figure 7.19: ESI-MS of the crude reaction mixture obtained using PyBOP (16 eq), HOAt (16 eq), collidina (32 eq), 24 h, 25^{o}C (Entry 4, Table 4.4

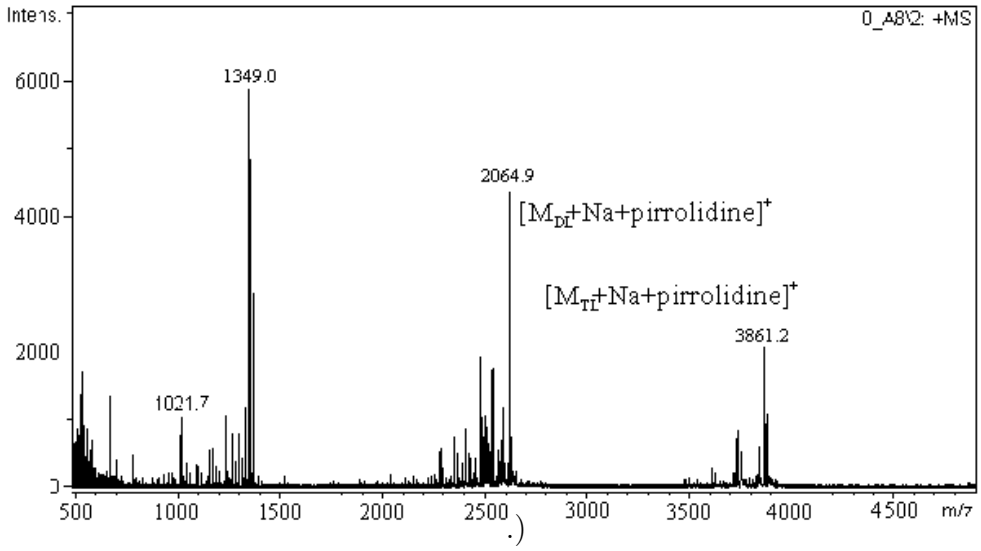

Figure 7.20: ESI-MS of the crude reaction mixture obtained using PyBrOP (16 eq), HOBt (16 eq), DIEA (32 eq), 24 h, 25^{o}C (Entry 5, Table 4.4

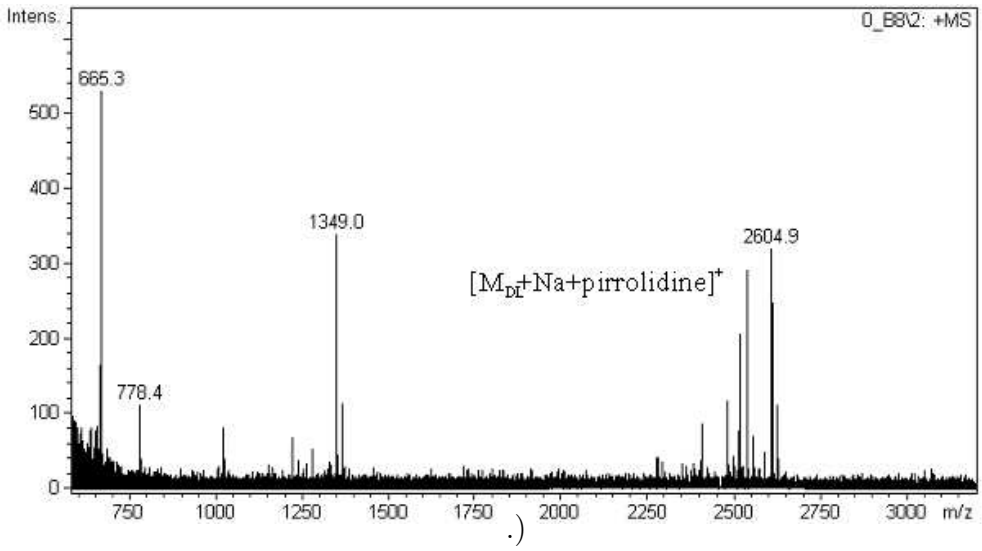

Figure 7.21: ESI-MS of the crude reaction mixture obtained using PyBrOP (16 eq), HOAt (16 eq), DIEA (32 eq), 24 h, 25^{o}C (Entry 6, Table 4.4

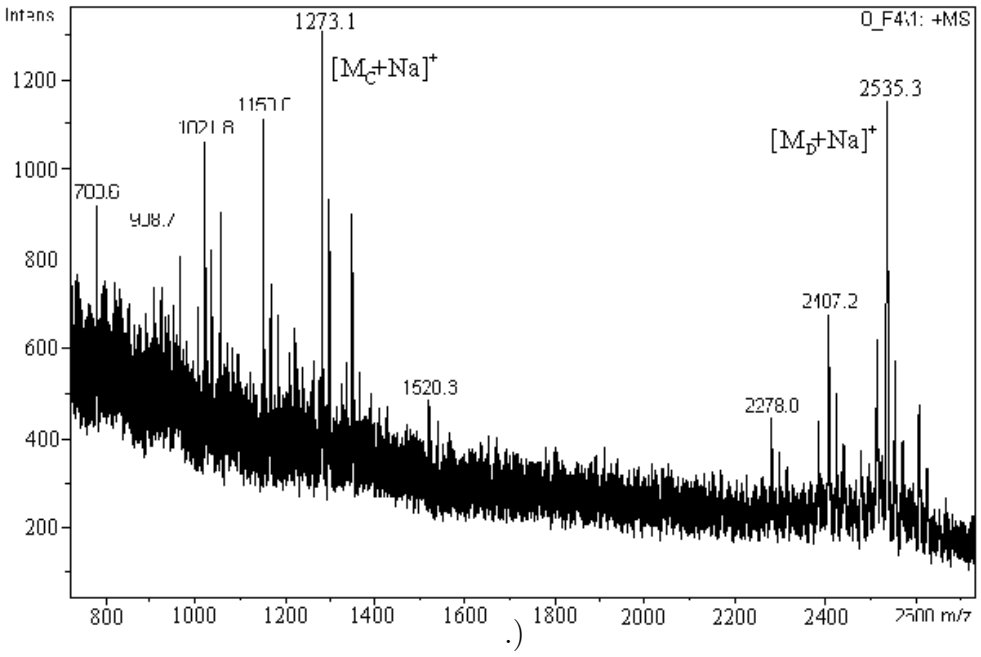

Figure 7.22: ESI-MS of the crude reaction mixture obtained using PyBrOP (16 eq), HOAt (16 eq), collidina (32 eq), 24 h, 25^{o}C (Entry 7, Table 4.4

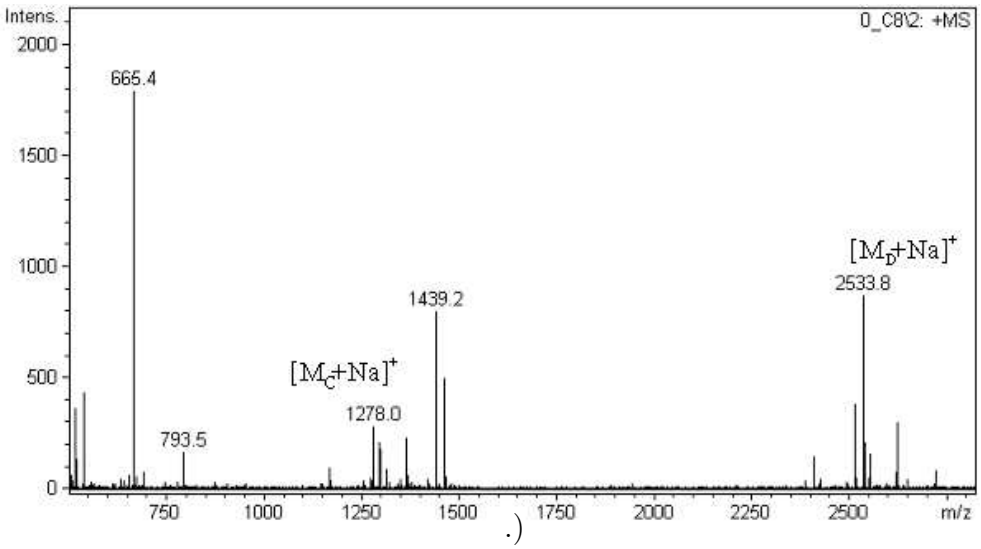

Figure 7.23: ESI-MS of the crude reaction mixture obtained using HATU (16 eq), HOAt (16 eq), DIEA (32 eq), 24 h, 25^{o}C (Entry 8, Table 4.4

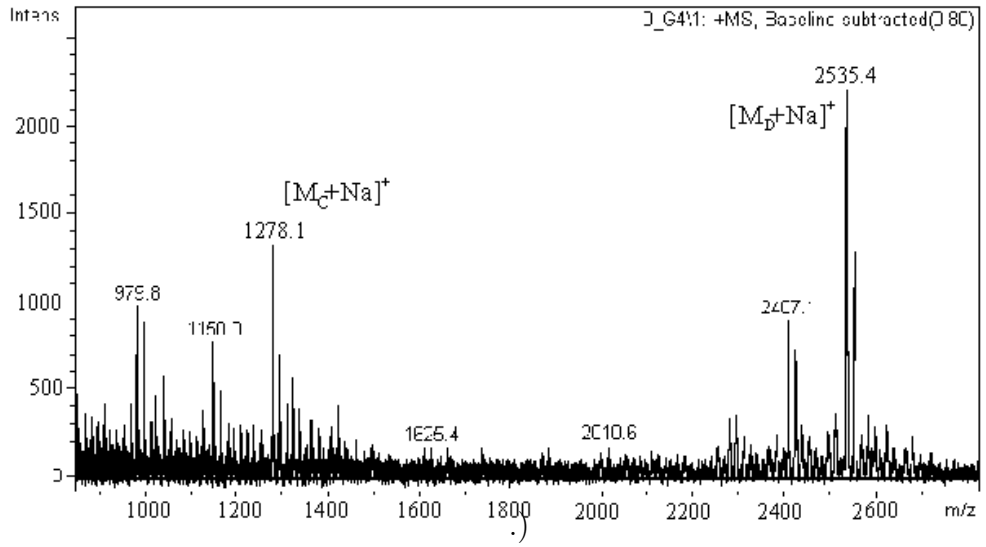

Figure 7.24: ESI-MS of the crude reaction mixture obtained using HATU (16 eq), HOAt (16 eq), collidina (32 eq), 24 h, 25^{o}C (Entry 9, Table 4.4

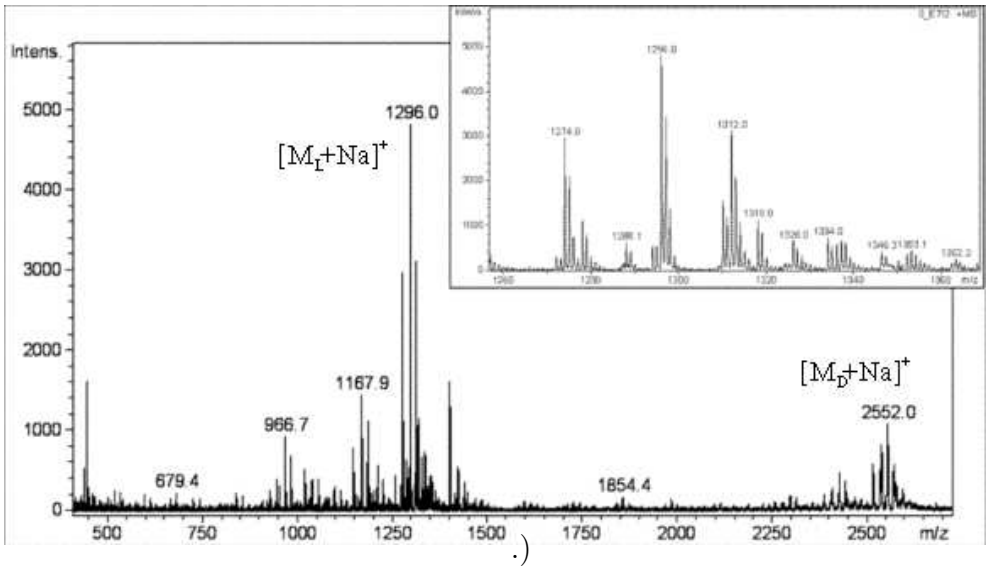

Figure 7.25: ESI-MS of the crude reaction mixture obtained using DIC (16 eq), HOBt (16 eq), 12 h, 25^{o}C (Entry 10, Table 4.4

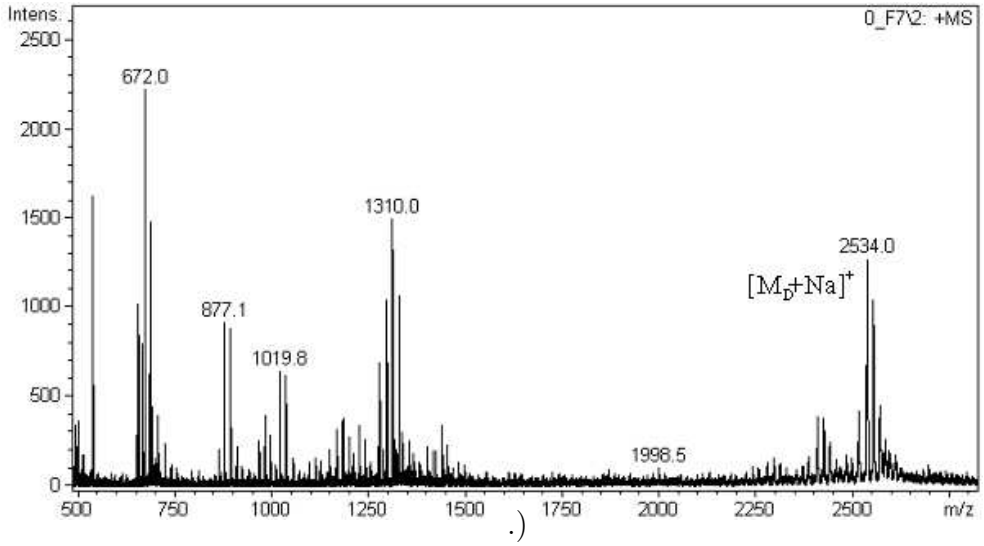

.)

Figure 7.26: ESI-MS of the crude reaction mixture obtained using DIC (16 eq), HOBt (16 eq), 24 h, 25^{o}C in DMF (Entry 11, Table 4.4

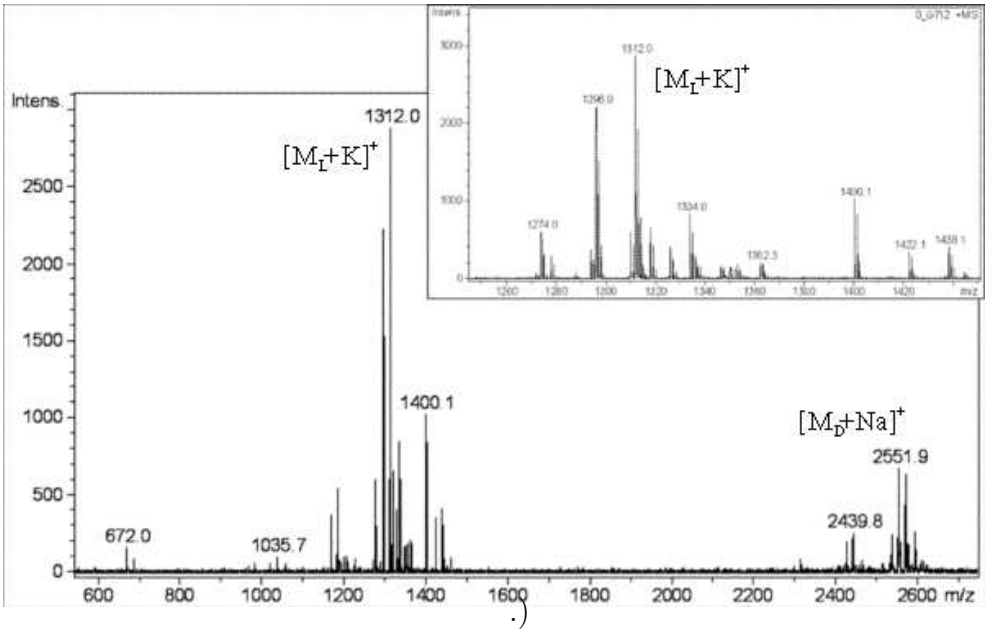

.)

Figure 7.27: ESI-MS of the crude reaction mixture obtained using DIC (8 eq), HOBt (8 eq), 24 h, 25^{o}C (Entry 12, Table 4.4

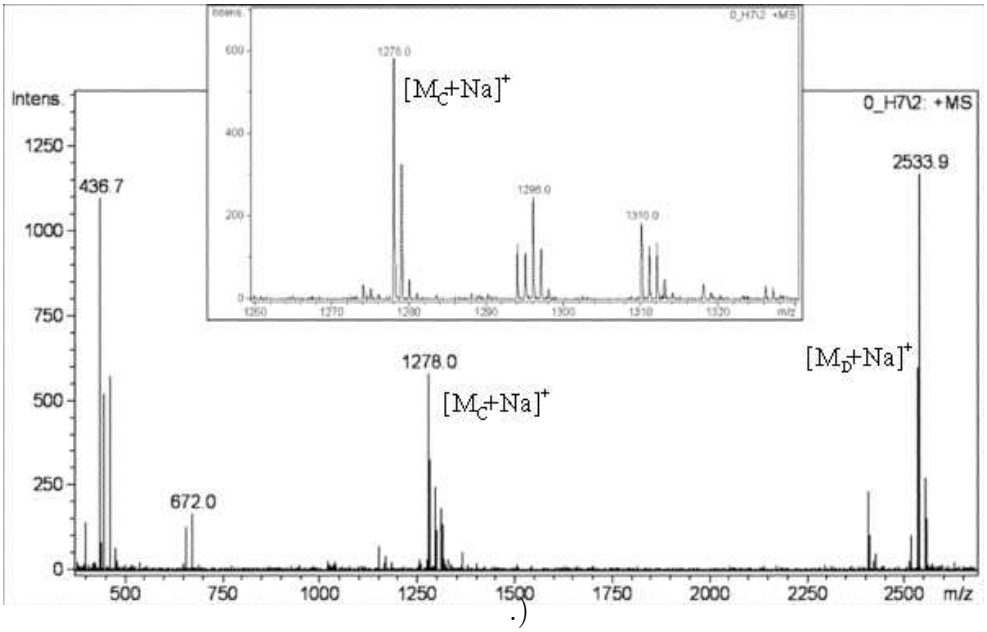

.)

Figure 7.28: ESI-MS of the crude reaction mixture obtained using DIC (16 eq), HOAt (16 eq), 24 h, 25^{o}C (Entry 13, Table 4.4

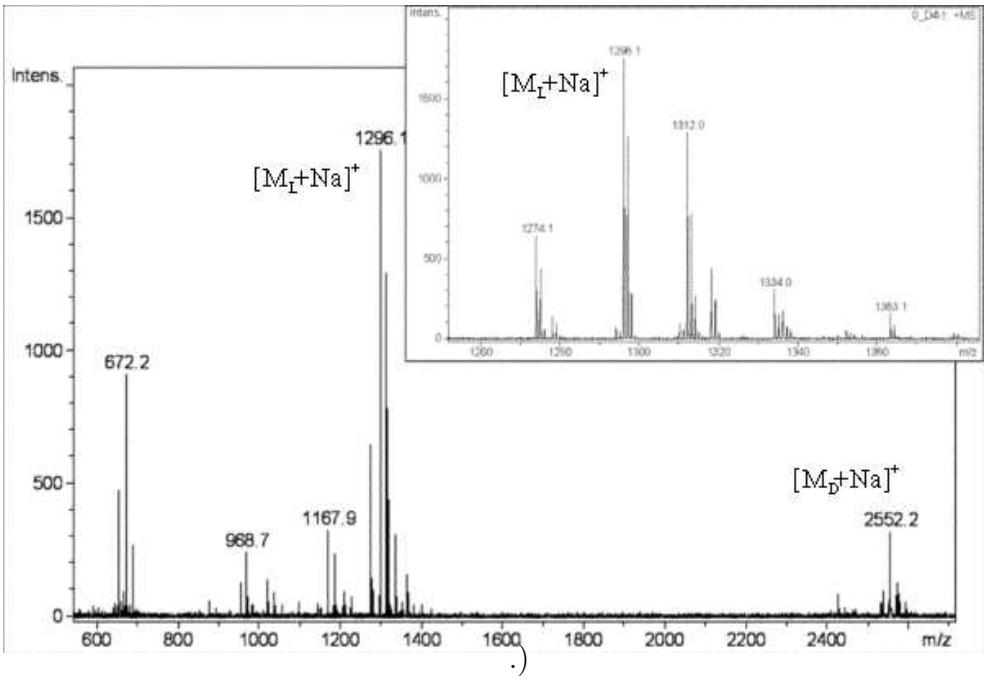

.)

Figure 7.29: ESI-MS of the crude reaction mixture obtained using DIC (8 eq), HOAt (8 eq), 12 h, 25^{o}C (Entry 14, Table 4.4

Table 7.1: Code and sequences of Trp-containing cyclic peptides library.

Code	Sequence	Code	Sequence
BPC296	c(KLKLKWKLKQ)	**BPC16**	c(KLKLKFKLKQ)
BPC298	c(KKKKKWLLLQ)	**BPC058**	c(KKKKKFLLLQ)
BPC300	c(KKKKLWKLLQ)	**BPC060**	c(KKKKLFKLLQ)
BPC302	c(KKKLKWKLLQ)	**BPC062**	c(KKKLKFKLLQ)
BPC304	c(KKLKKWKLLQ)	**BPC064**	c(KKLKKFKLLQ)
BPC306	c(KLKKKWKLLQ)	**BPC066**	c(KLKKKFKLLQ)
BPC308	c(LKKKKWKLLQ)	**BPC068**	c(LKKKKFKLLQ)
BPC310	c(KKKKLWLKLQ)	**BPC070**	c(KKKKLFLKLQ)
BPC312	c(KKKLKWLKLQ)	**BPC072**	c(KKKLKFLKLQ)
BPC314	c(KKLKKWLKLQ)	**BPC074**	c(KKLKKFLKLQ)
BPC316	c(KLKKKWLKLQ)	**BPC076**	c(KLKKKFLKLQ)
BPC318	c(LKKKKWLKLQ)	**BPC078**	c(LKKKKFLKLQ)
BPC320	c(KKKLLWKKLQ)	**BPC080**	c(KKKLLFKKLQ)
BPC322	c(KKLKLWKKLQ)	**BPC082**	c(KKLKLFKKLQ)
BPC324	c(KLKKLWKKLQ)	**BPC084**	c(KLKKLFKKLQ)
BPC325	c(LKKKLWKKLQ)	**BPC086**	c(LKKKLFKKLQ)
BPC328	c(KKLLKWKKLQ)	**BPC088**	c(KKLLKFKKLQ)
BPC330	c(KLKLKWKKLQ)	**BPC090**	c(KLKLKFKKLQ)
BPC332	c(LKKLKWKKLQ)	**BPC092**	c(LKKLKFKKLQ)
BPC334	c(KLLKKWKKLQ)	**BPC094**	c(KLLKKFKKLQ)
BPC336	c(LKLKKWKKLQ)	**BPC096**	c(LKLKKFKKLQ)
BPC338	c(LLKKKWKKLQ)	**BPC098**	c(LLKKKFKKLQ)
BPC340	c(KKKLKWLLKQ)	**BPC100**	c(KKKLKFLLKQ)
BPC342	c(KKKLKWLLKQ)	**BPC102**	c(KKKLKFLLKQ)
BPC344	c(KKLKKWLLKQ)	**BPC104**	c(KKLKKFLLKQ)
BPC346	c(KLKKKWLLKQ)	**BPC106**	c(KLKKKFLLKQ)
BPC348	c(LKKKKWLLKQ)	**BPC108**	c(LKKKKFLLKQ)
BPC350	c(KKKLLWKLKQ)	**BPC110**	c(KKKLLFKLKQ)
BPC352	c(KKLKLWKLKQ)	**BPC112**	c(KKLKLFKLKQ)
BPC354	c(KLKKLWKLKQ)	**BPC114**	c(KLKKLFKLKQ)
BPC356	c(LKKKLWKLKQ)	**BPC116**	c(LKKKLFKLKQ)
BPC358	c(KKLLKWKLKQ)	**BPC118**	c(KKLLKFKLKQ)
BPC360	c(LKKLKWKLKQ)	**BPC120**	c(LKKLKFKLKQ)

Table 7.2: Code and sequences of Trp-containing cyclic peptides library.

Code	**Sequence**	**Code**	**Sequence**
BPC362	c(KLLKKWKLKQ)	**BPC122**	c(KLLKKFKLKQ)
BPC364	c(LKLKKWKLKQ)	**BPC124**	c(LKLKKFKLKQ)
BPC366	c(LLKKKWKLKQ)	**BPC126**	c(LLKKKFKLKQ)
BPC368	c(KKKLLWLKKQ)	**BPC128**	c(KKKLLFLKKQ)
BPC370	c(KKLKLWLKKQ)	**BPC130**	c(KKLKLFLKKQ)
BPC372	c(KLKKLWLKKQ)	**BPC132**	c(KLKKLFLKKQ)
BPC374	c(LKKKLWLKKQ)	**BPC134**	c(LKKKLFLKKQ)
BPC376	c(KKLLKWLKKQ)	**BPC136**	c(KKLLKFLKKQ)
BPC378	c(KLKLKWLKKQ)	**BPC138**	c(KLKLKFLKKQ)
BPC380	c(LKKLKWLKKQ)	**BPC140**	c(LKKLKFLKKQ)
BPC382	c(KLLKKWLKKQ)	**BPC142**	c(KLLKKFLKKQ)
BPC384	c(LKLKKWLKKQ)	**BPC144**	c(LKLKKFLKKQ)
BPC386	c(LLKKKWLKKQ)	**BPC146**	c(LLKKKFLKKQ)
BPC388	c(KKLLLWKKKQ)	**BPC148**	c(KKLLLFKKKQ)
BPC390	c(KLKLLWKKKQ)	**BPC150**	c(KLKLLFKKKQ)
BPC392	c(LKKLLWKKKQ)	**BPC152**	c(LKKLLFKKKQ)
BPC394	c(KLLKLWKKKQ)	**BPC154**	c(KLLKLFKKKQ)
BPC396	c(LKLKLWKKKQ)	**BPC156**	c(LKLKLFKKKQ)
BPC398	c(LLKKLWKKKQ)	**BPC158**	c(LLKKLFKKKQ)
BPC400	c(KLLLKWKKKQ)	**BPC160**	c(KLLLKFKKKQ)
BPC402	c(LKLLKWKKKQ)	**BPC162**	c(LKLLKFKKKQ)
BPC404	c(LLKLKWKKKQ)	**BPC164**	c(LLKLKFKKKQ)
BPC406	c(LLLKKWKKKQ)	**BPC166**	c(LLLKKFKKKQ)
BPC408	c(KLLLKWKKLQ)	**BPC184**	c(KLLLKFKKLQ)
BPC410	c(KKKLKWKKLQ)	**BPC186**	c(KKKLKFKKLQ)
BPC412	c(LLLKKWKKLQ)	**BPC188**	c(LLLKKFKKLQ)
BPC414	c(LKKKKWKKLQ)	**BPC190**	c(LKKKKFKKLQ)
BPC416	c(LKLLKWKKLQ)	**BPC192**	c(LKLLKFKKLQ)
BPC418	c(KKLKKWKKLQ)	**BPC194**	c(KKLKKFKKLQ)
BPC420	c(LLKLKWKKLQ)	**BPC196**	c(LLKLKFKKLQ)
BPC422	c(KLKKKWKKLQ)	**BPC198**	c(KLKKKFKKLQ)
BPC424	c(LLLLKWKKLQ)	**BPC200**	c(LLLLKFKKLQ)
BPC426	c(KKKKKWKKLQ)	**BPC202**	c(KKKKKFKKLQ)

7.5.5 HPLC Spectra of a Trp-Containing Library of Cyclic Peptides

7.5.5.1 Characterization of BPC312

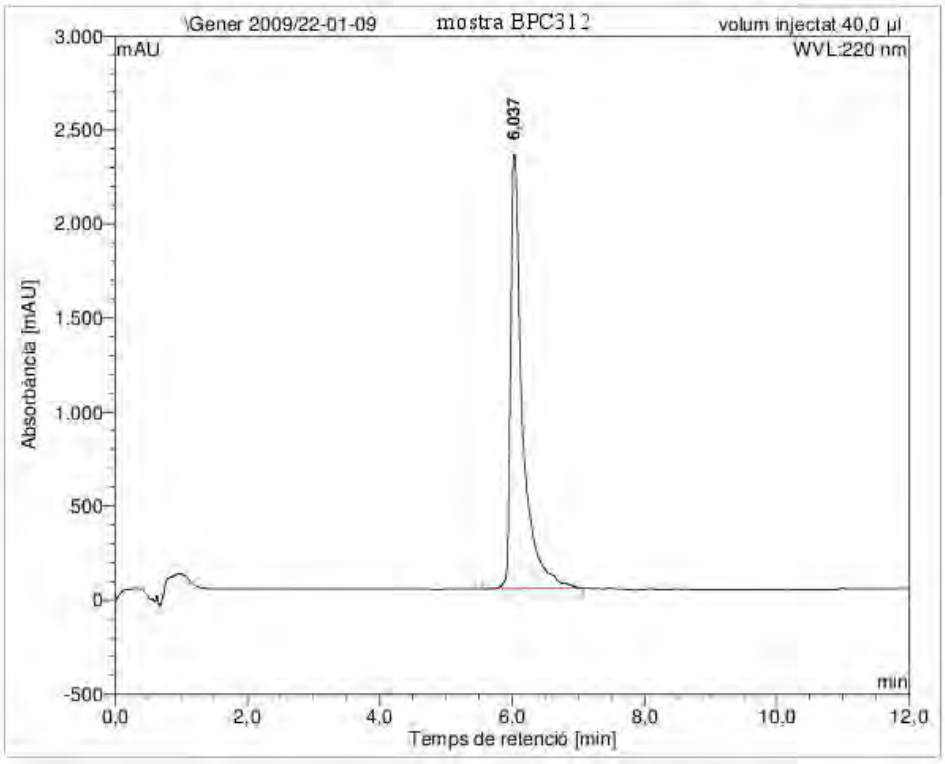

Figure 7.30: HPLC of BPC312.

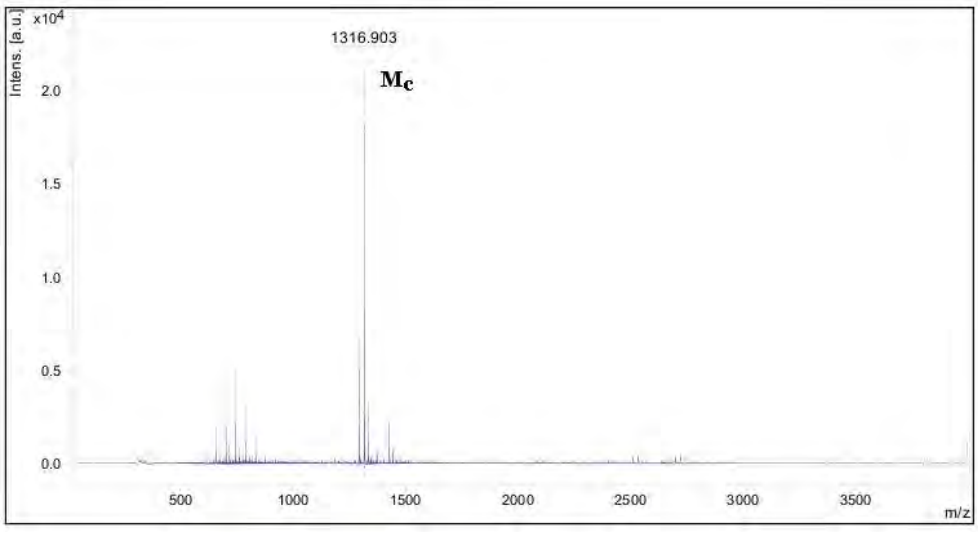

Figure 7.31: MALDI-TOF of BPC312.

7.5.5.2 Characterization of BPC326

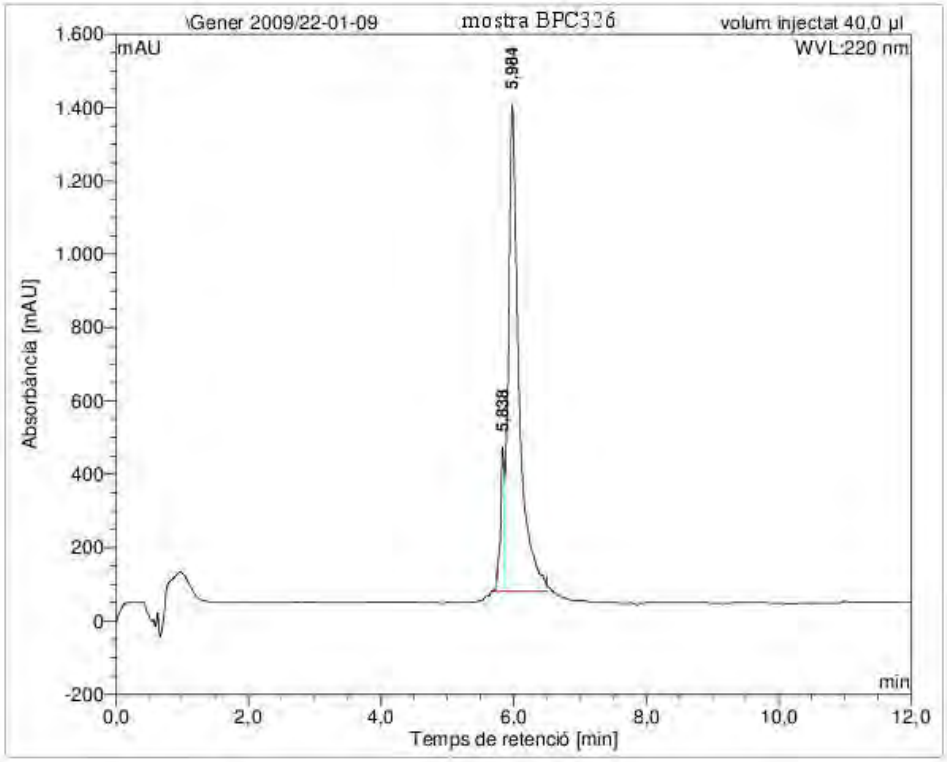

Figure 7.32: HPLC of BPC326.

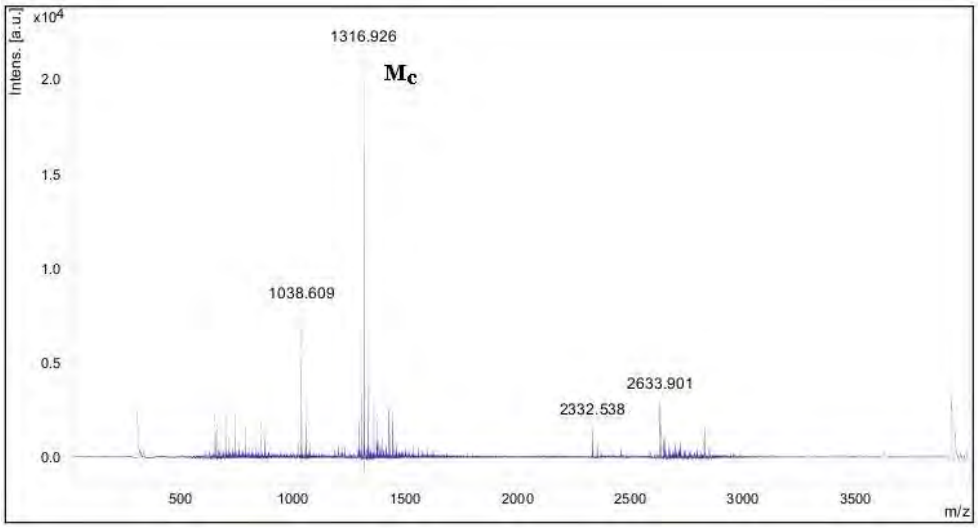

Figure 7.33: MALDI-TOF of BPC326.

7.5.5.3 Characterization of BPC338

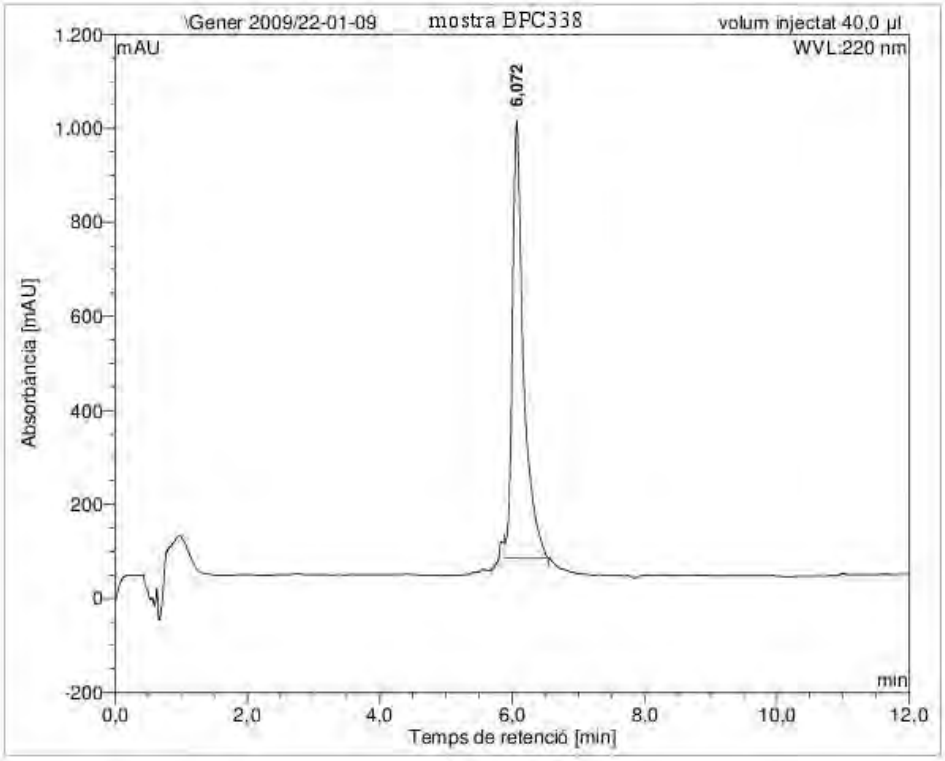

Figure 7.34: HPLC of BPC338.

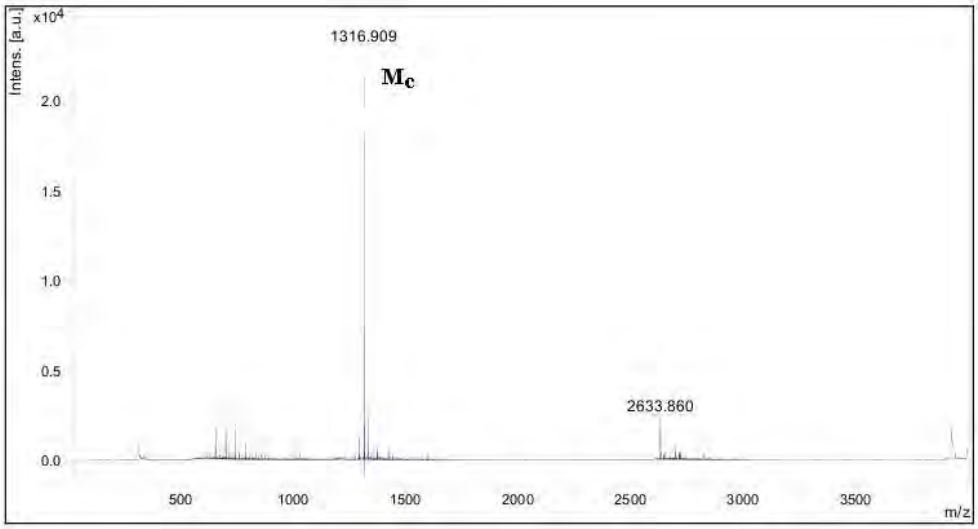

Figure 7.35: MALDI-TOF of BPC338.

7.5.5.4 Characterization of BPC354

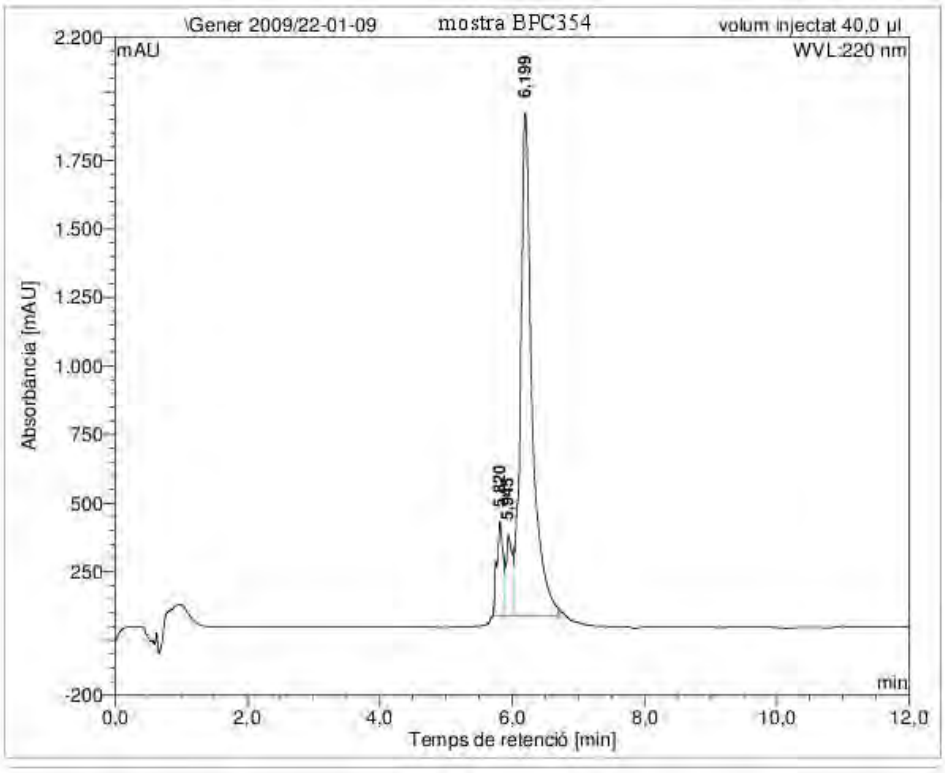

Figure 7.36: HPLC of BPC354.

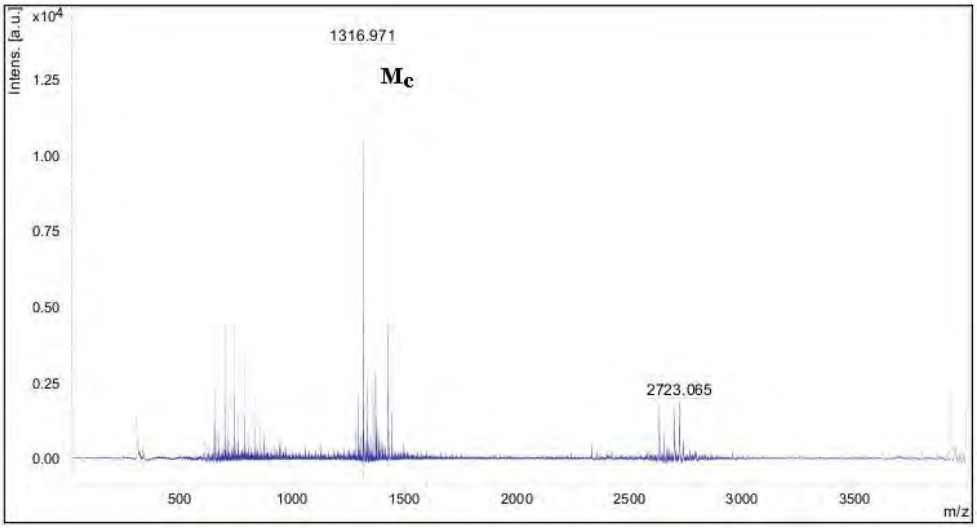

Figure 7.37: MALDI-TOF of BPC354.

7.5.5.5 Characterization of BPC356

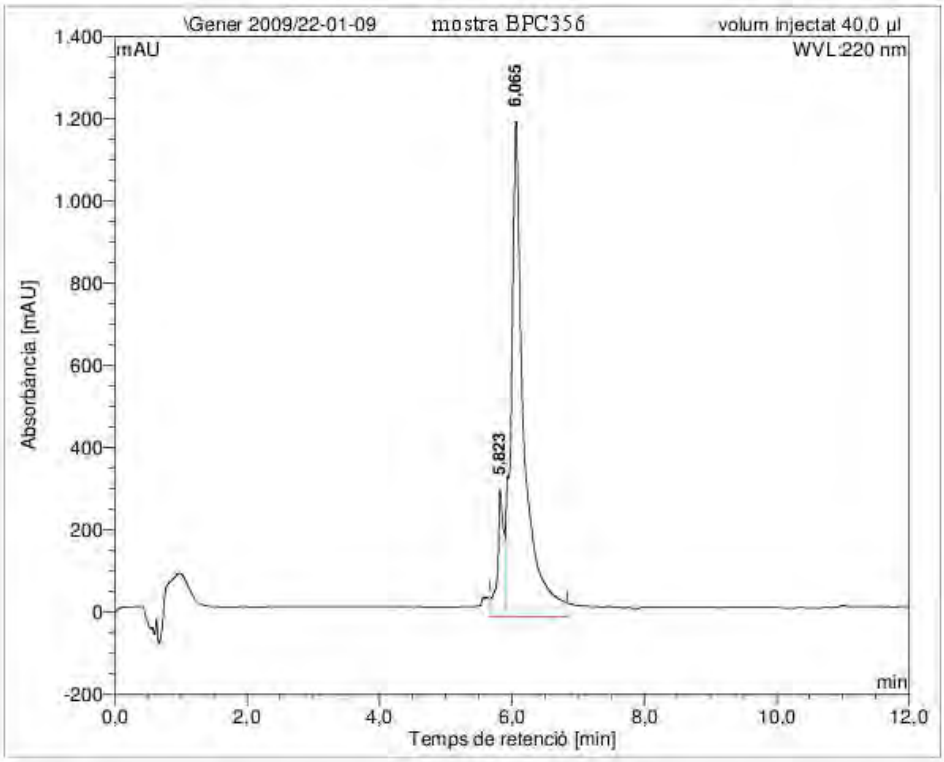

Figure 7.38: HPLC of BPC356.

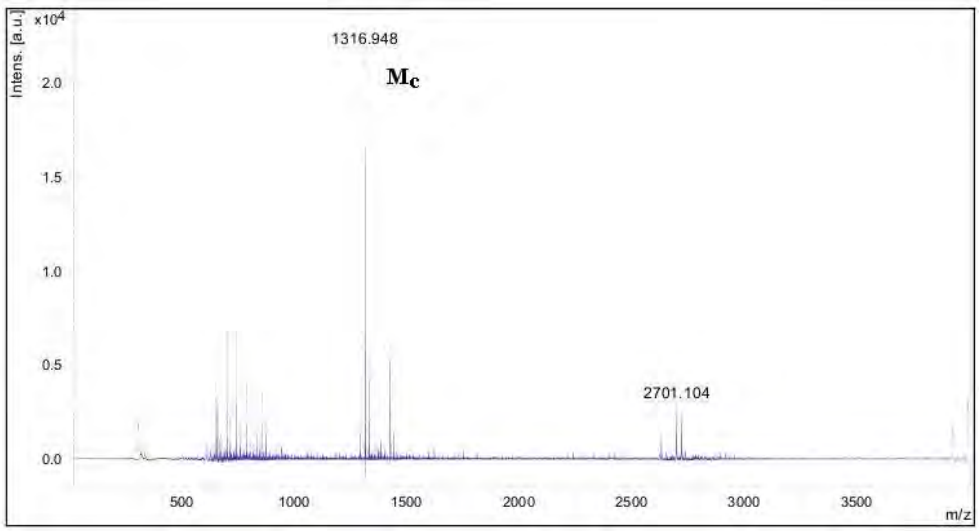

Figure 7.39: MALDI-TOF of BPC356.

7.5.5.6 Characterization of BPC372

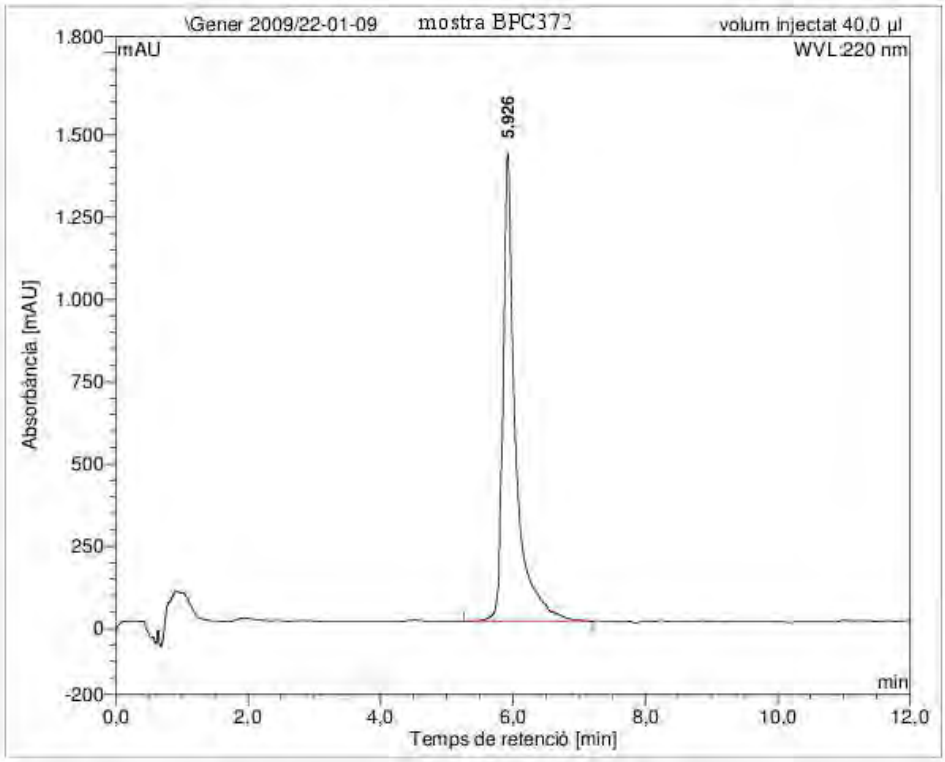

Figure 7.40: HPLC of BPC372

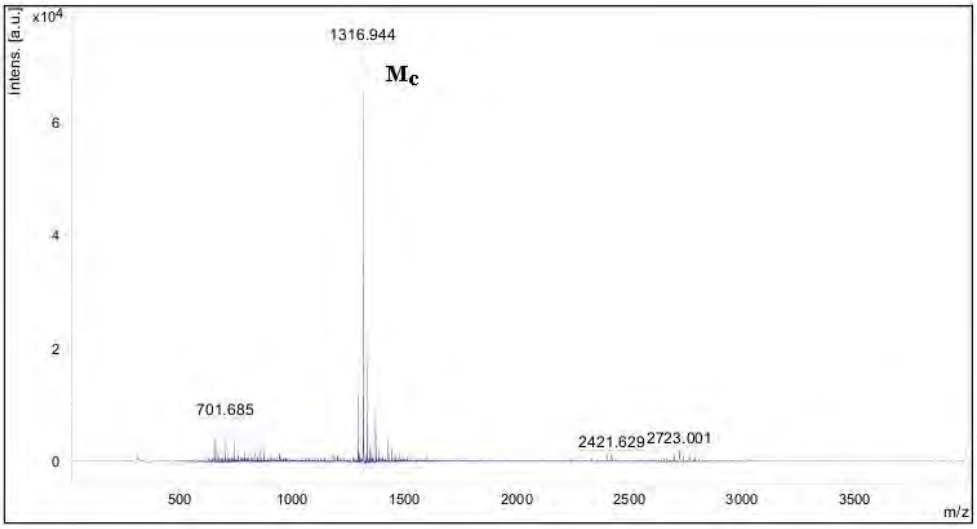

Figure 7.41: MALDI-TOF of BPC372.

7.5.5.7 Characterization of BPC360

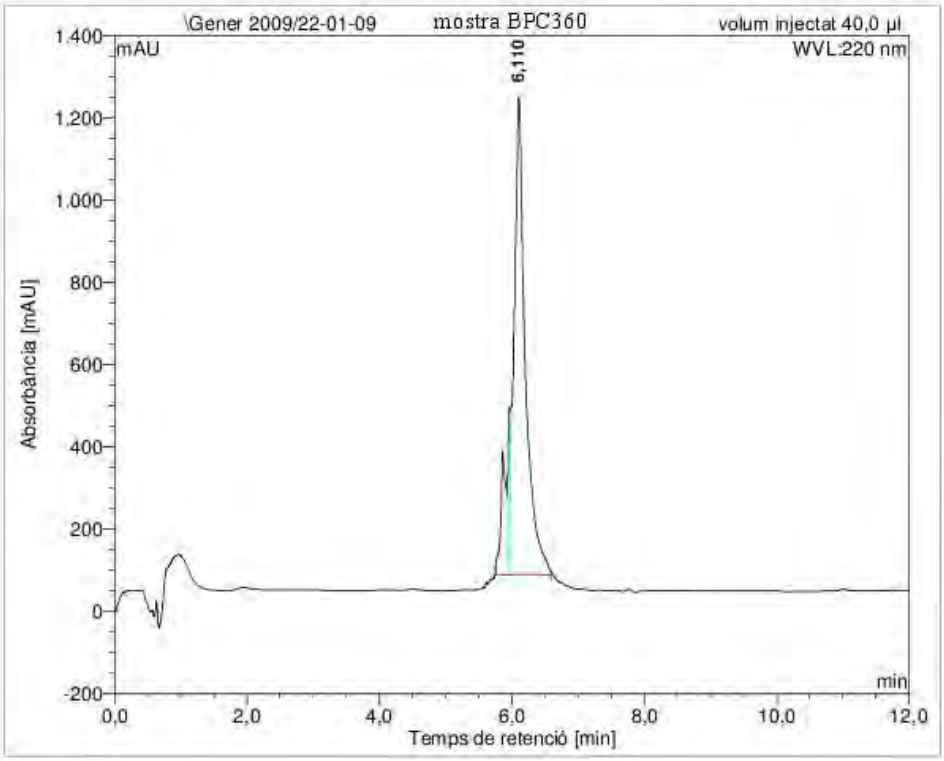

Figure 7.42: HPLC of BPC360

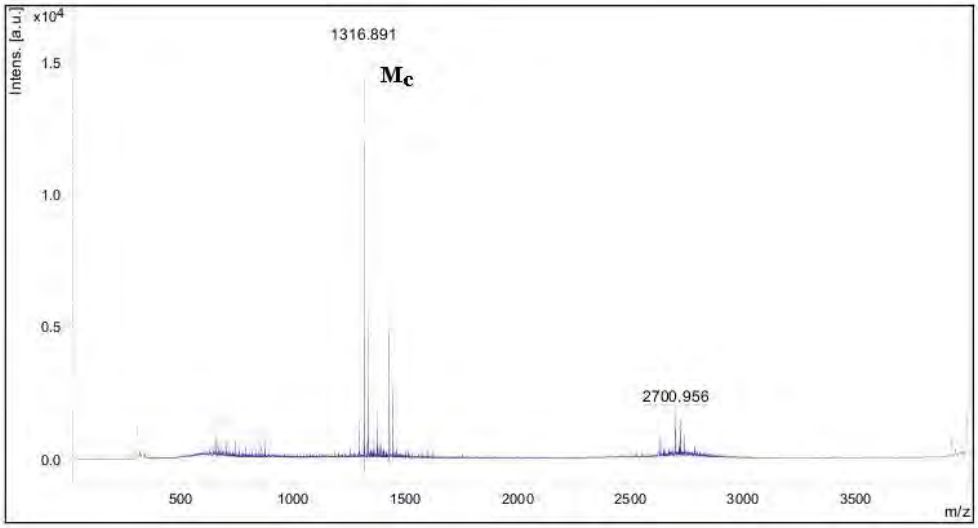

Figure 7.43: MALDI-TOF of BPC360.

7.6 Molecular Modelling of Cyclic Peptides

7.6.1 Supplementary Data for Interaction and Mechanism of Action of BPC194 Upon Membrane Models

Table 7.3: Summary of details of all the simulations performed on the cyclic (BPC194) and linear (BPC193) peptides together with secondary structure content during the simulation. FF stands for Force field CI for counter-ions and ER for electrostatic regime.

P:L	Code	Peptide	Structure	FF	CI	ER	Time (ns)	Non-S (%)[a]	β-S (%)[a]
Water	W_a	Cyclic	Random	43a2	-	RF	50	85	15
	W_b	Cyclic	Random	43a2	6 Cl^-	PME	50	99	1
	W_c	Cyclic	Random	53a6	6 Cl^-	PME	100	77	123
	Average	Cyclic	-	-	-	-	-	87±5	13±5
	W_d	Linear	α-helix	43a2	-	RF	160	72	27
	W_e	Linear	α-helix	53a6	6 Cl^-	PME	30	96	4
	W_f	Linear	Bend	43a2	-	RF	54	90	10
	W_g	Linear	Bend	43a2	6 Cl^-	PME	50	92	8
	W_h	Linear	Bend	53a6	6 Cl^-	PME	100	94	6
	W_i	Linear	Extended	43a2	-	RF	55	90	10
	W_j	Linear	β-hairpin	53a6	6 Cl^-	RF	100	68	32
	W_k	Linear	β-hairpin	53a6	6 Cl^-	PME	100	66	33
	Average	Linear	-	-	-	-	-	84±4	16±4
1:128	$1C_a$	Cyclic	Random	43a2	-	RF	80	91	9
	$1C_b$	Cyclic	Random	43a2	-	RF	50	90	10
	$1C_c$	Cyclic	Random	43a2	-	RF	50	70	30
	$1C_d$	Cyclic	Random	43a2	-	RF	50	87	13
	$1C_e$	Cyclic	Chair	43a2	-	RF	50	76	24
	$1C_f$	Cyclic	Chair	43a2	-	RF	50	73	27
	$1C_g$	Cyclic	Chair	43a2	-	RF	50	69	31
	Average	Cyclic	-	-	-	-	-	79±3	21±3

[a] The averages and standard errors are reported standard errors are calculated from the standard deviation between all peptides in all simulations.

[b] Structured

P:L	Code	Peptide	Structure	FF	CI	ER	Time (ns)	Non-S (%)[a]	β-S (%)[a]
:128	$1L_a$	Linear	Bend	43a2	-	RF	40	99	1
	$1L_b$	Linear	Extended	43a2	-	RF	100	100	0
	Average	Linear	-	-	-	-	-	100±0	100±0
2:60	$2L_a$	2 Linear	α-helix	43a2	-	RF	∼200	70	30
	$2L_b$	2 Linear	α-helix	43a2	-	RF	∼200	60	40
28	$4C_a$	Cyclic	Random	43a2	-	RF	100	69	30
	$4C_b$	Cyclic	Random	43a2	24 Cl^-	RF	100	63	37
	$4C_c$	Cyclic	Random	43a2	24 Cl^-	PME	40	68	32
	Average	Cyclic	-	-	-	-	-	67±4	33±4
	$4C_b$	Linear	Extended	43a2	24 Cl^-	RF	100	∼100	0
	$4C_c$	Linear	Extended	43a2	24 Cl^-	PME	40	100	0
	Average	Cyclic	-	-	-	-	-	100±0	0±0
0:128	$9C_a$	Cyclic	Random	43a2	-	RF	160	63	37
	$9C_b$	Cyclic	Random	43a2	-	RF	20	62	38
	$9C_c$	Cyclic	Random	43a2	-	RF	30	61	39
	$9C_d$	Cyclic	Random	43a2	-	RF	30	73	27
	$9C_e$	Cyclic	Random	43a2	54 Cl^-	RF	90	70	30
	$9C_f$	Cyclic	Random	43a2	54 Cl^-	RF	75	76	24
	$9C_g$	Cyclic	Random	43a2	54 Cl^-	RF	75	65	35
	$9C_h$	Cyclic	Random	43a2	54 Cl^-	PME	36	66	34
	$9C_i$	Cyclic	Random	43a2	54 Cl^-	PME	32	72	28
	$9C_j$	Cyclic	Random	43a2	54 Cl^-	PME	32	69	31
	Average	Cyclic	-	-	-	-	-	68±2	32±2
	$9L_a$	Linear	Extended	43a2	-	RF	142	∼100	∼0
	$9L_b$	Linear	Extended	43a2	-	RF	100	99	1
	$9L_c$	Linear	Extended	43a2	-	RF	41	100	0
	$9L_d$	Linear	Extended	43a2	-	RF	35	98	2
	$9L_e$	Linear	Extended	43a2	54 Cl^-	RF	87	99	1
	$9L_f$	Linear	Extended	43a2	54 Cl^-	RF	85	98	2
	$9L_g$	Linear	Extended	43a2	54 Cl^-	PME	24	99	1
	Average	Linear	-	-	-	-	-	99±0	1±0

[a] The averages and standard errors are reported standard errors are calculated from the standard deviation between all peptides in all simulations.

[b] Structured

Table 7.4: Distance between the parallel lysine residues of cyclic (BPC194) and linear (BPC193) peptides.

P:L	**K^1-K^8 (nm)**	**K^2-K^7 (nm)**	**K^4-K^5 (nm)**
Water	1.0	1.14	0.68
1:128	0.73	0.67	0.55
4:128	0.70	0.62	0.58
9:128	0.75	0.63	0.67

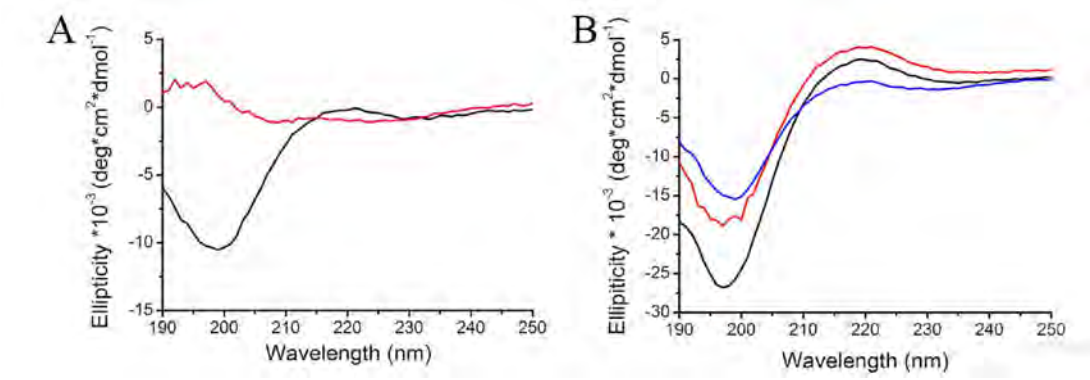

Figure 7.44: CD spectra. **A.** Cyclic BPC194 in aqueous buffer (black line) and in the presence of DOPG vesicles (red line) at a P:L ratio of 0.38. **B.** Linear peptide BPC193 in buffer, in the presence of DOPG membranes (at P:L ratio 0.38) or a secondary structure inducer TFE (black, red and blue line, respectively). Peptides 0.15μM, lipids 0.4μM, TFE-25% (vol/vol). This experiments were performed by Jacek T. Mika and Gemma Moiset (Mika 2011).

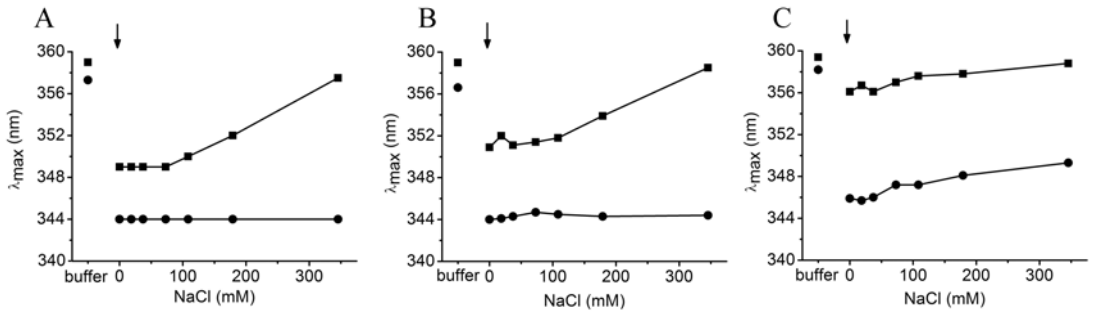

Figure 7.45: Peptide environment assessed by Trp fluorescence. Wavelengths of tryptophan fluorescence emission maxima (λ_{max}) of BPC418 (circles, solid line) and BPC417 (squares, dashed line) in buffer (first data point), upon addition of DOPG membranes (arrow), and following titration with NaCl up to 350 mM. The peptide concentration was 2μM; DOPG was added at different concentration, yielding **A.** P:L= 0.0073. **B.** P:L=0.071 and **C.** P:L= 0.88. Note that this experiments were performed with tryptophan analogues, which have shown also activity against the same bacteria. This experiments were performed by Jacek T. Mika and Gemma Moiset (For further data see Mika 2011).

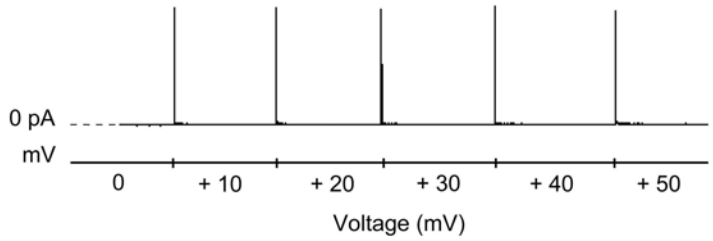

Figure 7.46: Linear peptide BPC193 is not able to stabilize pores. Current traces recorded after the addition of BPC194 peptide to DOPG membranes.

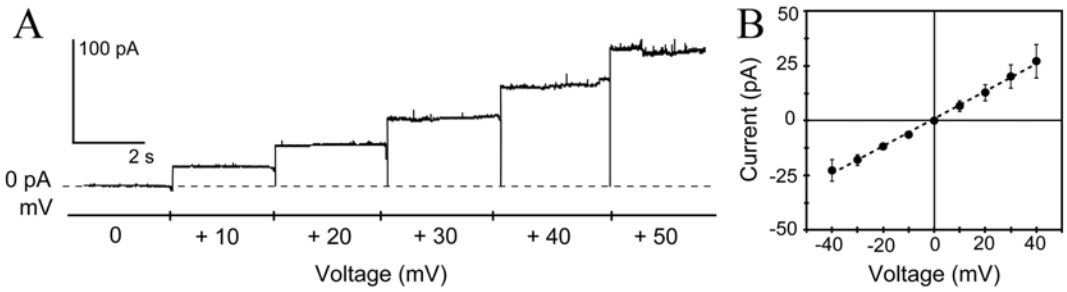

Figure 7.47: Cyclic peptide BPC194 is able to stabilize pores. **A.** Current traces recorded after the addition of BPC194 peptide to DOPG membranes. **B.** I/V curves plotted from seven independent current trace recording of BPC194. Since I/V curve is symmetric, the pores formed by BPC194 are not ion-selective. All independent recordings showed similar unitary pore conductance with an average value of 0.61 ± 0.12 nS. The estimated size of the pore was ranged between 1.5-1.9 nm.

7.7 Rational Design of Cyclic Peptides

7.7.1 Spectra of Cyclic Peptides

7.7.1.1 Characterization of BPC194

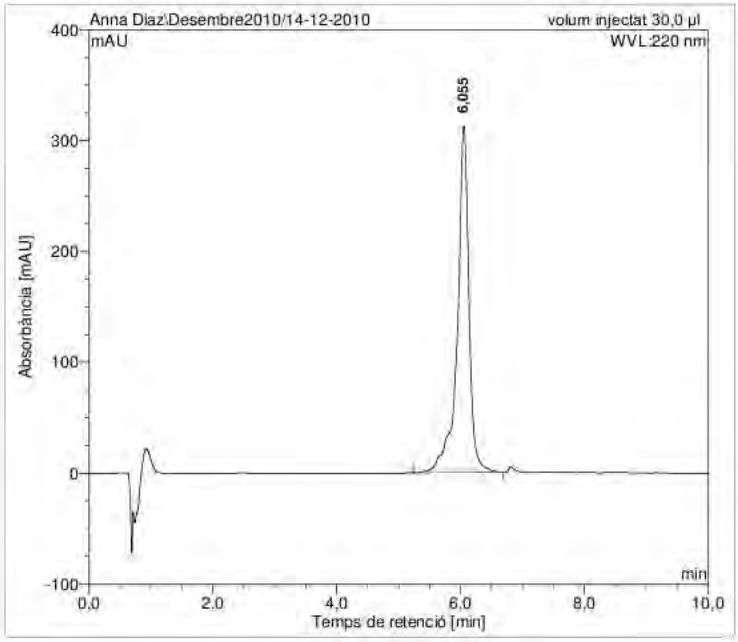

Figure 7.48: HPLC of BPC194. The cyclic peptide was synthetized for comparison purposes

7.7.1.2 Characterization of BPC480

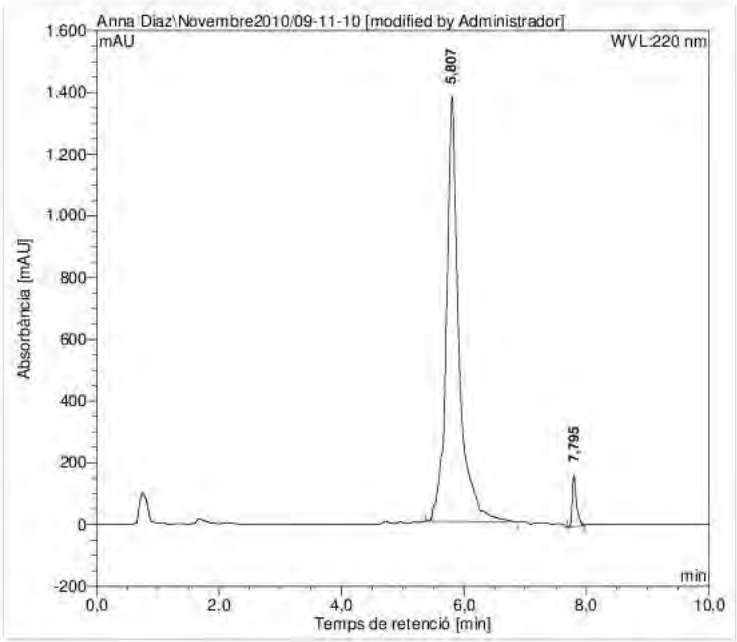

Figure 7.49: HPLC of BPC480

7.7.1.3 Characterization of BPC482

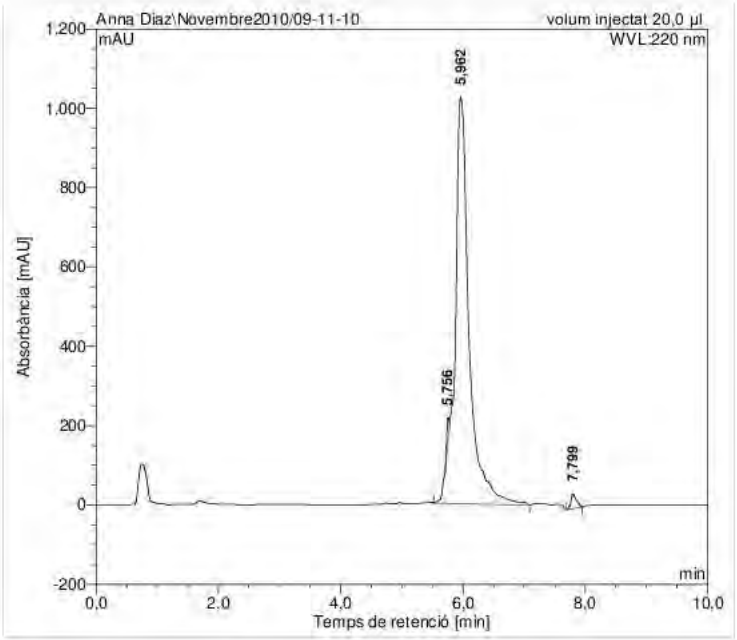

Figure 7.50: HPLC of BPC482

7.7.1.4 Characterization of BPC484

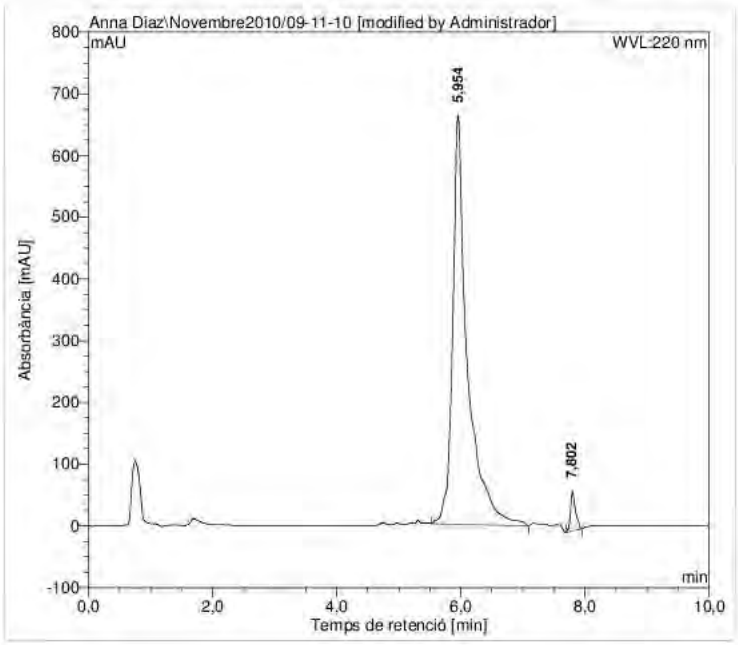

Figure 7.51: HPLC of BPC484

7.7.1.5 Characterization of BPC486

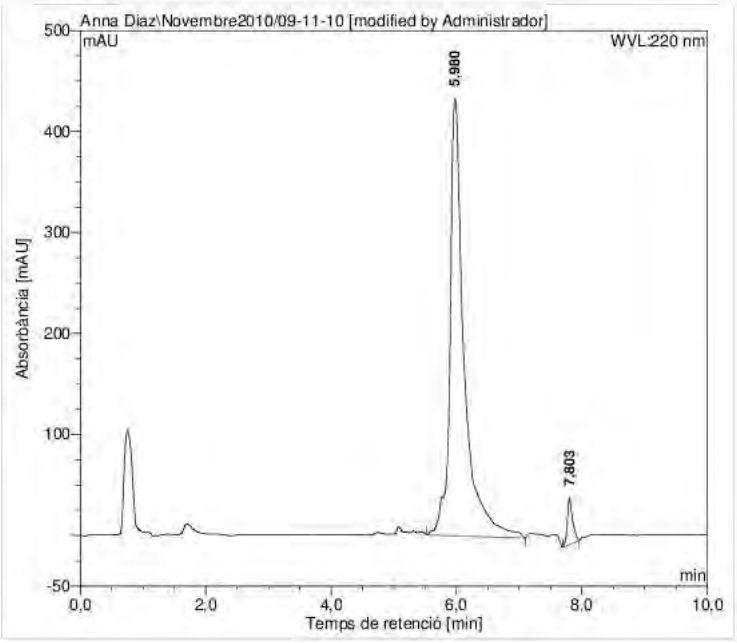

Figure 7.52: HPLC of BPC486

7.7.1.6 Characterization of BPC488

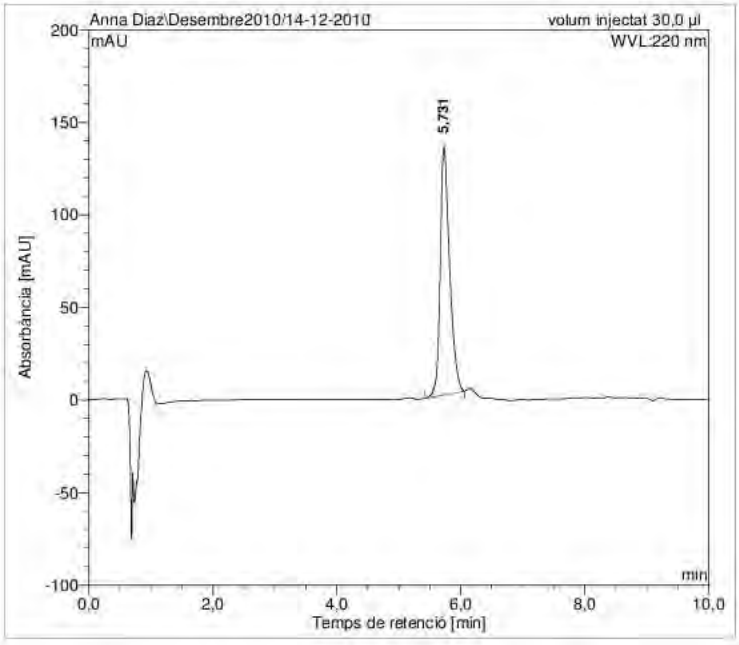

Figure 7.53: HPLC of BPC488

7.7.1.7 Characterization of BPC490

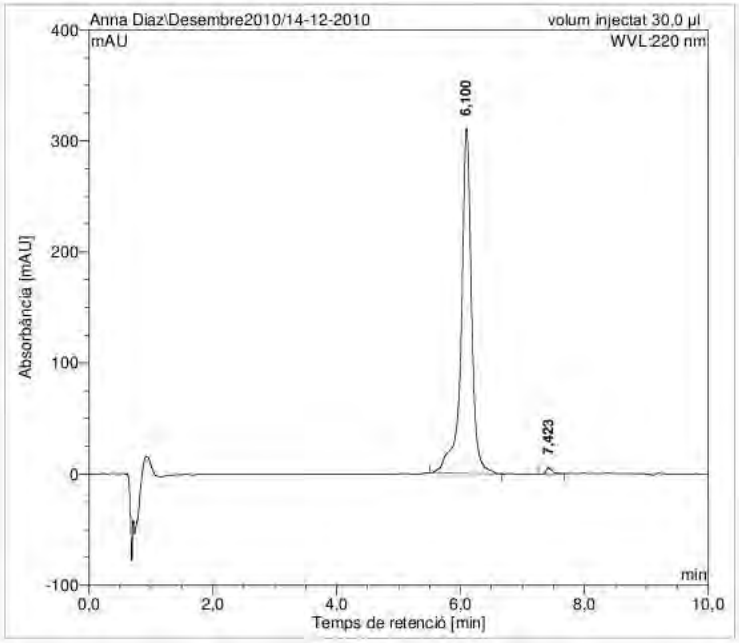

Figure 7.54: HPLC of BPC490

7.7.1.8 Characterization of BPC492

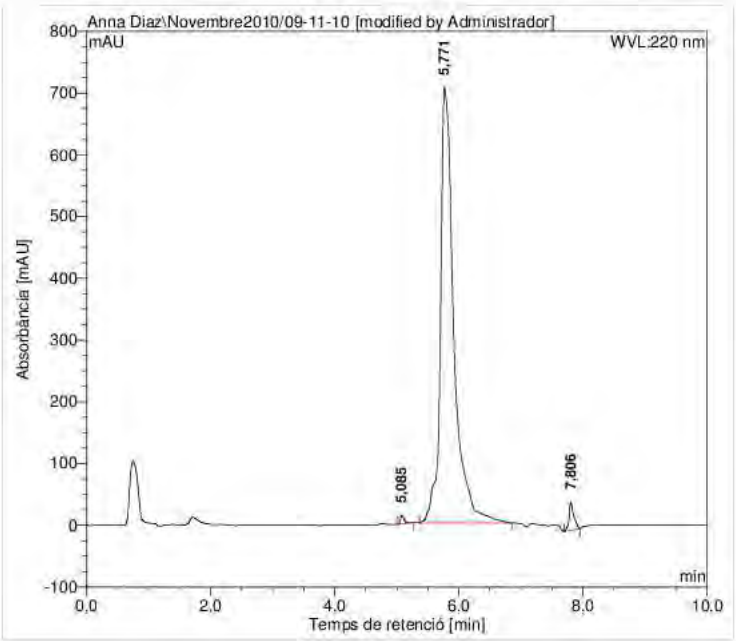

Figure 7.55: HPLC of BPC492

7.7.1.9 Characterization of BPC494

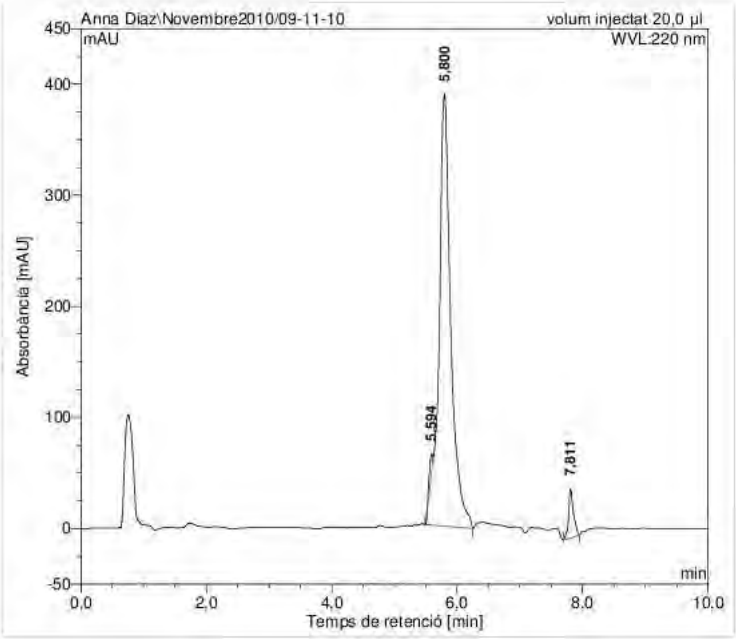

Figure 7.56: HPLC of BPC494

7.7.1.10 Characterization of BPC496

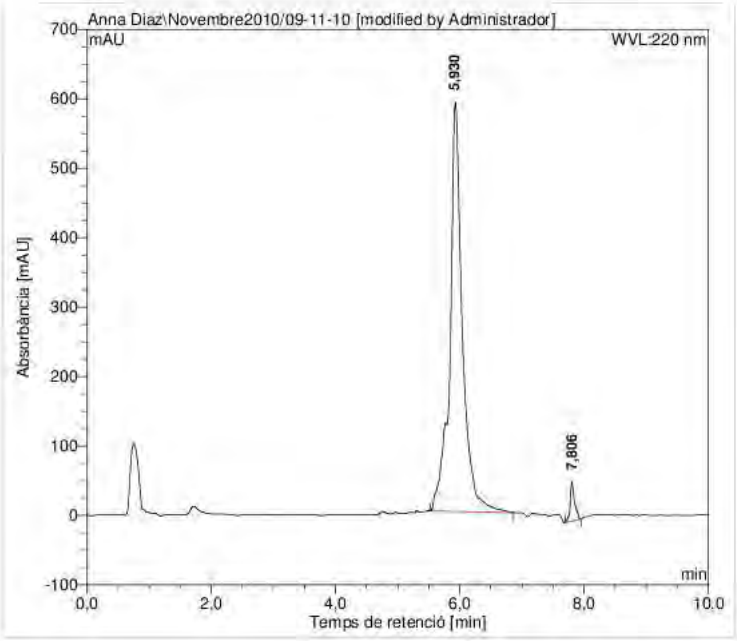

Figure 7.57: HPLC of BPC496

Bibliography

Albericio, F. 2000. Orthogonal protecting groups for N^{α}-amino and C-terminal carboxyl functions in solid-phase peptide synthesis *Peptide Sci.* 55:123139.

Andreu, D., Merrifield, R. B. Steiner, H., Boman, H. G. 1983. Solid-phase synthesis of cecropin A and related peptides *Proc. Natl. Acad. Sci.* 21:6475-6479.

Aneézo, C., A. H. de Vries, H. D. Höltje, D. P. Tieleman, and S. J. Marrink. 2003. Methodological issues in lipid bilayer simulations *J. Phys. Chem. B* 107:9424-9433.

Anfinsen, C. B. 1972. The formation of protein structure *Biochem. J.* 128:737-749.

Appelt, C., Eisenmenger, F., Kühne, R., Schmieder, P., Söderhäll, J. A. 2005. Interaction of the antimicrobial peptide cyclo(RRWWRF) with membranes by molecular dynamics simulations *Biophys. J.* 89:2296-2306.

Bechinger, B., Zasloff, M., Opella, S. J. 1993. Structure and orientation of the antibiotic peptide magainin in membranes by solid-state nuclear magnetic resonance spectroscopy *Protein Sci.* 2:2077-2084.

Bechinger, B. 1997. Structure and functions of channel-forming peptides: magainins, cecropins, melittin and alamethicin *J. Membrane Biol.* 156:197-211.

Bechinger, B. 1999. The structure, dynamics and orientation of antimicrobial peptides in membranes by multidimensional solid-state NMR spectroscopy *Biochim. Biophys. Acta.* 1462:157:183.

Bechinger, B., Aisenbrey, C., Bertani, P. 2004. The alignment, structure and dynamics of membrane-associated polypeptides by solid-state NMR spectroscopy *BBA-Biomembranes* 1666:190-204.

Bechinger, B. 2009. Rationalizing the membrane interactions of cationic amphipathic antimicrobial peptides by their molecular shape *Curr. Opin. Colloid. In.* 14:349-355.

Benz, R. W., Castro-Román, F., Tobias, D. J., White, S. H. 2005. Experimental Validation of Molecular Dynamics Simulations of Lipid Bilayers: A New Approach *Biophys. J.* 88:805-817.

Berendsen, H. J. C., J. P. M. Postma, W. F. van Gunsteren, and J. Hermans. 1981. Interaction models for water in relation to protein hydration *Intermolecular Forces.* 331-342.

Berendsen, H. J. C., Postma, J. P. M., van Gunsteren, W., DiNola, A., Haak, J. R. 1984. Molecular dynamics with coupling to an external bath *J. Chem. Phys.* 81:3684-3690.

Berendsen, H. J. C., J. P. M. Postma, W. F. van Gunsteren, A. D. Nola, and J. R. Haak. 1984. Molecular dynamics with coupling to an external bath *J. Chem. Phys.* 81:3684-3690.

Bessalle, R., Kapitkovsky, A., Gorea, A., Shalit, I., Fridkin, M. 1990. All-D-magainin: chirality, antimicrobial activity and proteolytic resistance *FEBS Lett.* 274:151-155.

Beven, L., Helluin, O., Molle, G., Duclohier, H., Wroblewski, H. 1999. Correlation between anti-bacterial activity and pore sizes of two classes of voltage-dependent channel-forming peptides *BBA-Biomembranes* 1421:53-63.

Bishop, J. L., Finlay, B. B. 2006. Friend or foe? Antimicrobial peptides trigger pathogen virulence *Trends Mol. Med.* 12:3-6.

Bisetty, K., Corcho, F. J., Canto, J., Kruger, H. G., Perez, J. J. 2006. A theoretical study of pentacyclo-undecane cage peptides of the type (Ac-X-Y-NHMe) *J. Pept. Sci.* 12:92-105.

Blondelle, S. E., Simpkins, L. R., Perez-Paya, E., Houghten, R. A. 1993. Influence of tryptophan residues on melittin's hemolytic activity *Biochim. Biophys. Acta. Protein. Struct. Mol. Enzymol.* 1202:331-336.

Blondelle, S. E., Lohner, K. 2000. Combinatorial libraries: a tool to design antimicrobial and antifungal peptide analogues having lytic specificities for structure-activity relationship studies *Biopolymers* 55:74-87.

Bocchinfuso, G., Palleschi, A., Orioni, B., Grande, G., Formaggio, F., Toniolo, C., Park, Y., Hahm, K. S., Stella, L. 2009. Different mechanism of action of antimicrobial peptides: insights from fluorescence spectroscopy experiments and molecular dynamics simulations *J. Pept. Sci.* 15:550-558.

Boland, M. P., Separovic, F. 2006. Membrane interactions of antimicrobial peptides from Australian tree frogs *Biochim. Biophys. Acta.* 1758:1178-1183.

Bosco, K. Ho., Thomas, A., Brasseur, R. 2009. Revisiting the Ramachandran plot: Hard-sphere repulsion, electrostatics, and H-bonding in the α-helix *Protein Science* 12:2508-2522.

Breukink, E., Wiedemann, I., van Kraaij, C., Kuipers, O. P., Sahl, H. G. de Kruijff, B. 1999. Use of the cell wall precursor lipid II by a pore-forming peptide antibiotic *Science* 5448:2361-2364.

Broekaert, W. F., Terras, F. R. G., Cammue, B. P. A., Osborn, R. W. 1995. Plant defensins: novel antimicrobial peptides as components of the host defense system *Plant Physiol.* 108:1353-1358.

Brogden, K. A., Ackermann, M., McCray, P. B., Tack, B. F. 2003. Antimicrobial peptides in animals and their role in host defences *Int. J. Antimicrob. Ag.* 22:465-478.

Brogden, K. A., 2005. Antimicrobial peptides: pore formers or metabolic inhibitors in bacteria? *Nat. Rev. Microbiol.* 3:238-250.

Bu, X., Wu, X., Xie, G., Guo, Z. 2002. Synthesis of Tyrocidine A and its analogues by spontaneous cyclization in aqueous solution *Org. Lett.* 4:2893-2895.

Bulet, P., Hetru, C., Dimarcq, J. L., Hoffmann, J. 1999. Antimicrobial peptides in insect; structure and function *Dev. Comp. Immunol.* 23:329-344.

Bürgi, R., Daura, X., Mark, A., van Gunsteren, W., Bellanda, M., Mammi, S., Peggion, E. 2001. Folding study of an Aib-rich peptide in DMSO by molecular dynamics simulations *J. Pept. Res.* 57:107118.

Carpino, L. A. Han, G. Y. 1970. 9-Fluorenylmethoxycarbonyl function, a new base-sensitive amino-protecting group *J. Am. Chem. Soc.* 92:5748-5749.

Carpino, L. A. 1993. 1-hydroxy-7-azabenzotriazole. An efficient peptide coupling additive *J. Am. Chem. Soc.* 115:4397-4398.

Carpino, L. A., El-Faham, A. 1995. Efficiency in peptide couing: 1-hydroxy-7-azabenzotriazole vs 3,4-dihydro-3-hydroxy-4-oxo-1,2,3-benzotriazine *J. Org. Chem.* 60:3561-3564.

Case, D. A., Darden, T. A., Cheatham, T.E. III, Simmerling, C.L., Wang, J., Duke, R. E., Luo, R., Merz, K. M., Pearlman, D. A., Crowley, M., Walker, R. C., Zhang, W., Wang, B., Hayik, S., Roitberg, A., Seabra, G., Wong, K. F., Paesani, F., Wu, X., Brozell, S., Tsui, V., Gohlke, H., Yang, L., Tan, C., Mongan, C., Hornak, V., Cui, G., Beroza, P., Mathews, D. H., Schafmeister, C., Ross, W. S., and Kollman, P. A. 2006. AMBER 9, University of California, San Francisco.

Chan, D. I., Prenner, E. J., Vogel, H. J. 2006. Tryptophan- and arginine-rich antimicrobial peptides: Structures and mechanisms of action *BBA-Biomembranes* 1758:1184-1202.

Chernomordik, L. V., Kozlov, M. M. 2008. Mechanics of membrane fusion *Nat. Struc. Mol. Biol.* 15:675-683.

Chou, C. K. 2000. Prediction of Tight Turns and Their Types in Proteins *Analyt. Biochem.* 286:1-16.

Cirac, A. D., Moiset, G., Mika, J. T., Koçer, A., Salvador, P., Poolman, B., Marrink, S. J., Sengupta, D. 2011. The molecular basis for antimicrobial activity of pore-forming cyclic peptides *Biophys. J.* 100:1-10.

Colilla, F.J., Rocher, A., Mendez, E. 1990. γ-Purothionins: amino acid sequence of two polypeptides of a new family of thionins from wheat endosperm *FEBS Lett.* 270:191-194.

Corcho, F. J., Filizola, M., Perez, J. J. 2000. Evaluation of the iterative simulated annealing technique in conformational search of peptides *Chem. Phys. Lett.* 319:65-70.

Corcho, F. J. S. 2003. Computational studies on the structure and dynamics of bioactive peptides *Escola Tecnica Superior d'Enginyeria Industrial de Barcelona*, Universitat Politecnica de Catalunya.

Cummings, J. E., Vanderlick, T. K. 2007. Aggregation and hemi-fusion of anionic vesicles induced by the antimicrobial peptide cryptdin-4 *Biochim. Biophys. Acta.* 1768:1796804.

Daidone, I., D'Abramo, M., Di Nola, A., Amadei, A. 2005. Theoretical characterization of α-helix and β-hairpin folding kinetics *J. Am. Chem. Soc.* 127:14825-14832.

Daidone, I., Amadei, A. and Di Nola, A. 2005. Thermodynamic and kinetic characterization of a β-hairpin peptide in solution: An extended phase space sampling by molecular dynamics simulations in explicit water *Proteins: Structure, Function, and Bioinformatics* 59:510518.

Dathe, M., Schümann, M., Wieprecht, T., Winkler, A., Beyermann, M., Krause, E., Matsuzaki, K., Murase, O., Bienert, M. 1996. Peptide helicity and membrane surface charge modulate the balance of electrostatic and hydrophobic interactions with lipid bilayers and biological membranes *Biochemistry* 35:1261212622.

Dathe, M., Wieprecht, T. 1999. Structural features of helical antimicrobial peptides: their potential to modulate activity on model membranes and biological

cells *BBA-Biomembranes* 15:71-87.

Dathe, M., Wieprecht, T. 1999. Hydrophobicity, hydrophobic moment and angle subtended by charged residues modulate antibacterial and haemolytic activity of amphipathic helical peptides *FEBS Lett.* 403:208-212.

Dathe, M., Nikolenko, H., Meyer, J., Beyermann, M., Bienert, M. 2001. Optimization of the antimicrobial activity of magainin peptides by modification of charge *FEBS Lett.* 501:146-150.

Daura, X., Jaun, B., Seebach, D., van Gunsteren, W. F., Mark, A. E. 1998. Reversible peptide folding in solution by molecular dynamics simulation *J. Mol. Biol.* 280:925-932.

Daura, X., van Gunsteren, W. F. Mark, A. E. 1999. Folding-unfolding thermodynamics of a β-heptapeptide from equilibrium simulations *Proteins: Structure, Function, and Bioinformatics* 34:269280.

Davies, J. S. 2003. The cyclization of peptides and depsipeptides *J. Pept. Sci.* 9:471501.

de Kroon, A. I.P.M., de Gier, J., de Kruijff, B. 1991. The effect of a membrane potential on the interaction of mastoparan X, a mitochondrial presequence, and several regulatory peptides with phospholipid vesicles *BBA-Biomembranes* 1068:111-124.

Devaux, P. F. 1991. Static and dynamic lipid asymmetry in cell membranes *Biochemistry* 30:1163-1173.

Dimarcq, J. L., Bulet, J., Hetru, C., Hoffmann, J. 1998. Cysteine-rich antimicrobial peptides in invertebrates *Biopolymers* 47:465-477.

Dolis, D., Moreau, C., Zachowski, A., Devaux, P. F. 1997. Aminophospholipid translocase and proteins involved in transmembrane phospholipid traffic *Biophys. Chem.* 68:221-231.

Domingues, M. M., Castanho, M. A. R. B., Santos, N. C. 2009. $rBPI_{21}$ promotes lipopolysaccharide aggregation and excerts its antimicrobial effect by (hemi)fusion of PG-membranes *PLoS ONE* 4:1-8.

Duan, Y., Kollman, P. A. 1998. Pathways to a protein folding intermediate observed in a 1-microsecond simulation in aqueous solution *Science* 282:740-744.

Efrat, A., Chernomordik, L. V., Kozlov, M. M. 2007. Point-like protrusion as a prestalk intermediate in membrane fusion pathway *Biophys. J.* 92:61-3.

Egberts, E., Berendsen, H. J. C. 1988. Molecular dynamics simulation of a smec-

tic liquid crystal with atomic detail *J. Chem. Phys.* 89:3718-3732.

Egberts, E., Marrink, S. J., Berendsen, H. J. C. 1994. Molecular dynamics simulations of a phospholipid membrane *Eur. Biophys. J.* 22:423-436.

Ehrlich, A., Heyne, H. U., Winter, R., Beyermann, M., Haber, H., Carpino, L. A., Bienert, M. 1996. Cyclization of all-L-pentapeptides by means of 1-hydroxy-7-azabenzotriazole-derived uronium and phosphonium reagents *J. Org. Chem.* 61:8831-8838.

Eisenberg, D., Schwarz, E., Komaromy, M., Wall, R. 1984. Analysis of membrane and surface protein sequences with the hydrophobic moment plot *J. Mol. Biol.* 179:125-142.

El-Faham, A., Subirós-Funosas, R., Prohens, R., Albericio, F. 2009. COMU: A safer and more effective replacement for benzotriazole-based uronium coupling reagents *Chem. Eur. J.* 15:9404-9416.

El-Faham, A., Albericio, F. 2010. COMU: A third generation of uronium-type coupling reagents *J. Pept. Sci.* 15:9404-9416.

Fahrner, R. L., Dieckmann, T., Harwig, S. S. L., Lehrer, R. I., Eisenberg, D., Feigon, J. 1996. Solution structure of protegrin-1, a broad-spectrum antimicrobial peptide from porcine leukocytes *Chem. Biol.* 3:543-550.

Falla, T. J., Karunaratne, D. N., Hancock, R. E. W. 1996. Mode of action of the antimicrobial peptide indolicidin *J. Biol. Chem.* 271:19298-19303.

Feliu, L., Oliveras, G., Cirac, A. D., Besalú, E., Rosés, C., Colomer, R., Bardají, E., Planas, M., Puig, T. 2010. Antimicrobial cyclic decapeptides with anticancer activity *Peptides* 31:2017-2026.

Ferre, R., Melo, M. N., Correia, A. D., Feliu, L., Bardají, E., Planas, M., Castanho. 2009. Synergistic effects of the membrane actions of cecropin-melittin antimicrobial hybrid peptide BP100 *Biophys. J.* 96:1815-1827.

Franklin, J. C., Ellena, J. F., Jayasinghe, S., Kelsh, L. P., Cafiso, D. S. 1994. Structure of micelle-associated alamethicin from H NMR. Evidence for conformational heterogeneity in a voltage-gated peptide *Biochemistry* 33:4036-4045.

Frecer, V., Ho, B., Ding, J. L. 2004. De novo design of potent antimicrobial peptides *Antimicrob. Agents Chemother.* 48:3349-3357.

Fung, S., Hruby, V. J. 2005. Design of cyclic and other templates for potent and selective peptide α-MSH analogues *Curr. Opin. Chem. Biol.* 9:352-358.

Ganz, T., Lehrer, R. I. 1998. Antimicrobial peptides of vertebrates *Curr. Opin.*

Immuno. 10:41-44.

Ganz, T. 2003. Defensins: antimicrobial peptides of innate immunity *Nat. Rev. Immunol.* 3:710-720.

Gause, G. F., Brazhnikova, M. G. 1944. Gramicidin S and its use in the treatment of infected wounds *Nature* 154:703-703.

Gazit, E., Lee, W. J., Brey, P. T., Shai, Y. 1994. Mode of action of the antibacterial cecropin B2: A spectrofluorometric study *Biochemistry* 33:10681-10692.

Gibbs, A. C., L. H. Kondejewski, W. Gronwald, A. M. Nip, R. S. Hodges, B. D. Sykes, and D. S. Wishart. 1998. Unusual β-sheet periodicity in small cyclic peptides *Nat. Struct. Biol.* 5:284-288.

Grant, G. A. 2002. Synthetic Peptides : A User's Guide, Oxford University Press, Oxford, New York.

Gudmundsson, G. H., Agerberth, B., Oderberg, J., Bergman, T., Olsson, B., Salcedo, R. 1996. The human gene *FALL39* and processing of the cathelin precursor to the antibacterial peptide LL-37 in granulocytes *Eur. J. Biochem.* 238:325-332.

Gurtovenko, A. A., Anwar, J., Vattulainen, I. 2010. Defect-mediated trafficking across cell membranes: insights from in silico modeling *Chem. Rev.* 110:6077-6103.

Hancock, R. E. W., Falla, T., Brown, M. 1995. Cationic bactericidal peptides, in Poole, R. K., Eds., Advances in Microbial Physiology, Academic Press 37:135-175.

Hancock, R. E. W. 1997. Peptide antibiotics *Lancet* 349:418-422.

Hancock, R. E. W., Chapple, D. S. 1999. Peptide antibiotics *Antimicrob. Agents Ch.* 43:1317-1323.

Hancock, R. E. W. 2001. Cationic peptides:effectors in innate immunity and novel antimicrobials *Lancet* 1:156-164.

Hancock, R. E. W. Rozek, A. 2002. Role of membranes in the activities of antimicrobial cationic peptides *FEMS Microbiol. Lett.* 206:143-149.

Harwig, S. S. L., Kokryakov, V. N., Swiderek, K. M., Aleshina, G. M., Zhao, C., Lehrer, R. I. 1995. Prophenin-1, an exceptionally proline-rich antimicrobial peptide from porcine leukocytes *FEBS Lett.* 362:65-69.

Hess, B., Bekker, H., Berendsen, H. J. C., Fraaije, J. G. E. M. 1997. LINCS: A linear constraint solver for molecular simulations *J. Comput. Chem.* 18:1463-

1471.

Hornak, V., Abel, R., Okur, A., Strockbine, B., Roitberg, A., Simmerling, C. 2006. Comparison of multiple Amber force fields and development of improved protein backbone parameters *Proteins* 65:712-725.

Hoskin, D. W., Ramamoorthy, A. 2008. Studies on anticancer activities of antimicrobial peptides *BBA-Biomembranes* 1778:357-375.

Houston, M. E. J., Kondejewski, L. H., Karunaratne, D. N., Gough, M., Fidai, S., Hodges, R. S., Huang, H. W. 2000. Action of antimicrobial peptides: Two-state model *Biochemistry* 39:8347-8352.

Howard, A. E., Kollman, P. E. 1988. An analysis of current methodologies for conformational searching of complex molecules *J. Med. Chem.* 31:1669-1675.

Hsu, J. Y. C., Yip, C. M. 2007. Molecular dynamics simulations of indolicidin association with model lipid bilayers *Biophys. J.* 92:100-102.

Huang, H. W. 2000. Action of antimicrobial peptides: two-state model *Biochemistry* 39:8347-8352.

Huang, H. W. 2006. Molecular mechanism of antimicrobial peptides: The origin of cooperativity *BBA-Biomembranes* 1758:1292-1302.

Humphrey, W., Dalke, A., Schulten, K. 1996. VMD: Visual molecular dynamics *J. Mol. Graph.* 14:33-38.

Hwang, P. M., Vogel, H. J. 1998. Structure-function relationships of antimicrobial peptides. *Biochem. Cell Biol.* 76:235-246.

Isidro-Llobet, A., Alvarez, M., Albericio, F. 2009. Amino acid-protecting groups *Chem. Rev.* 109:2455-2504.

IUPAC-IUB Joint Commission on Biochemical Nomenclature (JCBN). 1969. *Biochemistry* 9:3471-3479.

IUPAC-IUB Commission on Biochemical Nomenclature (JCBN). 1970.

IUPAC-IUB Joint Commission on Biochemical Nomenclature (JCBN). 1984. Nomenclature and symbolism for amino acids and peptides *Pure & Appl. Chem.* 56:595-624.

Jang, H., Ma, B., Woolf,T. B., Nussinov, R. 2006. Interaction of protegrin-1 with lipid bilayers: membrane thinning effect *Biophys. J.* 91:2848-2859.

Jang, H., Ma, B., Nussinov, R. 2007. Conformational study of the protegrin-1 (PG-1) dimer interaction with lipid bilayers and its effect *BMC Struct. Biol.*

7:21.

Jean François, F., Elezgaray, J., Berson, P., Vacher, P., Dufourc, E. J. 2008. Pore formation induced by an antimicrobial peptide: electrostatic effects *Biophys. J.* 95:5748-5756.

Jelokhani-Niaraki, M., Hodges, R. S., Meissner, J. E., Hassenstein, U. E., Wheaton, L. 2008. Interaction of gramicidin S and its aromatic amino-acid analog with phospholipid membranes it Biophys. J. 95:3306-3321.

Jelokhani-Niaraki, M., Prenner, E. J., Kay, C., M., McElhaney, R. N., Hodges, R. S. 2002. Conformation and interaction of the cyclic cationic antimicrobial peptides in lipid bilayers *J. Pept. Res.* 60:23-36.

Jenssen, H., Hamill, P., Hancock, R. E. W. 2006. Peptide antimicrobial agents *Clin. Microbiol. Rev.* 19:491-511.

Kabsch, W., Sander, C. 1983. Dictionary of protein secondary structure: Pattern recognition of hydrogen-bonded and geometrical features *Biopolymers* 22:2577-2637.

Kates, S. A., Sole, N. A., Johnson, C. R., Hudson, D., Barany, G., Albericio, F. 1993. A novel, convenient, three-dimensional orthogonal strategy for solid-phase synthesis of cyclic peptides *Tetrahedron Lett.* 34:1549-1552.

Kates, S. A., Albericio, F. 2000. Solid-phase synthesis a practical guide., Eds. Marcel Dekker, Inc. New York.

Kandasamy, S. K., Larson, R. G. 2004. Binding and insertion of α-helical antimicrobial peptides in POPC bilayers studied by molecular dynamics simulations *Chem. Phys. Lipids* 132:113-132.

Kawano, K., Yoneya, T., Miyata, T., Yoshikawa, K., Tokunaga, F., Terada, Y., Iwanaga, S. 1990. Antimicrobial peptide, tachyplesin I, isolated from hemocytes of the horseshoe crab (*Tachypleus tridentatus*). NMR determination of the β-sheet structure *J. Biol. Chem.* 265:15365-15367.

Khalfa, A., Tarek, M. 2010. On the antibacterial action of cyclic peptides: insights from coarse-grained MD simulations *J. Phys. Chem. B* 114:2676-2684.

Khandelia, H., Kaznessis, Y. N. 2007. Cation-π interactions stabilize the structure of the antimicrobial peptide indolicidin near membranes: molecular dynamics simulations *J. Phys. Chem. B* 111:242-250.

Khandelia, H., Kaznessis, Y. N. 2006. Molecular dynamics investigation of the influence of anionic and zwitterionic interfaces on antimicrobial peptides' struc-

ture: Implications for peptide toxicity and activity *Peptides* 27:1192-1200.

Kirkpatrick, S. 1984. Optimization by simulated annealing: Quantitative studies *J. Stat. Phys.* 34:975-986.

Klaenhammer, T. R. 1993. Genetics of bacteriocins produced by lactic acid bacteria *FEMS Microbiol. Rev.* 12:39-85.

Kokryakov, V. N., Harwig, S. S. L, Panyutich, E. A., Shevchenko, A. A., Aleshina, G. M., Shamova, O. V., Korneva, H. A., Lehrer, R. I. 1993. Protegrins: leukocyte antimicrobial peptides that combine features of corticostatic defensins and tachyplesins *FEBS Lett.* 327:231-236.

Kondejewski, L. H., Jelokhani-Niaraki, M., Farmer, S. W., Lix, B., Kay, C. M., Sykes, B. D., Hancock, R. E. W., Hodges, R. S. 1999. Dissociation of antimicrobial and hemolytic activities in cyclic peptide diastereomers by systematic alterations in amphipathicity *J. Biol. Chem.* 274:13181-13192.

Konz, D., Mohamed, M. A. 1999. How do peptide synthetases generate structural diversity? *Chem. Biol.* 6:39-48.

La Rocca, P., Shai, Y., Sansom, M. S. P. 1999. Peptide-bilayer interactions: simulations of dermaseptin B, an antimicrobial peptide *Biophys. Chem.* 76:145-159.

Landon, C., Sodano, P., Hetru, C., Hoffmann, J., Ptak, M. 1997. Solution structure of drosmycin, the first inducible antifugnal protein from insects *Protein Sci.* 6:1878-1884.

Langham, A. A., Khandelia, H. and Kaznessis, Y. N. 2006. How can a β-sheet peptide be both a potent antimicrobial and harmfully toxic? Molecular dynamics simulations of protegrin-1 in micelles *Peptide Sci.* 84:219231.

Langham, A. A., Ahmad, A. S., Kaznessis, Y. N. 2008. On the nature of antimicrobial activity: A model for protegrin-1 pores *J. Am. Chem. Soc.* 130:4338-4346.

Leach, A. R. 2001. Molecular modelling, principles and applications.

Lee, D. L. and Hodges, R. S. 2003. Structureactivity relationships of de novo designed cyclic antimicrobial peptides based on gramicidin S. *Peptide Sci.* 71:2848.

Lehrer, R. I., Ganz, T. 1999. Antimicrobial peptides in mammalian and insect host defence *Curr. Opin. Immuno.* 11:23-27.

Leontiadou, H., Mark, A. E., Marrink, S. J. 2006. Antimicrobial peptides in action *J. Am. Chem. Soc.* 128:12156-12161.

Lewis, P. N.; Momany, F. A.; Scheraga, H. A. 1973. Chain reversals in proteins *Biochem. Biophys. Acta.* 303:211-229.

Loncharich, R. J., Brooks, B. R., Pastor, R. W. 1992. Langevin dynamics of peptides: The frictional dependence of isomerization rates of N-acetylalanyl-N-methylamide *Biopolymers* 32:523-535.

Ludtke, S. J., He, K., Heller, W. T., Harroun, T. A., Yang, L., Huang, H. W. 1996. Membrane pores induced by magainin *Biochemistry* 35:13723-13728.

Mak, D. O. D., Webb, W. 1995. Two classes of alamethicin transmembrane channels: Molecular models from single-channel properties *Biophys. J.* 69:2323-2336.

Malesevic, M., Strijowski, U., Bächle, D., Sewald, N. 2004. An improved method for the solution cyclization of peptides under pseudo.high dilution conditions *J. Biotechnol.* 112:73-77.

Marion, D. Zasloff, M. Bax, A. 1988. A two-dimensional NMR study of the antimicrobial peptide magainin 2 *FEBS Lett.* 227:21-26.

Matsuzaki, K., Harada, M., Handa, T., Funakoshi, S., Fujii, N., Yajima, H., Miyajima, K. 1989. Magainin 1-induced leakage of entrapped calcein out of negatively-charged lipid vesicles *Biochim. Biophys. Acta.* 981:130-134.

Matsuzaki, K., Nakamura, A., Murase, O., Sugishita, K. I., Fujii, N., Miyajima, K. 1997. Modulation of magainin 2lipid bilayer interactions by peptide charge *Biochemistry* 26:2104-2111.

Matsuzaki, K., Murase, O., Fujii, N., Miyajima, K. 1996. An antimicrobial peptide, magainin 2, induced rapid flip-flop of phospholipids coupled with pore formation and peptide translocation *Biochemistry* 35:11361-11368.

Matsuzaki, K. 2009. Control of cell selectivity af antimicrobial peptides *Biochim. Biophys. Acta.* 1788:1687-1692.

Mátyus, E., Christian, K., Tieleman, D. P. 2007. Computer simulation of antimicrobial peptides *Curr. Med. Chem.* 14:2789-2798.

McCammon, J. A., Gelin, B. R., Karplus, M. 1977. Dynamics of folded proteins *Nature* 267:585-590.

Melo, M. N. Ferre, R., Castanho, M. A. R. B. 2009. Antimicrobial peptides: linking partition, activity and high membrane-bound concentration *Nat. Rev. Microbiol.* 7:245-250.

Mendez, E., Moreno, A., Collila, F., Pelaez, F., Limas, G.G., Mendez, R., So-

riano, F., Salinas, F., DeHaro, C. 1990. Primary structure and inhibition of protein synthesis in eukaryotic cell-free syste of a novel thionin, γ-hordothionin, from barley endosperm *Eur. J. Biochem.* 194:533-539.

Merrifield, R. B. 1963. Solid phase peptide synthesis 1. Synthesis of a tetrapeptide *J. Am. Chem. Soc.* 85:2149-2154.

Merrifield, R. B. 1986. Solid phase synthesis *Science* 232:341-347.

Mihailescu, D., Smith, J. C. 1999. Molecular dynamics simulation of the cyclic decapeptide antibiotic, gramicidin S, in dimethyl sulfoxide solution *J. Phys. Chem. B* 103:1586-1594.

Mihailescu, D., Smith, J. C. 2000. Atomic detail peptide-membrane interactions: Molecular dynamics simulation of gramicidin S in a DMPC Bilayer *Biophys. J.* 79:1718-1730.

Mika, J. T., Moiset, G., Cirac, A. D., Feliu, L., Bardají, E., Planas, M., Sengupta, D., Marrink, S. J., Poolman, B. 2011. *BBA-Membranes* X:X-X, *in Press.*

Miranda, L. P., Alewood, P. F. 2000. Challenges for protein chemical synthesis in the 21st century: bridging genomics and proteomics *Biopolymers* 55:217-226.

Mogi, T., Kita, K. 2009. Gramicidin S and polymyxins: the revival of cationic cyclic peptide antibiotics *Cell. Mol. Life Sci.* 23:3821-3826.

Monroc, S., Badosa, E., Feliu, L., Planas, M., Montesinos, E., Bardají, E. 2006a. De novo designed cyclic cationic peptides as inhibitors of plant pathogenic bacteria *Peptides* 27:2567-2574.

Monroc, S., Badosa, E., Besalú, E., Planas, M., Bardají, E., Montesinos, E., Feliu, L. 2006b. Improvement of cyclic decapeptides against plant pathogenic bacteria using a combinatorial chemistry approach *Peptides* 27:2575-2584.

Mootz, H. D., Marahiel, M. A. 1997. The tyrocidine biosynthesis operon of Bacillus brevis: complete nucleotide sequence and biochemical characterization of functional internal adenylation domains *J. Bacteriol.* 179:6843-6850.

Moult, J., James, M. N. G. 1986. An algorithm for determining the conformation of polypeptide segments in proteins by systematic search *Proteins: Structure, Function, and Bioinformatics* 1:146163.

Mottamal, M., Lazaridis, T. 2006. Voltage-dependent energetics of alamethicin monomers in the membrane *Biophys. Chem.* 122:50-57.

Nagata, Y. 1999. D-Amino acids in nature, in Palyi, G., Zucchi, C., Caglioti, L., Eds., Advances in BioChirality, Elsevier, Amsterdam, pp. 271-283.

Nagle, J. F., Tristram-Nagle, S. 2000. Lipid bilayer structure *Curr Opin. Struct. Biol.* 10:474-480.

Nakamura, T., Furunaka, H., Miyata, T., Tokunaga, F., Muta, T., Iwanaga, S., Niwa, M., Takao, T., Shimonishi, Y. 1988. Tachyplesin, a class of antimicrobial peptide from the hemocytes of the horseshoe crab (*Tachypleus tridentatus*). Isolation and chemical structure. *J. Biol. Chem.* 263:16709-16713.

Neu, H. C. 1992. The crisis in antibiotic resistance *Science* 257:1064-1073.

Nissen-Meyer, J., Nes, I. 1997. Ribosomally synthesized antimicrobial peptides: their function, structure, biogenesis, and mechanism of action *Arch. Biol.* 167:67-77.

Oishi, O., Yamashita, S., Nishimoto, E., Lee, S., Sugihara, G., Ohno, M. 1997. Conformations and orientations of aromatic amino acid residues of tachyplesin I in phospholipid membranes *Biochemistry* 36:4352-4359.

Oren, Z., Lerman, J. C., Gudmundsson, G. H., Agerberth, B., Shai, Y. 1999. Structure and organization of the human antimicrobial peptide LL-37 in phospholipid membranes: relevance to the molecular basis for its non-cell-selective activity *Biochem. J.* 341:501-513.

Orioni, B., Bocchinfuso, G., Kim, J. Y., Palleschi, A., Grande, G., Bobone, S., Park, Y., Kim, J. I., Hahm, K. S., Stella, L. 2009. Membrane perturbation by the antimicrobial peptide PMAP-23: A fluorescence and molecular dynamics study *Biochim. Biophys. Acta* 1788:1523-1533.

Oostenbrink, C., Soares, T.A., van der Vegt, N.F., van Gunsteren, W.F. 2005. Validation of the 53A6 GROMOS force field. *Eur. Biophys. J.* 34:273-284.

Pabst, G., S. Danner, S. Karmakar, G. Deutsch, and V. A. Raghunathan. 2007. On the propensity of phosphatidylglycerols to form interdigitated phases. *Biophys. J.* 93:513-525.

Park, C. B., Yi, K. S., Matsuzaki, K., Kim, M. S., Kim, S., C. 2000. Structureactivity analysis of buforin II, a histone H2A-derived antimicrobial peptide: The proline hinge is responsible for the cell-penetrating ability of buforin II *Proc. Natl. Acad. Sci.* 97:8245-8250.

Parsons, J. G., Sheehan, C. S., Wu, Z., James, I. W., Bray, A. M. 2003. A review of solid-phase organic synthesis on SynPhase$^{(TM)}$ Lanterns and SynPhase$^{(TM)}$ Crowns, in Morales, G. A., Bunin, B. A., Eds., Methods in Enzymology, Academic Press 369:39-74.

Pastor, R. W., Venable, R. M. 2002. Lipid Bilayers, NMR relaxation, and computer simulations *Acc. Chem. Res.* 35:438446.

Pauling, L., Corey, R. B. 1950. Two hydrogen-bonded spiral configurations of the polypeptide chain *J. Am. Chem. Soc.* 72:5349-5349.

Pauling, L., Corey, R. B. 1951. Atomic coordinates and structure factors for two helical configurations of polypeptide chain *Proc. Natl. Acad. Sci.* 37:235-240.

Pauling, L., Corey, R. B. 1951. The pleated sheet, a new layer configuration of polypeptide chains *Proc. Nat. Acad. Sci.* 37:251-256.

Pauling, L., Corey, R. B., Branson, H. R. 1951. The structure of proteins: two hydrogen bonded helical configurations of the polypeptide chain *Proc. Natl. Acad. Sci. USA* 37:205-211.

Pavone, V., Gaeta, G., Lombardi, A., Nastri, F., Maglio, O., Isernia, C., Saviano, M. 1996. Discovering protein secondary structures: Classification and description of isolated α-turns *Biopolymers* 38:705721.

Perron, G. G., Zasloff, M., Bell, G. 2006. Experimental evolution of resistance to an antimicrobial peptide *Proc. R. Soc. B.* 273:251-256.

Prenner, J. E., Lewis, R. N. A. H., McElhaney, R. N. 1999. The interaction of the antimicrobial peptide gramicidin S with lipid bilayer model and biological membranes *Biochim. Biophys.* Acta 1462:201-221.

Qian, S., Wang, W., Yang, L., Huang, H. W. 2008. Structure of the alamethicin pore reconstructed by x-ray diffraction analysis *Biophys. J.* 94:3512-3522.

Raj, P. A., Marcus, E., Sukumaran, D. K. 1998. Structure of human salivary histatin 5 in aqueous and nonaqueous solutions *Biopolymers* 45:5167.

Ramachandran, G. N., Sasisekharan, V. 1968. Conformation of polypeptides and proteins *Adv. Protein Chem.* 23:283-438.

Rapaport, D., Shai, Y. 1991. Interaction of fluorescently labeled paradaxin and its analogues with lipid bilayers *J. Biol. Chem.* 266:23769-23775.

Ripoll, D. R., Scheraga, H. A. 1988. On the multiple-minima problem in the conformational analysis of polypeptides. II. An electrostatically driven Monte Carlo methodtests on poly(L-alanine) *Biopolymers* 27:12831303.

Rizo, J., Gierasch, L. M. 1992. Constrained peptides: Models of bioactive peptides and protein substructure *Annu. Rev. Biochem.* 61:387-416.

Rivier, J., Brown, M., Vale, W. 1976. D-Trp8-somatostatin: An analog of somato-

statin more potent than the native molecule *Biochem. Biophys. Res. Comm.* 65:746-751.

Ryba, T. D., Depew, K. M., Marcaurelle, L. A. 2009. Large scale preparation of silicon-functionalized SynPhase lanterns for solid-phase synthesis *J. Comb. Chem.* 11:110-116.

Ryckaert, J. P., Ciccottu, G., Berendsen, H. J. C. J. 1997. Numerical integration of the cartesian equations of motion of a system with constraints: molecular dynamics of n-alkanes *Comput. Phys.* 23:327-341.

Saint, N., Marri, L., Marchini, D., Molle, G. 2003. The antibacterial peptide ceratotoxin A displays alamethicin-like behavior in lipid bilayers *Peptides* 24:1779-1784.

Saiz, L., Klein, M. L. 2002. Computer simulation studies of model biological membranes *Acc. Chem. Res.* 35:482489.

Sansom, M. S. 1991. The biophysics of peptide models of ion channels *Prog. Biophys. Mol. Biol.* 55:139-235.

Sarin, W. K., Kent, S. B. H., Merrifield, R. B. 1980. Properties of swollen polymer networks. Solvation and swelling of peptide-containing resins in solid-phase peptide synthesis *J. Am. Chem. Soc.* 102:54635470.

Scheraga, H. A. 1991. The multiple-minima problem in protein folding *AIP Conf. Proc.* 239:97107.

Seelig, J. 2004. Thermodynamics of lipid-peptide interactions *Biochim. Biophys. Acta* 1666:40-50.

Sengupta, D., Leontiadou, H., Mark, A. E., Marrink, S. J. 2008. Toroidal pores formed by antimicrobial peptides show significant disorder *BBA-Biomembranes* 1778:2308-2317.

Sewald, N., Jakubke, H. D. 2002. Peptides: chemistry and biology. WILEY-VCH Verlag GmbH, Weinheim.

Shepherd, C. M., Vogel, H. J., Tieleman, D. P. 2003. Interactions of the designed antimicrobial peptide MB21 and truncated dermaseptin S3 with lipid bilayers: molecular-dynamics simulations *Biochem J.* 370:233243.

Shai, Y. 2002. Mode of action of membrane active antimicrobial peptides *Biopolymers* 66:236-248.

Simmerling, C., Strockbine, B., Toitberg, A. E. 2002. All-atom structure prediction and folding simulations of a stable protein *J. Am. Chem. Soc.* 124:11258-

11259.

Smith, J. A., Pease, L. G. 1980. Reverse turns in peptides and proteins *Crit. Rev. Biochem.* 8:315-399.

Smith, C. W., Walter, R. 1978. Vasopressin analog with extraordinarily high antidiuretic potency: a study of conformation and activity *Science* 199:297-299.

Stavrakoudis, A., I. G. Tsoulos, Z. O. Shenkarev, and T. V. Ovchinnikova. 2009. Molecular dynamics simulation of antimicrobial peptide arenicin-2: beta-hairpin stabilization by noncovalent interaction *Peptide* 92:143-155.

Steiner, H., Hultmark, D., Engström, Å., Bennich, H., Boman, H. G. 1981. Sequence and specificity of two antibacterial proteins involved in insect immunity *Nature* 292:246-248.

Strahilevitz, J., Mor, A., Nicolas, P., Shai, Y. 1994. Spectrum of antimicrobial activity and assembly of dermaseptin-b and its precursor form in phospholipid membranes *Biochemistry* 33:10951-10960.

Struck, D. K., Hoekstra, D., Pagano, R. E. 1981. Use of resonance energy transfer to monitor membrane fusion *Biochemistry-Us* 20:4093-4099.

Subbalakshmi, C., Sitaram, N. 1998. Mechanism of antimicrobial action of indolicidin *FEMS Microbiol. Lett.* 160:91-96.

Subirós-Funosas, R., Prohens, R., Barbas, R., El-Faham, A., Albericio, F. 2009. Oxyma: an efficient additive for peptide synthesis to replace the benzenotriazole-based HOBt and HOAt with a lower risk of explosion *Chem. Eur. J.* 15:9394-9403.

Tarek, M. 2005. Membrane electroporation: A molecular dynamics simulation *Biophys. J* 88:4045-4053.

Tang, Y. Q., Yuan, J., Ösapay, G., Ösapay, K., Tran, D., Miller, C. J., Ouellette, A. J., Selsted, M. E. 1999. A Cyclic antimicrobial peptide produced in primate leukocytes by the ligation of two truncated α-defensins *Science* 286:498-502.

Thukral, L., Smith, J. C., Diadone, I. 2009. Common folding mechanism of a β-hairpin peptide via non-native turn formation revealed by unbiased molecular dynamics simulation *J. Am. Chem. Soc.* 131:18147-18152.

Tieleman, D. P., Berendsen, H. J. C. 1996. Molecular dynamics simulations of a fully hydrated dipalmitoylphosphatidylcholine bilayer with different macroscopic boundary conditions and parameters *J. Chem. Phys.* 105:4871-4880.

Tironi, I. G., Sperb, R., Smith, P. E., van Gunsteren, W. F. 1995. A general-

ized reaction field method for molecular dynamics simulations *J. Chem. Phys.* 102:5451-5459.

Tobias, D. J., Kechuan, T., Klein, M. L. 1997. Atomic-scale molecular dynamics simulations of lipid membranes *Curr. Opin. Coll. Int. Sci.* 2:15-26.

Toke, O. 2005. Antimicrobial peptides: new candidates in the fight against bacterial infections *Biopolymers* 80:717-735.

Tossi, A., Sandri, L., Giangaspero, A. 2000. Amphipathic, α-helical antimicrobial peptides *Biopolymers* 55:4-30.

Turner, J. D., Rouser, G. 1970. Precise quantitative determination of human blood lipids by thin-layer and triethylaminoethyl-cellulose column chromatography : I. Erythrocyte lipids *Anal. Chem.* 38:423-436.

Ulmschneider, M. B., Ulmschneider, J. P. 2008. Folding peptides into lipid bilayer membrane *J. Chem. Theory Comput.* 4:18071809.

Ulmschneider, J. P., Doux, J. P. F., Killian, J. A., Smith, J. C., Ulmschneider, M. B. 2009. Peptide partitioning and folding into lipid bilayers *J. Chem. Theory Comput.* 5:2202-2205.

Ultmark, D., Engström, Å., Bennich, H., Kapur, R. and Boman, H. G. 1982. Insect immunity: isolation and structure of cecropin D and four minor antibacterial components from cecropia pupae *Eur. J. Biochem.* 127:207-217.

Unger, T., Oren, Z., Shai, Y. 2001. The effect of cyclization of magainin 2 and melittin analogues on structure, function, and model membrane interactions: implication to their mode of action *Biochemistry* 40:6388-6397.

Utsugi, T., Schroit, A. J., Connor, J., Bucana, C. D., Fidler, I. J. 1991. Elevated expression of phosphatidylserine in the outer membrane leaflet of human tumor cells and recognition by activated human blood monocytes *Cancer Res.* 51:3062-3066.

Van den Bogaart, G., Kusters, I., Velàsquez, Mika, J. T., Krasnikov, V., Driessen, A. J. M., Poolman, B. 2008. Dual-color fluorescence-burst analysis to study pore formation and protein-protein interactions *Biophys. J.* 46:123-130.

van den Hooven, H. W., Doeland, C. C., van De Kamp, M., Konings, R. N., Hilbers, C. W., van De Ven, F. J. 1996. Three-dimensional structure of the lantibiotic nisin in the presence of membrane-mimetic micelles of dodecylphosphocholine and of sodium dodecylsulphate *Eur. J. Biochem.* 235:382-93.

van der Spoel, D., E. Lindahl, B. Hess, G. Groenhof, A. E. Mark, and H. J.

C. Berendsen. 2005. GROMACS: Fast, flexible, and free. *J. Comput. Chem.* 26:1701-1718.

van Gunsteren, W. F., Berendsen, H. J. C. 1990. Computer simulation of molecular dynamics methodology, applications and prespectives in chemistry *Angew. Chem. Int. Ed.* 29:992-1023.

van Gunsteren, W. F., Bürgi, R., Peter, C., Daura, X. 2001. The key to solving the protein-folding problem lies in an accurate description of the denatured state *Angew. Chem. Int. Ed.* 40:351355.

van Gunsteren, W. F., Krüger, P., Billeter, S. R., Mark, A. E., Eising, A. A., Scott, W. R. P., Hüneberger, P. H., Tironi, I. G. 1996. Biomolecular Simulation: The GROMOS96 Manual and User Guide.

Venkatachalam, C. M. 1968. Stereochemical criteria for polypeptides and proteins. V. Conformation of a system of three linked peptide units *Biopolymers* 6:1425-1436.

Vaz Gomes, A., de Waal, A., Berden, J. A., Westerhoff, H. V. 1993. Electric potentiation, cooperativity, and synergism of magainin peptides in protein-free liposomes *Biochemistry* 32:53655372.

Wade, D., Boman, A., Wåhlin, B., Drain, C. M., Andreu, D., Boman, H. G., Merrifield, R. B. 1990. All-D amino acid-containing channel-forming antibiotic peptides *Proc. Natl. Acad. Sci.* 12:4761-4765.

Waki, M., Izumiya, N. 1990. Recent advances in the biotechnology of β-lactams and microbial bioactive peptides. in Kleinhaug, H., van Doren, H, Eds., Biochemistry of peptide antibiotics. de Gruyter, Berlin, 205-244.

Wei, C. C., Ho, M. H., Wang, W. H., Sun, Y. C. 2005. Molecular dynamics simulation of folding of a short helical peptide with many charged residue *J. Phys. Chem. B* 109:19980-19986.

Wendoloski, J. J., Kimatian, S. J., Schutt, C. E., Salemme, F. R. 1989. Molecular dynamics simulation of a phospholipid micelle *Science* 243:636-638.

Wieprecht, T., Dathe, M., Krause, E., Beyermann, M., Maloy, W. L., MacDonald, D. L., Bienert, M. 1997. Modulation of membrane activity of amphypathic, antibacterial peptides by slight modifications of the hydrophobic moment *FEBS Lett.* 417:135-140.

Williams, R. W., Starman, R., Taylor, K. M. P., Gable, K., Beeler, T., Zasloff, M., Covell, D. 1990. Raman spectroscopy of synthetic antimicrobial frog pep-

tides magainin 2a and PGLa *Biochemistry* 29:4490-4496.

Wu, M., Hancock, R. E. W. 1999. Improved derivatives of bactenecin, a cyclic dodecameric antimicrobial cationic peptide *Antimicrob. Agents. Ch.* 43:1274-1276.

Wu, M., Hancock, R. E. W. 1999. Interaction of the cyclic antimicrobial cationic peptide bactenecin with the outer and cytoplasmic membrane *J. Biol. Chem.* 274:29-35.

Xu, Y., Sugár, I. P., Krishna, R. 1995. A variable target intensity-restrained global optimization (VARTIGO) procedure for determining three-dimensional structures of polypeptides from NOESY data: Application to gramicidin S *J. Biomol. NMR* 5:37-48.

Yang, L., Weiss, T. M., Lehrer, R. I., Huang, H. W. 2000. Crystallization of antimicrobial pores in membranes: magainin and protegrin *Biophys. J.* 79:2002-2009.

Yang, L., Harroun, T. A., Weiss, T. M., Ding, L., Huang, H. W. 2001. Barrel-stave model or toroidal model? A case study on melittin pores *Biophys. J.* 81:1475-1485.

Yeaman, M. R., Yount, N. 2003. Mechanism of antimicrobial peptide action and resistance *Pharmacol. Rev.* 55:27-55.

Yesylevskyy, S., Marrink, S. J., Mark, A. E. 2009. Alternative mechanisms for the interaction of the cell-penetrating peptides penetratin and the TAT peptide with lipid bilayers *Biophys. J.* 97:40-49.

Zanetti, M. 2004. Cathelicidins, multifunctional peptides of the innate immunity *J. Leukocyte Bio.* 75:39-48.

Zasloff, M. 1987. Magainins, a class of antimicrobial peptides from Xenopus skin: Isolation, characterization of two active forms, and partial cDNA sequence of a precursor *Proc. Natl. Acad. Sci. USA* 84:5449-5453.

Zasloff, M. 2002. Antimicrobial peptides of multicellular organisms. *Nature* 415:389-395.

Zhang, L., Dhillon, P., Yan, H., Farmer, S., Hancock, R. E. W. 2000. Interactions of bacterial cationic peptide antibiotic with outer and cytoplasmic membrane of *Pseudomonas aeruginosa Antimicrob. Agent. Ch.* 44:3317-3321.

Zhao, W., Róg, T., Gurtovenko, A. A., Vattulainen, I., Karttunen, M. 2007. Atomic-scale structure and electrostatics of anionic palmitoyloleoylphosphatidyl-

glycerol lipid bilayers with Na^+ counterions *Biophys. J.* 92:1114-1124.